

In light nuclear systems, with only a few degrees of freedom, it is possible to obtain accurate solutions for a wide variety of nuclear properties directly from realistic models of the NN interaction.

Within this deceptively simple picture, we can test our understanding of nuclear structure and dynamics over a wide range of energy, from the few keV of astrophysical relevance to the MeV regime of nuclear spectra to the tens to hundreds of MeV measured in nuclear response experiments. Through advances in computational techniques and facilities, the last few years have witnessed dramatic progress in the theory of light nuclei, as well as a variety of intriguing new experimental results. Important advances have occurred in studies of the spectra and structure of light nuclei, hadronic scattering, the response of light nuclei to external probes, and electroweak reactions involving few-nucleon systems at very low energy.

The picture of nuclei presented in this article, as nucleons interacting primarily through two-body interactions, should be adequate at low to modest values of energy and momentum transfer. Its usefulness lies in its conceptual simplicity: the nuclear properties are dominated by the two-nucleon interactions and one- and two-nucleon couplings to electroweak probes. This description is not new. Indeed, our knowledge of the basic components of the NN interaction—a short-range repulsion, an intermediate-range attraction, and a long-range attraction due to one-pion exchange—were all present in the work of Hamada and Johnston (1962) and Reid (1968).

The ability to perform reliable calculations within such a model is fairly new, however. Calculations with local interactions began in 1969 (Malfliet and Tjon, 1969a, 1969b), but convergence of the partial-wave expansion was convincingly demonstrated only in 1985 (Chen *et al.*, 1985). Four-nucleon ground-state calculations followed in 1990 (Carlson, 1990, 1991) and even more recently calculations of low-lying states in $A=5$ to 7 (Pudliner *et al.*, 1995). Also new is the connection, through chiral perturbation theory, of such a picture within QCD (Weinberg, 1990, 1991). Important conclusions of chiral perturbation theory, in particular the relative smallness of many-body forces, have been confirmed in the phenomenological models described in this article.

If progress involved only nuclear ground states, the picture would be interesting but of limited utility. However, important progress has been made in the scattering regime as well. Realistic calculations of three-nucleon (nd) scattering have been performed with momentum-space Faddeev techniques (Glöckle *et al.*, 1996). Comparisons are available with a wide range of experimental observables, including total cross sections, vector and tensor analyzing powers, spin-transfer coefficients, and scattering into specific final-state configurations. The overall agreement between theory and experiment is quite good, as many observables are well reproduced in the calculations. Nevertheless, some discrepancies remain unresolved. In particular, the difference between

calculated and experimental results on the polarization observable A_y are quite puzzling, possibly pointing to the need for improved models of the three-nucleon interaction and the inclusion of relativistic effects.

Significant progress has also been made in calculating low-energy electroweak reactions with realistic strong interactions and electroweak couplings. Reactions such as $^1\text{H}(p, e^+ \nu_e)^2\text{H}$, $^2\text{H}(p, \gamma)^3\text{He}$, $^2\text{H}(d, \gamma)^4\text{He}$, and $^3\text{He}(p, \nu_e)^4\text{He}$ have great astrophysical interest and are also important tests of our understanding of few-body reactions. They are sensitive both to ground-state and scattering-state wave functions and the electroweak current operators. Several methods have been used successfully in studying these low-energy capture reactions, including Faddeev, correlated hyperspherical harmonics (CHH), and Monte Carlo techniques.

The construction of realistic models of the nuclear current have proven essential to success in this area. Two-body currents associated with the NN interaction, particularly those associated with pion exchange, are crucial both on theoretical grounds, in order to satisfy current conservation, and on phenomenological grounds, as they provide a much improved description of the properties of light nuclei. The Faddeev and CHH calculations of the $^2\text{H}(p, \gamma)^3\text{He}$ and $^2\text{H}(n, \gamma)^3\text{H}$ cross sections are in good agreement with experimental values. The four-body capture reactions are particularly sensitive to the detailed model of the interactions and currents, as their cross sections vanish in the limit of no tensor force and no two-body currents. Discrepancies exist between variational estimates of the $^2\text{H}(d, \gamma)^4\text{He}$ and $^3\text{He}(n, \gamma)^4\text{He}$ cross sections and the corresponding experimental values, and it is not yet clear whether these discrepancies are to be ascribed to deficiencies in the variational wave function or to the model of two-body current operator (or both). These questions should be resolved in the near future.

Electron-scattering experiments provide further crucial tests of our understanding, in particular probing the electromagnetic current operator at higher values of the momentum transfer. Again, ground-state properties are well reproduced within this picture. The framework presented in this article has been shown to provide, at low and moderate values of the momentum transfer, a satisfactory description of the deuteron $A(Q)$ and $B(Q)$ structure functions and threshold disintegration, the charge and magnetic form factors of ^3H , ^3He , and ^4He , and the two-nucleon distribution functions of the helium isotopes as extracted from the (e, e') data. The only ground-state observables for which small but definite discrepancies exist between theory and experiment are the quadrupole moment and tensor polarization of the deuteron at intermediate values of the momentum transfer ($Q=0.5\text{--}1.0$ GeV/ c), and the ^3He magnetic form factor in the region of the first diffraction minimum. The discrepancy in the deuteron quadrupole moment is significant; it is a challenge to obtain precise agreement with all the deuteron data in either a relativistic or a nonrelativistic model.

Experiments with polarized and unpolarized electrons have measured inclusive and exclusive cross sections, longitudinal and transverse response functions, and asymmetry observables at intermediate energy and momentum transfer. The theoretical descriptions of these reactions have also progressed recently, with exact calculations of the response in $A=3$ with the Faddeev method, and Euclidean and Lorenz transforms of the response in $A=4$. The overall agreement with experiment is quite good in complete calculations—those that include realistic ground-state wave functions, two-body currents, and final-state interactions. In particular, the ratio of longitudinal to transverse strength, measured in electron scattering, is well described. The one-pion-exchange mechanism is important in each of these components and crucial to the overall success of the models. The failure to explain this ratio in calculations based on the naive plane-wave impulse approximation (PWIA) had led to speculations of in-medium modifications of the nucleon's form factors, the so-called “swelling” of the nucleon. In complete microscopic calculations no such modification of the form factors is necessary or even desirable.

The aim of this article is to review progress and highlight the prospects for microscopic studies of light nuclei. In the following sections, we present some of the methods used in calculating properties of few-nucleon systems and provide some highlights of the available comparisons with the huge quantity of experimental data. We begin with studies of nuclear spectra and structure, then discuss low-energy capture reactions, pd and nd scattering, and finally the nuclear response. Necessarily, some of the theoretical and experimental developments are treated cursorily, but we hope to convey a broad view of the intriguing and important studies in few-nucleon physics today.

II. NUCLEAR INTERACTION

We consider the simplest picture of a nucleus, a system of interacting neutrons and protons. In a nonrelativistic framework, the Hamiltonian is

$$\sum_i \frac{\mathbf{p}_i^2}{2m} + \sum_{i<j} v_{ij} + \sum_{i<j<k} V_{ijk} + \dots, \quad (2.1)$$

where the nucleons interact via two-, three-, and possibly many-body interactions. Studies of the nuclear interaction, both experimental and theoretical, have a long history, beginning essentially with the discovery of the neutron by Chadwick in 1932, and proceeding through the justification of this simple picture of nuclei within QCD by Weinberg (1991). A nice review of much of this history, along with a detailed description of current nucleon-nucleon (NN) interaction models, is given by Machleidt (1989). Here we merely explain some of the dominant features of the NN interaction and their importance in the structure and dynamics of light nuclei.

A. NN interactions

The NN interaction has an extraordinarily rich structure, as has been recognized for quite a long time. It is described in terms of the nucleon's spin ($\boldsymbol{\sigma}$) and isospin ($\boldsymbol{\tau}$), where both $\boldsymbol{\sigma}$ and $\boldsymbol{\tau}$ are SU_2 spinors. The former variable represents the intrinsic angular momentum (spin) of the nucleon, while the latter is a convenient representation for its two charge states—the proton and neutron. The generalized Pauli principle in this framework requires that two-nucleon states be antisymmetric with respect to the simultaneous exchange of the nucleons' space, spin, and isospin coordinates. The predominant isospin-conserving part of the NN interaction is written as linear combinations of components proportional to the two isoscalars, 1 and $\boldsymbol{\tau}_i \cdot \boldsymbol{\tau}_j$.

The long-range component of the NN interaction is due to one-pion exchange (OPE). If isospin-breaking terms are ignored, it is given, at long distances, by

$$v_{ij}^{OPE} = \frac{f_{\pi NN}^2 m_\pi}{4\pi} \frac{1}{3} [Y_\pi(r_{ij}) \boldsymbol{\sigma}_i \cdot \boldsymbol{\sigma}_j + T_\pi(r_{ij}) S_{ij}] \boldsymbol{\tau}_i \cdot \boldsymbol{\tau}_j, \quad (2.2)$$

$$Y_\pi(r_{ij}) = \frac{e^{-\mu r_{ij}}}{\mu r_{ij}}, \quad (2.3)$$

$$T_\pi(r_{ij}) = \left[1 + \frac{3}{\mu r_{ij}} + \frac{3}{(\mu r_{ij})^2} \right] \frac{e^{-\mu r_{ij}}}{\mu r_{ij}}, \quad (2.4)$$

where the mass m_π is the mass of the exchanged pion and

$$S_{ij} \equiv 3 \boldsymbol{\sigma}_i \cdot \hat{\mathbf{r}}_{ij} \boldsymbol{\sigma}_j \cdot \hat{\mathbf{r}}_{ij} - \boldsymbol{\sigma}_i \cdot \boldsymbol{\sigma}_j \quad (2.5)$$

is the tensor operator. At distances comparable to the inverse pion mass ($1/\mu \approx 1.4$ fm), one-pion exchange leads to a large tensor component in the NN interaction. In nuclear systems, then, the spatial and spin degrees of freedom are strongly correlated, and hence nuclear few- and many-body problems can be quite different from systems where the dominant interaction is independent of the particles' internal quantum numbers (spin and isospin), such as the Coulomb interaction in atomic and molecular problems or van der Waals forces in systems like bulk helium.

To further illustrate this point, we reproduce the plots of the deuteron's nucleon densities (Fig. 1) for two different orientations of the pair's spin, $S_z = \pm 1$ and $S_z = 0$, respectively (Forest *et al.*, 1996). These figures display surfaces of constant nucleon density for the two different spin orientations. As is apparent in the figure, the density is strongly correlated with the nuclear spin. Similar structures in the two-body distributions seem to occur in all light nuclei (Forest *et al.*, 1996). While this figure was constructed using a particular model of the NN interaction, the Argonne v_{18} model (Wiringa, Stoks, and Schiavilla, 1995), any NN interaction including short-range repulsive and long-range tensor components would produce a nearly indistinguishable plot.

At moderate and short distances, the NN interaction is much more complicated. However, the large body of pp and pn scattering data accumulated over the past

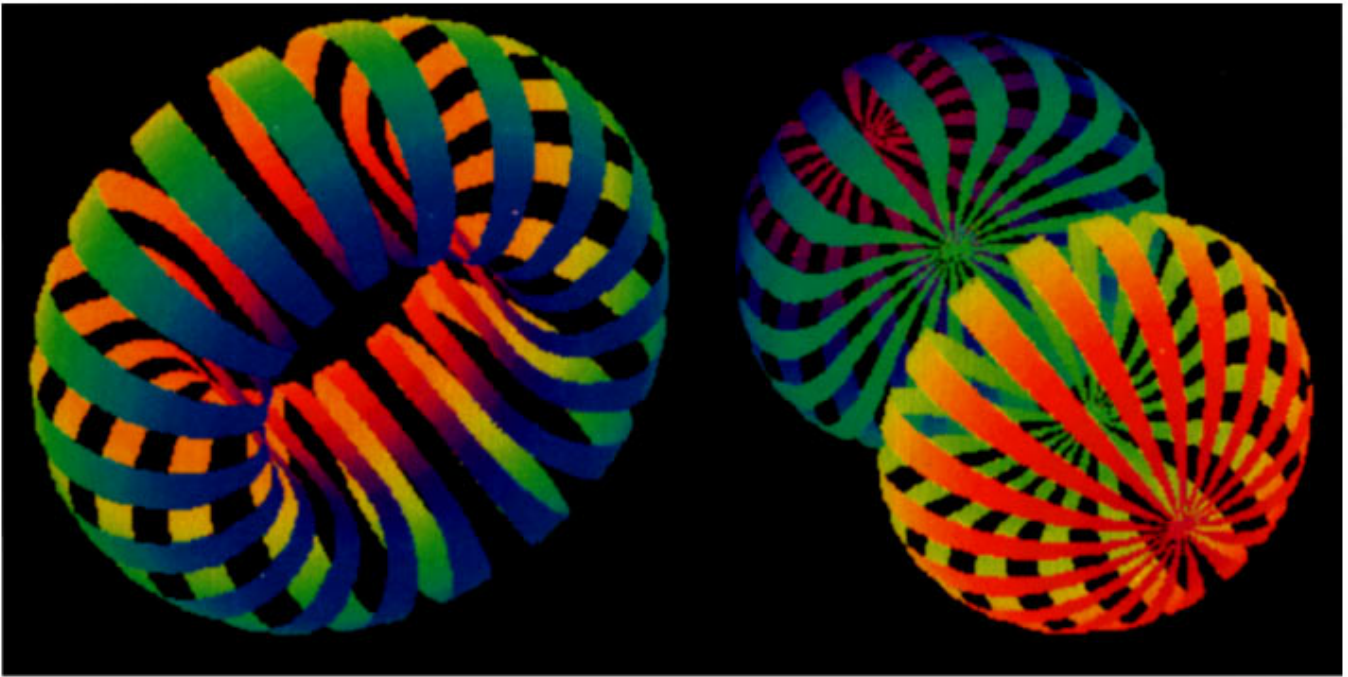


FIG. 1. (Color) Nucleon densities of the $S=1$ deuteron in its two spin projections, $S_z = \pm 1$ and $S_z = 0$, respectively. From Forest *et al.*, 1996.

half century provides, by now, very strong constraints, and indeed has been crucial in advancing our knowledge of the NN interaction.

One of the important early NN potentials was due to Reid (1968). It consisted of one-pion exchange at long distances and was of a partial-wave local form at short distances. That is, it can be written as

$$v_{ij} = \sum_{\alpha, \alpha'} v_{\alpha, \alpha'}(r) |\mathcal{Y}_\alpha\rangle \langle \mathcal{Y}_{\alpha'}|, \quad (2.6)$$

where the \mathcal{Y}_α are two-nucleon states of total isospin T and angular momentum J , the latter being composed of the spin S and relative orbital angular momentum L . The sums over α and α' run over these two-nucleon states. In the uncoupled channels ($S=0$ and $S=1$, $J=L$), the interaction is diagonal in α , while in the remaining triplet ($S=1$) channels, the tensor operator S_{ij} couples the $L=J \pm 1$ states. In the Reid interaction, the radial forms of the intermediate- and short-range parts of $v_{\alpha, \alpha'}(r)$ were simply taken as sums of Yukawa functions.

As more data became available, a variety of more sophisticated interaction models were introduced. At short and intermediate distances, these models can be quite different, ranging from one-boson-exchange (OBE) models to models with explicit two-meson exchanges to purely phenomenological parametrizations. Examples include the Paris (Cottingham *et al.*, 1973), Bonn (Machleidt, Holinde, and Elster, 1987), Nijmegen (Nagels, Rijken, and de Swart, 1978), and Argonne v_{14} (Wirringa, Smith, and Ainsworth, 1984) interaction models. The Nijmegen group employed Regge-pole theory to obtain an NN interaction model that includes numerous

one-boson-exchange terms with exponential form factors at the vertices, plus repulsive central Gaussian potentials arising from the Pomeron and tensor trajectories. This Nijmegen interaction is mildly nonlocal in the sense that it contains at most two powers of the nucleon pair's relative momentum. The resulting interaction can be written

$$v_{ij}(r) = \sum_p v^p(r) O_{ij}^p, \quad (2.7)$$

where the operators O_{ij}^p are products of

$$O_{ij}^p = [1, \boldsymbol{\sigma}_i \cdot \boldsymbol{\sigma}_j, S_{ij}, (\mathbf{L} \cdot \mathbf{S})_{ij}, \mathbf{p}_{ij}^2, \mathbf{p}_{ij}^2 \boldsymbol{\sigma}_i \cdot \boldsymbol{\sigma}_j, (\mathbf{L} \cdot \mathbf{S})_{ij}^2] \otimes [1, \boldsymbol{\tau}_i \cdot \boldsymbol{\tau}_j], \quad (2.8)$$

and $\mathbf{p}_{ij} = (\mathbf{p}_i - \mathbf{p}_j)/2$ is the relative momentum of the pair, while \mathbf{L} is the relative orbital angular momentum. The radial forms in the interaction are obtained from meson exchanges with phenomenological form factors. The coupling constants and form factor cutoffs are then adjusted to fit the deuteron properties and NN scattering data.

The Bonn group (Machleidt, Holinde, and Elster, 1987) used “old-fashioned” time-ordered perturbation theory and included a number of one-boson-exchange terms, as well as two-meson exchanges (2π , $\pi\rho$, and $\pi\omega$), correlated two-pion exchange in the form of the exchange of an effective scalar meson (the σ meson), effective three-pion exchange, and intermediate Δ isobars. Several forms of the Bonn interaction were presented; the “full” Bonn interaction is energy dependent and consequently difficult to use in many-body calculations. The Bonn B interaction is often used in realistic calculations. It is an energy-independent model con-

structured in momentum space; in coordinate space it contains nonlocalities with the range of the nucleon's Compton wavelength (≈ 0.2 fm).

The Argonne v_{14} (AV14) interaction (Wiringa, Smith, and Ainsworth, 1984) is of a more phenomenological form. At short and intermediate distances, its radial dependence is parametrized as a sum of functions proportional to T_π^2 [Eq. (2.4)] and consequently of two-pion-exchange range, plus short-range Woods-Saxon functions. The magnitude of these terms, as well as the parameters of the Woods-Saxon radial shapes, are adjusted to fit the data. As in the Nijmegen interaction, the Argonne v_{14} is a mildly nonlocal interaction containing at most two powers of the relative momentum. However, the Argonne v_{14} interaction uses the operators

$$O_{ij}^p = [1, \boldsymbol{\sigma}_i \cdot \boldsymbol{\sigma}_j, S_{ij}, (\mathbf{L} \cdot \mathbf{S})_{ij}, \mathbf{L}_{ij}^2, \mathbf{L}_{ij}^2 \boldsymbol{\sigma}_i \cdot \boldsymbol{\sigma}_j, (\mathbf{L} \cdot \mathbf{S})_{ij}^2] \otimes [1, \boldsymbol{\tau}_i \cdot \boldsymbol{\tau}_j]. \quad (2.9)$$

The first eight of these operators (those not involving two powers of the momentum) are unique in the sense that all such operators are implicitly contained in any realistic NN interaction model. The choice of the higher-order terms involving the second power of the orbital angular momentum operator is different from in the Nijmegen model, which uses \mathbf{p}^2 operators in place of \mathbf{L}^2 . The primary motivation for this choice is convenience in few- and many-body calculations, as the \mathbf{L}^2 terms do not contribute in relative S waves.

The Paris interaction (Cottingham *et al.*, 1973) is somewhat of a hybrid model. At intermediate nucleon-nucleon separations, it includes single ω exchange along with two-pion-exchange contributions calculated using πN phase shifts, $\pi\pi$ interactions, and dispersion relations. In addition, the Paris interaction contains short-range phenomenological terms. Indeed, all models should be considered phenomenological at short distances; they are either written phenomenologically from the start or, in the case of boson-exchange models, include phenomenological meson-nucleon form factors.

Even within the boson-exchange-type models, the interaction should not be taken literally as the exchange of single bosons. One-boson-exchange models often incorporate an effective scalar σ meson, which models the effects of correlated two-pion exchange; its mass and coupling constant are among the parameters that are adjusted to fit the two-nucleon data. Moreover, the relatively hard form factors obtained in NN interaction models can be thought of as simulating the exchange of heavier mesons with the same quantum numbers, or of simulating other physical effects outside the direct scope of the model.

While these models all produce a qualitatively similar picture of the NN interaction, with one-pion exchange at long range, an intermediate-range attraction, and a short-range repulsion, quantitatively they can be somewhat different. For example, the 1P_1 phase shifts for some of these models are plotted in Fig. 2. They vary for several reasons, chief among them that they have not all been fit to the same data. For example, models fit to np

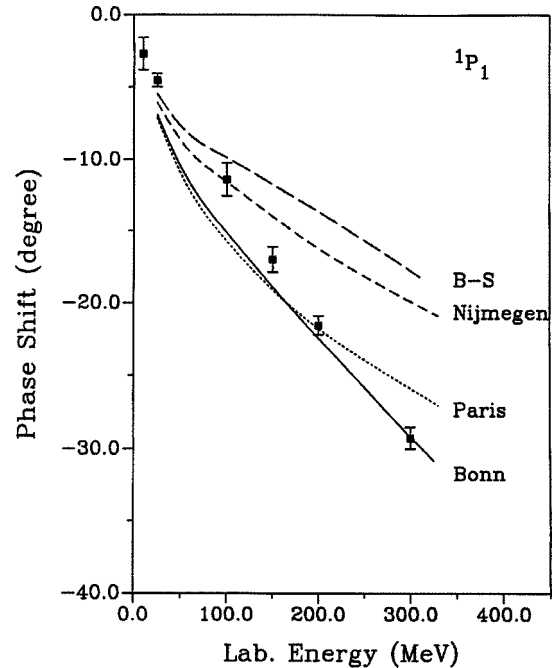


FIG. 2. Singlet 1P_1 phases in a variety of previous-generation interaction models. Not all interactions have been fit to the same data: Nijmegen, Nagels *et al.*, 1978; Paris, Cottingham *et al.*, 1973; Bonn, Machleidt *et al.*, 1987; B-S, Bryan and Scott, 1969.

data do not precisely fit the experimental pp data if only electromagnetic corrections are introduced.

Fortunately, high-quality phase-shift analyses of the pp and np data have become available recently (Arndt *et al.*, 1992; Stoks *et al.*, 1993). The Nijmegen analysis relies upon the (known) long-distance electromagnetic and one-pion-exchange interactions and makes a simple energy-dependent parametrization of the interior ($r_{ij} < 1.4$ fm) region. The data and analysis are quite accurate, yielding a χ^2 very near one per degree of freedom. The analysis is carried out for both pp and np experimental data, and the accuracy is sufficient to “reproduce the experimental charged and neutral-pion masses” from the nucleon-nucleon data (Stoks *et al.*, 1993). The Nijmegen group has also attempted to determine the πNN coupling constant from the phase-shift analysis (Stoks, Timmermans, and de Swart, 1993) and found a slightly lower value ($f_{\pi NN}^2/4\pi = 0.075$) than that obtained previously. This particular result is in agreement with recent analysis of πN data (Arndt, Workman, and Pavan, 1994), but is still a matter of some dispute (Arndt, Strakovsky, and Workman, 1995; Bugg and Machleidt, 1995; Ericson *et al.*, 1995). Another high-quality phase-shift analysis has been completed by the VPI group (Arndt *et al.*, 1992).

Recently, several NN interaction models have been fit to the experimental database. These include updated Nijmegen interactions (Nijm I, Nijm II, and Reid 93; Stoks *et al.*, 1994), the Argonne v_{18} (AV18) interaction (Wiringa, Stoks, and Schiavilla, 1995), and the CD Bonn interaction (Machleidt, Sammarruca, and Song, 1996). These models follow basically along the lines of their

TABLE I. Experimental deuteron properties compared to recent NN interaction models; meson-exchange effects in μ_d and Q_d are not included.

	Experiment	Argonne v_{18}	Nijm II	Reid 93	CD Bonn	Units
A_S	0.8846(8) ^a	0.8850	0.8845	0.8853	0.8845	fm ^{1/2}
η	0.0256(4) ^b	0.0250	0.0252	0.0251	0.0255	
r_d	1.971(5) ^c	1.967	1.9675	1.9686	1.966	fm
μ_d	0.857406(1) ^d	0.847				μ_0
Q_d	0.2859(3) ^e	0.270	0.271	0.270	0.270	fm ²
P_d		5.76	5.64	5.70	4.83	

^aEricson and Rosa-Clot, 1983.

^bRodning and Knutson, 1990.

^cMartorell, Sprung, and Zheng, 1995.

^dLindgren, 1965.

^eBishop and Cheung, 1979.

predecessors. However, in order to provide a precise fit, they are adjusted separately to the np and pp database, which requires them to contain charge-symmetry-breaking terms of both isovector ($\tau_{i,z} + \tau_{j,z}$) and isotensor ($3\tau_{i,z}\tau_{j,z} - \tau_i \cdot \tau_j$) type. Each of these models fits the NN database extremely well, with χ^2 per degree of freedom near one. The cost of this excellent fit is a rather large number of parameters; the Argonne v_{18} interaction has 40 adjustable parameters and the other modern interaction models have a similar number.

The most recent Nijmegen models are partial-wave local, in the same sense that the original Reid (1968) model was. While they retain a boson-exchange basis, the parameters are adjusted separately in each channel. The Nijmegen group has also produced an updated Reid-like model that is written as a sum of Yukawa functions. Such partial-wave local interactions provide a very specific choice of nonlocality in the full NN interaction. The CD Bonn interaction employs another choice for the nonlocal terms; the nonlocalities are essentially relativistic corrections and are discussed briefly below. Finally, the Argonne v_{18} interaction is maximally local, containing at most terms proportional to \mathbf{L}^2 .

As has been mentioned, each of these modern interactions contains isospin-breaking terms. At the level of accuracy required, the electromagnetic interaction must be specified along with the strong interaction in order to reproduce the data precisely. These electromagnetic interactions consist of one- and two-photon Coulomb terms, Darwin-Foldy and vacuum polarization contributions, and magnetic-moment interactions (Stoks and de Swart, 1990). The full NN interactions, then, are the sum of a (dominant) isospin-conserving strong interaction, specified electromagnetic interactions, and finally additional isospin-breaking terms. The latter, for example, are introduced in the Argonne v_{18} interaction as terms proportional to

$$O_{k=15\dots 18} = T_{ij}, \quad \boldsymbol{\sigma}_i \cdot \boldsymbol{\sigma}_j T_{ij}, \quad S_{ij} T_{ij}, \quad (\tau_{i,z} + \tau_{j,z}) \quad (2.10)$$

where the isotensor operator is

$$T_{ij} = 3\tau_{i,z}\tau_{j,z} - \tau_i \cdot \tau_j. \quad (2.11)$$

One-pion exchange includes effects of charged versus

neutral pion mass differences. In principle, one could use different coupling constants for the different charge channels; however, the Nijmegen analysis finds no necessity for this and the Argonne v_{18} interaction uses $f_{\pi NN}^2/4\pi = 0.075$ in all cases. This sophisticated fitting of the two-body np and pp data, as well as the nn scattering length, allows the study of isospin-breaking effects in three-, six-, and seven-nucleon systems.

The properties of the deuteron obtained with these interactions are given in Table I. The binding energy $E_d = 2.224575(9)$ MeV (van der Leun and Alderliesten, 1982) has been fit by construction; the asymptotic constants A_S (the S-wave normalization) and η (the D/S state ratio), which govern the wave function at large distances, are also quite accurate. The quadrupole moment Q_d and magnetic moment μ_d are underpredicted in the impulse approximation; however, the latter has significant corrections from two-body current operators and relativistic corrections, as discussed below.

The phase shifts for several channels are displayed in Figs. 3–6 (Wiringa, Stoks, and Schiavilla, 1995). In Fig. 3 the np and pp phases are shown to demonstrate explicitly the difference between the np and pp interaction. Several recent phase-shift analyses (Arndt *et al.*, 1992; Bugg and Bryan, 1992; Henneck, 1993; Stoks *et al.*, 1993) are also shown. In the 1S_0 channel ($S=0, T=1, L=0$), the two sets are both strongly attractive near threshold, indicating the presence of a nearly bound state in that channel. The phase shifts differ by nearly ten degrees near the maximum, however. For somewhat higher energies, the interaction remains attractive, but the phase shift turns negative near 250 MeV in the laboratory frame. The results of several phase-shift determinations are also shown in the figure.

The mixing parameter ϵ_1 is shown in Fig. 4, where it is again compared to several analyses. As is apparent, significant discrepancies remain among various analyses in that channel. This has been a subject of much debate, particularly with regard to comparisons of single- and multichannel phase-shift analyses. Nevertheless, the behavior of all the modern interaction models is quite similar in this regard. The ϵ_1 phase is particularly sensitive to the strength of the NN tensor interaction.

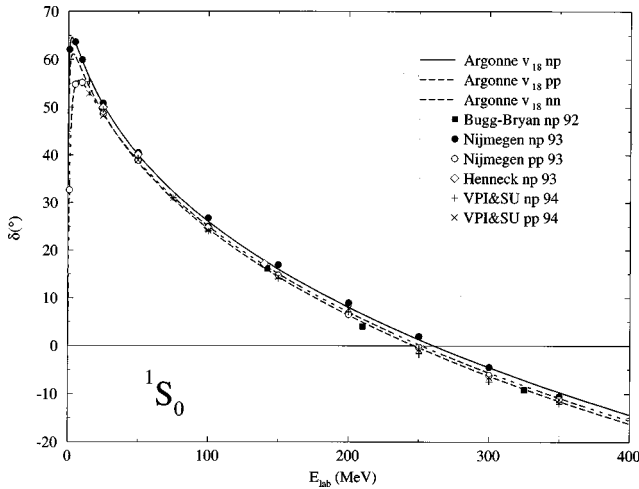


FIG. 3. 1S_0 phases of the Argonne v_{18} interaction compared to various np and pp phase-shift analyses: Argonne v_{18} , Wiringa, Stoks, and Schiavilla, 1995; Bugg-Bryan, Bugg and Bryan, 1992; Nijmegen, Stoks *et al.*, 1993; Henneck, Henneck, 1993; VPI-SU, Arndt, Workman, and Pavan, 1994. Figure from Wiringa *et al.*, 1995.

More typical is the case of the 3S_1 phase presented in Fig. 5, for which all modern interaction models produce nearly identical results, in agreement with the Nijmegen analysis. Finally, the 3P_J phase shifts are presented for the various interactions in Fig. 6.

Given this simple picture of (partial-wave) *local NN* interactions, one obvious concern is the importance of the choice of the specific radial forms for the individual components of the interaction. Friar *et al.* (1993) have investigated this question, solving for the triton binding energy with a wide variety of local-potential models. These interactions contain nonlocalities only at the level of two powers of the relative momentum (i.e., \mathbf{p}^2 or \mathbf{L}^2) and were found to yield nearly identical results for the

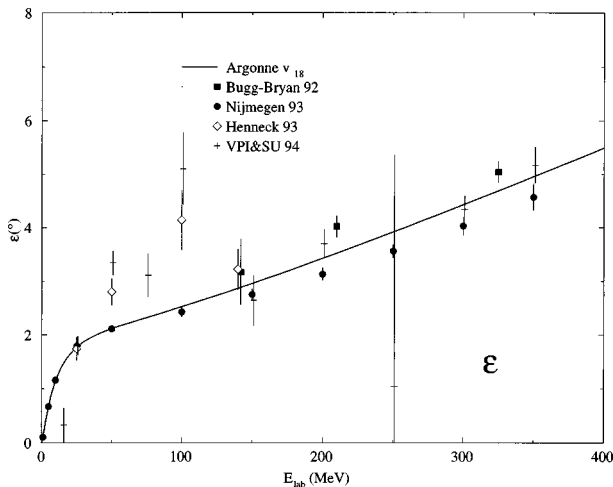


FIG. 4. 3S_1 - 3D_1 mixing parameter ϵ_1 from the Argonne v_{18} interaction and various phase-shift analyses: Argonne v_{18} , Wiringa, Stoks, and Schiavilla, 1995; Bugg-Bryan, Bugg and Bryan, 1992; Nijmegen, Stoks *et al.*, 1993; Henneck, Henneck, 1993; VPI-SU, Arndt, Workman, and Pavan, 1994. Figure from Wiringa *et al.*, 1995.

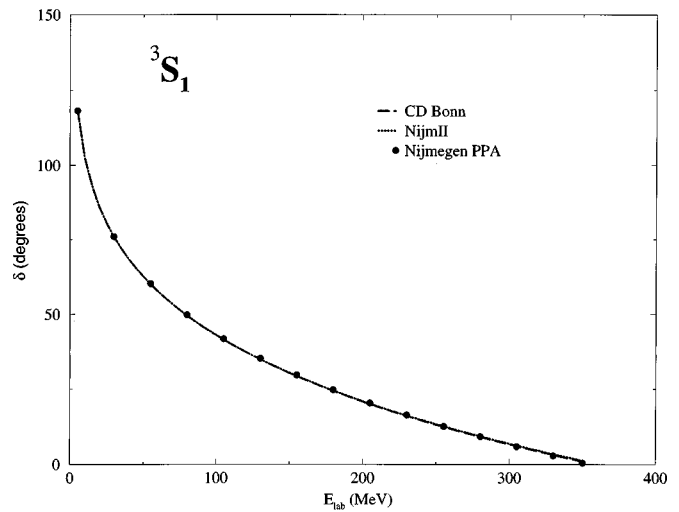


FIG. 5. 3S_1 phases from different modern NN interaction models: CD Bonn, Machleidt *et al.*, 1996; Nijm II, Stoks, Klomp, *et al.*, 1994; Nijmegen PPA, Stoks, Klomp, *et al.*, 1993. Figure from Wiringa, Stoks, and Schiavilla, 1995.

binding energy: 7.62 ± 0.01 MeV as compared to the experimental 8.48 MeV. Clearly, local two-body potentials are not sufficient to reproduce the three-nucleon binding energy.

B. Beyond static two-nucleon interactions

A natural question, then, is what other effects are important in reproducing binding energies of light nuclei? Two of them are immediately apparent: relativistic corrections and three-nucleon interactions. It has long been known that these effects cannot be completely separated—they are related both theoretically and phe-

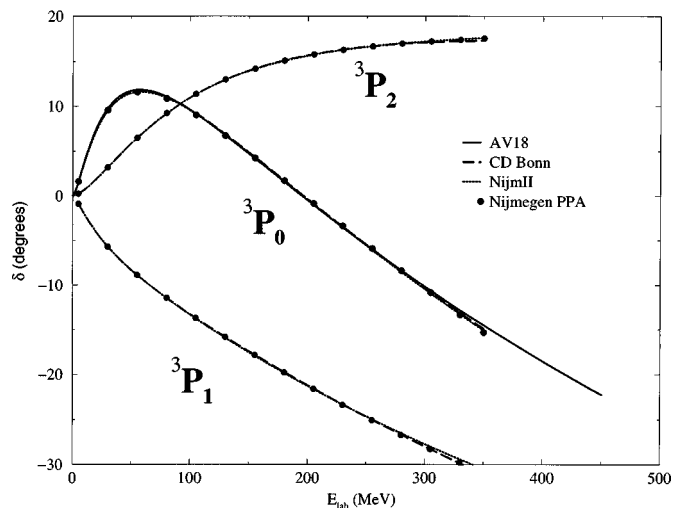


FIG. 6. 3P_J phases from different modern NN interaction models: AV18, Wiringa *et al.*, 1995; CD Bonn, Machleidt *et al.*, 1996; Nijm II, Stoks, Klomp, *et al.*, 1994; Nijmegen PPA, Stoks, Klomp, *et al.*, 1993. Figure from Wiringa, Stoks, and Schiavilla, 1995.

nomenologically, phenomenologically in the sense that simple estimates of their contributions are comparable.

The simplest way to estimate relativistic corrections is to consider a standard nonrelativistic calculation of the α particle. The total kinetic energy is on the order of 100 MeV, or 25 MeV per particle. Thus one would expect relativistic corrections on the order of 2% of this value, or 2 MeV. Three-body forces can be similar in size; at the longest distances the three-body force is of the well-known Fujita-Miyazawa type (Fujita and Miyazawa, 1957), corresponding to single-pion exchanges between three nucleons with the intermediate excitation of a Δ -isobar resonance. The presence of this relatively low-lying resonance requires a three-nucleon interaction at a similar level, roughly a few MeV in the α particle.

A wide variety of relativistic calculations of light nuclei have been carried out. One-boson-exchange mechanisms can be naturally extended to relativistic treatments; such a scheme naturally leads to a four-dimensional representation of the NN interaction. Rupp and Tjon (1992) have investigated trinucleon binding as well as other properties within a separable approximation to the Bethe-Salpeter equation, and have found an increase in binding compared to nonrelativistic approaches.

Several groups have pursued relativistic one-boson-exchange calculations within various three-dimensional reductions of the Bethe-Salpeter equation. These groups generally find a larger binding in the three-body system than is obtained in nonrelativistic calculations; for example, Machleidt, Sammarruca, and Song (1996) have fit the NN data within a one-boson-exchange model using a Blankenbecler-Sugar reduction. The resulting quasipotential equation can be cast in a form identical to the Lippman-Schwinger equation, thus allowing a direct comparison with standard nonrelativistic results. Clearly, though, any three-dimensional reduction is not unique. Upon extending the Blankenbecler-Sugar formalism to the three-nucleon system, Machleidt *et al.* find a triton binding energy of 8.19 MeV. Most of the additional binding is retained even in a nonrelativistic version of the calculation; the additional binding in such a calculation (8.0 MeV) is attributed to the nonlocal character of the interaction obtained within the Blankenbecler-Sugar formalism.

Trinucleon properties have also been investigated within the context of the Gross or spectator equation, in which one particle is placed on shell in all intermediate states. This scheme has the advantage of having the correct Dirac equation limit when one of the particles has a very large mass. The NN scattering and deuteron properties were originally investigated by Gross, Van Orden, and Holinde (1992). Recently, Stadler and Gross (1997) have introduced off-shell couplings in their one-boson-exchange model. The triton binding energy has been found to be sensitive to them. In particular, a set of parameters that reproduces NN data reasonably well also yields the correct binding energy.

It is important to realize, though, that many of these corrections are scheme dependent. For example, differ-

ent choices of πNN couplings, when converted to two- and three-nucleon interactions, are connected by unitary transformations. These different choices are exactly equivalent at the static level; however, when going beyond the static level, arbitrary parameters associated with the unitary transformation are introduced. Different choices in the nonstatic NN interaction also yield different three-nucleon interactions. Since they are unitarily equivalent, physical properties must be unchanged (Coon and Friar, 1986; Friar and Coon, 1994). The relationship between off-shell effects in the NN interaction and the choice of three-nucleon interactions have also been discussed by Polyzou and Glöckle (1990).

Without resorting to the specific one-boson-exchange mechanism, it is also possible to define the general properties of relativistic Hamiltonians that do not introduce antinucleon degrees of freedom. Within such a formalism the Poincaré invariance of the theory plays a pivotal role. The formal requirements of the theory have been presented in an article by Keister and Polyzou (1991). Information on the underlying dynamics is outside the requirements of Poincaré invariance and hence must be introduced from elsewhere. Fully relativistic calculations within the relativistic Hamiltonian formalism are not yet well developed. Glöckle, Lee, and Coester (1986) have investigated the triton in a simple model and find less binding than in comparable nonrelativistic calculations.

It is also possible to perform calculations within a v/c expansion scheme, where terms proportional to powers of the inverse of the nucleon mass are added to the Hamiltonian in order to preserve the Poincaré invariance to that order. Such a procedure is based upon the work of Foldy (1961), Krajcik and Foldy (1974), and Friar (1975).

One class of relativistic corrections that has been considered in such a scheme is purely kinematic. By replacing the nonrelativistic kinetic energy with the corresponding relativistic expression and including a frame dependence in the two- (and three-) nucleon interactions,

$$H = \sum_i \sqrt{\mathbf{p}_i^2 + m^2} + \sum_{i < j} v_{ij}(\mathbf{r}_{ij}; \mathbf{P}_{ij}) + \sum_{i < j < k} V_{ijk}(\mathbf{r}_{ij}, \mathbf{r}_{ik}; \mathbf{P}_{ijk}), \quad (2.12)$$

it is possible to construct a Hamiltonian with the correct transformation properties up to order $(v/c)^2$. In this equation, \mathbf{P}_{ij} and \mathbf{P}_{ijk} are the total momentum of the two- and three-body subsystems, respectively, while the dependence upon the relative coordinate is explicitly displayed. The Hamiltonian is nonlocal through the kinetic-energy operator and the frame dependence, but the nonlocality is rather small—on the order of the nucleon's Compton wavelength (Carlson, Pandharipande, and Schiavilla, 1993).

To perform such a calculation, it is necessary first to refit the NN data and two-body binding energy with the above Hamiltonian. The results of a comparison with a phase-equivalent nonrelativistic model are somewhat surprising, in that these relativistic corrections to three-

and four-body binding are in fact fairly small and repulsive: approximately 0.3 MeV of repulsion in the triton and almost 2 MeV in the α particle. Similar estimates for these kinematic effects have been found by Stadler and Gross (1997) in the framework mentioned above. The small effect is primarily understood as a cancellation between the change to a “softer” kinetic-energy operator and the revised NN interaction, which must be more repulsive to yield the same phase shifts. The resulting nucleon momentum distributions are in fact quite similar in these relativistic and nonrelativistic calculations (Carlson, Pandharipande, and Schiavilla, 1993).

Of course, other nonlocalities will appear in the NN interaction. At long distance these are introduced by relativistic corrections to one-pion exchange, and similar corrections would be expected in a one-boson-exchange picture through vector and scalar meson exchange. The v/c expansion scheme is currently being extended to treating the nonlocalities associated with one-pion exchange. These nonlocalities are required for a fully consistent treatment of the two-body charge operator and the nuclear Hamiltonian and are naturally present in a relativistic one-boson-exchange calculation. However, various technical difficulties make calculations of heavier systems more difficult within the one-boson-exchange scheme; more direct comparisons of the different relativistic calculations will undoubtedly prove instructive in understanding all the results obtained to date.

Three-nucleon interactions can also arise from the internal structure of the nucleon. Since all degrees of freedom other than the nucleons have been integrated out, the presence of virtual Δ resonances induces three-body forces. The longest-ranged term involves the intermediate excitation of a Δ , with pion exchanges involving two other nucleons. The two-pion-exchange three-nucleon interaction was originally written down by Fujita and Miyazawa (1957):

$$V_{ijk}^{2\pi} = A_{2\pi} \left[\{X_{ij}, X_{ik}\} \{\boldsymbol{\tau}_i \cdot \boldsymbol{\tau}_j, \boldsymbol{\tau}_i \cdot \boldsymbol{\tau}_k\} + \frac{1}{4} [X_{ij}, X_{ik}] [\boldsymbol{\tau}_i \cdot \boldsymbol{\tau}_j, \boldsymbol{\tau}_i \cdot \boldsymbol{\tau}_k] \right], \quad (2.13)$$

where

$$X_{ij} = Y_{\pi}(r_{ij}) \boldsymbol{\sigma}_i \cdot \boldsymbol{\sigma}_j + T_{\pi}(r_{ij}) S_{ij}, \quad (2.14)$$

and the two terms are anticommutators and commutators, respectively, of two operators X_{ij} .

This interaction is attractive in light nuclei. Of course, other effects enter as well; several groups (Picklesimer, Rice, and Brandenburg, 1992a, 1992b, 1992c, 1992d; Sauer, 1992) have performed calculations with explicit Δ -isobar degrees of freedom in the nuclear wave functions. They generally find that the attraction from the long-range two-pion-exchange three-nucleon interaction is canceled by dispersive effects at shorter distances and hence there is little net attraction.

Within a nucleons-only picture, several explicit models of the three-nucleon interaction have been proposed.

One of these put forward by the Tucson-Melbourne group (Coon *et al.*, 1979), was a three-nucleon interaction based upon a pion-nucleon scattering amplitude derived using partially conserved axial-vector current, current algebra, and phenomenological input. This interaction contains the long-range two-pion-exchange three-nucleon interaction, but also has additional structure at shorter distances. More recent versions (Coon and Peña, 1993) contain ρ exchange as well as pion-range forces between the three nucleons, with the π - ρ components of the interaction being repulsive in light nuclei. These models have been used in many different calculations, and the short-distance πNN cutoff can be adjusted to reproduce the triton binding energy. The cutoff dependence of the results is significantly smaller in models that include ρ exchange (Stadler *et al.*, 1995).

Another model has been derived by the Brazilian group (Robilotta and Isidro Filho, 1984, 1986; Robilotta *et al.*, 1985; Robilotta, 1987) by using tree-level diagrams of effective Lagrangians that are approximately invariant under chiral and gauge transformations. After proper adjustments of the parameters, the resulting force gives results in the trinucleon bound states similar to those of the Tucson-Melbourne model. Recent studies of this model are presented in Stadler *et al.* (1995).

A somewhat different approach has been taken by the Urbana Argonne group (Carlson, Pandharipande, and Wiringa, 1983; Pudliner *et al.*, 1995). Given the uncertainties in the three-nucleon interaction at distances shorter than pion exchange, the interaction is taken as the sum of the two-pion-exchange three-nucleon interaction plus a shorter-range term:

$$V_{ijk} = V_{ijk}^{2\pi} + V_{ijk}^R, \quad (2.15)$$

with

$$V_{ijk}^R = U_0 \sum_{\text{cyc}} T_{\pi}^2(r_{ij}) T_{\pi}^2(r_{ik}). \quad (2.16)$$

The second term is of two-pion-exchange range on each of the two legs. It is meant to simulate the dispersive effects that are required when integrating out Δ degrees of freedom. These terms are repulsive and are here taken to be independent of spin and isospin.

The constants $A_{2\pi}$ and U_0 in front of the two terms are adjusted to reproduce the triton binding energy and to provide additional repulsion in hypernetted-chain variational calculations of nuclear matter near equilibrium density. However, the resulting value for the $A_{2\pi}$ coefficient is close to that obtained from the analysis of observed pion-nucleon scattering. Clearly the energy levels of light nuclei must be well reproduced if accurate predictions of other observables at low- and intermediate-energy transfers are to be obtained. Since one of the major goals is to tie together the medium- and low-energy properties of light nuclei, it is natural to make simple assumptions about the nature of the three-nucleon interaction in pursuit of that goal.

Undoubtedly the real situation is much more complicated: relativistic effects and a significantly more compli-

cated three-nucleon interaction are certainly present. It will take far more than calculations of trinucleon binding energies to shed light on these questions. For example, calculations of three-nucleon scattering are, on occasion, at variance with the experimental data. The isospin dependence of the three-nucleon interaction could also prove crucial in studying light neutron-rich nuclei and neutron stars. Given recent improvements in experimental data and few-body techniques, it is quite possible that a more thorough understanding of these issues will soon be realized.

C. Effective chiral Lagrangian approaches

Before leaving the subject of nuclear interaction models, one must take note of the recent interest in NN potentials derived from effective chiral Lagrangians. The chiral expansion gives a systematic power-counting scheme in which the nucleon-nucleon interaction can be obtained. The advantage of such a scheme is a direct connection to QCD, in that in principle it should be possible to compute the coefficients of the low-energy effective theory directly from QCD.

Weinberg demonstrated that a systematic expansion exists in powers of p/Λ , where p is a typical nucleon momentum and Λ is a characteristic mass scale (Weinberg, 1990, 1991). He then proceeded to consider the leading terms in the expansion. Ordóñez, Ray, and van Kolck (1994) more recently extended the analysis to third order, considering the most general effective Lagrangian involving low-momentum pions, nonrelativistic nucleons, and Δ isobars. They also employed a Gaussian cutoff to regularize the theory. At present, the low-energy constants in the Lagrangian are adjusted to fit the NN data. While the interaction obtained in this manner provides a good fit to the NN data, the fit is not yet of the quality obtained in the more phenomenological models. In addition, the work mentioned above employs an energy-dependent interaction scheme, which is difficult to employ in a many-body context. Other schemes that do not employ a simple Gaussian cutoff result in contact interactions proportional to $\delta(r_{ij})$. Such terms are also problematic in any Schrödinger description of the nucleus (Phillips and Cohen, 1997).

However, the advantages of such a systematic treatment of the NN interaction are not to be ignored. They allow one to begin to place reasonable constraints on the size of three- and multinucleon interactions and indeed can be used to construct specific models. One of the important challenges is to join such systematic schemes to direct calculations of few- and many-nucleon systems.

III. BOUND-STATE METHODS

Given a model for the nuclear Hamiltonian, a first and important test is solving for the nuclear ground states. Although the nuclear interaction models described above are simple to write down, solutions have proven to be rather difficult to obtain. For the three-nucleon system, there is a long history of numerical solutions to

the Faddeev equations. The first calculation for model local potentials without tensor interactions was that of Malfliet and Tjon (1969a, 1969b). By now, a variety of methods have been used for studying light nuclear spectra. In this section we briefly describe Faddeev methods, correlated hyperspherical harmonics, and variational and Green's-function Monte Carlo methods. These have all proven successful for the three- and four-nucleon ground states, but nevertheless have different strengths, which we shall attempt to assess.

A. Faddeev methods

The Faddeev decomposition of the three- (and now four-) body problem has proven to be a tremendous computational tool in studies of light nuclei. In addition to being useful for studies of bound states and low-energy (below breakup) scattering, one of the primary advantages of the Faddeev decomposition is its applicability to higher-energy scattering problems. We first discuss the application to bound states, deferring the scattering problem until later.

The application of the Faddeev scheme to the bound-state problem has a long history. Solutions to these equations typically involve a partial-wave expansion, as described below. The first five-channel solutions with realistic interactions were obtained in the early to mid 70s both in momentum space (Harper, Kim, and Tubis, 1972; Brandenburg, Kim, and Tubis, 1974a, 1974b, 1975) and in coordinate space (Benayoun and Gignoux, 1972a, 1972b; Lavern and Gignoux, 1973). Comparisons between these groups yielded a triton binding energy of 7.0 MeV for the Reid soft-core interaction. Convergence of the partial-wave expansion was convincingly demonstrated by Chen *et al.* (1985) for a variety of interaction models. In particular, in 34 channel calculations they found a triton binding energy of 7.35 MeV for the Reid soft-core interaction. Similar calculations were subsequently performed in momentum space (Witala, Glöckle, and Kamada, 1991).

The Faddeev decomposition rewrites the Schrödinger equation as a sum of three equations in which (for two-particle interactions, at least) only one pair interacts at a time. The resulting equations are solved in either momentum or coordinate space. While the decomposition is identical, the methods employed in practice to obtain solutions are in fact quite different. The coordinate-space methods typically solve an integro-differential equation, so one of the primary concerns is necessarily the inclusion of correct asymptotic boundary conditions. Momentum-space calculations, on the other hand, typically proceed through the Green's function, and hence an important consideration is the treatment of the singularities in the scattering operators. In the sections below, we briefly depict applications to bound-state problems; later, low-energy and breakup scattering will be described.

1. Coordinate-space Faddeev methods

In coordinate space, the Schrödinger equation for three nucleons interacting with two-nucleon interactions only can be written

$$[E - H_0 - v_{12} - v_{13} - v_{23}]\Psi_3 = 0, \quad (3.1)$$

where H_0 is the (nonrelativistic) kinetic-energy operator and v_{ij} is the pair interaction between nucleons i and j .

The Faddeev decomposition consists of defining three sets of vectors \mathbf{x}_i , \mathbf{y}_i through cyclic permutations of i, j, k :

$$\mathbf{x}_i \equiv \mathbf{r}_j - \mathbf{r}_k, \quad (3.2)$$

$$\mathbf{y}_i \equiv 2[\mathbf{r}_i - (\mathbf{r}_j + \mathbf{r}_k)/2]/\sqrt{3} \quad (3.3)$$

and rewriting the Schrödinger equation as three equations:

$$[E - H_0 - v_{23}]\psi(\mathbf{x}_1, \mathbf{y}_1) = v_{23}[\psi(\mathbf{x}_2, \mathbf{y}_2) + \psi(\mathbf{x}_3, \mathbf{y}_3)],$$

$$[E - H_0 - v_{13}]\psi(\mathbf{x}_2, \mathbf{y}_2) = v_{13}[\psi(\mathbf{x}_3, \mathbf{y}_3) + \psi(\mathbf{x}_1, \mathbf{y}_1)],$$

$$[E - H_0 - v_{12}]\psi(\mathbf{x}_3, \mathbf{y}_3) = v_{12}[\psi(\mathbf{x}_1, \mathbf{y}_1) + \psi(\mathbf{x}_2, \mathbf{y}_2)],$$

which, when summed, reproduce the original Schrödinger equation for

$$\Psi_3 \equiv \psi(\mathbf{x}_1, \mathbf{y}_1) + \psi(\mathbf{x}_2, \mathbf{y}_2) + \psi(\mathbf{x}_3, \mathbf{y}_3). \quad (3.4)$$

The kinetic-energy operator is diagonal in \mathbf{x} and \mathbf{y} :

$$H_0 = -\frac{1}{m}\nabla_x^2 - \frac{1}{m}\nabla_y^2. \quad (3.5)$$

While rewriting the Schrödinger equation as three separate equations may appear convoluted, for identical particles the three solutions ψ are in fact simple permutations of each other. Hence solving one of these equations is equivalent to solving the full Schrödinger equation. Each equation involves only one of the pair potentials, so a significant simplification has been achieved. The primary advantage of this rearrangement is in its application to scattering problems, as we shall see. However, the method works equally well for bound states.

Rewriting the Schrödinger equation in this way requires us to specify the permutation properties of the Faddeev amplitudes ψ and also to discuss how the spin-isospin degrees of freedom are to be treated. The latter is an essential point in nuclear physics, because the number of degrees of freedom grows so rapidly with the number of nucleons. First, we consider the Pauli principle, which can be satisfied by enforcing antisymmetric conditions on the interacting pair in the Faddeev amplitude $\psi(\mathbf{x}_i, \mathbf{y}_i)$ via

$$\psi(\mathbf{x}_i, \mathbf{y}_i) = -E(jk)\psi(\mathbf{x}_i, \mathbf{y}_i). \quad (3.6)$$

In this equation $E(jk)$ is the total (space, spin, and isospin) permutation acting on particles j and k . For spin-polarized fermions this would imply $\psi(-\mathbf{x}_1, \mathbf{y}_1) = -\psi(\mathbf{x}_1, \mathbf{y}_1)$, while for nucleons the generalized Pauli principle simply requires that the pair orbital angular momentum ℓ , spin s^{jk} , and isospin t^{jk} satisfy $\ell + s^{jk} + t^{jk}$ equal to an odd integer.

The spin-isospin-dependent nature of the Hamiltonian requires one to solve, in general, for $4^3 = 64$ possible functions of \mathbf{x} and \mathbf{y} that can be classified by their total spin S and isospin T . Projecting onto a specific isospin state yields fewer components; for example, the

TABLE II. Dominant channels in the Faddeev and correlated hyperspherical harmonics (CHH) calculations of the $A=3$ ground state.

Channel	Pair			Spectator		Total J^π
	l	s	j	l	j	
1	0	0	0	0	1/2	$1/2^+$
2	0	1	1	0	1/2	$1/2^+, 3/2^+$
3	2	1	1	0	1/2	$1/2^+, 3/2^+$
4	0	1	1	2	3/2	$1/2^+, 3/2^+$
5	2	1	1	2	3/2	$1/2^+, 3/2^+$

^3He ground state ($T=1/2$, $T_z=1/2$) has a total of 16 spin-isospin states. In addition, the amplitudes $\psi(\mathbf{x}_i, \mathbf{y}_i)$ can be decomposed into partial waves in the angle μ between \mathbf{x} and \mathbf{y} , with an implicit dependence on the orientation of the spin-quantization axis. This decomposition converts a Faddeev equation in three variables into many equations in the two magnitudes x and y .

The usefulness of this partial-wave expansion depends upon the problem under consideration. For three- and four-body bound states the wave function is confined to a fairly small spatial region; hence the angular-momentum barrier ensures a fairly rapid convergence in partial waves. In order to perform this decomposition, a particular angular momentum coupling scheme must be chosen. Various angular-momentum coupling schemes have been employed—for example, jJ coupling, in which the interacting-pair total angular momentum $\mathbf{J}_i \equiv \mathbf{j}_j + \mathbf{j}_k = (\mathbf{l}_j + \mathbf{s}_j) + (\mathbf{l}_k + \mathbf{s}_k)$ is coupled to the total angular momentum of the spectator $\mathbf{j}_i \equiv \mathbf{l}_i + \mathbf{s}_i$. Similarly, the isospins can be coupled to a total isospin T .

For a calculation of the $J = \frac{1}{2}$ ground state in $A=3$, the interacting pair's spin and orbital angular momentum must be coupled to a specific total angular momentum. These states are then combined with the spin and orbital angular momentum of the spectator to yield the total $J = T = \frac{1}{2}$. Each term in this partial-wave expansion is called a channel. Accurate calculations of three-nucleon ground states typically keep all interacting-pair NN partial waves with $j \leq 4$, which requires 34 channels. The first five of these channels (those with $j \leq 2$) are given in Table II. Scattering calculations for $J = \frac{3}{2}$ require 62 channels for each parity; of course, the required number of channels increases with the total angular momentum of the system.

For realistic calculations, one would like to include three-nucleon interactions V_{ijk} as well as the Coulomb interaction. As the former are short-ranged functions, they can easily be added to the Faddeev equations. Three-nucleon interactions typically arise from “integrating out” the higher-energy degrees of freedom and hence can be decomposed into a cyclic sum: $V_{ijk} = V_{i;jk} + V_{j;ki} + V_{k;ij}$, where the first index indicates the particle in a higher-energy intermediate state. The Faddeev equations can then be written as

$$[E - H_0 - v_{23} - V_{1;23}]\psi(\mathbf{x}_1, \mathbf{y}_1) = (v_{23} + V_{1;23})[\psi(\mathbf{x}_2, \mathbf{y}_2) + \psi(\mathbf{x}_3, \mathbf{y}_3)], \quad (3.7)$$

plus permutations. The fact that the three-nucleon interactions are short ranged allows for significant freedom in how they are introduced in the Faddeev equations. Coulomb interactions could be handled similarly, in principle, but in fact there are more effective techniques for dealing with these long-ranged interactions. The Coulomb interaction and boundary conditions on the amplitudes ψ play a crucial role in scattering calculations, so we shall defer these discussions to a later section.

Given the decomposition of the amplitudes into partial waves, one must still solve for the various channels as a function of the magnitudes x and y . A detailed discussion of the numerical procedures involved is given by Payne (1987). The most efficient scheme for solving the Faddeev equations involves transforming the Faddeev equations into linear equations by writing the amplitudes as splines for the space x and y . In this way it is possible to set up the finer grids in the regions where the interaction is stronger.

For bound states, it is then useful to scale the binding energy out of the problem by writing the solution as a product of a term that has the correct exponential asymptotic behavior and an unknown function. The advantage of the coordinate-space formulation is that the Hamiltonian is local, or nearly so, and hence many of the matrices are quite sparse. In the end, the bound-state problem is an eigenvalue problem, and standard power methods (i.e., a Lanczos approach) can be used to solve for the eigenvalues and eigenvectors corresponding to the lowest-energy states.

2. Momentum-space Faddeev methods

In momentum space, the Faddeev equations are written as three integral equations:

$$\begin{aligned}\psi_1 &= G_0 T_1 (\psi_2 + \psi_3), \\ \psi_2 &= G_0 T_2 (\psi_3 + \psi_1), \\ \psi_3 &= G_0 T_3 (\psi_1 + \psi_2),\end{aligned}\quad (3.8)$$

where the ψ are again the Faddeev amplitudes, G_0 is the propagator for three noninteracting particles,

$$G_0 = \frac{1}{E - H_0}, \quad (3.9)$$

and the T_i are three-body scattering operators. Ignoring three-nucleon interactions for the moment, we see that the T_i are scattering operators for two interacting particles in a three-particle space. They are labeled by the index of the noninteracting particle and are obtained from a solution of the equation

$$T_i = v_{jk} + v_{jk} G_0 T_i. \quad (3.10)$$

The Faddeev amplitudes ψ_i are now written in terms of the momenta \mathbf{p} and \mathbf{q} , where

$$\begin{aligned}\mathbf{p}_i &\equiv (\mathbf{k}_j - \mathbf{k}_k)/2, \\ \mathbf{q}_i &\equiv 2[\mathbf{k}_i - (\mathbf{k}_j + \mathbf{k}_k)/2]/3.\end{aligned}\quad (3.11)$$

The T_i are diagonal in the spectator momentum \mathbf{q}_i and can be decomposed by the spin, isospin, and angular momentum of the two interacting particles coupled to those of the spectator particle. They are related to the standard two-body scattering operators $t^{(2)}$ by

$$\langle p q \alpha | T | p' q' \alpha' \rangle = \frac{\delta(q - q')}{q q'} t_{\alpha, \alpha'}^{(2)}(p, p', E - 3q^2/4m), \quad (3.12)$$

where the labels α, α' refer to spin, angular momentum, and isospin states. These ‘‘channels’’ are precisely the same as in the coordinate-space Faddeev equations. In this equation, the last argument of the two-body scattering operator $t^{(2)}$ is the energy of the two-particle subsystem. The three-body problem necessarily involves the off-shell two-body propagators; the energy $E - 3q^2/(4m)$ is what is available for the interacting pair.

Coupling the angular momentum, spin, and isospin again yields a series of coupled equations, here in the magnitudes p and q . With the channels labeled by α , the Faddeev equations (3.8) are of the form

$$\begin{aligned}\langle p q \alpha | \psi_1 \rangle &= \frac{1}{E - p^2/m - 3q^2/4m} \sum_{\alpha'} \int dp' p'^2 \int dq' q'^2 \langle p q \alpha | T_1 | p' q' \alpha' \rangle \\ &\times \sum_{\alpha''} \int dp'' p''^2 \int dq'' q''^2 \langle p' q' \alpha' | E | p'' q'' \alpha'' \rangle \langle p'' q'' \alpha'' | \psi_1 \rangle,\end{aligned}\quad (3.13)$$

where E is the sum of the two cyclic permutations $E = E(12)E(23) + E(13)E(23)$.

These equations are not as difficult to solve as they may at first appear, since the matrix elements of E are purely geometrical factors, and the T_1 operator is diagonal in q . Nevertheless, solving such a problem is a significant technical challenge. A complete discussion of the exchange operator is given in Glöckle (1983).

The equations are somewhat more difficult to solve in the presence of three-nucleon interactions. As in coordinate space, it is possible to add the three-nucleon equation in different ways. One particularly useful scheme is to use the symmetry of the solutions of Eq. (3.8) under particle interchange, to decompose the three-nucleon interaction as before ($V_{ijk} = V_{i,jk} + V_{j,ki} + V_{k,ij}$), and to rewrite the Faddeev equations as

$$\psi = G_0 T E \psi + G_0 (1 + T G_0) V_{ijk} (1 + E) \psi, \quad (3.14)$$

where the first term on the right-hand side is simply shorthand for Eq. (3.8) and the second term incorporates the effects of the three-nucleon interaction. The operator E here is again the sum of the two cyclic permutations. This form of the equations has been written down in Glöckle (1982) and used by Stadler, Glöckle, and Sauer (1991), for example.

A generalization of the Faddeev equation for four particles, the Faddeev-Yakubovsky equations (Yakubovsky, 1967), have recently been employed to solve the four-nucleon problem (Glöckle and Kamada, 1993a; 1993b; Glöckle *et al.*, 1994). The number of channels that must be included grows very rapidly in this case, and a further complication is that there are now six spatial dimensions rather than the three required for three-body calculations. As the decomposition of the wave function is very similar in the Faddeev and correlated hyperspherical harmonics methods, the four-particle case is deferred to the next section. Extensions to three-nucleon interactions in the Faddeev-Yakubovsky equations have been introduced by Glöckle and Kamada (1993a, 1993b).

While a certain degree of technical sophistication is required to solve these equations, there is a considerable simplification for bound states, in that there are no singularities in the Faddeev equations. Since the energy is negative, there are no zeros in the denominator in the equations for $t_{\alpha, \alpha'}^{(2)}$ and T , or in the full Faddeev equation. Hence the Faddeev equations take the form of a generalized eigenvalue equation. These can be solved by standard power methods, adjusting the energy E in the kernel until the equation is satisfied. Of course, for scattering problems the situation is more complex.

B. The correlated hyperspherical harmonics variational method

In recent years the correlated hyperspherical harmonics (CHH) variational method has been used to describe the bound states of the $A=3$ and 4 nuclei, as well as $d+n$ and $d+p$ scattering states at energies below the three-body breakup threshold (Kievsky, Viviani, and Rosati, 1994). The accuracy of these calculations is comparable to that achieved in “exact” Faddeev and Green’s-function Monte Carlo calculations, as will be shown in Sec. IV.

The wave function of a three-nucleon system with total angular momentum JJ_z and total isospin TT_z is expanded into a sum of Faddeev-like amplitudes as in Eq. (3.4). The amplitude $\psi(\mathbf{x}_i, \mathbf{y}_i)$ is expressed as

$$\psi(\mathbf{x}_i, \mathbf{y}_i) = \sum_{\alpha} F_{\alpha i} \phi_{\alpha}(x_i, y_i) \mathcal{Y}_{\alpha}(jk, i), \quad (3.15)$$

$$\mathcal{Y}_{\alpha}(jk, i) = \{ [Y_{L_{\alpha}}(\hat{\mathbf{y}}_i) Y_{\ell_{\alpha}}(\hat{\mathbf{x}}_i)]_{\Lambda_{\alpha}} [s_{\alpha}^{jk} s_{\alpha}^i]_{S_{\alpha}} \}_{JJ_z} [t_{\alpha}^{jk} t_{\alpha}^i]_{TT_z}, \quad (3.16)$$

where each channel α is specified by the orbital angular momenta ℓ_{α} , L_{α} , and Λ_{α} and the spin (isospin) s_{α}^{jk}

(t_{α}^{jk}) and s_{α}^i (t_{α}^i) of pair jk and particle i . Orbital and spin angular momenta are coupled in the LS scheme to give total angular momentum JJ_z . The correlation operator $F_{\alpha i}$ is taken to be of the Jastrow form, and its construction is discussed below. Since $\psi(\mathbf{x}_i, \mathbf{y}_i)$ must change sign under the exchange $j \rightleftharpoons k$ to ensure that the wave function is antisymmetric, it follows that $\ell_{\alpha} + s_{\alpha}^{jk} + t_{\alpha}^{jk}$ must be odd (the $F_{\alpha p}$ is assumed to be symmetric under the exchange $j \rightleftharpoons k$). Furthermore, $\ell_{\alpha} + L_{\alpha}$ must be even or odd depending on whether the state has even or odd parity. In principle, the sum over α should be extended to all channels compatible with the restrictions above. In practice, however, as in the Faddeev method, it is truncated and only a limited number of channels are included.

The CHH decomposition is quite similar to the Faddeev, the primary differences being (1) the inclusion of the correlation operators F in the definition of the wave function and (2) the further decomposition of ϕ_{α} into hyperspherical harmonics. The hyperspherical coordinates are introduced as

$$\rho = \sqrt{x_i^2 + y_i^2}, \quad (3.17)$$

$$\cos \phi_i = x_i / \rho, \quad (3.18)$$

where the hyper-radius ρ is independent of the particular permutation i that is being considered. The dependence of the radial amplitudes ϕ_{α} upon the the hyperspherical coordinates is thus expanded as

$$\phi_{\alpha}(x_i, y_i) = \sum_n \frac{u_n^{\alpha}(\rho)}{\rho^{5/2}} y_i^{L_{\alpha}} x_i^{\ell_{\alpha}} Y_n^{\alpha}(\phi_i). \quad (3.19)$$

The hyper-radial functions $u_n^{\alpha}(\rho)$ vanish exponentially for large ρ and are determined variationally as discussed below. The hyperspherical polynomials Y_n^{α} are defined as

$$Y_n^{\alpha}(\phi_i) = N_n^{\ell_{\alpha}, L_{\alpha}} P_n^{L_{\alpha} + 1/2, \ell_{\alpha} + 1/2}(\cos 2\phi_i), \quad (3.20)$$

where $N_n^{\ell_{\alpha}, L_{\alpha}}$ are normalization factors, $P_n^{\alpha, \beta}$ are Jacobi polynomials, and n is a non-negative integer, $n = 0, \dots, M_{\alpha}$, M_{α} being the selected number of basis functions in channel α .

The correlation factor $F_{\alpha i}$ takes into account the strong state-dependent correlations induced by the nucleon-nucleon interaction. It improves the behavior of the wave function at small internucleon separations, thus accelerating the convergence of the calculated quantities with respect to the required number of hyperspherical harmonics basis functions in Eq. (3.19). Two different forms have been employed for $F_{\alpha i}$:

$$F_{\alpha i} = f_{\alpha}(r_{jk}) \quad \text{PHH}, \quad (3.21)$$

$$= f_{\alpha}(r_{jk}) g_{\alpha}(r_{ij}) g_{\alpha}(r_{ik}) \quad \text{CHH}. \quad (3.22)$$

The projected hyperspherical harmonic (PHH) wave function only includes correlation effects between nucleons j and k in the active pair, while the CHH wave function includes in addition correlation effects between these and the spectator nucleon i . The product of corre-

lation functions in the CHH expansion introduces an explicit dependence on the coordinate $\mu_i = \hat{\mathbf{x}}_i \cdot \hat{\mathbf{y}}_i$, which leads to a different channel mixing than that which occurs in the PHH expansion. For soft-core interactions the convergence pattern with respect to the number of basis functions appears to be somewhat faster in the PHH expansion than in the CHH one, presumably because the PHH expansion does not contain the channel mixing mentioned above. However, the CHH expansion is also well suited to treating hard-core interactions, to which the PHH expansion and the Faddeev method are not applicable.

The correlation functions are obtained with a procedure similar to that used in the construction of symmetrized-product trial wave functions in variational Monte Carlo calculations. When two of the nucleons are close to each other and far removed from the others, it is expected that their relative motion will be predominantly influenced by their mutual interaction. The radial wave function for two particles in state $\beta = j_\beta \ell_\beta s_\beta^{jk} t_\beta^{jk}$ is then obtained from solutions of Schrödinger-like equations, which can be coupled or uncoupled depending on β (for an extended discussion, see below).

The Rayleigh-Ritz variational principle

$$\langle \delta_u \Psi_3 | H - E | \Psi_3 \rangle = 0 \quad (3.23)$$

is used to determine the hyper-radial functions $u_n^\alpha(\rho)$ in Eq. (3.19). Carrying out the variation $\delta_u \Psi_3$ with respect to the functions $u_n^\alpha(\rho)$, we obtain the following equation:

$$\sum_i \langle F_{ai} Y_n^\alpha(\phi_i) \mathcal{Y}_\alpha(jk, i) | H - E | \Psi_3 \rangle_\Omega = 0, \quad (3.24)$$

where Ω denotes the angular variables ϕ_i , $\hat{\mathbf{x}}_i$, and $\hat{\mathbf{y}}_i$. Performing the integrations over Ω and the spin-isospin sums leads to the set of coupled second-order differential equations,

$$\sum_{\alpha', n'} \left[A_{n, n'}^{\alpha, \alpha'}(\rho) \frac{d^2}{d\rho^2} + B_{n, n'}^{\alpha, \alpha'}(\rho) \frac{d}{d\rho} + C_{n, n'}^{\alpha, \alpha'}(\rho) + EN_{n, n'}^{\alpha, \alpha'}(\rho) \right] u_{n'}^{\alpha'}(\rho) = 0, \quad (3.25)$$

where $\alpha' = 1, \dots, \alpha_M$ and $n' = 0, \dots, M_{\alpha'}$. The total number of equations is

$$n_{\text{eq}} = \sum_{\alpha=1}^{\alpha_M} (M_\alpha + 1). \quad (3.26)$$

After discretization in the variable ρ , the set of differential equations (3.25) is converted to a generalized eigenvalue problem of the form

$$(\mathcal{Z} - E \cdot \mathcal{N})G = 0, \quad (3.27)$$

where G is a vector of dimension given by $n_{\text{eq}} \times n_\rho$, n_ρ being the number of grid points in ρ . Details on the numerical techniques employed—as well as explicit expressions for the coefficients $X_{K, K'}^{\alpha, \alpha'}(\rho)$, along with their derivation—can be found in Kievsky, Rosati, and Viviani (1993).

The CHH method has also been applied to systems with $A=4$ and 6, although calculations with realistic interactions have been carried out only for the α particle (Viviani, Kievsky, and Rosati, 1995). The $A=4$ wave function is decomposed in both the CHH and the Faddeev-Yakubovsky approaches as

$$\Psi_4 = \sum_i [\psi_A(\mathbf{x}_{A,i}, \mathbf{y}_{A,i}, \mathbf{z}_{A,i}) + \psi_B(\mathbf{x}_{B,i}, \mathbf{y}_{B,i}, \mathbf{z}_{B,i})], \quad (3.28)$$

where the sum is over distinct permutations of particles $ijkl$. The set of Jacobi variables $\mathbf{x}_{k,i}$, $\mathbf{y}_{k,i}$, and $\mathbf{z}_{k,i}$ corresponds for $k=A$ and B to the partitions 3+1 and 2+2, respectively, and is defined as

$$\begin{aligned} \text{set A} & & \text{set B} \\ \mathbf{z}_{A,i} &= \sqrt{3/2}(\mathbf{r}_l - \mathbf{R}_{kji}), & \mathbf{z}_{B,i} &= \mathbf{r}_l - \mathbf{r}_k, \\ \mathbf{y}_{A,i} &= \sqrt{4/3}(\mathbf{r}_k - \mathbf{R}_{ji}), & \mathbf{y}_{B,i} &= \sqrt{2}(\mathbf{R}_{lk} - \mathbf{R}_{ji}), \\ \mathbf{x}_{A,i} &= \mathbf{r}_j - \mathbf{r}_i, & \mathbf{x}_{B,i} &= \mathbf{r}_j - \mathbf{r}_i, \end{aligned} \quad (3.29)$$

where \mathbf{R}_{ij} (\mathbf{R}_{ijk}) is the center of mass of particles ij (ijk). In the LS -coupling scheme, the amplitudes ψ_A and ψ_B are expanded as

$$\psi_A(\mathbf{z}_{A,i}, \mathbf{y}_{A,i}, \mathbf{x}_{A,i}) = \sum_\alpha F_{\alpha p} \phi_{A\alpha}(x_{A,i}, y_{A,i}, z_{A,i}) \mathcal{Y}_{\alpha p}^A, \quad (3.30)$$

$$\begin{aligned} \mathcal{Y}_{\alpha p}^A &= \{[[[Y_{\ell_{1\alpha}}(\hat{\mathbf{z}}_{A,i}) Y_{\ell_{2\alpha}}(\hat{\mathbf{y}}_{A,i})]_{\ell_{12\alpha}} Y_{\ell_{3\alpha}}(\hat{\mathbf{x}}_{A,i})]_{L_\alpha} \\ &\quad \times [[s_i s_j]_{s_{\alpha\alpha}} s_k]_{s_{b\alpha} s_l} s_\alpha]_{JJ_z} [[t_i t_j]_{T_{\alpha\alpha}} t_k]_{T_{b\alpha}} t_l]_{TT_z}, \end{aligned} \quad (3.31)$$

and

$$\begin{aligned} \psi_B(\mathbf{x}_{B,p}, \mathbf{y}_{B,p}, \mathbf{z}_{B,p}) \\ = \sum_\alpha F_{\alpha p} \phi_{B\alpha}(x_{B,p}, y_{B,p}, z_{B,p}) \mathcal{Y}_{\alpha p}^B, \end{aligned} \quad (3.32)$$

$$\begin{aligned} \mathcal{Y}_{\alpha p}^B &= \{[[[Y_{\ell_{1\alpha}}(\hat{\mathbf{z}}_{B,p}) Y_{\ell_{2\alpha}}(\hat{\mathbf{y}}_{B,p})]_{\ell_{12\alpha}} Y_{\ell_{3\alpha}}(\hat{\mathbf{x}}_{B,p})]_{L_\alpha} \\ &\quad \times [[s_i s_j]_{s_{\alpha\alpha}} [s_k s_l]_{s_{b\alpha}}]_{s_\alpha} s_\alpha]_{JJ_z} [[t_i t_j]_{T_{\alpha\alpha}} [t_k t_l]_{T_{b\alpha}}]_{TT_z}, \end{aligned} \quad (3.33)$$

respectively. A channel α is now specified by the orbital-spin-isospin quantum numbers $\ell_{1\alpha}$, $\ell_{2\alpha}$, $\ell_{3\alpha}$, $\ell_{12\alpha}$, L_α , $S_{\alpha\alpha}$, $S_{b\alpha}$, S_α , $T_{\alpha\alpha}$, and $T_{b\alpha}$. The total orbital and spin angular momenta are then coupled to give JJ_z . The overall antisymmetry of the wave function requires that ψ_A and ψ_B change sign under the exchange $i \rightleftharpoons j$. As for the $A=3$ case, the correlation operator $F_{\alpha p}$ consists of the product of central-pair-correlation functions.

It is important to realize that either basis (3.31) or (3.33) is complete if all channels α are included in the sums (3.30) and (3.32). In this case, it would be sufficient to expand the wave function Ψ_4 in terms of either set of Jacobi variables. In practice, the sums over α are truncated, and it is advantageous from the standpoint of variational calculations (such as those described here) to

TABLE III. Quantum numbers corresponding to channels $\alpha = 1-22$ included in the partial-wave decomposition of the wave function Ψ_4 . Labels A and B correspond to partitions 3+1 and 2+2, respectively.

α	set	ℓ_1	ℓ_2	ℓ_3	ℓ_{12}	L	S_a	S_b	S	T_a	T_b	T
1	A	0	0	0	0	0	1	1/2	0	0	1/2	0
2	A	0	0	0	0	0	0	1/2	0	1	1/2	0
3	A	0	0	2	0	2	1	3/2	2	0	1/2	0
4	A	0	2	0	2	2	1	3/2	2	0	1/2	0
5	A	0	2	2	2	0	1	1/2	0	0	1/2	0
6	A	0	2	2	2	1	1	1/2	1	0	1/2	0
7	A	0	2	2	2	1	1	3/2	1	0	1/2	0
8	A	0	2	2	2	2	1	3/2	2	0	1/2	0
9	B	2	0	2	2	0	1	1	0	0	0	0
10	B	2	0	2	2	1	1	1	1	0	0	0
11	B	2	0	2	2	2	1	1	2	0	0	0
12	A	0	1	1	1	0	1	1/2	0	1	1/2	0
13	A	0	1	1	1	1	1	1/2	1	1	1/2	0
14	A	0	1	1	1	1	1	3/2	1	1	1/2	0
15	A	0	1	1	1	2	1	3/2	2	1	1/2	0
16	A	1	1	0	0	0	1	1/2	0	0	1/2	0
17	A	1	1	0	1	1	1	1/2	1	0	1/2	0
18	A	1	1	0	1	1	1	3/2	1	0	1/2	0
19	A	1	1	0	2	2	1	3/2	2	0	1/2	0
20	B	0	0	0	0	0	1	1	0	0	0	0
21	B	0	0	2	0	2	1	1	2	0	0	0
22	B	2	0	0	2	2	1	1	2	0	0	0

take into account both configurations 3+1 and 2+2. Table III lists the channels included in the most recent calculations.

The expression for the hyper-radius is now generalized to

$$\rho = \sqrt{x_{A,i}^2 + y_{A,i}^2 + z_{A,i}^2} = \sqrt{x_{B,i}^2 + y_{B,i}^2 + z_{B,i}^2}, \quad (3.34)$$

which again is independent of the permutation i , and the hyperangles appropriate for the partitions A and B are given by

$$\begin{aligned} \cos\phi_{3i} &= x_{A,i}/\rho = x_{B,i}/\rho, \\ \cos\phi_{2i}^A &= y_{A,i}/(\rho\sin\phi_{3i}), \\ \cos\phi_{2i}^B &= y_{B,i}/(\rho\sin\phi_{3i}). \end{aligned} \quad (3.35)$$

The radial amplitudes $\phi_{A\alpha}$ and $\phi_{B\alpha}$ are expanded in terms of hyperspherical harmonics basis functions as

$$\begin{aligned} \phi_{A\alpha}(x_{A,i}, y_{A,i}, z_{A,i}) \\ = \sum_{n,m} \frac{u_{nm}^\alpha(\rho)}{\rho^4} z_{A,i}^{\ell_{1\alpha}} y_{A,i}^{\ell_{2\alpha}} x_{A,i}^{\ell_{3\alpha}} Y_{nm}^\alpha(\phi_{2i}^A, \phi_{3i}), \end{aligned} \quad (3.36)$$

$$\begin{aligned} \phi_{B\alpha}(x_{B,p}, y_{B,p}, z_{B,p}) \\ = \sum_{n,m} \frac{w_{nm}^\alpha(\rho)}{\rho^4} z_{B,p}^{\ell_{1\alpha}} y_{B,p}^{\ell_{2\alpha}} x_{B,p}^{\ell_{3\alpha}} Y_{nm}^\alpha(\phi_{2p}^B, \phi_{3p}), \end{aligned} \quad (3.37)$$

where

$$\begin{aligned} Y_{nm}^\alpha(\beta, \gamma) &= N_{nm}^\alpha (\sin\beta)^{2m} P_n^{K_{2\alpha}, \ell_{3\alpha} + (1/2)}(\cos 2\beta) \\ &\times P_m^{\ell_{1\alpha} + (1/2), \ell_{2\alpha} + (1/2)}(\cos 2\gamma). \end{aligned} \quad (3.38)$$

The labels m and n of the Jacobi polynomials run in principle over all non-negative integers; $K_{2\alpha} = \ell_{1\alpha} + \ell_{2\alpha} + 2m + 2$, and N_{nm}^α are normalization factors. By using the expansions above, one can write the wave function schematically as

$$\Psi_4 = \sum_{\alpha, n, m} \frac{U_{nm}^\alpha(\rho)}{\rho^4} \mathcal{H}_{nm}^\alpha(\rho, \Omega), \quad (3.39)$$

where U stands for u or w , depending on whether channel α is constructed with partition 3+1 or 2+2, respectively. The factors \mathcal{H} include the remaining dependences on ρ and angular variables, the latter denoted collectively as Ω . The linear differential equations resulting from the minimization of the Hamiltonian are then solved by the same techniques outlined above.

C. Monte Carlo methods

Monte Carlo methods have often proven useful in the study of strongly interacting quantum systems, and few-nucleon systems are no exception. They are primarily useful when explicit numerical schemes such as Faddeev or CHH methods cannot be carried out because the dimensions of the necessary grids grow too large. Two principle Monte Carlo schemes have been developed—variational and Green's-function Monte Carlo.

Variational Monte Carlo is an approximate variational method that uses Monte Carlo techniques to perform standard numerical quadratures. Green's-function (or diffusion) Monte Carlo methods, on the other hand, employ Monte Carlo methods to evaluate the imaginary-time path integrals relevant for a light nucleus. They typically use the variational Monte Carlo wave functions as a starting point and cool them in order to measure ground-state observables. In this section we describe the application of these methods to ground-state properties; each can also be employed to gain information about nuclear dynamics.

1. Variational Monte Carlo

Variational Monte Carlo (VMC) employs an explicit form of a trial wave function, typically containing 20–30 variational parameters. These parameters are optimized by minimizing the expectation value of the energy; Monte Carlo methods, specifically the Metropolis *et al.* (1953) algorithm, are used to evaluate the spatial integrals.

The trial wave functions used in VMC calculations typically have a simple form:

$$|\Psi_T\rangle = \left[\mathcal{S} \prod_{i < j < k} F_{ijk} \right] \left[\mathcal{S} \prod_{i < j} F_{ij} \right] |\Psi_J\rangle, \quad (3.40)$$

where \mathcal{S} represents the symmetrization operator, respectively, acting over the A -particle space. In this equation for $|\Psi_T\rangle$, the Jastrow state $|\Psi_J\rangle$ carries the quantum

number information and, for $A > 4$, much of the long-distance physics. Important clustering properties and binding or threshold effects are incorporated here. The Jastrow wave function $|\Psi_J\rangle$ is written as

$$|\Psi_J\rangle = \mathcal{A} \left[\prod_{i < j \in s} f_{ss}^c(r_{ij}) \prod_{i \in s, j \in p} f_{sp}^c(r_{ij}) \prod_{i \in p, j \in p} f_{pp}^c(r_{ij}) |\Phi\rangle \right], \quad (3.41)$$

where \mathcal{A} is the antisymmetrization operator. The central-pair correlations f^c are functions of the pair distance only. However, the long-distance behavior may be different for nucleons in different shells, and hence the f^c are labeled by the single-particle orbits of the two nucleons. The determination of these Jastrow factors is described below. For these larger systems, $|\Phi\rangle$ is written as a sum over a small number of shell-model configurations and the coefficients of the various configurations are variational parameters.

For example, in recent calculations of six-body nuclei (Pudliner *et al.*, 1995),

$$\begin{aligned} |\Phi(JMTT_z)\rangle &= \mathcal{A} [\Phi_\alpha(00) \phi_p(r_{5,\alpha}) \phi_p(r_{6,\alpha})] \\ &\times \sum_{L,S} \beta_{JLS} [Y_1(\Omega_{5,\alpha}) Y_1(\Omega_{6,\alpha})]_L [\chi_5 \chi_6]_S]_{JM} \\ &\times [\eta_5 \eta_6]_{T,T_z}, \end{aligned} \quad (3.42)$$

where $|\Phi_\alpha(00)\rangle$ is an antisymmetrized product of four-nucleon spinors coupled to $J = T = 0$ with no spatial dependence, and the spatial dependence in the p-wave orbitals ϕ_p is taken from the solution of a single nucleon in a Woods-Saxon well. Additional clustering properties—for example, the α - d breakup in $A = 6$, as well as three-body correlations—can also be incorporated in the Jastrow wave function if they are found to be important. Note that the wave function is translationally invariant in that it involves only pair separations and the separation between p-shell nucleons and s-shell clusters. The wave functions Ψ_J are constructed to be eigenstates of the total momentum \mathbf{J} . Since the pair-correlation operators commute with \mathbf{J} , the total wave function also has good total angular momentum.

The “two-body” spin-isospin correlation operators F_{ij} in Eq. (3.40) carry the short- and intermediate-range physics, including the tensor correlations and the isospin dependence in the short-range repulsion. They are parametrized as

$$F_{ij} = \left[1 + \sum_{m=2,8} u_m(\mathbf{r}_{ij}; \mathbf{R}) O_{ij}^m \right], \quad (3.43)$$

and contain operators O_{ij}^m that are a subset of those employed in the interaction:

$$O_{ij}^m = [1, \boldsymbol{\sigma}_i \cdot \boldsymbol{\sigma}_j, S_{ij}, (\mathbf{L} \cdot \mathbf{S})_{ij}] \otimes [1, \boldsymbol{\tau}_i \cdot \boldsymbol{\tau}_j]. \quad (3.44)$$

The product $f^c(r_{ij}) F_{ij}$ is required to satisfy the short-distance properties of the wave function as two nucleons are brought close together. The dependence upon the pair distance r_{ij} is obtained as a solution of Schrödinger-

like equations in the various two-body channels. These correlations are obtained from equations similar to those used for the low-density limit of Fermi hypernetted-chain variational calculations of nuclear matter (Wiringa, Fiks, and Fabrocini, 1988; Arriaga, Pandharipande, and Wiringa, 1995). Schematically, they are written as

$$-(1/m) \nabla^2 [f(r) \phi(\mathbf{r})]_{JST} + [v_{ij} + \lambda(r)] [f(r) \phi(\mathbf{r})]_{JST} = 0. \quad (3.45)$$

This equation is solved for the various J, S, T channels and the correlations are recast into the operator form, as in Eq. (3.43). The functions $\phi(\mathbf{r})$ contain the appropriate spherical harmonics for the given channel. For the spin-triplet channels the combination $[f(r) \phi(\mathbf{r})]_{JST}$ satisfies two coupled equations with $L = J - 1$ and $L = J + 1$ (Wiringa, 1991). The variational parameters are included in the functional form of $\lambda(r)$. For s-shell nuclei, the form is adjusted so that

$$[f_{ss}^c(r)]^{A-1} \rightarrow \exp(-\gamma r)/r, \quad (3.46)$$

where γ is related to the separation energy of the last nucleon. Spin dependence in the breakup channels can be treated by including a nonzero long-distance behavior in the spin-dependent correlations $u_m(r)$. For larger systems, however, the product of the f_{sp} or f_{pp} in $|\Psi_J\rangle$ multiplied by the F_{ij} is adjusted to go to a constant. The pair-correlation functions F_{ij} are defined to carry the spin-isospin dependence of only particles i and j . However, the associated amplitudes u_m are functions of the coordinates of all the nucleons; the presence of the remaining particles requires a quenching of the noncentral correlations. The full structure of this quenching is described by Arriaga, Pandharipande, and Wiringa (1995).

The structure of the three-nucleon correlations F_{ijk} can, in principle, be quite complicated. The most important correlation is that due to the three-nucleon interaction V_{ijk} ; the operator form is taken from

$$F_{ijk} = 1 - \beta V_{ijk}, \quad (3.47)$$

where β is again a variational parameter. Additional three-body correlations have been investigated by Arriaga, Pandharipande, and Wiringa (1995).

Given the wave function, one can, in principle, evaluate the expectation value of any operator using Metropolis Monte Carlo techniques. Variational Monte Carlo methods have often been employed in studies of other quantum systems, including, for example, atoms and molecules, the electron gas, and liquid and solid helium. The state dependence of the interaction, though, requires a somewhat different treatment than is traditionally used in VMC calculations. Typically, one uses the Metropolis method to obtain points distributed proportional to a probability density $W(\mathbf{R})$, often choosing $W(\mathbf{R}) = |\langle \Psi_T(\mathbf{R}) | \Psi_T(\mathbf{R}) \rangle|$, where the angle brackets indicate sums over the internal degrees of freedom, the spins and isospins. Hence an estimate of an expectation value is obtained from

$$\langle O \rangle = \frac{\int d\mathbf{R} \langle \Psi_T(\mathbf{R}) | O | \Psi_T(\mathbf{R}) \rangle}{\int d\mathbf{R} \langle \Psi_T(\mathbf{R}) | \Psi_T(\mathbf{R}) \rangle} \approx \frac{\sum_i \langle \Psi_T(\mathbf{R}_i) | O | \Psi_T(\mathbf{R}_i) \rangle / W(\mathbf{R}_i)}{\sum_i \langle \Psi_T(\mathbf{R}_i) | \Psi_T(\mathbf{R}_i) \rangle / W(\mathbf{R}_i)}. \quad (3.48)$$

In the case of the Hamiltonian, we are averaging the “local” energy $\langle \Psi_T | H | \Psi_T \rangle / W(\mathbf{R})$ over the points to yield an estimate of the ground-state energy.

Several variations on the standard methods are incorporated to treat light nuclei. First, instead of computing the full wave function $|\Psi_T\rangle$ in Eq. (3.40), one can sample over the order of pair- and triplet-correlation operators F_{ij} and F_{ijk} that are implied by the symmetrization operators \mathcal{S} in Eq. (3.40). These orders must be sampled independently for the left- and right-hand wave functions and a positive-definite choice made for a probability density $W(\mathbf{R})$.

In all cases, Monte Carlo methods are used to evaluate the coordinate-space integrals, while spin-isospin sums are explicitly evaluated. The number of spin degrees of freedom grows as 2^A , while the isospin grows a little more slowly due to charge and (approximate) isospin conservation. The efficiency of the variational calculations can be dramatically improved by calculating energy differences between different wave functions. Nevertheless, these explicit spin-isospin summations require computing time that grows exponentially with A , a requirement that has limited standard variational Monte Carlo calculations of nuclear systems to light nuclei. In principle, it should be possible to sample over at least some of the degrees of freedom, but an exact practical scheme that yields a variance small enough to be useful has yet to be found. However, cluster VMC algorithms invoke a cluster approximation to sum over a connected set of spin-isospin degrees of freedom and have been applied to studying the ground state of ^{16}O (Pieper, Wiringa, and Pandharipande, 1990, 1992) and spin-orbit splitting in ^{15}N (Pieper and Pandharipande, 1993). Such calculations are also a useful starting point, for example, for Glauber calculations of electron scattering in heavier systems (Pandharipande and Pieper, 1992).

Once the variational parameters have been optimized, the expectation value of any ground-state observable can be evaluated using Eq. (3.48). Off-diagonal observables, such as momentum distributions, can be similarly evaluated. They simply require an additional integration variable corresponding to the off-diagonal displacement. Experimental quantities of interest include charge and magnetic form factors, sum rules, etc. In addition, other quantities can be computed that are not directly observable experimentally, but that are useful in approximate theories of reactions, including momentum distributions of nucleons and nucleon clusters. A summary of some

recent results is given below; additional results are presented by Arriaga, Pandharipande, and Wiringa (1995) and Forest *et al.* (1996).

2. Green's-function Monte Carlo

Diffusion or Green's-function Monte Carlo (GFMC) methods rely upon the path-integral approach to evaluate the imaginary-time propagation of the wave function:

$$|\Psi_0\rangle = \lim_{\tau \rightarrow \infty} \exp[-(H - E_0)\tau] |\Psi_T\rangle, \quad (3.49)$$

where $|\Psi_0\rangle$ is the ground state of H with energy E_0 , and $|\Psi_T\rangle$ is a trial state. In order to evaluate this propagation, one splits up the imaginary time τ into small time slices $\Delta\tau$, and iterates an equation of the form

$$|\Psi(\tau + \Delta\tau)\rangle = \exp[-(H - E_0)\Delta\tau] |\Psi(\tau)\rangle. \quad (3.50)$$

This method has a long history, starting with calculations of the α particle using a spin-isospin-independent interaction by Kalos (1962). It has also been used extensively for problems in atomic and condensed-matter physics. The first application to state-dependent interactions was provided by Carlson (1987), and more realistic interactions were used in Carlson, 1988 and Carlson, 1991. Recently calculations for $A=6$ and 7 have been performed, which are the first direct microscopic calculations of these p-shell nuclei (Pudliner *et al.*, 1995, Pudliner *et al.* 1997).

The first element in performing such a calculation is an evaluation of the matrix elements of the short-time propagator:

$$\begin{aligned} \langle \mathbf{R}', \chi' | \exp(-H\Delta\tau) | \mathbf{R}, \chi \rangle &\equiv G(\mathbf{R}', \mathbf{R}; \Delta\tau) \approx \left[\prod_{i=1, A} G_{0,i}(|\mathbf{r}_i - \mathbf{r}'_i|) \right] \\ &\times \sum_{\chi_1, \chi_2} \langle \chi' | \left[1 - \frac{\Delta\tau}{2} \sum_{i < j < k} V_{ijk}(\mathbf{R}') \right] | \chi_1 \rangle \\ &\times \langle \chi_1 | \mathcal{S} \prod_{i < j} \left[\frac{g_{ij}(\mathbf{r}'_i, \mathbf{r}_{ij})}{g_{0,ij}(\mathbf{r}'_i, \mathbf{r}_{ij})} \right] | \chi_2 \rangle \langle \chi_2 | \\ &\times \left[1 - \frac{\Delta\tau}{2} \sum_{i < j < k} V_{ijk}(\mathbf{R}) \right] | \chi \rangle, \end{aligned} \quad (3.51)$$

where the χ represent A -nucleon spin-isospin states, $G_{0,i}$ and $g_{0,ij}$ are the free one- and two-body imaginary-time propagators, respectively, and g_{ij} is the interacting two-body propagator.

The free propagators are simple Gaussians:

$$G_{0,i} = N_1 \exp \left[-m \frac{(\mathbf{r}'_i - \mathbf{r}_i)^2}{2\Delta\tau} \right], \quad (3.52)$$

$$g_{0,ij} = N_2 \exp \left[-m \frac{(\mathbf{r}'_{ij} - \mathbf{r}_{ij})^2}{4\Delta\tau} \right], \quad (3.53)$$

with normalizations N_i such that the norm of the flux is preserved ($\int d\mathbf{r}_i G_{0,i} = 1$). The pair propagator g_{ij} is the

imaginary-time equivalent of the two-body T matrix. It is a matrix in the two-body spin-isospin space and must be calculated numerically. The propagator satisfies an evolution equation,

$$\langle \chi'_{ij} | \left[\frac{\partial}{\partial \tau} + H_{ij} \right] g_{ij}(\mathbf{r}', \mathbf{r}; \tau) | \chi_{ij} \rangle = 0, \quad (3.54)$$

where

$$H_{ij} = -(1/m)\nabla_{ij}^2 + v_{ij} \quad (3.55)$$

and χ_{ij} and χ'_{ij} are two-nucleon spin-isospin states. The g_{ij} also satisfy a boundary condition

$$\langle \chi'_{ij} | g_{ij}(\mathbf{r}', \mathbf{r}; \tau=0) | \chi_{ij} \rangle = \delta(\mathbf{r}-\mathbf{r}') \delta_{\chi'_{ij}, \chi_{ij}}. \quad (3.56)$$

Techniques for calculating and storing g_{ij} are described in detail by Pudliner *et al.* (1977).

Once the propagator $G(\mathbf{R}, \mathbf{R}'; \Delta\tau)$ is constructed, a practical algorithm must be implemented to carry out the iteration of the wave function [Eq. (3.50)]. The scheme currently used for sampling the paths is described in detail by Pudliner *et al.* (1997); here, we simply sketch the basic ideas. Since the wave functions (propagators) are vectors (matrices) in spin-isospin space, a scalar quantity must be defined to sample the paths. In principle, any set of paths can be chosen as long as the probability used to choose the paths is divided out when computing expectation values. To minimize the variance, though, it is important to follow as closely as possible standard importance-sampling techniques used in traditional Green's-function and diffusion Monte Carlo (Pudliner *et al.*, 1997). In essence, this requires sampling from a kernel so that the probability of a configuration at \mathbf{R} is proportional to

$$\sum_{\chi} \langle \Psi_T(\mathbf{R}) | \chi \rangle \langle \chi | \Psi(\mathbf{R}; \tau) \rangle.$$

In the limit that the trial wave function Ψ_T is exact and the propagator is sampled exactly, this method would produce the correct ground-state energy with no variance.

To this end, we introduce an importance function I that depends upon the full trial and GFMC wave functions. The calculations proceed by sampling paths from $I[\Psi_T(\mathbf{R}), \Psi(\mathbf{R}; \tau)]$. The importance function must be real and positive; a convenient choice is

$$I[\Psi_T(\mathbf{R}), \Psi(\mathbf{R}; \tau)] = \left| \sum_{\chi} \langle \Psi_T(\mathbf{R}) | \chi \rangle \langle \chi | \Psi(\mathbf{R}; \tau) \rangle \right| + \epsilon \sum_{\chi} \left| \langle \Psi_T(\mathbf{R}) | \chi \rangle \langle \chi | \Psi(\mathbf{R}; \tau) \rangle \right|, \quad (3.57)$$

where ϵ is a small positive coefficient. The second term ensures that all paths are allowed with a positive probability. In this equation and those that follow, the dependence upon the symmetrization \mathcal{S} in the pair and triplet orders will be suppressed, both in the wave function, Eq. (3.40), and in the propagator, Eq. (3.51). The pair and triplet orders are, in fact, sampled in both cases. Details of the sampling and weighting of paths are described by Pudliner *et al.* (1997).

Branching techniques are used to split (delete) paths with large (small) importance functions $I[\Psi_T(\mathbf{R}), \Psi(\mathbf{R}; \tau)]$ in a statistically unbiased manner. After branching, expectation values can be recovered from the equivalent of Eq. (3.48) evaluated between the trial and propagated GFMC wave functions:

$$\langle O(\tau) \rangle \approx \frac{\sum_{\mathbf{R}_i} \langle \Psi_T(\mathbf{R}_i) | O | \Psi(\mathbf{R}_i; \tau) \rangle / I[\Psi_T(\mathbf{R}_i), \Psi(\mathbf{R}_i; \tau)]}{\sum_{\mathbf{R}_i} \langle \Psi_T(\mathbf{R}_i) | \Psi(\mathbf{R}_i; \tau) \rangle / I[\Psi_T(\mathbf{R}_i), \Psi(\mathbf{R}_i; \tau)]}. \quad (3.58)$$

This is the basis of the importance-sampled GFMC algorithm for noncentral interactions. Iterating this equation propagates the amplitudes of the wave function in a way designed to minimize statistical fluctuations in calculated expectation values.

The matrix element in Eq. (3.58) is a ‘‘mixed’’ estimate; it is of the form

$$\langle O \rangle_{\text{mix}} = \frac{\langle \Psi_T | O \exp(-H\tau) | \Psi_T \rangle}{\langle \Psi_T | \exp(-H\tau) | \Psi_T \rangle}. \quad (3.59)$$

The value O_{mix} is the matrix element of the trial (variational) and the true ground state. The mixed estimate is sufficient to evaluate the ground-state energy, since the Hamiltonian commutes with the propagator. Indeed, an upper bound to the true ground-state energy E_0 is obtained for any value of τ :

$$\langle H \rangle_{\text{mix}} = \frac{\langle \Psi_T | \exp(-H\tau/2) H \exp(-H\tau/2) | \Psi_T \rangle}{\langle \Psi_T | \exp(-H\tau/2) \exp(-H\tau/2) | \Psi_T \rangle} \geq E_0. \quad (3.60)$$

Of course, the actual convergence is governed by the accuracy of the trial wave function and the spectrum of the Hamiltonian. Often knowledge of the spectrum can be used to estimate the remaining error in a calculation that necessarily proceeds only to a finite τ .

For quantities other than the energy, one typically estimates the true ground-state expectation value by extrapolating from the mixed and variational estimates:

$$\langle O \rangle \approx 2 \langle O \rangle_{\text{mix}} - \frac{\langle \Psi_T | O | \Psi_T \rangle}{\langle \Psi_T | \Psi_T \rangle}, \quad (3.61)$$

which is accurate to first order in the difference between Ψ and Ψ_T . The variational wave functions used in this work are typically quite accurate, so this estimate is usually sufficient. For momentum-independent quantities, one can also retain a time history of the path in order to reconstruct an estimate of the form

$$\langle O \rangle = \frac{\langle \Psi_T | \exp(-H\tau/2) O \exp(-H\tau/2) | \Psi_T \rangle}{\langle \Psi_T | \exp(-H\tau/2) \exp(-H\tau/2) | \Psi_T \rangle}. \quad (3.62)$$

For momentum-dependent operators O , however, the statistical fluctuations associated with this estimate can be quite large.

Two caveats remain in present-day GFMC calculations of light nuclei. First, due to the well-known ‘‘sign problem’’ in all path integral simulations of fermions, the statistical error grows rapidly with τ . Present-day

TABLE IV. Triton binding energy comparison for different methods.

Hamiltonian	Method	${}^3\text{H}$ B (MeV)	${}^3\text{He}$ B (MeV)
AV14	PHH	7.683	7.032
	Faddeev/Q	7.680 ^a	
	Faddeev/R	7.670 ^b	7.014
	GFMC	7.670(8) ^b	
AV18/IX	GFMC	8.471(12) ^c	
	PHH	8.475 ^c	
	Expt.	8.48	7.72

^aGlöckle *et al.*, 1995.^bChen *et al.*, 1985.^cPudliner *et al.*, 1997.^dKievsky, Viviani, and Rosati, 1995.^eViviani, 1997.

calculations are typically limited to τ of the order of $0.05\text{--}0.1\text{ MeV}^{-1}$. This is not as severe a situation as one might suppose, since we have quite accurate variational wave functions available for these nuclei and we have a significant knowledge of the excitation spectra in these systems. For calculations of six- and seven-body nuclei, it is useful to perform a shell-model-like diagonalization in variational Monte Carlo to determine the optimum amplitudes for the various symmetry components of the p-wave part of the wave function (Pudliner *et al.*, 1997). Nevertheless, for some problems it may be quite useful to have a path-integral approximation that provides another type of approximation to the true ground state. For example, the fixed-node (Anderson, 1975; Ceperley and Alder, 1980) and constrained-path methods (Zhang, Carlson, and Gubernatis, 1995) have proven quite valuable in condensed-matter problems. These constraints can often be relaxed to yield an even better estimate of observables.

The other concern is that, in all currently available GFMC calculations, an approximate interaction that contains no \mathbf{p}^2 terms has been used in the propagation. Perturbation theory is then used to determine the expectation value of the difference between the two Hamiltonians. This approximation has proven to be quite accurate in studies of the three- and four-body systems. Although the equations above are still correct for an interaction with \mathbf{p}^2 , \mathbf{L}^2 , or $(\mathbf{L}\cdot\mathbf{S})^2$ interactions, a direct implementation of the method will yield large statistical errors. Again, variational schemes based upon constraints to the path integral may prove useful.

Green's-function Monte Carlo has proven to be quite accurate in the three-, and now four-, body systems in which it has been tested. Recent applications to larger systems (Pudliner *et al.*, 1995, 1997) provide the first real tests of these microscopic models beyond $A=4$. It is also possible to compute low-energy scattering with path-integral techniques, as well as to obtain information about a variety of dynamic nuclear-response functions. A selection of results will be presented later in this article.

IV. LIGHT NUCLEAR SPECTRA

The spectra of light nuclear systems provide the first test of nuclear interaction models. Only if the spectra are well reproduced can one expect to calculate accurately other low-energy and low-momentum observables, like radii, form factors, and scattering lengths. In this section we present a brief review of results in light nuclei, the most recent calculations of which include systems up to $A=7$.

These calculations also provide a substantial test of the consistency of chiral perturbation theory in nuclei; it is *a priori* unclear how well a microscopic picture framed in terms of nucleon degrees of freedom with only two- and (small) three-nucleon interactions can reproduce nuclear spectra and structure.

A. Three- and four-nucleon systems

The simplest system, $A=3$, was the original test of realistic interaction models. As described previously, there is a considerable history of Faddeev solutions of the three-nucleon bound-state problem, in both coordinate and momentum space. More recently, correlated hyperspherical harmonics (CHH; Kievsky, Rosati, and Viviani, 1993) and Green's-function Monte Carlo (GFMC; Carlson, 1995) calculations have also been performed for $A=3$, basically as tests of the methods. The binding energies obtained with the various methods are in excellent agreement, typically within 10 keV or less. The GFMC calculations are limited to an accuracy of 20 keV by statistical fluctuations and the approximations in the treatment of \mathbf{p}^2 -components of the interaction. A comparison of results obtained with different methods for the Argonne interaction models is given in Table IV. In all cases the agreement between different methods is very good.

As noted previously, local two-nucleon interaction models underbind the triton by 800 keV compared to experiment. This naturally leads to too large a charge radius and also affects the nd scattering lengths. A vari-

TABLE V. Triton binding energy comparison for different interactions. See text for a discussion of these results.

Hamiltonian	B (MeV)	χ^2/N_d	Type
Nijm II	7.62 ^a	1.03	local
Reid 93	7.63 ^a	1.03	local
Argonne v_{18} (AV18)	7.62 ^a	1.09	local
Nijm I	7.72 ^a	1.03	nonlocal one-boson exchange
CD Bonn	8.00 ^b	1.03	nonlocal
CD Bonn	8.19 ^b	1.03	rel. BbS Eq.
Gross	8.50 ^c	2.40	rel. Gross Eq.
CD-Bonn+Tucson-Melbourne (TM)	8.48 ^d		TNI ($\Lambda/m_\pi=4.856$)
Nijm II+TM	8.48 ^d		TNI ($\Lambda/m_\pi=4.99$)
AV18+TM	8.48 ^d		TNI ($\Lambda/m_\pi=5.21$)
AV18+TNI IX	8.47 ^e		Urbana TNI IX

^aFriar *et al.*, 1993.

^bMachleidt, Sammarruca, and Song, 1996.

^cStadler and Gross, 1997.

^dNogga, Hüber, Kamada, and Glöckle, 1997.

^ePudliner *et al.*, 1997.

ety of recent results for realistic interaction models are presented in Table V. The local interaction models (Nijm II, Reid 93, and Argonne v_{18}) produce a binding energy of 7.62 ± 0.01 MeV for the triton, as compared to the experimental 8.48 MeV. The Nijm I interaction is nonlocal in the central channel and gives a slightly larger binding of 7.72 MeV.

The relativistic calculations of Machleidt, Sammarruca, and Song (1996) and Stadler and Gross (1997) give greater binding energies. In the first instance, both relativistic and nonrelativistic (but nonlocal) calculations were performed. The NN interaction was adjusted to provide an excellent fit to the np and pp data, and the resulting binding energy was about halfway between the local NN interactions and the experimental value. The Gross equations have also been solved for a realistic NN interaction model (Stadler and Gross, 1997). In this case, fewer parameters were used in the one-boson-exchange model, and hence the statistical fit to the NN database was not as good. They included off-shell scalar σNN couplings and were able to reproduce the experimental triton binding energy and a reasonable fit to the NN phase shifts with a suitable choice of these couplings. Gross and Stadler emphasize that this type of model is equivalent to another one-boson-exchange model without such off-shell couplings, but with an additional specific family of N -body forces.

Upon including specific three-body interactions, a natural choice is to adjust the three-nucleon interaction strength to yield the correct binding energy. In the framework of the Tucson-Melbourne three-nucleon interaction model, this has been done by adjusting the cutoff at the πNN vertex; harder cutoffs produce a larger effect. Table V lists several combinations of realistic NN interactions with specific cutoffs that reproduce the experimental binding energies (Nogga, Hüber, Kamada,

and Glöckle, 1997). In the Urbana/Argonne three-nucleon interaction models VIII and IX, the strength is constrained to fit the triton binding energy when used with the Argonne (isospin-conserving) v_{14} or v_{18} interactions, respectively. As discussed later, adjusting the three-nucleon interaction in this way also yields nd scattering lengths that are in agreement with experimental values.

Clearly, though, it is also important to go beyond $A=3$. Chiral perturbation theory, for example, predicts that four-nucleon interactions are much less important than three-nucleon ones, which are, in turn, much smaller than two-nucleon interactions. This can only be tested by studying larger systems. It is also important to study neutron-rich and proton-rich systems to understand the isospin dependence of the three-nucleon interaction. Ideally, one would like to be able to proceed from light nuclei to light p-shell nuclei to neutron stars with the same Hamiltonian and similar accuracy. While this has still not been achieved, significant progress has been made.

The four-body system is the next step, and it has been studied by several groups. While the nucleons are in predominantly spatially symmetric configurations for both the three- and four-body ground states, the α particle is tightly bound. This tight binding, an approximately 20-MeV nucleon separation energy, yields a rather high central density. In addition, the fact that there are four triplets in the four-body system as compared to one in $A=3$ implies that the three-nucleon interaction is comparatively more important here.

Again, the alpha particle is severely underbound in the presence of static two-nucleon interactions only. Tjon (1975) originally noticed the strong correlation in three- and four-body binding energies. Carlson (1991) provided the first complete calculations with realistic

TABLE VI. ${}^4\text{He}$ binding energies with and without three-nucleon interaction; comparison of different methods: correlated hyperspherical harmonics (CHH), Faddeev-Yakubovsky (FY), variational Monte Carlo (VMC), and Green's-function Monte Carlo (GFMC). Error bars in CHH calculations are estimates of the effects of channel truncation.

Hamiltonian	AV14	AV14+TNI 8
CHH	24.17(5) ^a	27.48 ^b
FY	24.01 ^b	
VMC		27.6(1) ^c
GFMC	24.23(3) ^c	28.3(2) ^f

^aViviani, 1997.

^bViviani, Kievsky, and Rosati, 1995.

^cGlöckle *et al.*, 1995.

^dArriaga, Pandharipande, and Wiringa, 1995.

^ePudliner *et al.*, 1977.

^fCarlson and Schiavilla, 1994a.

two- (and three-) nucleon interactions, and found that a three-nucleon interaction fit to the measured triton binding energy also produced a result for the α -particle binding energy close to the experimental value. More recently, several other groups have calculated $A=4$ binding energy using both Faddeev-Yakubovsky (Glöckle and Kamada, 1993a, 1993b) and CHH (Viviani, Kievsky, and Rosati, 1995) methods. Although the agreement between these calculations is not quite as good as that for the three-body system, it is nevertheless satisfactory, as indicated by a comparison of results presented in Table VI.

With two-nucleon interactions alone, the results are accurate to within 0.2 MeV. In the CHH calculations the authors provide an estimate of 0.05 MeV for the error arising from channel truncation, which yields an estimate consistent with the GFMC results. These newer, more accurate GFMC results are also consistent with the older result of 24.2 ± 0.2 MeV (Carlson and Schiavilla, 1994a). The Faddeev-Yakubovsky results are slightly (0.2 MeV) lower than the others. For the Argonne v_{18} interaction, recent calculations are in similar good agreement: the CHH method (Viviani, 1997) yields a binding energy of 24.11 MeV compared to the GFMC result of 24.1 ± 0.1 MeV.

When three-nucleon interactions are added, the agreement is not quite as good. The CHH and GFMC calculations differ by approximately 0.8 MeV. However, the $A=4$ CHH calculation in the presence of a three-nucleon interaction has an estimated truncation error of 0.4 MeV, and it will soon be possible to perform a larger, more complete calculation. At present, the best variational Monte Carlo calculation is slightly higher than the CHH calculation, but both yield significantly less binding than the GFMC result, which coincides with the experimental binding energy. These results should be considered in substantial agreement. Note that the kinetic energy in this system is of the order of 100 MeV; the energies are calculated to an accuracy much better

than 1% of this value. Of course, it would be useful to reduce the difference through more accurate calculations.

It is worthwhile to consider other expectation values to understand the α -particle structure. For example, while the kinetic energy and NN interaction contributions are of the order of 100 MeV, the three-nucleon interaction is of the order of 10 MeV. Hence the two-nucleon interaction is still dominant; in fact, a further breakdown of the individual contributions to $\langle v_2 \rangle$ indicates that (1) the short-range repulsion and intermediate-range attraction are sizable but of opposite sign, and (2) the one-pion-exchange potential is extremely important, having an expectation value of almost 75% of the full NN interaction. Finally, we note that the alpha particle has a D-state percentage of nearly 15%, largely arising from the one-pion-exchange interaction.

B. Light p-shell nuclei

In the low-lying states of light p-shell nuclei, a considerably different regime of the NN interaction is tested. Here negative-parity states become important for the first time. At present, only Monte Carlo methods have been used to study these systems with realistic interaction models; certainly, this will change in the years ahead.

Historically, p-shell nuclei have been studied with the nuclear shell model. Recently, a great deal of progress has been made in so-called “no-core” shell-model calculations (Zheng *et al.*, 1995). These yield quite good spectral results starting from a microscopic NN G matrix. As an average energy constant has been added to these shell-model calculations, it is difficult to compare the corresponding results directly with those from the microscopic calculations described below. However, comparisons of the two approaches, particularly regarding ground- and excited-state expectation values, are likely to be quite valuable.

The first p-shell “nucleus” is ${}^5\text{He}$, which is not bound. The two lowest-lying states are negative-parity resonances consisting predominantly of a $p_{1/2}$ or $p_{3/2}$ neutron outside of an α -particle core. The low-energy scattering techniques described in Sec. VIII are adequate to treat this system; in the calculations described here the neutron is confined within a radius of 12.5 fm from the α particle. Assuming this distance to be large enough so that there are essentially no interactions between the two clusters, the experimental n - α phase shifts (Bond and Firk, 1977) can be directly converted to energies. For the radius chosen, the $p_{3/2}$ state is nearly at resonance, while the $p_{1/2}$ state is slightly above.

For the AV18/IX model, the GFMC calculation of the $3/2^-$ states gives an energy of $-26.5(2)$ MeV, as compared to the experimental -27.2 (Pudliner *et al.*, 1995). The $1/2^-$ state is well reproduced; the GFMC calculation gives $-25.7(2)$ MeV, compared to the experimen-

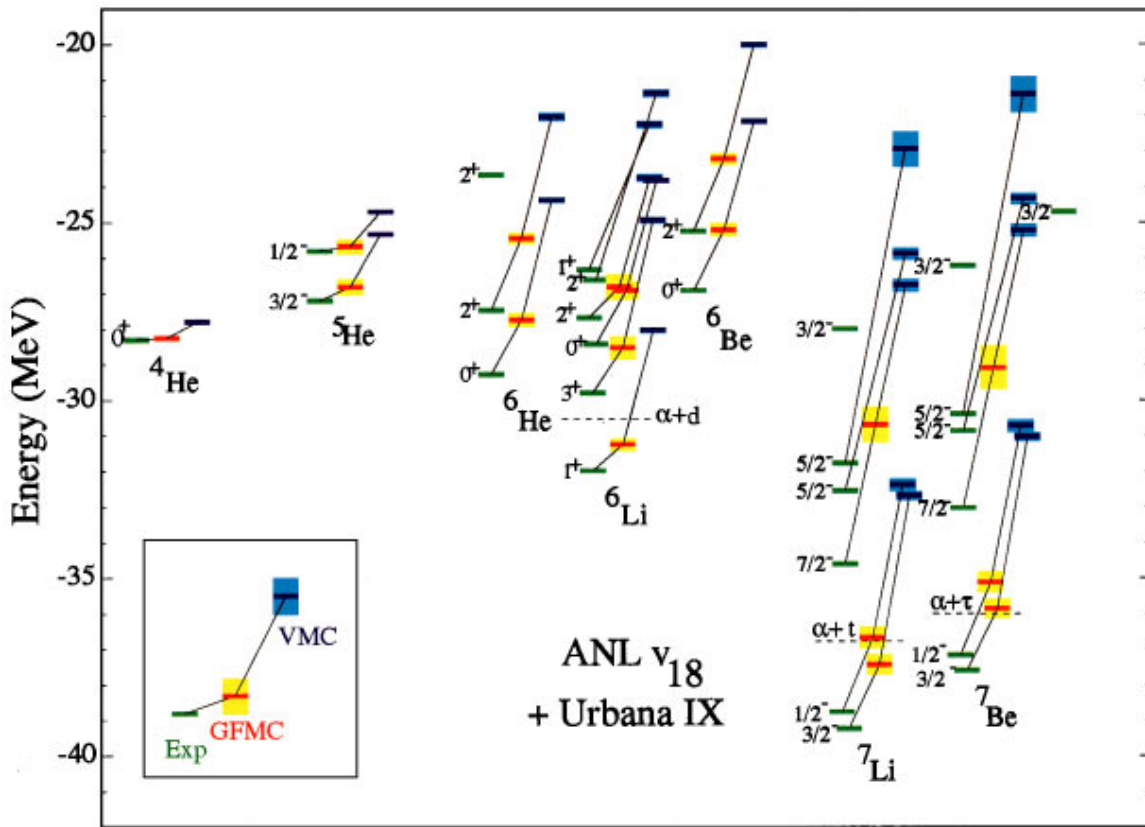


FIG. 7. (Color) Energy spectra of $A=4-7$ nuclei, obtained in variational Monte Carlo (VMC) and Green's-function Monte Carlo (GFMC) calculations with the Argonne v_{18} two-nucleon and Urbana model IX three-nucleon interactions. Both the central value and the one-standard-deviation error estimate are shown. GFMC results are a variational bound obtained by averaging from $\tau = 0.04-0.06 \text{ MeV}^{-1}$.

tal -25.8 . Thus this calculation yields approximately two-thirds of the experimental spin-orbit splitting in ${}^5\text{He}$.

Green's-function Monte Carlo calculations produce a series of decreasing upper bounds to the true energy as the iteration time τ is increased. For ${}^5\text{He}$, the calculations appear to be well converged—indeed, little dependence upon τ is seen for any observable for $\tau > 0.03 \text{ MeV}^{-1}$. Hence the only uncertainty remaining is the degree to which the difference between the full isospin-dependent Hamiltonian and a simpler static v_8 model can be treated in perturbation theory. While this is apparently quite a good approximation in $A=3$ and 4 , for larger systems it remains to be tested.

The initial sets of calculations for $A=6-7$ have recently been completed (Pudliner *et al.*, 1995, 1997), and the results are quite encouraging. Figure 7 compares the GFMC spectra to experiment for these systems; the overall agreement is quite satisfactory. While the absolute energies are slightly higher than experiment, the level splittings appear to be well described. These calculations provide a significant test of the three-nucleon interaction. While the errors in the calculation are on the order of 1 MeV , the three-nucleon-interaction expectation values are approximately 10 MeV .

In Fig. 8 we show the convergence with imaginary time for one of the most recent six-body calculations.

Similar calculations in $A=4$ and 5 show that the results are well converged. Statistical fluctuations that occur in all path-integral calculations of fermion systems (Schmidt and Kalos, 1984) limit the calculations to τ

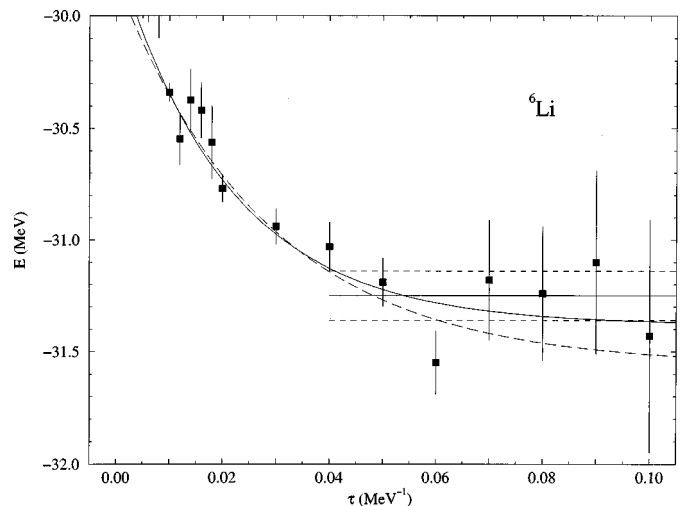


FIG. 8. Convergence with imaginary time τ of the Green's-function Monte Carlo (GFMC) calculations of $A=6$. Curves are fits to ground-state plus excitations, and the horizontal lines are the average from $\tau=0.04-0.06 \text{ MeV}^{-1}$ plus and minus one standard deviation.

TABLE VII. Experimental and quantum Monte Carlo energies of $A=3-7$ nuclei in MeV (Pudliner *et al.*, 1997), for variational Monte Carlo (VMC), Green's-function Monte Carlo (GFMC), and experiment.

${}^A Z(J^\pi; T)$	VMC	GFMC	Expt.
${}^2\text{H}(1^+; 0)$	-2.2248(5)		-2.2246
${}^3\text{H}(\frac{1}{2}^+; \frac{1}{2})$	-8.32(1)	-8.47(1)	-8.48
${}^4\text{He}(0^+; 0)$	-27.76(3)	-28.30(2)	-28.30
${}^6\text{He}(0^+; 1)$	-24.87(7)	-27.64(14)	-29.27
${}^6\text{He}(2^+; 1)$	-23.01(7)	-25.84(11)	-27.47
${}^6\text{Li}(1^+; 0)$	-28.09(7)	-31.25(11)	-31.99
${}^6\text{Li}(3^+; 0)$	-25.16(7)	-28.53(32)	-29.80
${}^6\text{Li}(0^+; 1)$	-24.25(7)	-27.31(15)	-28.43
${}^6\text{Li}(2^+; 0)$	-23.86(8)	-26.82(35)	-27.68
${}^6\text{Be}(0^+; 1)$	-22.79(7)	-25.52(11)	-26.92
${}^7\text{He}(\frac{3}{2}^-; \frac{3}{2})$	-20.43(12)	-25.16(16)	-28.82
${}^7\text{Li}(\frac{3}{2}^-; \frac{1}{2})$	-32.78(11)	-37.44(28)	-39.24
${}^7\text{Li}(\frac{1}{2}^-; \frac{1}{2})$	-32.45(11)	-36.68(30)	-38.76
${}^7\text{Li}(\frac{7}{2}^-; \frac{1}{2})$	-27.30(11)	-31.72(30)	-34.61
${}^7\text{Li}(\frac{5}{2}^-; \frac{1}{2})$	-26.14(11)	-30.88(35)	-32.56
${}^7\text{Li}(\frac{3}{2}^-; \frac{3}{2})$	-19.73(12)	-24.79(18)	-28.00

$\leq 0.06 \text{ MeV}^{-1}$, and hence only the relatively high-lying components of the trial wave function are projected out. The two curves are fits to the data for $\tau > 0.01 \text{ MeV}^{-1}$, with a ground-state plus excited-state contribution. The dashed curve fits the data only up to $\tau = 0.06 \text{ MeV}^{-1}$, while the solid curve includes all the data up to 0.1 MeV^{-1} . The latter yields a ground-state energy approximately one standard deviation below the average from $\tau = 0.04-0.06 \text{ MeV}^{-1}$, which is shown as horizontal lines in the figure. A variety of tests of the GFMC method have been performed. These tests confirm that the GFMC is able to correct for very poor choices of short-ranged correlations, but is not able to adequately suppress all low-lying excitations within the present limit of $\tau = 0.06 \text{ MeV}^{-1}$. In order to perform the most accurate calculations possible, the starting variational Monte Carlo (VMC) wave functions have been optimized with respect to the presence of different symmetry compo-

nents in the single-particle part of the wave function. These small-basis diagonalizations reproduce the standard dominant spatially symmetric components of the ground-state wave function that were originally obtained in shell-model calculations.

Ground-state energies for $A=3-7$ are presented in Table VII, and a variety of expectation values for specific ground states are presented in Table VIII. In the tables, the energy is an upper bound obtained from averaging results from $\tau = 0.04$ to 0.06 MeV^{-1} . It may be possible to improve these calculations further. For example, it is possible to compute estimates for an arbitrary mixture of states with different symmetries, as is currently done in the VMC calculations. In addition, it should be possible to place constraints on the path-integral calculations to extend them to much larger τ . Indeed, such approximate techniques have proven to be very valuable in condensed-matter simulations.

This is particularly important for studying low-energy and low-momentum transfer properties of the nuclei. The present VMC calculations do not provide enough binding compared to the lowest breakup threshold and hence have been adjusted to give the experimental ground-state radius of Li. The radii as well as the magnetic and quadrupole moments in the VMC calculations are given in Table IX. Due to the limit of the present GFMC calculations to $\tau = 0.06 \text{ MeV}^{-1}$, it is not clear that they have converged to the true ground-state values, for this Hamiltonian.

Green's-function Monte Carlo has also been employed to study isospin-breaking in light nuclei. The calculations use an average isoscalar interaction and evaluate the electromagnetic and strong-interaction isospin-breaking terms in perturbation theory. Using the Argonne v_{18} model, Pudliner *et al.* (1997) have reproduced the isovector energy differences between the ${}^3\text{H}$ - ${}^3\text{He}$ and ${}^6\text{He}$ - ${}^6\text{Be}$ fairly well, as shown in Table X (Pudliner *et al.*, 1997). The isotensor energy differences involve more difficult cancellations and are not as well reproduced.

In summary, realistic models of the NN interaction can now be explicitly solved for up to 7-body systems. To date, the calculations confirm that the standard picture of these nuclei as interacting through realistic two-

TABLE VIII. Green's-function Monte Carlo (GFMC) energy components in MeV for $A=6,7$ ground states.

${}^A Z(J^\pi; T)$	K	v_{ij}	V_{ijk}	v_{ij}^γ	v_{ij}^π	$V_{ijk}^{2\pi}$
${}^2\text{H}(1^+; 0)$	19.81	-22.05	0.0	0.018	-21.28	0.0
${}^3\text{H}(\frac{1}{2}^+; \frac{1}{2})$	50.0(8)	-57.6(8)	-1.20(7)	0.04	-43.8(2)	-2.2(1)
${}^4\text{He}(0^+; 0)$	112.1(8)	-136.4(8)	-6.5(1)	0.86(1)	-99.4(2)	-11.8(1)
${}^6\text{He}(0^+; 1)$	140.3(15)	-165.9(15)	-7.2(2)	0.87(1)	-109.0(4)	-13.6(2)
${}^6\text{Li}(1^+; 0)$	150.8(10)	-180.9(10)	-7.2(1)	1.71(1)	-128.9(5)	-13.7(3)
${}^6\text{Be}(0^+; 1)$	134.8(16)	-160.5(16)	-6.8(2)	2.97(2)	-108.0(4)	-12.8(2)
${}^7\text{He}(\frac{3}{2}^-; \frac{3}{2})$	146.0(17)	-171.2(17)	-7.4(2)	0.86(1)	-109.9(6)	-14.1(2)
${}^7\text{Li}(\frac{3}{2}^-; \frac{1}{2})$	186.4(28)	-222.6(30)	-8.9(2)	1.78(2)	-152.5(7)	-17.1(4)

TABLE IX. Variational Monte Carlo (VMC) values for proton rms radii (in fm), quadrupole moments (in fm²), and magnetic moments (in n.m.) all in the impulse approximation. Only Monte Carlo statistical errors are shown.

	$\langle r_p^2 \rangle^{1/2}$		μ		Q	
	VMC	Experiment	VMC	Experiment	VMC	Experiment
${}^2\text{H}(1^+;0)$	1.967	1.953	0.847	0.857	0.270	0.286
${}^3\text{H}(\frac{1}{2}^+; \frac{1}{2})$	1.59(1)	1.60	2.582(1)	2.979		
${}^3\text{He}(\frac{1}{2}^+; \frac{1}{2})$	1.74(1)	1.77	-1.770(1)	-2.128		
${}^4\text{He}(0^+;0)$	1.47(1)	1.47				
${}^6\text{He}(0^+;1)$	1.95(1)					
${}^6\text{Li}(1^+;0)$	2.46(2)	2.43	0.828(1)	0.822	-0.33(18)	-0.083
${}^6\text{Be}(0^+;1)$	2.96(4)					
${}^7\text{Li}(\frac{3}{2}^-; \frac{1}{2})$	2.26(1)	2.27	2.924(2)	3.256	-3.31(29)	-4.06
${}^7\text{Be}(\frac{3}{2}^-; \frac{1}{2})$	2.42(1)		-1.110(2)		-5.64(45)	

and three-nucleon interactions is capable of adequately reproducing the nuclear spectra and much of the strong-interaction dynamics. Certainly discrepancies remain, but the calculations have advanced to the stage that these can be confronted. In particular, relativistic effects and the spin-isospin structure of the three-nucleon interaction can be addressed.

V. THE NUCLEAR ELECTROWEAK CURRENT OPERATOR

The simplest description of nuclei is based on a non-relativistic many-body theory of interacting nucleons. Within this framework, the nuclear electromagnetic and weak-current operators are expressed in terms of those associated with the individual protons and neutrons—the so-called impulse approximation (IA). Such a description, though, is certainly incomplete. The nucleon-nucleon interaction is mediated at large internucleon distances by pion exchange, and indeed seems to be well represented, even at short and intermediate distances, by meson-exchange mechanisms, which naturally lead to effective many-body current operators. It should be realized that these meson-exchange current operators arise, as does the nucleon-nucleon interaction itself, as a consequence of the elimination of the mesonic degrees of freedom from the nuclear state vector. Clearly, such

an approach is justified only at energies below the threshold for meson (specifically, pion) production, since above this threshold these non-nucleonic degrees of freedom have to be explicitly included in the state vector.

The investigation of meson-exchange current effects on nuclear electroweak observables has a long history. The need for their inclusion was soon realized after Yukawa (1935) postulated that pions mediate the nuclear force. Villars (1947) and Miyazawa (1951) first considered their contributions to the magnetic moments of nuclei and found that they accounted for most of the existing discrepancies between experimental values and previous IA predictions. However, it was not until 1972, when Riska and Brown showed how pion-exchange currents could resolve the long-standing 10% discrepancy between the calculated and measured cross section for radiative proton-neutron capture, that the importance of such interaction currents was established at a quantitative level. Since then, there have been several calculations of two-body current effects in other processes, such as the deuteron electrodisintegration at threshold,¹ the charge² and magnetic form factors³ of the trinucleons, the β decay of tritium⁴ and the magnetic moments and

TABLE X. Isovector and isotensor energy differences in MeV; one-photon exchange and total, including charge symmetry-breaking and charge-dependent components of v_{NN} .

	$\langle v \rangle$	ΔE (GFMC)	ΔE (Expt.)
${}^3\text{He}-{}^3\text{H}$	0.680(1)	0.756(1)	0.764
${}^6\text{Be}-{}^6\text{He}$	2.095(4)	2.239(17)	2.345
${}^7\text{Be}-{}^7\text{Li}$	1.501(3)	—	1.644
${}^7\text{B}-{}^7\text{He}$	3.326(8)	—	4.10
${}^6\text{Be}+{}^6\text{He}-2\times{}^6\text{Li}^*$	0.558(3)	0.767(32)	0.670
${}^7\text{B}+{}^7\text{He}-{}^7\text{Li}^*-{}^7\text{Be}^*$	0.713(3)	—	0.69

¹These include the calculations of Hockert *et al.* (1973), Lock and Foldy (1975), Fabian and Arenhövel (1976, 1978), Leidemann and Arenhövel (1983), Mathiot (1984), Leidemann, Schmitt, and Arenhövel (1990), and Schiavilla and Riska (1991).

²These include the calculations of Kloet and Tjon (1974), Riska and Radomski (1977), Hadjimichael, Goulard, and Bornais, (1983), Struieve *et al.* (1987), and Schiavilla, Pandharipande, and Riska (1990).

³These include the calculations of Barroso and Hadjimichael (1975), Riska (1980), Maize and Kim (1984), and Schiavilla, Pandharipande, and Riska (1989).

⁴These include the calculations of Blomqvist (1970), Riska and Brown (1970), Chemtob and Rho (1971), Ciechanowicz and Truhlik (1984), Saito, Ishikawa, and Sasakawa (1990), and Carlson *et al.* (1991).

weak-axial-current matrix elements of medium- and heavy-weight nuclei.⁵ However, because of uncertainties in the many-body wave functions of heavy nuclei, the few-nucleon systems have played a rather special role, since for their ground (and, very recently, continuum) states, the Schrödinger equation can be solved with a high degree of accuracy using a variety of different techniques (see Sec. III). These studies have conclusively proven that a satisfactory quantitative description of electroweak observables requires a current operator consisting, at a minimum, of one- and two-body components.

Two-body electromagnetic and weak-current operators have conventionally been derived as the nonrelativistic limit of Feynman diagrams, in which the meson-baryon couplings have been obtained either from effective chiral Lagrangians (Riska, 1984) or from semi-empirical models for the off-shell pion-nucleon amplitude (Chemtob and Rho, 1971). These methods of constructing effective current operators, however, do not address the problem of how to model the composite structure of the hadrons in the phenomenological meson-baryon vertices. This structure is often parametrized in terms of form factors. For the electromagnetic case, however, gauge invariance actually puts constraints on these form factors by linking the divergence of the two-body currents to the commutator of the charge operator with the nucleon-nucleon interaction. The latter contains form factors, too, but these are determined phenomenologically by fitting nucleon-nucleon data. Thus the continuity equation reduces the model dependence of the two-body currents by relating them to the form of the interaction. This point of view has been emphasized by Riska and collaborators (Riska, 1985a, 1985b; Riska and Poppius, 1985; Blunden and Riska, 1992; Tsushima, Riska, and Blunden, 1993) and others (Buchmann, Leidemann, and Arenhövel, 1985; Ohta, 1989a, 1989b), and is adopted in the treatment of two-body currents that we discuss below.

The nuclear electromagnetic $\rho(\mathbf{q})$ and $\mathbf{j}(\mathbf{q})$ and axial $\mathbf{A}_a(\mathbf{q})$ current operators are expanded into a sum of one-, two-, and many-body terms that operate on the nucleon degrees of freedom:

$$\rho(\mathbf{q}) = \sum_i \rho_i^{(1)}(\mathbf{q}) + \sum_{i<j} \rho_{ij}^{(2)}(\mathbf{q}) + \dots, \quad (5.1)$$

$$\mathbf{j}(\mathbf{q}) = \sum_i \mathbf{j}_i^{(1)}(\mathbf{q}) + \sum_{i<j} \mathbf{j}_{ij}^{(2)}(\mathbf{q}) + \dots, \quad (5.2)$$

$$\mathbf{A}_a(\mathbf{q}) = \sum_i \mathbf{A}_{a,i}^{(1)}(\mathbf{q}) + \sum_{i<j} \mathbf{A}_{a,ij}^{(2)}(\mathbf{q}) + \dots, \quad (5.3)$$

where a is an isospin index.

⁵These include the calculations of Dubach, Koch, and Donnelly (1976), Dubach (1980), Mathiot and Desplanques (1981), Suzuki *et al.* (1981a, 1981b), Donnelly and Sick (1984), and Towner (1987).

The one-body operators $\rho_i^{(1)}$ and $\mathbf{j}_i^{(1)}$ are obtained from the covariant single-nucleon current

$$j^\mu = \bar{u}(\mathbf{p}') \left[F_1(Q^2) \gamma^\mu + F_2(Q^2) \frac{i\sigma^{\mu\nu} q_\nu}{2m} \right] u(\mathbf{p}), \quad (5.4)$$

where \mathbf{p} and \mathbf{p}' are the initial and final momenta, respectively, of a nucleon of mass m , and $F_1(Q^2)$ and $F_2(Q^2)$ are its Dirac and Pauli form factors taken as a function of the four-momentum transfer $Q^2 = -q_\mu q^\mu > 0$, with $q_\mu = p'_\mu - p_\mu$. The Bjorken and Drell convention (Bjorken and Drell, 1964) is used for the γ matrices, and $\sigma^{\mu\nu} = (i/2)[\gamma^\mu, \gamma^\nu]$. The j_μ is expanded in powers of $1/m$ and, including terms up to order $1/m^2$, the charge ($\mu=0$) component can be written as

$$\rho_i^{(1)}(\mathbf{q}) = \rho_{i,\text{NR}}^{(1)}(\mathbf{q}) + \rho_{i,\text{RC}}^{(1)}(\mathbf{q}), \quad (5.5)$$

with

$$\rho_{i,\text{NR}}^{(1)}(\mathbf{q}) = \epsilon_i e^{i\mathbf{q} \cdot \mathbf{r}_i}, \quad (5.6)$$

$$\rho_{i,\text{RC}}^{(1)}(\mathbf{q}) = \left(\frac{1}{\sqrt{1 + Q^2/4m^2}} - 1 \right) \epsilon_i e^{i\mathbf{q} \cdot \mathbf{r}_i} - \frac{i}{4m^2} (2\mu_i - \epsilon_i) \mathbf{q} \cdot (\boldsymbol{\sigma}_i \times \mathbf{p}_i) e^{i\mathbf{q} \cdot \mathbf{r}_i}, \quad (5.7)$$

while the current components ($\mu=1,2,3$) are expressed as

$$\mathbf{j}_i^{(1)}(\mathbf{q}) = \frac{1}{2m} \epsilon_i \{ \mathbf{p}_i, e^{i\mathbf{q} \cdot \mathbf{r}_i} \} - \frac{i}{2m} \mu_i \mathbf{q} \times \boldsymbol{\sigma}_i e^{i\mathbf{q} \cdot \mathbf{r}_i}, \quad (5.8)$$

where $\{ \dots, \dots \}$ denotes the anticommutator. Here we have defined

$$\epsilon_i \equiv \frac{1}{2} [G_E^S(Q^2) + G_E^V(Q^2) \tau_{z,i}], \quad (5.9)$$

$$\mu_i \equiv \frac{1}{2} [G_M^S(Q^2) + G_M^V(Q^2) \tau_{z,i}], \quad (5.10)$$

and \mathbf{p} , $\boldsymbol{\sigma}$, and $\boldsymbol{\tau}$ are the nucleon's momentum, Pauli spin, and isospin operators, respectively. The two terms proportional to $1/m^2$ in $\rho_{i,\text{RC}}^{(1)}$ are the well-known Darwin-Foldy and spin-orbit relativistic corrections (deForest and Walecka, 1966; Friar, 1973).

The superscripts S and V of the Sachs form factors G_E and G_M denote, respectively, isoscalar and isovector combinations of the proton and neutron electric and magnetic form factors (Sachs, 1962). The G_E and G_M are related to the Dirac and Pauli form factors in Eq. (5.4) via

$$G_E(Q^2) = F_1(Q^2) - \frac{Q^2}{4m^2} F_2(Q^2), \quad (5.11)$$

$$G_M(Q^2) = F_1(Q^2) + F_2(Q^2) \quad (5.12)$$

and are normalized so that

$$G_E^S(Q^2=0) = G_E^V(Q^2=0) = 1, \quad (5.13)$$

$$G_M^S(Q^2=0) = \mu_p + \mu_n = 0.880 \mu_N, \quad (5.14)$$

$$G_M^V(Q^2=0) = \mu_p - \mu_n = 4.706 \mu_N, \quad (5.15)$$

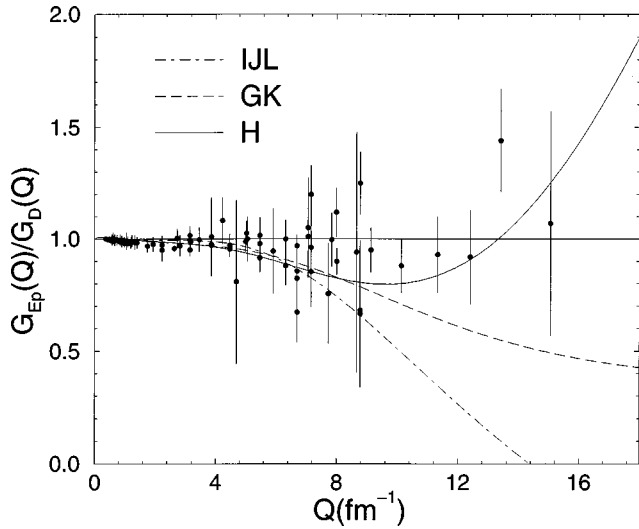


FIG. 9. The proton electric form-factor data (Kirk *et al.*, 1973; Borkowski *et al.*, 1975a, 1975b; Höhler *et al.*, 1976; Simon *et al.*, 1980; Walker *et al.*, 1989) compared with the dipole (D) and parametrizations of Iachello, Jackson, and Lande (1973) (IJL); Gari and Krümpelmann (1986) (GK); Höhler *et al.* (1976) (H). The ratio G_{Ep}/G_D is plotted.

where μ_p and μ_n are the magnetic moments of the proton and neutron in terms of the nuclear magneton μ_N . The Q^2 dependence of the Sachs form factors is determined by fitting electron-nucleon scattering data (Galster *et al.*, 1971; Iachello, Jackson, and Lande, 1973; Höhler *et al.*, 1976; Gari and Krümpelmann, 1986). The proton electric and magnetic form factors are experimentally fairly well known over a wide range of momentum transfers (Kirk *et al.*, 1973; Borkowski *et al.*, 1975a, 1975b; Höhler *et al.*, 1976; Simon *et al.*, 1980; Walker *et al.*, 1989) (see Figs. 9 and 10). In contrast, the present data on the neutron form factors (Albrecht *et al.*, 1968; Rock *et al.*, 1982; Platchkov *et al.*, 1990; Gari and Krümpelmann, 1992), particularly the electric one, are

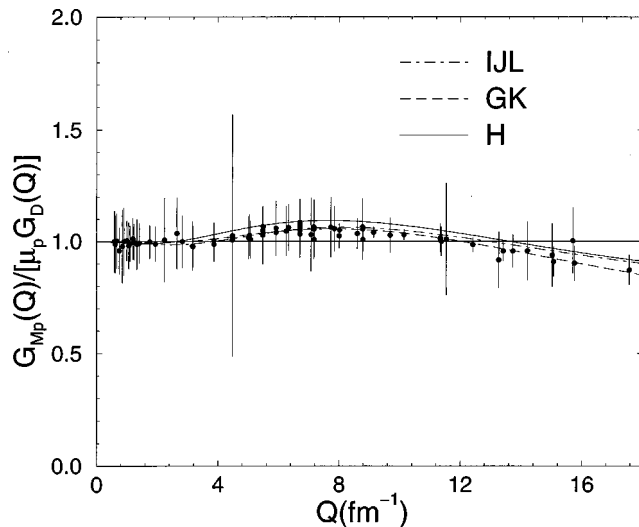


FIG. 10. Same as in Fig. 9, but for the proton magnetic form factor.

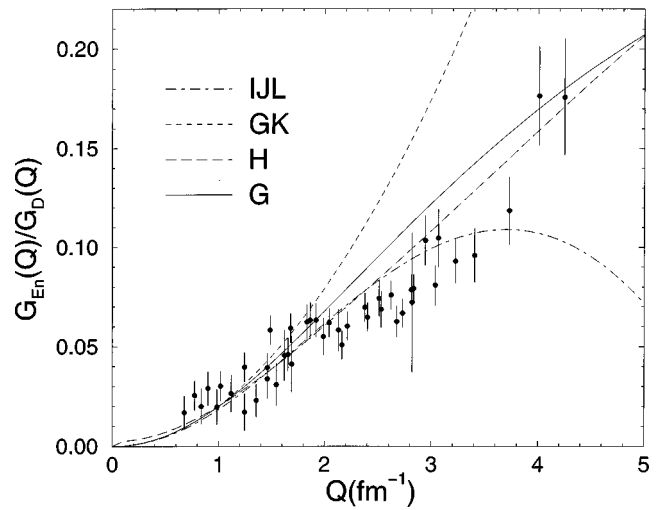


FIG. 11. The neutron electric form-factor data (Albrecht *et al.*, 1968; Rock *et al.*, 1982; Platchkov *et al.*, 1990; Gari and Krümpelmann, 1992) compared with parametrizations of Iachello, Jackson, and Lande (1973) (IJL); Gari and Krümpelmann (1986) (GK); Höhler *et al.* (1976) (H); and Galster *et al.* (1971) (G). The ratio G_{En}/G_D is plotted.

not as accurate and, therefore, the available semiempirical parametrizations for them differ widely, particularly at high-momentum transfers, as shown in Figs. 11 and 12. Until this uncertainty in the detailed behavior of the electromagnetic form factors of the nucleon is narrowed, quantitative predictions of electronuclear observables at high-momentum transfers will remain rather tentative. We shall reexamine this issue later in this review.

The one-body operator $\mathbf{A}_{a,i}^{(1)}$ is obtained from the non-relativistic limit of the nucleon axial current given by

$$A_a^\mu = \bar{u}(\mathbf{p}') \left[G_A(Q^2) \gamma^\mu + \frac{G_P(Q^2)}{2m} q^\mu \right] \gamma_5 \frac{\tau_a}{2} u(\mathbf{p}). \quad (5.16)$$

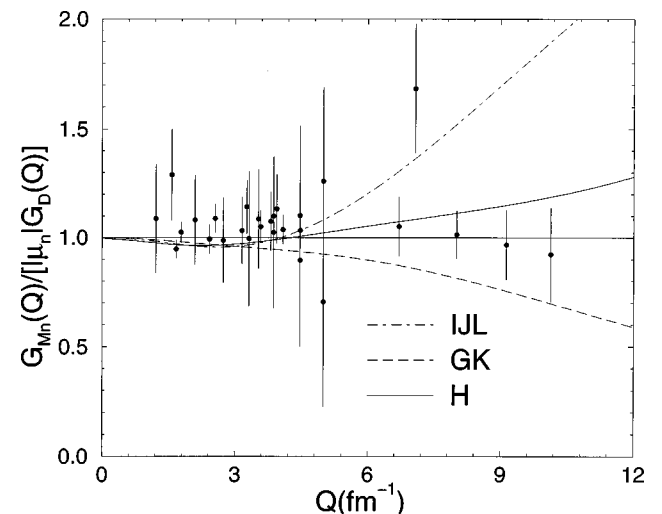


FIG. 12. Same as in Fig. 9, but for the neutron magnetic form factor.

The Q^2 dependence of the axial (G_A) and induced pseudoscalar (G_P) form factors are parametrized, respectively, as

$$G_A(Q^2) = \frac{g_A}{(1 + Q^2/\Lambda_A^2)^2}, \quad (5.17)$$

$$G_P(Q^2) = \frac{G_P(0)[g_{\pi NN}(Q^2)/g_{\pi NN}(0)]}{1 + Q^2/m_\pi^2}, \quad (5.18)$$

where $g_A = 1.262 \pm 0.006$, as determined from neutron β decay (Bopp *et al.*, 1986), and $(m_\mu/2m)G_P(Q^2 = m_\mu^2) = 8.2 \pm 2.4$, as obtained from muon capture in hydrogen (Bernabéu, 1982). Here m_μ is the muon mass. The value for the cutoff mass Λ_A is found to be approximately 1 GeV/ c^2 from an analysis of pion electroproduction data (Amaldi, Fubini, and Furlan, 1979) and measurements of the reaction $\nu_\mu + p \rightarrow n + \mu^+$ (Kitagaki *et al.*, 1983). In the induced pseudoscalar form factor $G_P(Q^2)$, the Q^2 dependence is dominated by the pion-pole contribution, and $g_{\pi NN}(Q^2)$ is the πNN strong-interaction form factor. Retaining only the leading contribution in $1/m$ in the nonrelativistic reduction of A_a^μ leads to the well-known expression for the Gamow-Teller transition operator

$$\mathbf{A}_{a,i}^{(1)}(\mathbf{q}) = -\frac{g_A}{2} \tau_{a,i} \boldsymbol{\sigma}_i e^{i\mathbf{q}\cdot\mathbf{r}_i}. \quad (5.19)$$

The next-to-leading-order correction involves, in the limit $Q^2 = 0$, a nonlocal operator, which arises from the time component ($\mu = 0$) of A_a^μ and is given by

$$A_{a,i}^{(1)}(\mathbf{q}) = -\frac{g_A}{4m} \tau_{a,i} \boldsymbol{\sigma}_i \cdot \{\mathbf{p}_i, e^{i\mathbf{q}\cdot\mathbf{r}_i}\}. \quad (5.20)$$

Our interest in the present review is focused on weak transitions involving very small momentum transfers Q^2 , and therefore the Q^2 dependence of the axial form factor has been suppressed.

The axial charge operator has pseudoscalar character, and there is no obvious observable in the few-nucleon systems which could be significantly affected by transitions induced by such an operator (Nozawa, Kohyama, and Kubodera, 1982). For example, in the β decays of ^3H and ^6He and in the weak-capture reactions $^1\text{H}(p, e^+ \nu_e)^2\text{H}$ and $^3\text{He}(p, e^+ \nu_e)^4\text{He}$, the matrix elements of the axial charge operator vanish, since the former involve transitions in which the initial and final states have the same parity, while the latter proceed predominantly via $J^\pi: 0^+ \Rightarrow 1^+$ transitions. However, the axial charge operator, particularly its two-body component, influences the rates of several $\Delta T = 1$ $J^\pi: 0^+ \Rightarrow 0^-$ transitions (Guichon, Giffon, and Samour, 1978; Jäger, Kirchbach, and Truhlik, 1984; Kirchbach, Jäger, and Gmitro, 1984; Kirchbach, Kamalov, and Jäger, 1984; Nozawa *et al.*, 1984; Towner, 1984; Kirchbach, 1986), such as, for example, the rates of the mirror transitions $^{16}\text{N}(0^-, 120 \text{ keV}) \rightarrow ^{16}\text{O}(0^+, \text{g.s.}) + e^- + \nu_e$ or $\mu_- + ^{16}\text{O} \rightarrow ^{16}\text{N}(0^-, 120 \text{ keV}) + \nu_\mu$ (Riska, 1984). We shall not discuss the axial charge operator any further in the present review.

The electromagnetic current operator must satisfy the continuity equation

$$\mathbf{q} \cdot \mathbf{j}(\mathbf{q}) = [H, \rho(\mathbf{q})], \quad (5.21)$$

where the Hamiltonian H includes two- and three-nucleon interactions

$$H = \sum_i \frac{\mathbf{p}_i^2}{2m} + \sum_{i < j} v_{ij} + \sum_{i < j < k} V_{ijk}. \quad (5.22)$$

To lowest order in $1/m$, the continuity equation (5.21) separates into separate continuity equations for the one-, two-, and many-body current operators,

$$\mathbf{q} \cdot \mathbf{j}_i^{(1)}(\mathbf{q}) = \left[\frac{\mathbf{p}_i^2}{2m}, \rho_{i,\text{NR}}^{(1)}(\mathbf{q}) \right], \quad (5.23)$$

$$\mathbf{q} \cdot \mathbf{j}_{ij}^{(2)}(\mathbf{q}) = [v_{ij}, \rho_{i,\text{NR}}^{(1)}(\mathbf{q}) + \rho_{j,\text{NR}}^{(1)}(\mathbf{q})], \quad (5.24)$$

and a similar equation involving three-nucleon currents and interactions.

The one-body current in Eq. (5.8) is easily shown to satisfy Eq. (5.23). The isospin and momentum dependence of the two- and three-nucleon interactions, however, lead to nonvanishing commutators with the nonrelativistic one-body charge operator and thus link the longitudinal part of the corresponding two- and three-body currents to the form of these interactions. In the present review, we shall limit our discussion to two-body currents, since, so far, no systematic investigation of three-body current (and charge) operators has been carried out.

This section is divided into four subsections. The first, Sec. V.A, deals with the two-body current operators that are required by gauge invariance. We denote them as “model independent” [adopting a nomenclature introduced by Riska (1989)], since they are constructed from the nucleon-nucleon interaction and contain no free parameters. We discuss in Sec. V.B those two-body currents, denoted as “model dependent,” which, being purely transverse, are not constrained by the continuity equation. To this class belong the currents associated with the $\rho\pi\gamma$ and $\omega\pi\gamma$ mechanisms, as well as those due to excitation of intermediate Δ -isobar resonances. However, it should be noted that the isoscalar $\rho\pi\gamma$ transition current has been linked (in the framework of the topological soliton or Skyrme-model approach to nucleon and nuclear structure) to the chiral anomaly (Nyman and Riska, 1986, 1987; Wakamatsu and Weise, 1988). This connection is extensively discussed in the review article by Riska (1989).

In Sec. V.C, we derive the structure of the most important two-body charge operators. The latter are model dependent and may be viewed as relativistic corrections. The use of these two-body charge operators in conjunction with nonrelativistic wave functions is founded more on phenomenological success than on solid theoretical argument. From this standpoint, however, theoretical predictions for the charge form factors of nuclei with $A = 2-6$ (based on calculations carried out within such a simple approach) have come remarkably close to the data, as will be shown later in the present review. A

study that systematically and consistently deals with the constraints that relativistic covariance imposes on both the electromagnetic current and the interaction models, as well as on the nuclear wave functions in systems with $A > 2$, is still lacking, although progress in this direction has been made in the past few years (Rupp and Tjon, 1992; Carlson, Pandharipande, and Schiavilla, 1993; Forest *et al.*, 1995; Stadler and Gross, 1997). The deuteron, however, has been studied extensively in relativistic approaches; relativistically covariant calculations of the deuteron structure functions and tensor polarization have been carried out within the framework of quasipotential reductions of the Bethe-Salpeter equation with one-boson-exchange interaction models (Hummel and Tjon, 1989, 1990; Van Orden, Devine, and Gross, 1995).

In Sec. V.D, we list the expressions for the axial two-body current operators commonly used in the study of weak transitions involving few-body nuclei (Carlson *et al.*, 1991). Their derivation is discussed in the review article by Towner (1987) and is not repeated here. We only emphasize that, in contrast to the electromagnetic case, the axial current operator is not conserved. Its two-body components cannot be directly linked to the nucleon-nucleon interaction and, in this sense, are completely model dependent. Indeed, the partially conserved axial-vector current (PCAC) relations, which play a role analogous to that of current conservation in the electromagnetic case, lead to model-independent predictions only for the axial exchange charge operator.

A. Electromagnetic two-body current operators from the two-nucleon interaction

All realistic NN interactions include isospin-dependent central, spin-spin, and tensor components,

$$[v^\tau(r_{ij}) + v^{\sigma\tau}(r_{ij})\boldsymbol{\sigma}_i \cdot \boldsymbol{\sigma}_j + v^{t\tau}(r_{ij})S_{ij}]\boldsymbol{\tau}_i \cdot \boldsymbol{\tau}_j, \quad (5.25)$$

where the $\sigma\tau$ and $t\tau$ terms include the long-range one-pion-exchange potential. The $\boldsymbol{\tau}_i \cdot \boldsymbol{\tau}_j$ operator, which does not commute with the charge operators in Eq. (5.24), is formally equivalent to an implicit momentum dependence (Sachs, 1948). This can be seen when we consider the product of space-, spin-, and isospin-exchange operators, denoted, respectively, as E_{ij} , E_{ij}^σ , and E_{ij}^τ , where

$$E_{ij} = \exp\left[i \int_{\mathbf{r}_i}^{\mathbf{r}_j} d\mathbf{s} \cdot (\mathbf{p}_i - \mathbf{p}_j)\right], \quad (5.26)$$

$$E_{ij}^\sigma = \frac{1 + \boldsymbol{\sigma}_i \cdot \boldsymbol{\sigma}_j}{2}, \quad (5.27)$$

$$E_{ij}^\tau = \frac{1 + \boldsymbol{\tau}_i \cdot \boldsymbol{\tau}_j}{2}. \quad (5.28)$$

They must satisfy $E_{ij}E_{ij}^\sigma E_{ij}^\tau = -1$. The line integral in Eq. (5.26) is along any path leading from \mathbf{r}_i to \mathbf{r}_j . Thus two-body current operators associated with the $\boldsymbol{\tau}_i \cdot \boldsymbol{\tau}_j$ -dependent interactions, Eq. (5.25), can be constructed by minimal substitution in the space-exchange operator:

$$\mathbf{p}_i \rightarrow \mathbf{p}_i - \boldsymbol{\epsilon}_i \mathbf{A}(\mathbf{r}_i), \quad (5.29)$$

where $\mathbf{A}(\mathbf{r}_i)$ is the vector potential. However, due to the arbitrariness of the integration path in Eq. (5.26), such a prescription does not lead to unique two-body currents (Nyman, 1967). Therefore an assumption has to be made about the dynamic origin of the interactions in Eq. (5.25) in order to construct the associated currents.

At intermediate and large internucleon separation distances, the v^τ , $v^{\sigma\tau}$, and $v^{t\tau}$ interactions are assumed to be due to π -meson and ρ -meson exchanges. The πNN and ρNN coupling Lagrangians are given by

$$L_{\pi NN}(x) = \frac{f_{\pi NN}}{m_\pi} \bar{\psi}(x) \gamma^\mu \gamma_5 \boldsymbol{\tau} \psi(x) \cdot \partial_\mu \boldsymbol{\pi}(x), \quad (5.30)$$

$$L_{\rho NN}(x) = g_{\rho NN} \bar{\psi}(x) \left[\left(\gamma^\mu + \frac{\kappa_\rho}{2m} \sigma^{\mu\nu} \partial_\nu \right) \boldsymbol{\rho}_\mu(x) \right] \cdot \boldsymbol{\tau} \psi(x), \quad (5.31)$$

where $\boldsymbol{\pi}(x)$ and $\boldsymbol{\rho}(x)$ are the π - and ρ -meson $T=1$ fields; $\psi(x)$ is the $T=\frac{1}{2}$ nucleon field; m_π and m_ρ are the meson masses; $f_{\pi NN}$, $g_{\rho NN}$, and κ_ρ are the pseudovector πNN , and the vector and tensor ρNN coupling constants ($f_{\pi NN}^2/4\pi=0.075$, $g_{\rho NN}^2/4\pi=0.55$, and $\kappa_\rho=6.6$), respectively. By performing a nonrelativistic reduction of the one-boson-exchange Feynman amplitudes, one obtains the π - and ρ -meson-exchange interactions in momentum space as

$$[v_{\rho S}(k) + [v_\pi(k) + 2v_\rho(k)]k^2 \boldsymbol{\sigma}_i \cdot \boldsymbol{\sigma}_j - [v_\pi(k) - v_\rho(k)]S_{ij}(\mathbf{k})] \boldsymbol{\tau}_i \cdot \boldsymbol{\tau}_j, \quad (5.32)$$

where

$$v_{\rho S}(k) \equiv g_{\rho NN}^2 \frac{1}{k^2 + m_\rho^2}, \quad (5.33)$$

$$v_\pi(k) \equiv -\frac{f_{\pi NN}^2}{3m_\pi^2} \frac{1}{k^2 + m_\pi^2}, \quad (5.34)$$

$$v_\rho(k) \equiv -\frac{g_{\rho NN}^2}{12m^2} \frac{(1 + \kappa_\rho)^2}{k^2 + m_\rho^2}. \quad (5.35)$$

The tensor operator in momentum space is defined as

$$S_{ij}(\mathbf{k}) = k^2 \boldsymbol{\sigma}_i \cdot \boldsymbol{\sigma}_j - 3 \boldsymbol{\sigma}_i \cdot \mathbf{k} \boldsymbol{\sigma}_j \cdot \mathbf{k}. \quad (5.36)$$

The isovector two-body currents corresponding to π and ρ exchanges can be derived by minimal substitution $\partial_\mu \rightarrow \partial_\mu \pm iA_\mu(x)$ in the πNN and ρNN coupling Lagrangians, Eqs. (5.30) and (5.31), and in the free π - and ρ -meson Lagrangians:

$$L_\pi(x) = \frac{1}{2} \partial_\mu \boldsymbol{\pi}(x) \cdot \partial^\mu \boldsymbol{\pi}(x) - \frac{m_\pi^2}{2} \boldsymbol{\pi}(x) \cdot \boldsymbol{\pi}(x), \quad (5.37)$$

$$L_\rho(x) = -\frac{1}{4} [\partial_\mu \boldsymbol{\rho}_\nu(x) - \partial_\nu \boldsymbol{\rho}_\mu(x)] \cdot [\partial^\mu \boldsymbol{\rho}^\nu(x) - \partial^\nu \boldsymbol{\rho}^\mu(x)] - \frac{m_\rho^2}{2} \boldsymbol{\rho}^\mu(x) \cdot \boldsymbol{\rho}_\mu(x). \quad (5.38)$$

The nonrelativistic reduction of the Feynman amplitudes shown in Fig. 13 leads to the momentum-space two-body operators:

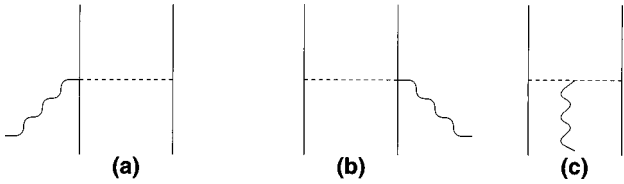


FIG. 13. Feynman diagram representation of the isovector two-body currents associated with pion exchange: Solid lines, nucleons; dashed lines, pions; wavy lines, photons.

$$\mathbf{j}_{ij,\pi}^{(2)}(\mathbf{k}_i, \mathbf{k}_j) = 3i(\boldsymbol{\tau}_i \times \boldsymbol{\tau}_j)_z G_E^V(Q^2) \left[v_\pi(k_j) \boldsymbol{\sigma}_i (\boldsymbol{\sigma}_j \cdot \mathbf{k}_j) - v_\pi(k_i) \boldsymbol{\sigma}_j (\boldsymbol{\sigma}_i \cdot \mathbf{k}_i) + \frac{\mathbf{k}_i - \mathbf{k}_j}{k_i^2 - k_j^2} [v_\pi(k_i) - v_\pi(k_j)] (\boldsymbol{\sigma}_i \cdot \mathbf{k}_i) (\boldsymbol{\sigma}_j \cdot \mathbf{k}_j) \right], \quad (5.39)$$

$$\mathbf{j}_{ij,\rho}^{(2)}(\mathbf{k}_i, \mathbf{k}_j) = -3i(\boldsymbol{\tau}_i \times \boldsymbol{\tau}_j)_z G_E^V(Q^2) \left[v_\rho(k_j) \boldsymbol{\sigma}_i \times (\boldsymbol{\sigma}_j \times \mathbf{k}_j) - v_\rho(k_i) \boldsymbol{\sigma}_j \times (\boldsymbol{\sigma}_i \times \mathbf{k}_i) - \frac{v_\rho(k_i) - v_\rho(k_j)}{k_i^2 - k_j^2} \times [(\mathbf{k}_i - \mathbf{k}_j) (\boldsymbol{\sigma}_i \times \mathbf{k}_i) \cdot (\boldsymbol{\sigma}_j \times \mathbf{k}_j) + (\boldsymbol{\sigma}_i \times \mathbf{k}_i) \boldsymbol{\sigma}_j \cdot (\mathbf{k}_i \times \mathbf{k}_j) + (\boldsymbol{\sigma}_j \times \mathbf{k}_j) \boldsymbol{\sigma}_i \cdot (\mathbf{k}_i \times \mathbf{k}_j)] + \frac{\mathbf{k}_i - \mathbf{k}_j}{k_i^2 - k_j^2} [v_{\rho S}(k_i) - v_{\rho S}(k_j)] \right], \quad (5.40)$$

where \mathbf{k}_i and \mathbf{k}_j are the fractional momenta delivered to nucleons i and j with $\mathbf{q} = \mathbf{k}_i + \mathbf{k}_j$, and the form factor $G_E^V(Q^2)$ has been included to take into account the electromagnetic structure of the nucleon. The continuity equation requires that the same form factor be used to describe the electromagnetic structure of the hadrons in the longitudinal part of the current operator and in the charge operator. Again, the continuity equation places no restrictions on the electromagnetic form factors that may be used in the transverse parts of the current. Ignoring this ambiguity, the choice made here [$G_E^V(Q^2)$] satisfies the “minimal” requirement of current conservation. However, for a somewhat different discussion of this point we refer the reader to Gross and Henning (1992).

The first two terms in Eqs. (5.39) and (5.40) are seagull currents corresponding to diagrams (a) and (b) of Fig. 13, while the remaining terms are the currents due to π meson and ρ meson in flight. These operators, with the $v_\pi(k)$, $v_\rho(k)$, and $v_{\rho S}(k)$ propagators suitably modified by the inclusion of form factors, have commonly been used in the investigation of exchange current effects in nuclei. A first systematic derivation of pion- and heavy-meson-exchange current operators was in fact given by Chemtob and Rho in their seminal 1971 paper. While these simple two-body currents satisfy the continuity equation with the corresponding meson-

exchange interactions, they do not satisfy the continuity equation with the realistic models for the nucleon-nucleon interaction that are used to construct nuclear wave functions. A method of obtaining current operators that satisfy the continuity equation for any given v_{ij}^τ , $v_{ij}^{\sigma\tau}$, and $v_{ij}^{t\tau}$ interactions has been proposed by Riska (1985b) and, independently, by Arenhovel and co-workers (Buchmann, Leidemann, and Arenhovel, 1985). In this method these interactions are attributed to exchanges of families of π -like pseudoscalar (PS) and ρ -like vector (V) mesons. The sum of all $T=1$ PS -exchange and V -exchange terms is then obtained as

$$v_{PS}(k) = [v^{\sigma\tau}(k) - 2v^{t\tau}(k)]/3, \quad (5.41)$$

$$v_V(k) = [v^{\sigma\tau}(k) + v^{t\tau}(k)]/3, \quad (5.42)$$

$$v_{VS}(k) = v^\tau(k), \quad (5.43)$$

where

$$v^\tau(k) = 4\pi \int_0^\infty r^2 dr j_0(kr) v^\tau(r), \quad (5.44)$$

$$v^{\sigma\tau}(k) = \frac{4\pi}{k^2} \int_0^\infty r^2 dr [j_0(kr) - 1] v^{\sigma\tau}(r), \quad (5.45)$$

$$v^{t\tau}(k) = \frac{4\pi}{k^2} \int_0^\infty r^2 dr j_2(kr) v^{t\tau}(r). \quad (5.46)$$

The expression for $v^{\sigma\tau}(k)$ reflects the fact that in all nucleon-nucleon interaction models derived from a relativistic scattering amplitude a δ -function term has been dropped from the spin-spin component. The current operators $\mathbf{j}_{ij,PS}^{(2)}$ and $\mathbf{j}_{ij,V}^{(2)}$, obtained by using $v_{PS}(k)$, $v_V(k)$, and $v_{VS}(k)$ in place of $v_\pi(k)$, $v_\rho(k)$, and $v_{\rho S}(k)$ in Eqs. (5.39) and (5.40), satisfy the continuity equation with the v^τ , $v^{\sigma\tau}$, and $v^{t\tau}$ potentials in the model interaction used to fit the nucleon-nucleon scattering data and to calculate nuclear ground- and scattering-state wave functions. In particular, there is no ambiguity left as to the proper form of the short-range behavior of the two-body current operator, as this is determined by the interaction model. Configuration-space expressions may be obtained from

$$\mathbf{j}_{ij,a}^{(2)}(\mathbf{q}) = \int d\mathbf{x} e^{i\mathbf{q}\cdot\mathbf{x}} \int \frac{d\mathbf{k}_i}{(2\pi)^3} \frac{d\mathbf{k}_j}{(2\pi)^3} \times e^{i\mathbf{k}_i\cdot(\mathbf{r}_i-\mathbf{x})} e^{i\mathbf{k}_j\cdot(\mathbf{r}_j-\mathbf{x})} \mathbf{j}_{ij,a}^{(2)}(\mathbf{k}_i, \mathbf{k}_j), \quad (5.47)$$

where $a = PS$ or V , and are given explicitly by Schiavilla, Pandharipande, and Riska (1989).

Although the Riska prescription obviously cannot be unique, it has nevertheless been shown to provide, at low and moderate values of momentum transfer (typically, below ≈ 1 GeV/ c), a satisfactory description of most observables in which isovector two-body currents play a large (if not dominant) role, such as the deuteron threshold electrodisintegration (Buchmann, Leidemann, and Arenhovel, 1985; Schiavilla and Riska, 1991), the neutron and proton radiative captures on protons

(Schiavilla and Riska, 1991) and deuterons (Viviani, Schiavilla, and Kievsky, 1996) at low energies, and the magnetic moments and form factors of the trinucleons (Schiavilla, Pandharipande, and Riska, 1989; Schiavilla and Viviani, 1996).

In addition to spin-spin and tensor components, all realistic interactions contain spin-orbit and quadratic momentum-dependent terms. The construction of the associated two-body current operators is less straightforward. A procedure similar to that used above to derive the π -like and ρ -like currents has been generalized to the case of the two-body currents from the spin-orbit interactions (Carlson *et al.*, 1990). It consists, in essence, of attributing the two-body currents to exchanges of σ -like and ω -like mesons for the isospin-independent terms, and to ρ -like mesons for the isospin-dependent ones. The explicit form of the resulting currents, as well as their derivation, can be found in the original reference (Carlson *et al.*, 1990).

The quadratic momentum-dependent terms represent, on the one hand, relativistic corrections to the central and spin-orbit interactions, which are proportional to \mathbf{p}^2 (\mathbf{p} is the relative momentum) and, on the other hand, quadratic spin-orbit interactions. To construct the associated two-body current operators is, in general, difficult or impossible, because of the many approximations typically used to simplify the structure of these interaction components. Furthermore, some interactions, such as the Argonne models (Wiringa, Smith, and Ainsworth, 1984; Wiringa, Stoks, and Schiavilla, 1995), contain terms proportional to \mathbf{L}^2 , which do not appear in any natural way in boson-exchange models. Hence, in view of the fact that the numerical significance of these operators is small anyway, the two-body currents associated with the quadratic momentum dependence are obtained by minimal substitution [see Eq. (5.29)] into the corresponding interaction components (Schiavilla, Pandharipande, and Riska, 1989).

The currents associated with the momentum dependence of the interaction are fairly short ranged and have both isoscalar and isovector terms. Their contribution to isovector observables is found to be numerically much smaller than that due to the leading π -like current (Schiavilla, Pandharipande, and Riska, 1989; Schiavilla and Viviani, 1996). However, they give non-negligible corrections to isoscalar observables, such as the deuteron magnetic moment and $B(Q)$ -structure function (Schiavilla and Riska, 1991; Wiringa, Stoks, and Schiavilla, 1995), and isoscalar combination of the magnetic moments and form factors of the trinucleons (Schiavilla, Pandharipande, and Riska, 1989; Schiavilla and Viviani, 1996), as will be reported later in this article.

B. "Model-dependent" electromagnetic two-body current operators

The two-body currents discussed in the previous subsection are constrained by the continuity equation and do not contain any free parameters, since they are determined directly from the nucleon-nucleon interaction.

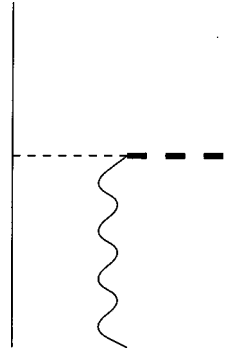


FIG. 14. Feynman diagram representation of the isoscalar $\rho\pi\gamma$ and isovector $\omega\pi\gamma$ transition currents: Solid line, nucleons; dashed line, pions; thick-dashed line, vector mesons (either ρ or ω); wavy line, photons.

They can therefore be viewed as "model independent." There are, however, additional two-body currents that are purely transverse. These will be referred to as "model-dependent" two-body currents.

The class of model-dependent currents that has been considered in the literature contains two-body operators associated with electromagnetic transition couplings between different mesons or with excitation of intermediate nucleon resonances (specifically, the Δ isobar).

1. The $\rho\pi\gamma$ and $\omega\pi\gamma$ current operators

Among the currents due to transition couplings, the $\rho\pi\gamma$ and $\omega\pi\gamma$ mechanisms, illustrated by the Feynman diagrams in Fig. 14, have been considered most commonly in the literature (Chemtob, Moniz, and Rho, 1974; Gari and Hyuga, 1976). The associated two-body operators have short range, because of the large ρ - and ω -meson masses and, therefore, their contribution to electromagnetic observables at low and moderate values of momentum transfers ($Q \ll 1$ GeV/c) is typically small. These currents can be derived from the Feynman diagrams in Fig. 14 by considering the transition current matrix elements given by

$$\begin{aligned} \langle \pi^a(k) | j_\mu(0) | \rho^b(p, \epsilon) \rangle \\ = - \frac{G_{\rho\pi\gamma}(Q^2)}{m_\rho} \delta_{ab} \epsilon_{\mu\nu\sigma\tau} p^\nu k^\sigma \epsilon^\tau, \end{aligned} \quad (5.48)$$

and a similar expression for the $\omega\pi\gamma$ transition current matrix element, with $G_{\rho\pi\gamma}(Q^2)/m_\rho$ replaced by $G_{\omega\pi\gamma}(Q^2)/m_\omega$ (ϵ is the polarization vector of the vector meson). The values of the transition form factors $G_{\rho\pi\gamma}$ and $G_{\omega\pi\gamma}$ at the photon point are known to be $G_{\rho\pi\gamma}(Q^2=0) \equiv g_{\rho\pi\gamma} = 0.56$ (Berg *et al.*, 1980) and $G_{\omega\pi\gamma}(Q^2=0) \equiv g_{\omega\pi\gamma} = 0.68$ (Chemtob and Rho, 1971) from the measured widths of the $\rho \rightarrow \pi + \gamma$ and $\omega \rightarrow \pi + \gamma$ decays, while the Q^2 dependence is modeled using vector-meson dominance:

$$G_{\rho\pi\gamma}(Q^2) = g_{\rho\pi\gamma} / (1 + Q^2/m_\rho^2), \quad (5.49)$$

$$G_{\omega\pi\gamma}(Q^2) = g_{\omega\pi\gamma} / (1 + Q^2/m_\omega^2). \quad (5.50)$$

A nonrelativistic reduction to lowest order of the amplitudes in Fig. 14 leads to the momentum-space expressions:

$$\mathbf{j}_{\rho\pi\gamma}(\mathbf{k}_i, \mathbf{k}_j) = i \frac{f_\pi g_\rho G_{\rho\pi\gamma}(Q^2)}{m_\pi m_\rho} \boldsymbol{\tau}_i \cdot \boldsymbol{\tau}_j \mathbf{k}_i \times \mathbf{k}_j \times \left[\frac{\boldsymbol{\sigma}_i \cdot \mathbf{k}_i}{(k_i^2 + m_\pi^2)(k_j^2 + m_\rho^2)} - \frac{\boldsymbol{\sigma}_j \cdot \mathbf{k}_j}{(k_i^2 + m_\rho^2)(k_j^2 + m_\pi^2)} \right], \quad (5.51)$$

$$\mathbf{j}_{\omega\pi\gamma}(\mathbf{k}_i, \mathbf{k}_j) = i \frac{f_\pi g_\omega G_{\omega\pi\gamma}(Q^2)}{m_\omega m_\pi} \mathbf{k}_i \times \mathbf{k}_j \times \left[\frac{\boldsymbol{\sigma}_i \cdot \mathbf{k}_i}{(k_i^2 + m_\pi^2)(k_j^2 + m_\omega^2)} \tau_{i,z} - \frac{\boldsymbol{\sigma}_j \cdot \mathbf{k}_j}{(k_i^2 + m_\omega^2)(k_j^2 + m_\pi^2)} \tau_{j,z} \right]. \quad (5.52)$$

Note that the next-to-leading-order terms in the nonrelativistic expansion of the $\rho\pi\gamma$ amplitude are proportional to $(1 + \kappa_\rho)/m^2$, where κ_ρ is the large ρNN tensor coupling. They have been found to substantially reduce the contribution of the leading term, Eq. (5.51), in a calculation of the deuteron $B(Q)$ structure function (Schiavilla and Riska, 1991). The importance of these $1/m^2$ corrections was first stressed by Hummel and Tjon (1989) in a relativistic boson-exchange-model calculation of the deuteron form factors, based on the Blankenbecler-Sugar reduction of the Bethe-Salpeter equation.

Monopole form factors at the pion and vector-meson strong-interaction vertices, given by

$$f_a(k) = \frac{\Lambda_a^2 - m_a^2}{\Lambda_a^2 + k^2}, \quad a = \pi, \rho, \quad (5.53)$$

are introduced to take into account the finite size of nucleons and mesons. It should be emphasized that the contributions due to these operators are rather sensitive to the values used for the (poorly known) vector-meson coupling constants to the nucleon and cutoff parameters Λ_a , $a = \pi, \rho$, and ω (Carlson, Pandharipande, and Schiavilla, 1991). In recent calculations, the values of these have been taken as $\Lambda_\pi = 0.9$ GeV and $\Lambda_\rho = \Lambda_\omega = 1.35$ GeV from studies of the magnetic form factor of the deuteron (Wiringa, Stoks, and Schiavilla, 1995) and radiative capture of neutrons on ^2H (Viviani, Schiavilla, and Kievsky, 1996) and ^3He (Schiavilla *et al.*, 1992).

2. Currents associated with Δ -isobar degrees of freedom

The theoretical framework adopted in the present review article views the nucleus as made up of nucleons and assumes that all other subnucleonic degrees of freedom can be eliminated in favor of effective two- and many-body operators acting on the nucleons' coordi-

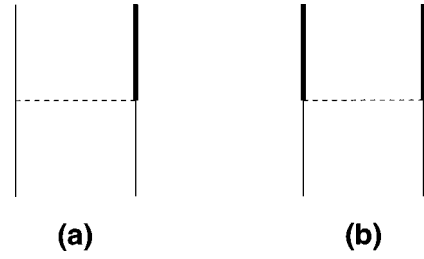


FIG. 15. Feynman diagram representation of the $NN \rightarrow N\Delta$ and $NN \rightarrow \Delta\Delta$ transition interactions due to one-pion exchange: Solid lines, nucleons; thick solid lines, Δ isobars; dashed lines, pions.

nates. The validity of this greatly simplified description—in which color-carrying quarks and gluons (the degrees of freedom of quantum chromodynamics, the fundamental theory of the strong interaction) are assembled into colorless clusters (the nucleons), and these clusters are taken as effective constituents of the nucleus—is based on the success it has achieved in the quantitative prediction of many nuclear observables. However, it is interesting to consider corrections to this picture by taking into account the degrees of freedom associated with colorless quark-gluon clusters other than the nucleons as additional constituents of the nucleus. At least when treating phenomena that do not explicitly involve meson production, it is reasonable to expect that the lowest excitation of the nucleon, the Δ isobar, plays a leading role (Green, 1976; Sauer, 1986).

In such an approach, the wave function of a nucleus is written as

$$\Psi_{N+\Delta} = \Psi(NN \dots NN) + \Psi^{(1)}(NN \dots N\Delta) + \Psi^{(2)}(NN \dots \Delta\Delta) + \dots, \quad (5.54)$$

where Ψ is that part of the total wave function consisting only of nucleons; the term $\Psi^{(1)}$ is the component in which a single nucleon has been transformed into a Δ isobar, and so on. These Δ -isobar admixtures are generated by transition interactions, the long-range part of which are obtained from a $\pi N\Delta$ coupling Lagrangian of the form

$$L_{\pi N\Delta}(x) = \frac{f_{\pi N\Delta}}{m_\pi} \bar{\psi}^\mu(x) \mathbf{T} \psi(x) \cdot \partial_\mu \boldsymbol{\pi}(x) + \text{H.c.}, \quad (5.55)$$

where $\psi^\mu(x)$ is the isospin-spin 3/2 field of the Δ . The nonrelativistic reduction of the Feynman amplitudes in Fig. 15 leads to $NN \rightarrow N\Delta$ and $NN \rightarrow \Delta\Delta$ interactions, given by (Sugawara and von Hippel, 1968)

$$v_{NN \rightarrow N\Delta}(ij) = [v^{\sigma\tau\text{II}}(r_{ij}) \boldsymbol{\sigma}_i \cdot \mathbf{S}_j + v'^{\tau\text{II}}(r_{ij}) S_{ij}^{\text{II}}] \boldsymbol{\tau}_i \cdot \mathbf{T}_j, \quad (5.56)$$

$$v_{NN \rightarrow \Delta\Delta}(ij) = [v^{\sigma\tau\text{III}}(r_{ij}) \mathbf{S}_i \cdot \mathbf{S}_j + v'^{\tau\text{III}}(r_{ij}) S_{ij}^{\text{III}}] \mathbf{T}_i \cdot \mathbf{T}_j, \quad (5.57)$$

with

$$v^{\sigma\tau a}(r) = \frac{(ff)_a m_\pi}{4\pi} \frac{e^{-x}}{3x}, \quad (5.58)$$

$$v^{\text{tra}}(r) = \frac{(ff)_a m_\pi}{4\pi} \frac{1}{3} \left(1 + \frac{3}{x} + \frac{3}{x^2} \right) \frac{e^{-x}}{x}, \quad (5.59)$$

$a = \text{II}, \text{III}$, $x = m_\pi r$, and $(ff)_a \equiv f_{\pi NN} f_{\pi N\Delta}$, $f_{\pi N\Delta} f_{\pi N\Delta}$ for $a = \text{II}, \text{III}$, respectively. Here \mathbf{S} and \mathbf{T} are spin- and isospin-transition operators, which convert the nucleon into a Δ isobar. The matrix elements of their spherical components S_μ , $S_{\mu=\pm 1} = \mp (S_x \pm iS_y)/\sqrt{2}$, and $S_0 = S_z$, are given by

$$\langle 3/2s_\Delta | S_\mu | 1/2s \rangle = \langle 1\mu, 1/2s | 3/2s_\Delta \rangle \epsilon_\mu^*, \quad (5.60)$$

where $\epsilon_\pm = \mp 1(\hat{\mathbf{x}} \pm i\hat{\mathbf{y}})/\sqrt{2}$, $\epsilon_0 = \hat{\mathbf{z}}$, and similarly for T_μ . The S_{ij}^{II} and S_{ij}^{III} are tensor operators in which the Pauli spin operators of particle i (or j), and particles i and j , are replaced by corresponding spin-transition operators.

The coupling constants $f_{\pi N\Delta}$ and $f_{\pi\Delta\Delta}$ are not well known. The static quark model predicts for them the values $f_{\pi N\Delta}^2/4\pi = 0.233$ and $f_{\pi\Delta\Delta}^2/4\pi = 0.00324$, while the Chew-Low theory gives $f_{\pi N\Delta}^2/4\pi = 0.324$ (Brown and Weise, 1975). However, the observed Δ -decay width provides a value for $f_{\pi N\Delta}^2/4\pi$ that is about 10% larger than that obtained in the Chew-Low theory (Sugawara and von Hippel, 1968).

There are, of course, additional contributions, arising from other processes, such as $N\Delta \rightarrow \Delta\Delta$ and $\Delta\Delta \rightarrow \Delta\Delta$ transitions, or due to exchanges of heavier mesons, such as the ρ meson. In models of interactions with explicit N and Δ degrees of freedom, these contributions are constrained by fits to the NN elastic-scattering data and deuteron properties (Wiringa, Smith, and Ainsworth, 1984; Sauer, 1986).

Once the NN , $N\Delta$, and $\Delta\Delta$ interactions have been determined, there still remains the problem of how to generate isobar configurations in a many-nucleon system. Essentially, the methods fall into two categories: perturbation theory and coupled channels.

In perturbation theory, one- and two- Δ components are generated via

$$\Psi^{(1)} = \frac{1}{m - m_\Delta} \sum_{i < j} [v(ij)_{NN \rightarrow \Delta N} + v(ij)_{NN \rightarrow N\Delta}] \Psi, \quad (5.61)$$

$$\Psi^{(2)} = \frac{1}{2(m - m_\Delta)} \sum_{i < j} v(ij)_{NN \rightarrow \Delta\Delta} \Psi, \quad (5.62)$$

where the kinetic-energy contributions in the denominators of Eqs. (5.61) and (5.62) have been neglected (static Δ approximation). This approximation has been often (in fact, almost exclusively) used in the literature to estimate the effect of Δ degrees of freedom on electroweak observables (Riska, 1989). However, it produces $N\Delta$ and $\Delta\Delta$ wave functions that are too large at short distances (Schiavilla *et al.*, 1992).

The most reliable way of generating isobar admixtures in nuclei is through the coupled-channel method. Because of its complexity, however, due to the large number of $N\Delta$ channels involved, it has been applied only

to relatively simple systems, to date the deuteron⁶ and triton.⁷ It is reviewed by Sauer (1986) and in a series of articles by Picklesimer, Rice, and Brandenburg (1991, 1992a, 1992b, 1992c, 1992d). A somewhat simpler approach, but one that has been used in studies of $A=3$ and 4 nuclei electroweak transitions (Schiavilla *et al.*, 1992; Viviani, Schiavilla, and Kievsky, 1996) and magnetic form factors (Schiavilla and Viviani, 1996), consists of a generalization of the correlation-operator technique (Kallio *et al.*, 1974; Schiavilla *et al.*, 1992), which has proven very useful in the variational theory of light nuclei, particularly in the context of variational Monte Carlo calculations. In such an approach, known as the transition-correlation-operator method, the nuclear wave function is written as

$$\Psi_{N+\Delta} = \left[S \prod_{i < j} (1 + U_{ij}^{\text{tr}}) \right] \Psi, \quad (5.63)$$

where S is the symmetrizer, and the transition operators U_{ij}^{tr} convert NN pairs into $N\Delta$ and $\Delta\Delta$ pairs.

In principle, the U_{ij}^{tr} and Ψ could be determined variationally by using a Hamiltonian containing an interaction that includes both nucleon and Δ degrees of freedom, such as the Argonne v_{28} model. Variational calculations of this type have not yet been attempted, however. Instead, in the studies carried out so far, Ψ is taken from solutions of a Hamiltonian with nucleons-only interactions, while the U_{ij}^{tr} is obtained from two-body bound and low-energy scattering state solutions of the full $N\Delta$ coupled-channel problem.

The $N \rightleftharpoons \Delta$ and $\Delta \rightarrow \Delta$ electromagnetic currents are given by

$$\mathbf{j}_i^{(1)}(\mathbf{q}; N \rightarrow \Delta) = -\frac{i}{2m} G_{\gamma N\Delta}(Q^2) e^{i\mathbf{q} \cdot \mathbf{r}_i} \mathbf{q} \times \mathbf{S}_i T_{z,i}, \quad (5.64)$$

$$\mathbf{j}_i^{(1)}(\mathbf{q}; \Delta \rightarrow \Delta) = -\frac{i}{24m} G_{\gamma\Delta\Delta}(Q^2) e^{i\mathbf{q} \cdot \mathbf{r}_i} \mathbf{q} \times \boldsymbol{\Sigma}_i (1 + \Theta_{z,i}), \quad (5.65)$$

and the expression for $\mathbf{j}_i^{(1)}(\mathbf{q}; \Delta \rightarrow N)$ is obtained from that for $\mathbf{j}_i^{(1)}(\mathbf{q}; N \rightarrow \Delta)$ by replacing \mathbf{S} and \mathbf{T} with their Hermitian conjugates. Here $\boldsymbol{\Sigma}$ (Θ) is the Pauli operator for the Δ spin (isospin).

The electromagnetic form factors $G_{\gamma N\Delta}(Q^2)$ and $G_{\gamma\Delta\Delta}(Q^2)$ are parametrized as

$$G_{\gamma N\Delta}(Q^2) = \frac{\mu_{\gamma N\Delta}}{(1 + Q^2/\Lambda_{N\Delta,1}^2)^2 \sqrt{1 + Q^2/\Lambda_{N\Delta,2}^2}}, \quad (5.66)$$

$$G_{\gamma\Delta\Delta}(Q^2) = \frac{\mu_{\gamma\Delta\Delta}}{(1 + Q^2/\Lambda_{\Delta\Delta}^2)^2}. \quad (5.67)$$

⁶For examples, see van Faassen and Tjon, 1984; Leidemann and Arenhövel, 1987; Dymarz *et al.*, 1990; Dymarz and Khanna, 1990a, 1990b.

⁷For examples, see Hajduk and Sauer, 1979; Hajduk, Sauer, and Struве, 1983; Picklesimer, Rice, and Brandenburg, 1991, 1992a, 1992b, 1992c, 1992d.

In the static quark model, the $N \rightarrow \Delta$ transition magnetic moment $\mu_{\gamma N\Delta}$ is related to the nucleon isovector magnetic moment by the relation $\mu_{\gamma N\Delta} = (3\sqrt{2}/5)\mu_N^V = 3.993$ n.m. This value is significantly larger than that obtained in an analysis of γN data in the Δ -resonance region, $\mu_{\gamma N\Delta} = 3$ n.m. (Carlson, 1986). This analysis also gives $\Lambda_{N\Delta,1} = 0.84$ GeV/c and $\Lambda_{N\Delta,2} = 1.2$ GeV/c. The Δ magnetic moment $\mu_{\gamma\Delta\Delta}$ is taken equal to 4.35 n.m., by averaging the values obtained from a soft-photon analysis of pion-proton bremsstrahlung data near the Δ^{++} resonance (Lin and Liou, 1991), and $\Lambda_{\Delta\Delta} = 0.84$ GeV. In principle, Δ excitation can also occur via an electric quadrupole transition. Its contribution, however, has been neglected, since the associated pion-photoproduction amplitude is found to be experimentally small at resonance (Ericson and Weise, 1988). Also neglected is the Δ convection current.

Electromagnetic observables require the calculation of a matrix element, which can be schematically written as

$$\mathbf{j}_{fi} = \frac{\langle \Psi_{N+\Delta,f} | \mathbf{j} | \Psi_{N+\Delta,i} \rangle}{[\langle \Psi_{N+\Delta,f} | \Psi_{N+\Delta,f} \rangle \langle \Psi_{N+\Delta,i} | \Psi_{N+\Delta,i} \rangle]^{1/2}}, \quad (5.68)$$

where the initial- and final-state wave functions $|\Psi_{N+\Delta,x}\rangle$ ($x=i$ or f) contain both N and Δ degrees of freedom. The numerator in Eq. (5.68) can be expressed as

$$\langle \Psi_{N+\Delta,f} | \mathbf{j} | \Psi_{N+\Delta,i} \rangle = \langle \Psi_f | \mathbf{j} (N \text{ only}) | \Psi_i \rangle + \Delta\text{-terms}, \quad (5.69)$$

where $\mathbf{j}(N \text{ only})$ denotes all one- and two-body contributions to $\mathbf{j}(\mathbf{q})$ that involve only nucleon degrees of freedom, i.e., $\mathbf{j}(N \text{ only}) = \mathbf{j}^{(1)}(N \rightarrow N) + \mathbf{j}^{(2)}(NN \rightarrow NN)$, while the Δ terms include all possible $N \rightleftharpoons \Delta$ transitions and $\Delta \rightarrow \Delta$ electromagnetic currents in the system, as well as normalization corrections to the “nucleonic” matrix elements. Of course, the latter also influence the normalization of the full wave function $\Psi_{N+\Delta}$.

The contributions involving a single Δ have been included in a coupled-channel calculation of the $A=3$ magnetic form factors (Hajduk, Sauer, and Struive, 1983; Struive *et al.*, 1987). Contributions with both one- and two- Δ admixtures in the wave functions have also been studied with the transition-correlation-operator method in the $A=3$ magnetic form factors (Schiavilla and Viviani, 1996), and $A=3$ and 4 radiative- and weak-capture reactions at low energies (Schiavilla *et al.*, 1992; Viviani, Schiavilla, and Kievsky, 1996).

Perturbation theory estimates of the importance of Δ -isobar degrees of freedom in photonuclear observables typically include only the contributions from single $N \rightleftharpoons \Delta$ transitions and also ignore the change in wavefunction normalization. Thus the two-body operator corresponding to this approximation is written as

$$\begin{aligned} \mathbf{j}_{\Delta\text{PT},ij} &= \mathbf{j}(\mathbf{q}; \Delta \rightarrow N) \frac{v_{NN \rightarrow \Delta N,ij}}{m - m_\Delta} \\ &+ \frac{v_{\Delta N \rightarrow NN,ij}}{m - m_\Delta} \mathbf{j}_i(\mathbf{q}; N \rightarrow \Delta) + i \rightleftharpoons j \\ &= i \frac{G_{\gamma N\Delta}(Q^2)}{9m} e^{i\mathbf{q} \cdot \mathbf{r}_i} \{ 4 \tau_{z,j} [f_\Delta(r_{ij}) \boldsymbol{\sigma}_j + g_\Delta(r_{ij}) \\ &\quad \times \hat{\mathbf{r}}_{ij}(\boldsymbol{\sigma}_j \cdot \hat{\mathbf{r}}_{ij})] - (\boldsymbol{\tau}_i \times \boldsymbol{\tau}_j)_z [f_\Delta(r_{ij})(\boldsymbol{\sigma}_i \times \boldsymbol{\sigma}_j) \\ &\quad + g_\Delta(r_{ij})(\boldsymbol{\sigma}_i \times \hat{\mathbf{r}}_{ij})(\boldsymbol{\sigma}_j \cdot \hat{\mathbf{r}}_{ij})] \} \times \mathbf{q} + i \rightleftharpoons j, \end{aligned} \quad (5.70)$$

where

$$f_\Delta(r) \equiv \frac{v^{\sigma\tau\Pi}(r) - v^t \tau^\Pi(r)}{m - m_\Delta}, \quad (5.71)$$

$$g_\Delta(r) \equiv 3 \frac{v^t \tau^\Pi(r)}{m - m_\Delta}. \quad (5.72)$$

The preceding discussion shows that explicit inclusion of Δ admixtures in the nuclear wave function influences the predictions for electromagnetic observables in two ways: first, via direct electromagnetic couplings, and second by renormalization corrections. Typically, these effects lead to a substantial reduction of the predictions based on the perturbative treatment. This subject will be taken up again in Secs. VI and IX.

C. Electromagnetic two-body charge operators

Several uncertainties arise when considering the two-body charge operator, in contrast to the two-body current operator. While the main parts of the two-body current are linked to the form of the nucleon-nucleon interaction through the continuity equation, the most important two-body charge operators are model dependent and may be viewed as relativistic corrections. Until a systematic method for a simultaneous nonrelativistic reduction of both the interaction and the electromagnetic current operator is developed, the definite form of the two-body charge operators remains uncertain, and one has to rely on perturbation theory.

Two-body charge operators fall into two classes. The first includes those effective operators that represent non-nucleonic degrees of freedom, such as nucleon-antinucleon pairs or nucleon resonances, and that arise when those degrees of freedom are eliminated from the state vector. The second class includes those dynamic exchange charge effects that would appear even in a description explicitly including non-nucleonic excitations in the state vector. In a description based on meson-exchange mechanisms, these involve electromagnetic transition couplings between different mesons. The proper forms of the former operators depend on the method of eliminating the non-nucleonic degrees of freedom; therefore evaluating their matrix elements with the usual nonrelativistic nuclear wave functions represents only the first approximation to a systematic reduction (Friar, 1977). We shall first consider the two-

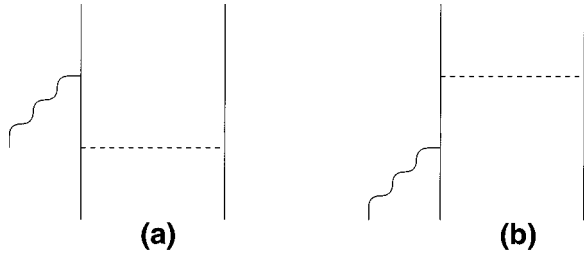


FIG. 16. Feynman diagram representation of the Born amplitudes for photoproduction of virtual mesons: Solid lines, nucleons; dashed lines, mesons; wavy lines, photons.

body charge operators of this class, to which belongs the long-range pion-exchange charge operator.

The two-body charge operator due to pion exchange is derived by considering the low-energy limit of the relativistic Born diagrams associated with the virtual-pion photoproduction amplitude (Riska, 1984). When these are evaluated with pseudovector pion-nucleon coupling, the following operator is obtained for diagram (a) of Fig. 16:

$$\begin{aligned} & \frac{1}{2} [F_1^S(Q^2) + F_1^V(Q^2) \tau_{z,i}] \frac{1}{E_{\text{in}} - E} v_{ij,\pi}(\mathbf{k}_j) \\ & + \frac{f_{\pi NN}^2}{2mm_\pi^2} \frac{1}{2} [F_1^S(Q^2) + F_1^V(Q^2) \tau_{z,i}] \boldsymbol{\tau}_i \cdot \boldsymbol{\tau}_j \frac{\boldsymbol{\sigma}_i \cdot \mathbf{q} \boldsymbol{\sigma}_j \cdot \mathbf{k}_j}{m_\pi^2 + k_j^2} \\ & + O(E_{\text{in}} - E). \end{aligned} \quad (5.73)$$

A similar operator is also obtained that corresponds to the time ordering in diagram (b) of Fig. 16. Here \mathbf{q} is the momentum transfer to the nucleus, \mathbf{k}_j is the momentum transferred by the pion to nucleon j , and E_{in} and E are the energies of the initial and intermediate states, respectively. In Eq. (5.73), $v_{ij,\pi}(\mathbf{k}_j)$ is the one-pion-exchange potential in momentum space:

$$v_{ij,\pi}(\mathbf{k}) = 3v_\pi(k) \boldsymbol{\tau}_i \cdot \boldsymbol{\tau}_j \boldsymbol{\sigma}_i \cdot \mathbf{k} \boldsymbol{\sigma}_j \cdot \mathbf{k}. \quad (5.74)$$

The first term in Eq. (5.73) contains the intermediate-state Green's function and one-pion-exchange potential. It is therefore contained in the bound-state matrix elements of the single-nucleon charge operator (i.e., in the impulse approximation). The second term represents a part of the exchange charge operator. There is an additional contribution due to the energy dependence of the pion propagator (Friar, 1977; Coon and Friar, 1986; Schiavilla, 1996a). To these operators, one must add the operator associated with direct coupling of the photon to the exchanged pion (Friar, 1977; Coon and Friar, 1986; Schiavilla, 1996a). However, this latter operator, as well as that due to retardation effects in the pion propagator, gives rise to nonlocal isovector contributions that are expected to provide only small corrections to the leading local term and that have typically been neglected in studies of charge-exchange effects in nuclei. For example, in the few-nucleon systems, these operators would only contribute to the isovector combination of the ${}^3\text{He}$ and ${}^3\text{H}$ charge form factors, a combination that is a factor of 3 smaller than

the isoscalar. Thus the two-body charge operator due to pion exchange is simply taken as

$$\begin{aligned} \rho_{ij,\pi}(\mathbf{k}_i, \mathbf{k}_j) = & -\frac{3}{2m} \{ [F_1^S(Q^2) \boldsymbol{\tau}_i \cdot \boldsymbol{\tau}_j + F_1^V(Q^2) \tau_{z,j}] \\ & \times v_\pi(k_j) \boldsymbol{\sigma}_i \cdot \mathbf{q} \boldsymbol{\sigma}_j \cdot \mathbf{k}_j + [F_1^S(Q^2) \boldsymbol{\tau}_i \cdot \boldsymbol{\tau}_j \\ & + F_1^V(Q^2) \tau_{z,i}] v_\pi(k_i) \boldsymbol{\sigma}_i \cdot \mathbf{k}_i \boldsymbol{\sigma}_j \cdot \mathbf{q} \}, \end{aligned} \quad (5.75)$$

where $\mathbf{k}_i + \mathbf{k}_j = \mathbf{q}$.

The effect of the pion-exchange charge operator is enhanced by a similar operator that is associated with ρ -meson exchange and that can be derived in the same way, by considering the nonrelativistic reduction of the virtual ρ -meson photoproduction amplitudes in two-body diagrams of the form in Fig. 16. One then eliminates the singular term that represents an iteration of the wave function. The form of the resulting operator is (Riska, 1984)

$$\begin{aligned} \rho_{ij,\rho}(\mathbf{k}_i, \mathbf{k}_j) = & -\frac{3}{2m} \{ [F_1^S(Q^2) \boldsymbol{\tau}_i \cdot \boldsymbol{\tau}_j + F_1^V(Q^2) \tau_{z,j}] v_\rho(k_j) \\ & \times (\boldsymbol{\sigma}_i \times \mathbf{q}) \cdot (\boldsymbol{\sigma}_j \times \mathbf{k}_j) + [F_1^S(Q^2) \boldsymbol{\tau}_i \cdot \boldsymbol{\tau}_j \\ & + F_1^V(Q^2) \tau_{z,i}] v_\rho(k_i) (\boldsymbol{\sigma}_j \times \mathbf{q}) \cdot (\boldsymbol{\sigma}_i \times \mathbf{k}_i) \}, \end{aligned} \quad (5.76)$$

where again nonlocal terms and/or terms proportional to powers of $1/(1 + \kappa_\rho)$ have been neglected. Due to its short range, the contribution associated with this operator is typically an order of magnitude smaller than that due to pion exchange.

The π - and ρ -meson-exchange charge operators contain coupling constants and bare meson propagators, which are usually modified by *ad hoc* vertex form factors in order to take into account the finite extent of the nucleons. However, this model dependence can be eliminated by replacing v_π and v_ρ with the v_{PS} and v_V defined in Eqs. (5.41) and (5.42). These replacements are the ones required for the construction of a two-body current operator that satisfies the continuity equation. It is reasonable to apply them to the two-body charge operators as the generalized meson propagators constructed in this way take into account the nucleon structure in a way that is consistent with the nucleon-nucleon interaction. An additional reason for using the present construction is that it has been shown to lead to predictions for the magnetic form factors of the trinucleons that are in good agreement with the experimental data (Schiavilla, Pandharipande, and Riska, 1989; Schiavilla and Viviani, 1996).

The $T=1$ pseudoscalar and vector exchanges provide the largest contribution to the charge operator, and contain no adjustable parameters. The other contributions that have been considered, namely, those associated with the ω exchange, and $\rho\pi\gamma$ and $\omega\pi\gamma$ mechanisms, are relatively smaller, and we use experimental coupling constants and vertex form factors to calculate them. The ω -meson-exchange charge operator is taken as (Gari and Hyuga, 1976)

$$\begin{aligned} \rho_{ij,\omega}(\mathbf{k}_i, \mathbf{k}_j) = & \frac{g_{\omega NN}^2}{8m^3} \left[[F_1^S(Q^2) + F_1^V(Q^2)\tau_{z,i}] \right. \\ & \times \frac{(\boldsymbol{\sigma}_i \times \mathbf{q}) \cdot (\boldsymbol{\sigma}_j \times \mathbf{k}_j)}{k_j^2 + m_\omega^2} + [F_1^S(Q^2) \\ & \left. + F_1^V(Q^2)\tau_{z,j}] \frac{(\boldsymbol{\sigma}_j \times \mathbf{q}) \cdot (\boldsymbol{\sigma}_i \times \mathbf{k}_i)}{k_i^2 + m_\omega^2} \right], \quad (5.77) \end{aligned}$$

where small terms proportional to the tensor coupling κ_ω ($\kappa_\omega = -0.12$) have been neglected.

All the exchange charge operators above belong to the first class of exchange operators and appear as non-singular seagull terms in the nonrelativistic reduction of the virtual photoproduction amplitudes for the exchanged mesons. The exchange charge operators that correspond to the $\rho\pi\gamma$ and $\omega\pi\gamma$ couplings shown in Fig. 14 belong to the (second) class of genuine dynamic exchange operators, those with transverse four-vector currents. The $\rho\pi\gamma$ - and $\omega\pi\gamma$ -exchange charge operators corresponding to the diagrams in Fig. 14 have the form

$$\begin{aligned} \rho_{\rho\pi\gamma}(\mathbf{k}_i, \mathbf{k}_j) = & -\frac{f_{\pi NN} g_{\rho NN} (1 + \kappa_\rho)}{2m_\pi m_\rho m} G_{\rho\pi\gamma}(Q^2) \\ & \times \boldsymbol{\tau}_i \cdot \boldsymbol{\tau}_j \left[\frac{\boldsymbol{\sigma}_i \cdot \mathbf{k}_i (\boldsymbol{\sigma}_j \times \mathbf{k}_j) \cdot (\mathbf{k}_i \times \mathbf{k}_j)}{(k_i^2 + m_\pi^2)(k_j^2 + m_\rho^2)} \right. \\ & \left. - \frac{\boldsymbol{\sigma}_j \cdot \mathbf{k}_j (\boldsymbol{\sigma}_i \times \mathbf{k}_i) \cdot (\mathbf{k}_i \times \mathbf{k}_j)}{(k_i^2 + m_\rho^2)(k_j^2 + m_\pi^2)} \right], \quad (5.78) \end{aligned}$$

$$\begin{aligned} \rho_{\omega\pi\gamma}(\mathbf{k}_i, \mathbf{k}_j) = & -\frac{f_{\pi NN} g_{\omega NN}}{2m_\pi m_\omega m} G_{\omega\pi\gamma}(Q^2) \\ & \times \left[\frac{\boldsymbol{\sigma}_i \cdot \mathbf{k}_i (\boldsymbol{\sigma}_j \times \mathbf{k}_j) \cdot (\mathbf{k}_i \times \mathbf{k}_j)}{(k_i^2 + m_\pi^2)(k_j^2 + m_\omega^2)} \tau_{z,i} \right. \\ & \left. - \frac{\boldsymbol{\sigma}_j \cdot \mathbf{k}_j (\boldsymbol{\sigma}_i \times \mathbf{k}_i) \cdot (\mathbf{k}_i \times \mathbf{k}_j)}{(k_i^2 + m_\omega^2)(k_j^2 + m_\pi^2)} \tau_{z,j} \right], \quad (5.79) \end{aligned}$$

The derivation of the $\rho\pi\gamma$ - and $\omega\pi\gamma$ -exchange charge operators is straightforward, given the transition current matrix elements $\langle \pi^a(k) | j_\mu(0) | V(p, \epsilon) \rangle$, with $V = \rho, \omega$. More recently it has been shown that the isoscalar $\rho\pi\gamma$ -exchange charge operator can also be derived from the anomalous baryon current that carries the baryon charge in the topological soliton (or Skyrme) model (Nyman and Riska, 1986, 1987; Wakamatsu and Weise, 1988). This derivation is independent of the detailed form of the effective chiral Lagrangian in the soliton model and links the $\rho\pi\gamma$ -exchange current operator to the chiral anomaly.

In the ω -, $\rho\pi\gamma$ -, and $\omega\pi\gamma$ -exchange charge operators, the meson-nucleon vertices have been taken to be point-like. The finite extent of nucleons and mesons is taken into account by modifying the free meson propagators in the above expressions by introducing high-momentum cutoff factors of the conventional monopole form. In the $\rho\pi\gamma$ - and $\omega\pi\gamma$ -exchange charge operators, the pion and

vector-meson propagators are multiplied, respectively, by $f_\pi(k)$ and $f_V(k)$, $V = \rho, \omega$. However, in the ω -exchange charge operator, the propagator is multiplied by $f_\omega^2(k)$. The values used for Λ_π and Λ_V are 0.9 and 1.35 GeV/c, as discussed before. It should be reiterated that the contributions due to two-body charge operators from vector-meson (ρ -like and ω) exchanges, as well as transition couplings ($\rho\pi\gamma$ and $\omega\pi\gamma$), are typically an order of magnitude (or more) smaller than those due to π -like exchanges (Schiavilla, Pandharipande, and Riska, 1990; Schiavilla and Viviani, 1996).

D. The axial two-body current operators

Among the axial two-body current operators, the leading terms of pionic range are those associated with excitation of Δ -isobar resonances. These arise from $N \Rightarrow \Delta$ and $\Delta \rightarrow \Delta$ axial couplings, which are modeled as

$$\mathbf{A}_{a,i}^{(1)}(\mathbf{q}; N \rightarrow \Delta) = -\frac{g_{\beta N \Delta}}{2} T_{a,i} \mathbf{S}_i e^{i\mathbf{q} \cdot \mathbf{r}_i}, \quad (5.80)$$

$$\mathbf{A}_{a,i}^{(1)}(\mathbf{q}; \Delta \rightarrow \Delta) = -\frac{g_{\beta \Delta \Delta}}{2} \Theta_{a,i} \boldsymbol{\Sigma}_i e^{i\mathbf{q} \cdot \mathbf{r}_i}. \quad (5.81)$$

The $\Delta \rightarrow N$ current is obtained by replacing the spin and isospin transition operators in Eq. (5.80) by their Hermitian conjugates. The coupling constants $g_{\beta N \Delta}$ and $g_{\beta \Delta \Delta}$ are not known. In the static quark model, they are related to the axial coupling of the nucleon by the relations $g_{\beta N \Delta} = (6\sqrt{2}/5)g_A$ and $g_{\beta \Delta \Delta} = (9/5)g_A$. These values have often been used in the literature in the calculation of Δ -induced axial current contributions to weak transitions (Carlson *et al.*, 1991; Saito, Wu, Ishikawa, and Sasakawa, 1990). However, given the uncertainties in the naive quark-model predictions, a more reliable estimate for the $g_{\beta N \Delta}$ coupling constant is obtained by determining it phenomenologically in the following way: It is well known that the one-body axial current [Eq. (5.3)] leads to a 4% underprediction of the measured Gamow-Teller matrix element in tritium β decay. Since the contribution of the $\Delta \rightarrow \Delta$ axial current (as well as those due to other axial two-body operators to be discussed below) are found to be numerically very small, this 4% discrepancy can be used to determine $g_{\beta N \Delta}$. This procedure produces, in the context of a transition-correlation-operator calculation of the type discussed above, a value for $g_{\beta N \Delta}$ about 30% larger than the quark-model estimate (Schiavilla *et al.*, 1992).

There are additional axial two-body current operators, although their contributions to weak transitions in the few-nucleon systems have been found to be numerically far less important than those from Δ degrees of freedom. These operators are associated with axial πNN and ρNN contact interactions and axial $\rho\pi$ couplings and were first described in a systematic way by Chemtob and Rho (1971). Their derivation has been given in a number of articles, including the original reference mentioned above and the more recent review by

Towner (1987). Their expressions in momentum space follow. Axial pion-exchange seagull (pair) current:

$$\mathbf{A}_{a,ij}^{(2)}(\mathbf{q};\pi S) = \frac{g_A}{2m} \frac{f_{\pi NN}^2}{m_\pi^2} \frac{\boldsymbol{\sigma}_j \cdot \mathbf{k}_j}{m_\pi^2 + k_j^2} f_\pi^2(k_j) \{ (\boldsymbol{\tau}_i \times \boldsymbol{\tau}_j)_a \boldsymbol{\sigma}_i \times \mathbf{k}_j - i\boldsymbol{\tau}_{a,j} [\mathbf{q} + i\boldsymbol{\sigma}_i \times (\mathbf{p}_i + \mathbf{p}'_i)] \} + i \rightleftharpoons j, \quad (5.82)$$

axial ρ -meson-exchange seagull (pair) current:

$$\begin{aligned} \mathbf{A}_{a,ij}^{(2)}(\mathbf{q};\rho S) = & -g_A \frac{g_\rho^2(1 + \kappa_\rho)^2}{8m^3} \frac{f_\rho^2(k_j)}{m_\rho^2 + k_j^2} \\ & \times \{ \boldsymbol{\tau}_{a,j} [(\boldsymbol{\sigma}_j \times \mathbf{k}_j) \times \mathbf{k}_j \\ & - i [\boldsymbol{\sigma}_i \times (\boldsymbol{\sigma}_j \times \mathbf{k}_j)] \times (\mathbf{p}_i + \mathbf{p}'_i)] \\ & + (\boldsymbol{\tau}_i \times \boldsymbol{\tau}_j)_a [\mathbf{q} \boldsymbol{\sigma}_i \cdot (\boldsymbol{\sigma}_j \times \mathbf{k}_j) \\ & + i(\boldsymbol{\sigma}_j \times \mathbf{k}_j) \times (\mathbf{p}_i + \mathbf{p}'_i) \\ & - [\boldsymbol{\sigma}_i \times (\boldsymbol{\sigma}_j \times \mathbf{k}_j)] \times \mathbf{k}_j \} + i \rightleftharpoons j, \quad (5.83) \end{aligned}$$

axial $\rho\pi$ current:

$$\begin{aligned} \mathbf{A}_{a,ij}^{(2)}(\mathbf{q};\rho\pi) \\ = -g_A \frac{g_\rho^2}{m} \frac{\boldsymbol{\sigma}_j \cdot \mathbf{k}_j}{(m_\rho^2 + k_i^2)(m_\pi^2 + k_j^2)} f_\rho(k_i) f_\pi(k_j) (\boldsymbol{\tau}_i \times \boldsymbol{\tau}_j)_a \\ \times [(1 + \kappa_\rho) \boldsymbol{\sigma}_i \times \mathbf{k}_i - i(\mathbf{p}_i + \mathbf{p}'_i)] + i \rightleftharpoons j. \quad (5.84) \end{aligned}$$

Here \mathbf{q} is the total momentum transfer $= \mathbf{k}_i + \mathbf{k}_j$, $\mathbf{k}_{i(j)}$ is the momentum transfer to nucleon i (j), \mathbf{p}_i and \mathbf{p}'_i are the initial and final momenta of nucleon i , and $f_{\pi(\rho)}(k) =$ pion (ρ -meson)-nucleon monopole vertex form factor. The expression for πS represents the conventional pair current operator given in the literature. It is obtained with pseudoscalar pion-nucleon coupling. With pseudovector coupling, the pion momentum \mathbf{k}_j in the first term in brackets would be replaced by the external momentum \mathbf{q} , and an additional term $(\mathbf{p}_i + \mathbf{p}'_i)$ would appear with the isospin structure $(\boldsymbol{\tau}_i \times \boldsymbol{\tau}_j)_a$. Furthermore, the ρS operator includes only those terms proportional to $(1 + \kappa_\rho)^2$. Finally, configuration-space expressions may again be obtained by carrying out the Fourier transforms in Eq. (5.47).

VI. ELASTIC AND INELASTIC ELECTROMAGNETIC FORM FACTORS

In this section we give an overview of the current status of elastic and inelastic electromagnetic form-factor calculations in the $A=2-6$ nuclei. Our discussion will be in the context of a unified approach to nuclear dynamics based on realistic two- and three-nucleon interactions and consistent two-body charge and current operators.

A variety of techniques, including Faddeev-Yakubovsky (FY), correlated hyperspherical harmonics (CHH), variational Monte Carlo (VMC), and Green's-function Monte Carlo (GFMC) methods, have been used to calculate the bound-state wave functions of ^3H , ^3He , and ^4He with high accuracy (see Secs. III and IV and references therein). For the same (realistic) input

Hamiltonian, the binding energies obtained with the FY, CHH, and GFMC methods typically differ by less than 0.5% for $A=3$ and 1% for $A=4$. Very recently, the VMC and GFMC calculations have also been extended to the $A=6$ and 7 systems. Thus the electromagnetic form factors of these few-body nuclei, along with the deuteron structure functions and threshold electrodisintegration at backward angles, are the observables of choice for testing the quality of models for the nucleon-nucleon interaction and associated two-body charge and current operators.

While the literature on the electromagnetic structure of the deuteron and trinucleons is very extensive—and no attempt will be made here to systematically discuss it all—this is not the case for the α particle and low-lying states of ^6Li , for which realistic wave functions have become available only relatively recently. Indeed, the ^6Li form factors have been exclusively studied up until now by using phenomenological shell-model (Donnelly and Walecka, 1973; Vergados, 1974; Bergstrom, 1975) or cluster (Bergstrom, 1979; Bergstrom, Kowalski, and Neuhausen, 1982; Lehman and Parke, 1983a, 1983b; Kukulin *et al.*, 1990; Kukulin *et al.*, 1995) wave functions. However, given our premise, such calculations are not as directly tied to the NN interaction and currents.

Rather complete calculations of the $A=2$ and 3 electromagnetic form factors have been carried out by a number of groups,⁸ using wave functions derived from a Hamiltonian with two-nucleon interactions, such as the Paris (Cottingham *et al.*, 1973), Bonn (Machleidt, Holinde, and Elster, 1987) and Argonne v_{14} (Wiringa, Smith, and Ainsworth, 1984) and v_{18} (Wiringa, Stoks, and Schiavilla, 1995) models, and including (for $A=3$) three-nucleon interactions, such as the Tucson-Melbourne (Conn *et al.*, 1979) and Urbana/Argonne (Carlson, Pandharipande, and Wiringa, 1983; Pudliner *et al.*, 1995) models. Some of these calculations have also explicitly taken into account Δ -isobar admixtures in the $A=2$ (Dymarz *et al.*, 1990; Dymarz and Khanna, 1990a, 1990b; Leidemann and Arenhövel, 1987) and $A=3$ (Hajduk, Sauer, and Strueve, 1983; Strueve *et al.*, 1987; Schiavilla and Viviani, 1986) wave functions. While GFMC wave functions, corresponding to the Argonne v_{18} and Urbana model-IX Hamiltonian (AV18/IX), are now available (Pudliner *et al.*, 1995; Pieper and Wiringa, 1996), the less accurate VMC wave functions have been used to date for the ^6Li form-factor calculations (Wiringa and Schiavilla, 1996). The AV18/IX and the older Argonne v_{14} two-nucleon and Urbana model-VIII three-nucleon (AV14/VIII) models reproduce the experimental binding energies and charge radii of ^3H ,

⁸For $A=2$, see, for example, Chemtob, Moniz, and Rho (1974), Gari and Hyuga (1976), Schiavilla and Riska (1991), Plessas, Christian, and Wagenbrunn (1995). For $A=3$, see Brandenburg, Kim, and Tubis (1974a), Kloet and Tjon (1974), Hadjimichael, Goulard, and Bornais (1983), Maize and Kim (1984), Strueve *et al.* (1987), Schiavilla, Pandharipande, and Riska (1989), Schiavilla, Pandharipande, and Riska (1990).

${}^3\text{He}$, and ${}^4\text{He}$. However, for the $A=6$ systems the (AV18/IX-based) GFMC calculations indicate that the experimental binding energy of the ${}^6\text{Li}$ ground state is near agreement with the calculated value, while those of the ${}^6\text{He}$ and ${}^6\text{Be}$ ground states and low-lying excited states of ${}^6\text{Li}$ are underestimated by theory at the 2% and 3–5 % levels, respectively (Pieper and Wiringa, 1996).

Form-factor calculations in few-body nuclei have used electromagnetic charge and current operators including one- and two-body components. We here summarize their most important features. The dominant two-body current operator is the isovector one due to π -meson exchange. While its general structure is dictated by the low-energy theorems and is therefore on solid theoretical ground (Chemtob and Rho, 1971), there is nevertheless considerable uncertainty with regard to its short-range behavior due to the composite nature of nucleons and pions. In most calculations, this has been taken into account by including form factors at the πN vertices. However, the resulting operator will not generally satisfy the continuity equation with the two-nucleon interaction used to generate the wave functions. Riska (1985b) and, independently, Buchmann, Leidemann, and Arenhövel (1985), have suggested prescriptions for constructing “ π -like” and, in fact, “ ρ -like” two-body currents from the isospin-dependent spin-spin and tensor components of the two-nucleon interaction (the most commonly used “Riska” prescription has been reviewed in Sec. V). These prescriptions, although not unique, lead to conserved two-body currents, which have been characterized by Riska as “model independent” (Riska, 1989). Additional, but numerically far less important, “model-independent” two-body currents are obtained from the momentum dependence of the interaction (Buchmann, Leidemann, and Arenhövel, 1985; Riska, 1985a; Riska and Poppius, 1985; Schiavilla, Pandharipande, and Riska, 1989; Carlson *et al.*, 1990). In contrast to the π -like current, these are fairly short ranged, and have both isoscalar and isovector terms.

Some of the calculations reported in the literature have also included two-body current operators due to the $\rho\pi\gamma$ and $\omega\pi\gamma$ mechanisms (which are, respectively, isoscalar and isovector), as well as contributions (predominantly isovector) associated with the presence of Δ -isobar degrees of freedom. The former as well as the latter are purely transverse, and therefore unconstrained by the interaction—that is, they are “model dependent” in the Riska classification scheme. Again, the short-range behavior of these currents and, in particular, the $\gamma N\Delta$ and $\pi N\Delta$ transition couplings, are poorly known.

Isovector magnetic observables, such as the threshold electrodisintegration of the deuteron at backward angles (Hockert *et al.*, 1973) and the magnetic form factors of the trinucleons (Hadjimichael, Goulard, and Bornais, 1983), are dominated by the π -like two-body currents mentioned above in the momentum-transfer range 2.5–3.5 fm^{-1} . Contributions from the remaining two-body currents become significant only at higher momentum transfer Q ($Q > 5 \text{ fm}^{-1}$). Two-body contributions to

isoscalar observables, such as the deuteron $B(Q)$ structure function, only provide a small correction to the impulse approximation (IA) predictions based on the single-nucleon convection and spin-magnetization currents at low and moderate values of Q (below 5 fm^{-1}). At higher Q , isoscalar contributions due to the momentum-dependent components of the two-nucleon interaction and the $\rho\pi\gamma$ coupling increase significantly. However, it should be emphasized that the $\rho\pi\gamma$ corrections become numerically very sensitive to the precise values used for the cutoff parameters at the πNN and ρNN vertices.

While the main parts of the two-body currents are linked to the form of the nucleon-nucleon interaction through the continuity equation, the most important two-body charge operators are model dependent and should be considered as relativistic corrections. Indeed, a consistent calculation of two-body charge effects in nuclei would require the inclusion of relativistic effects in both the interaction models and nuclear wave functions. Such a program is just at its inception for systems with $A > 2$. Of course, fully relativistic calculations of the deuteron form factors based on quasipotential reductions of the Bethe-Salpeter equation, of the type reported by Hummel and Tjon (1989, 1990) and Van Orden, Devine, and Gross (1995), do include the effects mentioned above. However, they are not immune from ambiguities of their own (Coester and Riska, 1994).

There are nevertheless rather clear indications for the relevance of two-body charge operators from the failure of the impulse approximation in predicting the charge form factors of the three- and four-nucleon systems (Hadjimichael, Goulard, and Bornais, 1983; Strueve *et al.*, 1987; Schiavilla, Pandharipande, and Riska, 1990). The model commonly used includes the π -, ρ -, and ω -meson-exchange charge operators, as well as the $\rho\pi\gamma$ and $\omega\pi\gamma$ charge transition couplings, in addition to the single-nucleon Darwin-Foldy and spin-orbit relativistic corrections. It should be emphasized, however, that, for $Q < 5 \text{ fm}^{-1}$, the contribution due to the π -exchange charge operator is typically at least an order of magnitude larger than that of any of the remaining two-body mechanisms and one-body relativistic corrections.

The present section is divided into five subsections. The first presents a summary of the basic formalism for discussing electro- (and photo-)induced transitions between discrete nuclear levels. No derivation of the relevant formulas will be given, as these can be found in a number of authoritative review articles (deForest and Walecka, 1966; Donnelly and Sick, 1984). The next three subsections deal, in turn, with the deuteron, the three- and four-nucleon, and six-nucleon systems, while Sec. VI.E contains some concluding remarks, along with tables of the $A=2-6$ nuclei ground-state moments.

A final note concerns the form-factor calculations presented below. The most comprehensive studies of light-nuclei form factors have been based on Argonne two-nucleon and Urbana three-nucleon interactions, and “model-independent” two-body charge and current operators constructed from the Argonne model (Schiavilla,

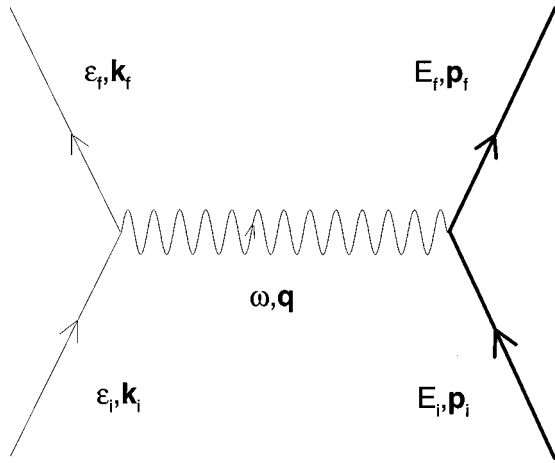


FIG. 17. Electron scattering in the one-photon-exchange approximation: Solid lines, electrons; thick-solid lines, hadrons; wavy line, photons.

Pandharipande, and Riska, 1989, 1990; Wiringa, 1991, Schiavilla and Viviani, 1996; Wiringa and Schiavilla, 1996). We therefore take the results of these calculations as a “baseline” and discuss, in relation to them, those obtained by other groups using different interaction and current models.

A. Elastic and inelastic electron scattering from nuclei: A review

In the one-photon-exchange approximation, the electron-scattering cross section involving a transition from an initial nuclear state $|J_i\rangle$ of spin J_i and rest mass m_i to a final nuclear state $|J_f\rangle$ of spin J_f , rest mass m_f , and recoiling energy E_f can be expressed in the laboratory frame as (deForest and Walecka, 1996; Donnelly and Sick, 1984)

$$\frac{d\sigma}{d\Omega} = 4\pi\sigma_M f_{\text{rec}}^{-1} [v_L F_L^2(q) + v_T F_T^2(q)], \quad (6.1)$$

where

$$\sigma_M = \left(\frac{\alpha \cos\theta/2}{2\epsilon_i \sin^2\theta/2} \right)^2, \quad (6.2)$$

$$v_L = \frac{Q^4}{q^4}, \quad (6.3)$$

$$v_T = \tan^2\frac{\theta}{2} + \frac{Q^2}{2q^2}, \quad (6.4)$$

and the recoil factor f_{rec} is given by

$$f_{\text{rec}} = 1 + \frac{\epsilon_f - \epsilon_i \cos\theta}{E_f} \approx 1 + \frac{2\epsilon_i}{m_i} \sin^2\frac{\theta}{2}. \quad (6.5)$$

The electron kinematic variables are defined in Fig. 17. The last expression for f_{rec} in Eq. (6.5) is obtained by neglecting terms of order $(\omega/m_i)^2$ and higher, where

$$\frac{\omega}{m_i} = \frac{Q^2 + m_f^2 - m_i^2}{2m_i^2}. \quad (6.6)$$

The nuclear structure information is contained in the longitudinal and transverse form factors denoted, respectively, by $F_L^2(q)$ and $F_T^2(q)$. By fixing q and ω and varying θ it is possible to separate $F_L^2(q)$ from $F_T^2(q)$ in a procedure known as a Rosenbluth separation. Alternatively, by working at $\theta=180^\circ$ one ensures that only the transverse form factor contributes to the cross section and so may be isolated (in this case, we observe that the combination $\sigma_M \tan^2\theta/2 \rightarrow (\alpha/2\epsilon_i)^2$ as $\theta \rightarrow 180^\circ$, and is therefore finite in this limit).

The longitudinal and transverse form factors are expressed in terms of reduced matrix elements of Coulomb, electric, and magnetic multipole operators as (deForest and Walecka, 1966; Donnelly and Sick, 1984)

$$F_L^2(q) = \frac{1}{2J_i+1} \sum_{J_f=0}^{\infty} |\langle J_f || T_J^{\text{Coul}}(q) || J_i \rangle|^2, \quad (6.7)$$

$$F_T^2(q) = \frac{1}{2J_i+1} \sum_{J_f=1}^{\infty} [|\langle J_f || T_J^{\text{El}}(q) || J_i \rangle|^2 + |\langle J_f || T_J^{\text{Mag}}(q) || J_i \rangle|^2], \quad (6.8)$$

where we have defined

$$T_{JM}^{\text{Coul}}(q) \equiv \int d\mathbf{x} j_J(qx) Y_{JM}(\hat{\mathbf{x}}) \rho(\mathbf{x}), \quad (6.9)$$

$$T_{JM}^{\text{El}}(q) \equiv \frac{1}{q} \int d\mathbf{x} [\nabla \times j_J(qx) \mathbf{Y}_{JM}^M(\hat{\mathbf{x}})] \cdot \mathbf{j}(\mathbf{x}), \quad (6.10)$$

$$T_{JM}^{\text{Mag}}(q) \equiv \int d\mathbf{x} j_J(qx) \mathbf{Y}_{JM}^M(\hat{\mathbf{x}}) \cdot \mathbf{j}(\mathbf{x}), \quad (6.11)$$

with

$$\mathbf{Y}_{JM}^M(\hat{\mathbf{x}}) \equiv \sum_{M_L, \mu} \langle LM_L, 1\mu | JM \rangle Y_{LM_L}(\hat{\mathbf{x}}) \hat{\mathbf{e}}_\mu, \quad (6.12)$$

$\hat{\mathbf{e}}_0 \equiv \hat{\mathbf{e}}_z$, and $\hat{\mathbf{e}}_{\pm 1} \equiv \mp(\hat{\mathbf{e}}_x \pm i\hat{\mathbf{e}}_y)/\sqrt{2}$. Here $\rho(\mathbf{x})$ and $\mathbf{j}(\mathbf{x})$ are the nuclear charge and current-density operators, and $j_J(qx)$ are spherical Bessel functions. The reduced matrix elements in Eqs. (6.7) and (6.8) are related to the matrix elements of the Fourier transforms $\rho(\mathbf{q})$ and $\mathbf{j}(\mathbf{q})$, introduced in Sec. V, via (deForest and Walecka, 1966)

$$\begin{aligned} & \langle J_f M_f | \rho(\mathbf{q}) | J_i M_i \rangle \\ &= 4\pi \sum_{J=0}^{\infty} \sum_{M=-J}^J i^J Y_{JM}^*(\hat{\mathbf{q}}) \frac{\langle J_i M_i, JM | J_f M_f \rangle}{\sqrt{2J_f+1}} \\ & \times \langle J_f || T_J^{\text{Coul}}(q) || J_i \rangle, \end{aligned} \quad (6.13)$$

$$\begin{aligned}
 & \langle J_f M_f | \hat{\mathbf{e}}_\lambda(\mathbf{q}) \cdot \mathbf{j}(\mathbf{q}) | J_i M_i \rangle \\
 &= -\sqrt{2\pi} \sum_{J=1}^{\infty} \sum_{M=-J}^J i^J \sqrt{2J+1} \mathcal{D}_{\lambda M}^J(0\theta_q 0) \\
 & \quad \times \frac{\langle J_i M_i, J M | J_f M_f \rangle}{\sqrt{2J_f+1}} [\lambda \langle J_f || T_J^{\text{Mag}}(q) || J_i \rangle \\
 & \quad + \langle J_f || T_J^{\text{El}}(q) || J_i \rangle], \tag{6.14}
 \end{aligned}$$

where $\lambda = \pm 1$, $\hat{\mathbf{e}}_\lambda(\mathbf{q})$ are the spherical components of the virtual-photon transverse polarization vector, and the $\mathcal{D}_{\lambda M}^J$ are standard rotation matrices. The expressions above correspond to the virtual photon's being absorbed at an angle θ_q with respect to the quantization axis of the nuclear spins. The more familiar expressions for the multipole expansion of the charge and current matrix elements are recovered by taking \mathbf{q} along the spin-quantization axis, so that $Y_{JM}^*(\hat{\mathbf{q}}) \rightarrow \delta_{M,0} \sqrt{2J+1} / \sqrt{4\pi}$ and $\mathcal{D}_{\lambda M}^J(0\theta_q 0) \rightarrow \delta_{\lambda, M}$.

It is useful to consider the parity and time-reversal properties of the multipole operators (de Forest and Walecka, 1966). Thus the scalar and polar vector characters of, respectively, the charge and current-density operators under parity transformations imply that T_{JM}^{Coul} and T_{JM}^{El} have parity $(-1)^J$, while T_{JM}^{Mag} has parity $(-1)^{J+1}$. The resulting selection rules are $\pi_i \pi_f = (-1)^J$ [$\pi_i \pi_f = (-1)^{J+1}$] for Coulomb and electric (magnetic) transitions, where π_i and π_f are the parities of the initial and final states.

The Hermitian character of the operators $\rho(\mathbf{x})$ and $\mathbf{j}(\mathbf{x})$, as well as their transformation properties under time reversal, $\rho(\mathbf{x}) \rightarrow \rho(\mathbf{x})$ and $\mathbf{j}(\mathbf{x}) \rightarrow -\mathbf{j}(\mathbf{x})$, can be shown to lead to the following relations:

$$\langle J_f || T_J^{\text{Coul}}(q) || J_i \rangle = (-1)^{J_f+J-J_i} \langle J_i || T_J^{\text{Coul}}(q) || J_f \rangle, \tag{6.15}$$

$$\langle J_f || T_J^{\text{El, Mag}}(q) || J_i \rangle = (-1)^{J_f+J-J_i+1} \langle J_i || T_J^{\text{El, Mag}}(q) || J_f \rangle. \tag{6.16}$$

These relations, along with the parity selection rules stated above, require, in particular, that elastic transitions, for which $J_f = J_i$, can only be induced by even- J Coulomb and odd- J magnetic multipole operators.

Finally, in the low- q or long-wavelength limit, the multipole operators defined above can be shown to behave as (deForest and Walecka, 1966; Donnelly and Sick, 1984)

$$T_{JM}^{\text{Coul}}(q) \approx \sqrt{\frac{2J+1}{4\pi}} \frac{q^J}{(2J+1)!!} Q_{JM}, \tag{6.17}$$

$$Q_{JM} \equiv \sqrt{\frac{4\pi}{2J+1}} \int d\mathbf{x} x^J Y_{JM}(\hat{\mathbf{x}}) \rho(\mathbf{x}), \tag{6.18}$$

$$T_{JM}^{\text{Mag}}(q) \approx -\frac{1}{i} \sqrt{\frac{2J+1}{4\pi}} \sqrt{\frac{J+1}{J}} \frac{q^J}{(2J+1)!!} \mu_{JM}, \tag{6.19}$$

$$\mu_{JM} \equiv \sqrt{\frac{4\pi}{2J+1}} \frac{1}{J+1} \int d\mathbf{x} [\mathbf{x} \times \mathbf{j}(\mathbf{x})] \cdot \nabla [x^J Y_{JM}(\hat{\mathbf{x}})], \tag{6.20}$$

and

$$\begin{aligned}
 T_{JM}^{\text{El}}(q) &\approx \frac{1}{i} \sqrt{\frac{J+1}{J}} \frac{q^{J-1}}{(2J+1)!!} \int d\mathbf{x} x^J Y_{JM}(\hat{\mathbf{x}}) \nabla \cdot \mathbf{j}(\mathbf{x}) \\
 &= -\sqrt{\frac{2J+1}{4\pi}} \sqrt{\frac{J+1}{J}} \frac{m_f - m_i}{q} \frac{q^J}{(2J+1)!!} Q_{JM}, \tag{6.21}
 \end{aligned}$$

where in the last equation use has been made of the continuity equation $\nabla \cdot \mathbf{j}(\mathbf{x}) = -i[H, \rho(\mathbf{x})]$ and of the fact that the initial and final states are eigenstates of the Hamiltonian. In particular, for elastic scattering ($J_f = J_i$), the reduced matrix elements of $T_{JM}^{\text{Coul}}(q)$ and $T_{JM}^{\text{Mag}}(q)$ are proportional to the ground-state charge and magnetic moments, defined as

$$Q_J \equiv \langle J_i, M_i = J_i | Q_{J0} | J_i, M_i = J_i \rangle, \tag{6.22}$$

$$\mu_J \equiv 2m \langle J_i, M_i = J_i | \mu_{J0} | J_i, M_i = J_i \rangle, \tag{6.23}$$

where the magnetic moments μ_J are in terms of nuclear magnetons μ_N . It is then easily found that

$$\langle J_i || T_J^{\text{Coul}} || J_i \rangle \approx \sqrt{\frac{2J+1}{4\pi}} \frac{\sqrt{2J_i+1}}{\langle J_i J_i, J0 | J_i J_i \rangle} \frac{q^J}{(2J+1)!!} Q_J, \tag{6.24}$$

$$\begin{aligned}
 & \langle J_i || T_J^{\text{Mag}} || J_i \rangle \\
 & \approx -\frac{1}{i} \sqrt{\frac{2J+1}{4\pi}} \sqrt{\frac{J+1}{J}} \frac{\sqrt{2J_i+1}}{\langle J_i J_i, J0 | J_i J_i \rangle} \frac{q^J}{(2J+1)!!} \frac{\mu_J}{2m}, \tag{6.25}
 \end{aligned}$$

where J satisfies the condition $0 \leq J \leq 2J_i$, and is even in Eq. (6.24), while it is odd in Eq. (6.25). In particular, it is found that

$$\langle J_i || T_{J=0}^{\text{Coul}}(q) || J_i \rangle \approx \sqrt{\frac{2J_i+1}{4\pi}} Z, \tag{6.26}$$

and for $J_i \geq 1$

$$\begin{aligned}
 & \langle J_i || T_{J=2}^{\text{Coul}}(q) || J_i \rangle \\
 & \approx \frac{1}{6\sqrt{5}\pi} \sqrt{\frac{(J_i+1)(2J_i+1)(2J_i+3)}{J_i(2J_i-1)}} q^2 Q_{J=2}, \tag{6.27}
 \end{aligned}$$

where $2Q_{J=2}$ is the usual ground-state electric quadrupole moment, while for $J_i \geq 1/2$

$$\langle J_i || T_{J=1}^{\text{Mag}}(q) || J_i \rangle \approx -\frac{1}{i} \frac{1}{\sqrt{6\pi}} \sqrt{\frac{(J_i+1)(2J_i+1)}{J_i}} \frac{q}{2m} \mu_{J=1}, \tag{6.28}$$

where $\mu_{J=1}$ is the usual ground-state magnetic dipole moment.

B. The deuteron

1. Deuteron electromagnetic form factors

The deuteron elastic $1^+ \rightarrow 1^+$ electromagnetic transition is induced by T_0^{Coul} , T_2^{Coul} , and T_1^{Mag} form factors in the notation introduced above. However, it is customary

to discuss the electromagnetic structure of the deuteron ground state in terms of charge, quadrupole, and magnetic form factors related to T_0^{Coul} , T_2^{Coul} , and T_1^{Mag} via

$$\sqrt{\frac{4\pi}{3}}T_0^{\text{Coul}}(Q) = (1 + \eta)G_C(Q), \quad (6.29)$$

$$\sqrt{\frac{4\pi}{3}}T_2^{\text{Coul}}(Q) = \frac{2\sqrt{2}}{3}\eta(1 + \eta)G_Q(Q), \quad (6.30)$$

$$-\sqrt{\frac{4\pi}{3}}iT_1^{\text{Mag}}(Q) = \frac{2}{\sqrt{3}}\sqrt{\eta(1 + \eta)}G_M(Q), \quad (6.31)$$

where $\eta \equiv Q^2/(2m_d)^2$, m_d being the deuteron mass. These form factors are normalized as

$$G_C(0) = 1, \quad (6.32)$$

$$G_Q(0) = m_d^2 Q_d, \quad (6.33)$$

$$G_M(0) = \frac{m_d}{m}\mu_d, \quad (6.34)$$

where Q_d and μ_d are the quadrupole and magnetic moments of the deuteron. The elastic electron-scattering cross section from an unpolarized deuteron is then expressed in terms of the $A(Q)$ and $B(Q)$ structure functions as

$$\frac{d\sigma}{d\Omega} = \sigma_M f_{\text{rec}}^{-1} [A(Q) + B(Q)\tan^2\theta/2], \quad (6.35)$$

with

$$A(Q) = G_C^2(Q) + \frac{2}{3}\eta G_M^2(Q) + \frac{8}{9}\eta^2 G_Q^2(Q), \quad (6.36)$$

$$B(Q) = \frac{4}{3}\eta(1 + \eta)G_M^2(Q). \quad (6.37)$$

A Rosenbluth separation of the elastic e - d cross section will not allow a separation of the charge and quadrupole form factors. To achieve this goal, electron-scattering experiments from tensor-polarized deuteron targets have been carried out in recent years (Schulze *et al.*, 1984; Dmitriev *et al.*, 1985; Gilman *et al.*, 1990; The *et al.*, 1991), leading to an experimental determination of the tensor polarization observable $T_{20}(Q)$, given by

$$T_{20}(Q) = -\sqrt{2}\frac{x(x+2)+y/2}{1+2(x^2+y)}, \quad (6.38)$$

where the variables x and y are defined as

$$x = \frac{2}{3}\eta\frac{G_Q(Q)}{G_C(Q)}, \quad (6.39)$$

$$y = \frac{2}{3}\eta\left[\frac{G_M(Q)}{G_C(Q)}\right]^2 f(\theta), \quad (6.40)$$

and the auxiliary function $f(\theta)$ is $\frac{1}{2} + (1 + \eta)\tan^2\theta/2$.

In Figs. 18 and 19 the calculated charge and quadrupole form factors (Plessas, Christian, and Wagenbrunn, 1995; Wiringa, Stoks, and Schiavilla, 1995) are compared with data, after The *et al.* (1991). The calculations are

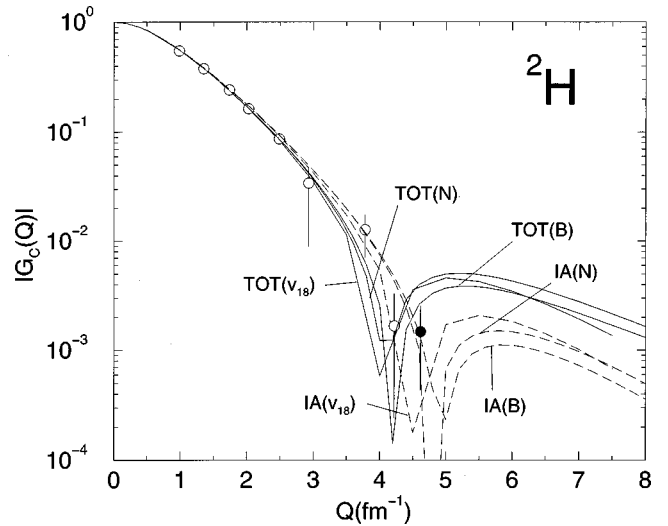


FIG. 18. The charge form factor of the deuteron, obtained in the impulse approximation (IA) and with inclusion of two-body charge contributions and relativistic corrections (TOT), compared with data from Schulze *et al.* (1984), The *et al.* (1991), Dmitriev *et al.* (1985), and Gilman *et al.* (1990) [empty and filled circles denote, respectively, positive and negative experimental values for $G_C(Q)$]. Theoretical results corresponding to the Argonne v_{18} (v_{18} ; Wiringa, Stoks, and Schiavilla, 1995), Bonn B (B; Plessas, Christian, and Wagenbrunn, 1995), and Nijmegen (N; Plessas, Christian, and Wagenbrunn, 1995) interactions are displayed. The Höhler parametrization is used for the nucleon electromagnetic form factors.

based on the Argonne v_{18} (Wiringa, Stoks, and Schiavilla, 1995), Nijmegen (Stoks *et al.*, 1994), and Bonn-B (Machleidt, Holinde, and Elster, 1987) interactions and the Höhler parametrization (Höhler *et al.*, 1976) of the nucleon electromagnetic form factors. The curves labeled TOT in the figures include the contributions due to the two-body charge operators as well as to the Darwin-Foldy and spin-orbit relativistic corrections to the single-nucleon charge operator. The effect of these

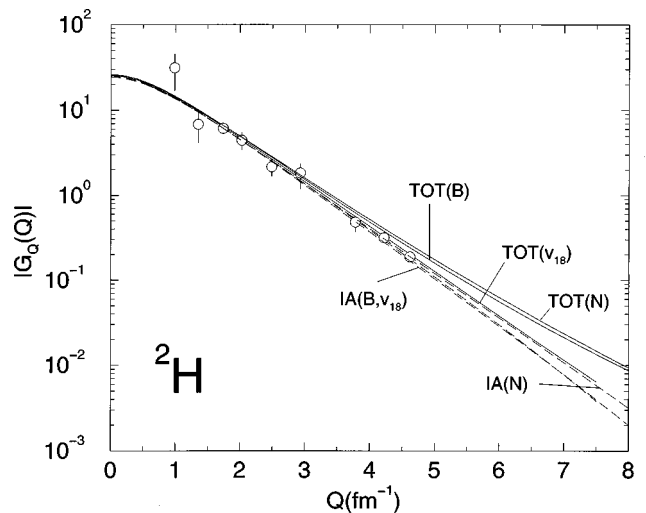


FIG. 19. Same as in Fig. 18, but for the quadrupole form factor of the deuteron.

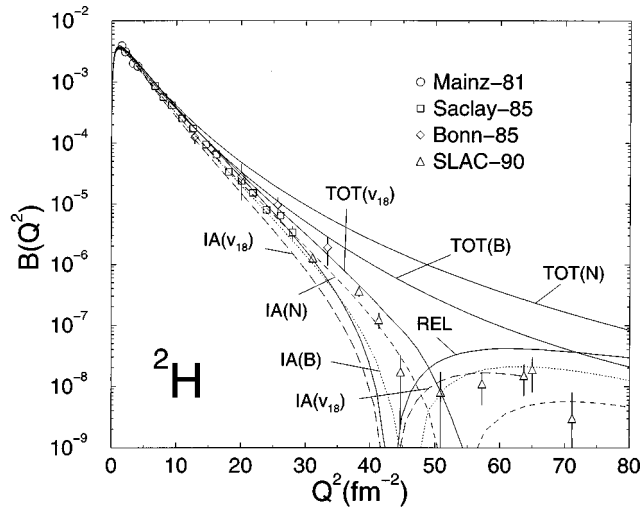


FIG. 20. The deuteron $B(Q^2)$ structure function, obtained in the impulse approximation (IA) and with inclusion of two-body current contributions and relativistic corrections (TOT), compared with data from Simon, Schmitt, and Walther (1981; Mainz-81), Cramer *et al.* (1985; Bonn-85) Auffret *et al.* (1985a; Saclay-85), and Arnold *et al.* (1987). Theoretical results corresponding to the Argonne v_{18} (v_{18} ; Wiringa, Stoks, and Schiavilla, 1995), Bonn B (B; Plessas, Christian, and Wagenbrunn, 1995), and Nijmegen (N; Plessas, Christian, and Wagenbrunn, 1995) interactions are displayed. Also shown is the relativistically covariant full calculation of Van Orden, Devine, and Gross (1995). The Höhler parametrization is used for the nucleon electromagnetic form factors.

contributions on $G_C(Q)$ is significant and brings the zero predicted by the impulse approximation towards lower values of momentum transfers. However, in $G_Q(Q)$ their effect is relatively unimportant at moderate values of momentum transfers (below 5 fm^{-1}). The main two-body correction is that due to the π -like exchange charge operator. Including the corrections due to vector-meson exchanges, the $\rho\pi\gamma$ mechanism, and the Darwin-Foldy and spin-orbit terms amounts to only a very small additional contribution. The results for the charge and quadrupole form factors are qualitatively similar to those obtained with simple meson-exchange charge operators and deuteron wave functions corresponding to alternative potential models (for example, Gari and Hyuga, 1976). The important role of the two-body charge operators in bringing the zero in the charge form factor to a lower value of momentum transfer is similar to that in the case of the bound three- and four-nucleon systems, where this effect is required for agreement with the measured charge form factors (see below).

The results for the structure function $B(Q)$ Plessas, Christian, and Wagenbrunn, 1995; Wiringa, Stoks, and Schiavilla, 1995), which is related to $G_M(Q)$ via Eq. (6.37), are compared in Fig. 20 with data from Simon, Schmitt, and Walther (1981), Auffret *et al.* (1985a), Cramer *et al.* (1985), and Arnold *et al.* (1987). Since the deuteron is a $T=0$ state, the long-range π -like two-body current, being isovector, does not contribute. Thus

$B(Q)$ is sensitive to the isoscalar model-independent two-body currents associated with the momentum dependence of the interaction, as well as the model-dependent $\rho\pi\gamma$ term. The $B(Q)$ calculated with the Argonne v_{18} interaction (Wiringa, Stoks, and Schiavilla, 1995) is found to be in reasonable agreement with data in the Q^2 range $0-45 \text{ fm}^{-2}$, and has a zero at around 60 fm^{-2} (in the impulse approximation the zero is shifted to Q^2 about 43 fm^{-2}). However, the Bonn-B and Nijmegen-based calculations substantially overestimate the data (Plessas, Christian, and Wagenbrunn, 1995).

In Wiringa, Stoks, and Schiavilla (1995), the leading two-body contributions are from the spin-orbit and quadratic spin-orbit currents and interfere destructively. The present slight overestimate of the data in the Q^2 range $0-40 \text{ fm}^{-2}$ indicates that the degree of cancellation between these contributions is not quite enough. Of course, this is an interaction-dependent statement. It depends, in particular, on the detailed behavior of the (short-range) spin-orbit and quadratic spin-orbit components of the interaction. In the case of the older Argonne v_{14} model, the associated currents led to an excellent fit of the $B(Q)$ structure function in the same momentum-transfer range (Schiavilla and Riska, 1991). Note that the contributions from these currents are ignored in the Plessas, Christian, and Wagenbrunn (1995) calculation.

The contribution from the $\rho\pi\gamma$ current is very sensitive to the values used for the cutoff masses Λ_π and Λ_ρ in the monopole form factors at the πNN and ρNN vertices. Indeed, the large values used for these cutoffs ($\Lambda_\pi=1.2 \text{ GeV}/c$ and $\Lambda_\rho=2 \text{ GeV}/c$) lead to the substantial overprediction of the data in the Bonn-B and Nijmegen-based calculations, as can be seen from Fig. 20. However, in the Argonne-based calculation, these values are taken as $\Lambda_\pi=0.75 \text{ GeV}/c$ and $\Lambda_\rho=1.25 \text{ GeV}/c$, making the $\rho\pi\gamma$ contribution rather small over the momentum-transfer range considered here. It is also important to point out that there are corrections to the leading operator proportional to κ_ρ —the large ρ -meson tensor coupling to the nucleon ($\kappa_\rho=6.6$)—neglected in the calculations discussed above. The associated contributions interfere destructively with those from the leading operator, reducing the latter significantly (Hummel and Tjon, 1989; Schiavilla and Riska, 1991). Thus the choice of softer cutoff masses may be justified as simulating these higher-order corrections.

The calculated $A(Q)$ structure function and $T_{20}(Q)$ tensor polarization (Plessas, Christian, and Wagenbrunn, 1995; Wiringa, Stoks, and Schiavilla, 1995) are compared in Figs. 21 and 22 with data. For $A(Q)$, experimental data are from Arnold *et al.* (1975), Simon, Schmitt, and Walthier (1981), Cramer *et al.* (1985), and Platchkov *et al.* (1990); for $T_{20}(Q)$, they are from Schulze *et al.* (1984), Dmitriev *et al.* (1985), Gilman *et al.* (1990), and The *et al.* (1991). These observables are mostly sensitive to the charge and quadrupole form factors. In both of them the π -like two-body charge operator plays a major role (Plessas, Christian, and Wagenbrunn, 1995; Wiringa, Stoks, and Schiavilla, 1995).

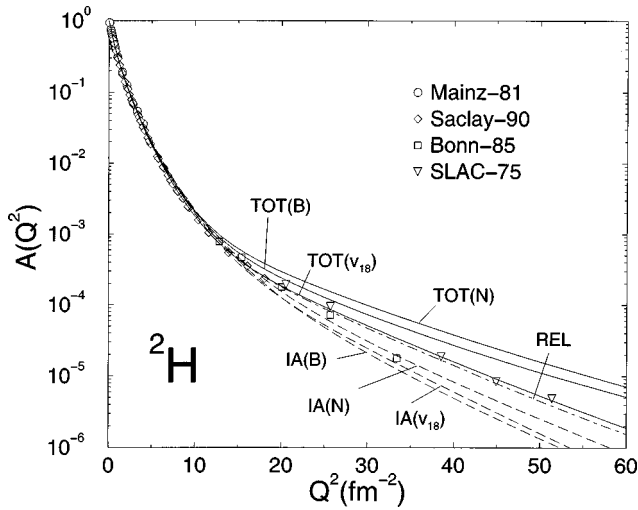


FIG. 21. The deuteron $A(Q^2)$ structure function, obtained in the impulse approximation (IA) and with inclusion of two-body charge and current contributions and relativistic corrections (TOT), compared with data from Simon, Schmitt, and Walther (1981; Mainz-81), Cramer *et al.* (1985; Bonn-85), Platchkov *et al.* (1990; Saclay-90), and Arnold *et al.* (1975; SLAC-75). Theoretical results corresponding to the Argonne v_{18} (v_{18} ; Wiringa, Stoks, and Schiavilla, 1995), Bonn-B (B; Plessas, Christian, and Wagenbrunn, 1995) interactions are displayed. Also shown is the relativistically covariant full calculation of Van Orden, Devine, and Gross (1995). The Höhler parametrization is used for the nucleon electromagnetic form factors.

However, while the associated contribution leads to a prediction for $A(Q)$ in excellent agreement with the data over the whole range of momentum transfer, it produces a significant discrepancy between theory and experiment in the case of the tensor polarization. Neglecting the magnetic contribution to $T_{20}(Q)$ gives

$$T_{20}(Q) \approx -\sqrt{2} \frac{x(x+2)}{1+2x^2}, \quad (6.41)$$

and at Q_0 , where $G_C(Q)$ vanishes, $T_{20}(Q_0) = -1/\sqrt{2}$. Thus the relative shift between the calculated and experimental $T_{20}(Q_0)$ implies a corresponding shift between the charge form-factor zeros, as is evident from Fig. 18.

In Figs. 20–22 we also show the results obtained in a covariant, gauge-invariant calculation of the $A(Q)$, $B(Q)$, and $T_{20}(Q)$ observables (Van Orden, Devine, and Gross, 1995), based on the Gross equation (Gross, 1969, 1974, 1982) and a one-boson-exchange interaction model (Gross, Van Orden, and Holinde, 1992). The Gross equation is a quasipotential equation in which the relative energy is constrained by restricting one of the nucleons to its positive-energy mass shell. The one-boson-exchange kernel contains π , η , ρ , and ω mesons, as well as the fictitious scalar mesons σ and σ_1 of isoscalar and isovector character, respectively. It is determined by fitting the Nijmegen np phase shifts and the deuteron binding energy, and gives for the SAID database (Arndt *et al.*, 1992) a χ^2 per datum of ≈ 2.5 in the

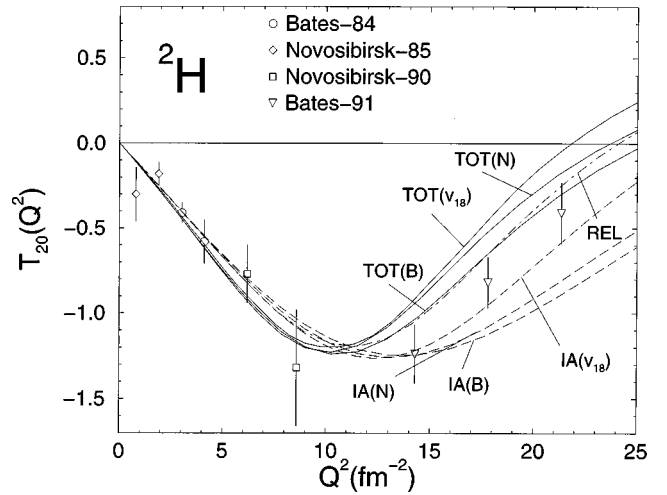


FIG. 22. The deuteron tensor polarization $T_{20}(Q^2)$, obtained in the impulse approximation (IA) and with inclusion of two-body charge and current contributions and relativistic corrections (TOT), compared with data from Schulze *et al.* (1984; Bates-84), The *et al.* (1991; Bates-91) Dmitriev *et al.* (1985; Novosibirsk-85), and Gilman *et al.* (1990; Novosibirsk-90). Theoretical results corresponding to the Argonne v_{18} (v_{18} ; Wiringa, Stoks, and Schiavilla, 1995), Bonn B (B; Plessas, Christian, and Wagenbrunn, 1995), Nijmegen (N; Plessas, Christian, and Wagenbrunn, 1995) interactions are displayed. Also shown is the relativistically covariant full calculation of Van Orden, Devine, and Gross (1995). The Höhler parametrization is used for the nucleon electromagnetic form factors.

energy range 0–350 MeV, which is somewhat higher than that obtained for recent interaction models ($\chi^2/\text{datum} \approx 1$). The electromagnetic current consists of nucleon one-body and $\rho\pi\gamma$ two-body terms. Off-shell form factors are included in the one-body currents, while the form factor for the (transverse) $\rho\pi\gamma$ transition current is taken from a quark-model calculation.

Significant differences exist between the relativistic and nonrelativistic calculations of $B(Q)$ and $T_{20}(Q)$. To clarify the situation, a number of comments are in order. First, the two-body charge operators associated with π -, ρ - and ω -meson exchange, which arise only in the nonrelativistic reduction of the photoproduction amplitudes for these virtual mesons, are included in the relativistic IA calculation (not shown in the figures) to all orders. Second, boost effects, such as those associated with the Lorentz contraction of the wave function and Wigner rotation of the nucleons' spins (Friar, 1975, 1977), are typically not included in the nonrelativistic calculations. It has been shown that the tensor polarization can be expressed in the impulse approximation, and neglecting small magnetic contributions, as (Forest *et al.*, 1996)

$$T_{20}(Q) = -\sqrt{2} \frac{F_{C,M=0}^2(Q) - F_{C,M=1}^2(Q)}{F_{C,M=0}^2(Q) + 2F_{C,M=1}^2(Q)}, \quad (6.42)$$

where $F_{C,M}(Q)$ is the Fourier transform of the density for a deuteron in state M ($=0, \pm 1$). Thus the minimum in $T_{20}(Q)$ is related to the vanishing of the $M=1$ form factor. The deuteron in an $M=1$ state has the shape of a

dumbbell oriented along the z axis, while in an $M=0$ state it has the shape of a torus lying in the xy plane (Forest *et al.*, 1996). Naively, one therefore expects that the Lorentz contraction would affect the $M=1$ more than the $M=0$ density, and this fact would produce a shift in the minimum position for $T_{20}(Q)$. However, a rough estimate indicates that such a shift is of the order of a couple percent for a deuteron traveling along the z axis with a velocity $Q/4m$ (in the Breit frame), with $Q \approx 2 \text{ fm}^{-1}$. A more realistic estimate of these boost corrections in a relativistic framework also found them to be rather small in the momentum-transfer range covered by experiment (Hummel and Tjon, 1990). Therefore the substantial differences between the nonrelativistic and relativistic predictions are more likely due to dynamic differences. For example, Van Orden, Devine, and Gross (1995) have shown that the $B(Q)$ structure function, in particular its zero position, is very sensitive to the (very) small P-wave components due to $N\bar{N}$ admixtures in the deuteron wave function, which are clearly of relativistic origin. However, it is also important to point out that different quasipotential schemes, using similar one-boson-exchange interaction models, nevertheless produce significantly different predictions for the deuteron observables (Hummel and Tjon, 1989; Van Orden, Devine, and Gross, 1995). A satisfactory resolution of these issues is still lacking.

2. The backward electrodisintegration of the deuteron at threshold

The inclusive electron-scattering cross section is written, in the one-photon-exchange approximation, as (de Forest and Walecka, 1966)

$$\frac{d^2\sigma}{d\omega d\Omega} = \sigma_M [v_L R_L(q, \omega) + v_T R_T(q, \omega)], \quad (6.43)$$

where the longitudinal and transverse response functions are given by

$$R_\alpha(q, \omega) = \frac{1}{2J_i + 1} \sum_{M_i} \sum_f |\langle f | O_\alpha(\mathbf{q}) | i; J_i M_i \rangle|^2 \times \delta(\omega + E_i - E_f), \quad (6.44)$$

where $O_\alpha(\mathbf{q})$ is either the charge operator ($\alpha=L$), or the transverse component of the current operator ($\alpha=T$). For a transition to a discrete final state $|f\rangle$ of angular momentum J_f the multipole expansion of $O_\alpha(\mathbf{q})$ leads to Eqs. (6.7) and (6.8).

In the ${}^2\text{H}(e, e')pn$ reaction, the final state is in the continuum, and its wave function is written as

$$|\mathbf{q}; \mathbf{p} S M_S T M_T\rangle = e^{i\mathbf{q}\cdot\mathbf{R}} \psi_{\mathbf{p}, S M_S T M_T}^{(-)}(\mathbf{r}), \quad (6.45)$$

where $\mathbf{r} = \mathbf{r}_1 - \mathbf{r}_2$ and $\mathbf{R} = (\mathbf{r}_1 + \mathbf{r}_2)/2$ are the relative and center-of-mass coordinates. The incoming-wave scattering-state wave function of the two nucleons having relative momentum \mathbf{p} and spin-isospin states $S M_S, T M_T$ is approximated as (Renard, Tran Thanh Van, and Le Bellac, 1965; Fabian and Arenhövel, 1979; Schiavilla and Riska, 1991)

$$\begin{aligned} \psi_{\mathbf{p}, S M_S T M_T}^{(-)}(\mathbf{r}) \approx & \frac{1}{\sqrt{2}} [e^{i\mathbf{p}\cdot\mathbf{r}} - (-1)^{S+T} e^{-i\mathbf{p}\cdot\mathbf{r}}] \chi_{M_S}^S \chi_{M_T}^T \\ & + \frac{4\pi}{\sqrt{2}} \sum_{J \leq J_{\max}} \sum_{L L'} i^L \delta_{LST} [Z_{L S M_S}^{J M_J}(\hat{\mathbf{p}})]^* \\ & \times \left[\frac{1}{r} u_{L' L}^{(-)}(r; p, JST) \right. \\ & \left. - \delta_{L' L} j_L(pr) \right] \mathcal{Y}_{L' S J}^{M_J} \chi_{M_T}^T, \end{aligned} \quad (6.46)$$

where

$$\delta_{LST} = 1 - (-1)^{L+S+T}, \quad (6.47)$$

$$Z_{L S M_S}^{J M_J}(\hat{\mathbf{p}}) = \sum_{M_L} \langle L M_L, S M_S | J M_J \rangle Y_{L M_L}(\hat{\mathbf{p}}). \quad (6.48)$$

The δ_{LST} factor ensures the antisymmetry of the wave function, while the Clebsch-Gordan coefficients restrict the sum over L and L' . The radial functions $u_{L' L}^{(-)}$ are obtained by solving the Schrödinger equation in the JST channel, and they behave asymptotically as

$$\begin{aligned} \frac{1}{r} u_{L' L}^{(-)}(r; p, JST) \underset{r \rightarrow \infty}{\sim} & \frac{1}{2} [\delta_{L' L} h_L^{(1)}(pr) \\ & + (S_{L' L}^{JST})^* h_L^{(2)}(pr)], \end{aligned} \quad (6.49)$$

where $S_{L' L}^{JST}$ is the S matrix in the JST channel and the Hankel functions are defined as $h_L^{(1,2)}(x) = j_L(x) \pm i n_L(x)$, j_L and n_L being the spherical Bessel and Neumann functions, respectively. In the absence of interaction, $u_{L' L}^{(-)}(r; p, JST)/r \rightarrow \delta_{L' L} j_L(pr)$, and $\psi^{(-)}(\mathbf{r})$ reduces to an antisymmetric plane wave. Interactions effects are retained in all partial waves with $J \leq J_{\max}$. For the threshold electrodisintegration it is found that these interaction effects are negligible for $J_{\max} > 2$ (Fabian and Arenhövel, 1979; Schiavilla and Riska, 1991).

The response functions are expressed as

$$R_\alpha(q, \omega) = \sum_{S, T=0,1} R_\alpha^{ST}(q, \omega), \quad (6.50)$$

where the contributions from the individual spin-isospin states are

$$\begin{aligned} R_\alpha^{ST}(q, \omega) = & \frac{1}{3} \sum_{M_J M_S} \int \frac{d\mathbf{p}}{(2\pi)^3} \frac{1}{2} |A_\alpha^{ST}(\mathbf{q}, \mathbf{p}; M_J, M_S)|^2 \\ & \times \delta(\omega + m_d - \sqrt{q^2 + m_p^2}), \end{aligned} \quad (6.51)$$

with A_α^{ST} defined as

$$\begin{aligned} A_\alpha^{ST}(\mathbf{q}, \mathbf{p}; M_J, M_S) \\ \equiv \langle \mathbf{q}; \mathbf{p}, S M_S T, M_T = 0 | O_\alpha(\mathbf{q}) | d; J = 1, M_J \rangle. \end{aligned} \quad (6.52)$$

Here m_p is the internal energy of the recoiling pair of nucleons, and the factor $\frac{1}{2}$ in Eq. (6.51) is included to avoid double counting.

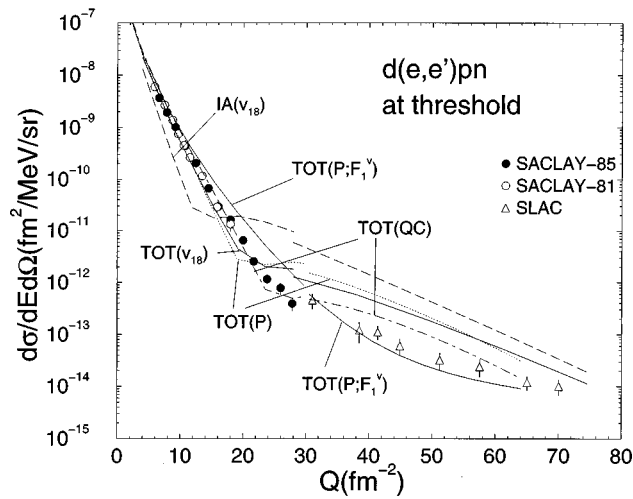


FIG. 23. The cross sections for backward electrodisintegration of the deuteron near threshold, obtained in the impulse approximation (IA) and with inclusion of two-body current contributions and relativistic corrections (TOT), compared with data from Cox, Wynchank, and Collie (1965; SLAC), Bernheim *et al.* (1981; Saclay-81), Auffret *et al.* (1985b; Saclay-85), and Arnold *et al.* (1990; SLAC). Theoretical results corresponding to the Argonne v_{18} (v_{18} ; Schiavilla, 1996b), Paris (P; Leidemann, Schmitt, and Arenhövel, 1990), and r -space version C of the Bonn (QC; Leidemann, Schmitt, and Arenhövel, 1990) interactions are displayed. The dipole parametrization (including the Galster factor for $G_{E,n}$) is used for the nucleon electromagnetic form factors. In particular, the Sachs form factor $G_E^V(Q^2)$ is used in the isovector model-independent two-body current operators. For the Paris interaction, the results obtained by using the Dirac form factor $F_1^V(Q^2)$ in these two-body currents are also shown [curve labeled TOT(P; F_1^V)]. Data and theory have been averaged between 0 and 3 MeV for $Q^2 < 30 \text{ fm}^{-2}$ and between 0 and 10 MeV for $Q^2 > 30 \text{ fm}^{-2}$ pn relative energy, corresponding to the break in the curves.

The main component of the cross section for backward electrodisintegration of the deuteron near threshold is the magnetic dipole transition between the bound deuteron and the $T=1$ 1S_0 scattering state (Hockert *et al.*, 1973). At large values of momentum transfer, this transition rate is dominated by the isovector (model-independent) π -like and ρ -like two-body currents (Buchmann, Leidemann, and Arenhövel, 1985; Schiavilla and Riska, 1991).

The calculated cross sections for backward electrodisintegration are compared in Fig. 23 with the experimental values given in Cox, Wynchank, and Collie (1965), Bernheim *et al.* (1981), Auffret *et al.* (1985b), and Arnold *et al.* (1990). The data have been averaged over the intervals 0–3 MeV and 0–10 MeV of the recoiling pn pair center-of-mass energy for the Saclay [$Q \leq 1 \text{ GeV}/c$, Bernheim *et al.* (1981), Auffret *et al.* (1985b)] and SLAC [$Q > 1 \text{ GeV}/c$, Arnold *et al.* (1990)] kinematic regions, respectively. The theoretical results have instead been calculated at center-of-mass energies of 1.5 MeV and 5 MeV for the Saclay and SLAC kinematics, respectively. However, it has been shown that the effect of the width of the energy interval above threshold (of the final state)

over which the cross-section values are averaged is small (Schiavilla and Riska, 1991). In the figure, the results obtained in the impulse approximation and, in addition, with inclusion of the two-body current contributions (Leidemann, Schmitt, and Arenhövel, 1990; Schiavilla, 1996b) are shown separately for the Paris (Cottingham *et al.*, 1973), Bonn QC (Machleidt, 1989), and Argonne v_{18} (Wiringa, Stoks, and Schiavilla, 1995) interactions. The dipole parametrization is used for the electromagnetic form factors of the nucleon (including the Galster factor for the electric form factor of the neutron, Galster *et al.*, 1971).

While the low-momentum transfer data are in reasonable agreement with theory, those at high Q ($> 1 \text{ GeV}/c$) are substantially overestimated by the calculations based on the Paris (Leidemann, Schmitt, and Arenhövel, 1990) and Argonne v_{18} (Schiavilla, 1996b) models. A number of remarks are in order, however. First, in the calculations shown in Fig. 23, the isovector Sachs form factor $G_E^V(Q^2)$ is used in the expressions for the leading π -like and ρ -like two-body currents. In fact, if $F_1^V(Q^2)$ were to be used, the data would be substantially overestimated by theory in the Q^2 range 5–25 fm^{-2} , as is shown for the case of the Paris interaction.

Second, the better overall fit to the data provided by the Bonn QC interaction is a consequence of the fact that in the impulse approximation the cancellation between the S- and D-state contributions to the pn 1S_0 transition occurs at a somewhat higher Q value than for the Paris and Argonne v_{18} models (Leidemann, Schmitt, and Arenhövel, 1990). This is presumably due to the weaker Bonn QC tensor force.

Third, the predicted cross-section values are sensitive to the parametrization used for the nucleon electromagnetic form factors, in particular $G_E^V(Q^2)$. This sensitivity can be traced back to the unknown behavior of the neutron electric form factor at large Q^2 . Indeed, as shown in Fig. 24, the difference between the results obtained with the dipole and Gari and Krümpelmann (1986) parametrizations is as large as that between the present predictions and the data, although use of the Gari and Krümpelmann form factors would increase the observed discrepancy by more than a factor of 2. In any case, the uncertainty in the behavior of the nucleon electromagnetic form factors (far larger than that in the experimental data) prevents definitive quantitative predictions being made at $Q > 5 \text{ fm}^{-1}$.

C. The $A=3$ and 4 systems

1. The magnetic form factors of ^3H and ^3He

Because of a destructive interference in the matrix elements for the magnetic dipole transition between the S- and D-state components of the wave functions, the impulse approximation predictions for the ^3He and ^3H magnetic form factors have distinct minima at around 2.5 fm^{-1} and 3.5 fm^{-1} , respectively, in disagreement with the experimental data (Collard *et al.*, 1965; McCar-

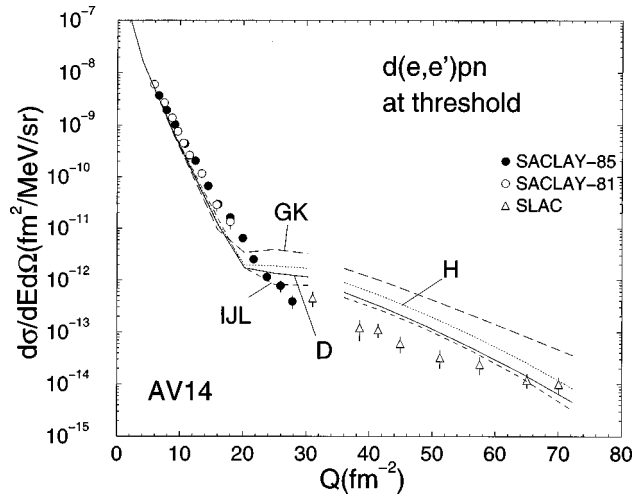


FIG. 24. The cross sections for backward electrodisintegration of the deuteron near threshold, obtained with the IJL (Iachello, Jackson, and Lande, 1973), GK (Gari and Krümpelmann, 1986), H (Höhler *et al.* 1976), D (Galster *et al.*, 1971) parametrizations of the nucleon electromagnetic form factors, compared with data from Cox, Wynchank, and Collie (1965; SLAC), Bernheim *et al.* (1981; Saclay-81), Auffret *et al.* (1985b; Saclay-85), and Arnold *et al.* (1990; SLAC). All theoretical results correspond to the Argonne v_{14} interaction and include two-body current contributions and relativistic corrections (Schiavilla and Riska, 1991). The Sachs form factor $G_E^V(Q^2)$ is used in the isovector model-independent two-body current operators. Data and theory have been averaged as in Fig. 23.

thy, Sick, and Whitney, 1977; Arnold *et al.*, 1978; Szalata *et al.*, 1977; Cavedon *et al.*, 1982; Dunn *et al.*, 1983; Juster *et al.*, 1985; Ottermann *et al.*, 1985; Beck *et al.*, 1987; Amroun *et al.*, 1994). The situation is closely related to that of the backward cross section for electrodisintegration of the deuteron, which is in fact dominated by two-body current contributions for values of momentum transfer above 2.5 fm^{-1} .

The calculated magnetic form factors of ^3H and ^3He (Strueve *et al.*, 1987; Schiavilla and Viviani, 1996) are compared with the experimental data in Figs. 25 and 26. The ground-state wave functions have been calculated either with the correlated hyperspherical harmonics (CHH) method using the AV18/IX model and including one- and two- Δ admixtures with the transition-correlation-operator technique (Schiavilla *et al.*, 1992) or with the coupled-channel Faddeev method using a Paris interaction modified to include explicit Δ -isobar excitations via π -meson and ρ -meson exchange (phase-equivalent to the original Paris model; Hajduk, Sauer, and Strueve, 1983). The AV18/IX ^3He and ^3H wave functions give binding energies and charge radii which reproduce the experimental values (Viviani, Schiavilla, and Kievsky, 1996). However, the Paris-based calculations underbind the trinucleons by about 800 keV (Hajduk, Sauer, and Strueve, 1983). This underbinding is a consequence of the partial cancellation between the attractive contribution from the three-body interaction mediated by intermediate Δ isobars, and the repulsive

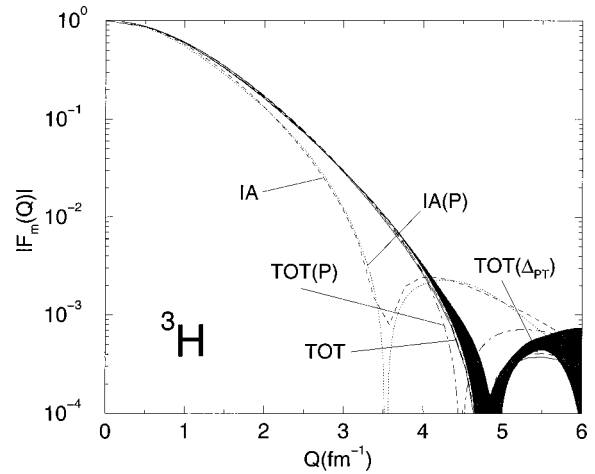


FIG. 25. The magnetic form factors of ^3H , obtained in the impulse approximation (IA) and with inclusion of two-body current contributions and Δ admixtures in the bound-state wave function (TOT), compared with data (shaded area) from Amroun *et al.* (1994). Theoretical results correspond to the Argonne v_{18} two-nucleon and Urbana IX three-nucleon (Schiavilla and Viviani, 1996) and Paris two-nucleon (P; Strueve *et al.*, 1987) interactions. They use, respectively, correlated hyperspherical harmonics and Faddeev wave functions and employ the dipole parametrization (including the Galster factor for $G_{E,n}$) for the nucleon electromagnetic form factors. Note that the Sachs form factor $G_E^V(Q^2)$ is used in the isovector model-independent two-body current operators for the Argonne-based calculations, while the Dirac form factor $F_1^V(Q^2)$ is used in the Paris-based calculations. Also shown are the Argonne results [curve labeled TOT(Δ_{PT})] obtained by including the two-body currents associated with intermediate excitation of a single Δ isobar in perturbation theory.

one due to dispersive effects.

There are also differences in the π -like (and ρ -like) two-body currents, which give the dominant contribution to the $A=3$ magnetic form factor. While these are constructed from the two-nucleon interaction in the case of the AV18/IX calculation, they have a form derived from simple meson-exchange models in the Paris-based

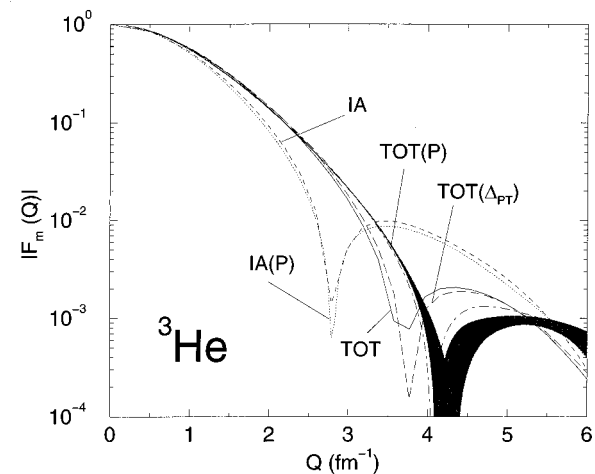


FIG. 26. Same as in Fig. 25, but for ^3He .

calculation and are not therefore strictly consistent with the interaction. In particular, the usual *ad hoc* treatment of the short-range part implies that the continuity equation is satisfied only approximately. Even more importantly, the Paris-based calculations use, in the leading isovector currents, the form factor $F_1^V(Q^2)$ rather than $G_E^V(Q^2)$, which substantially increases their contribution.

In the figures, the curves labeled Δ_{PT} are obtained by including the Δ components perturbatively in the ground states, as is commonly done in the literature.

While the measured ^3H magnetic form factor is in excellent agreement with theory over a wide range of momentum transfers, there is a significant discrepancy between the measured and calculated values of the ^3He magnetic form factor in the region of the diffraction minimum, particularly for the case of the AV18/IX calculation. This discrepancy persists even when different parametrizations of the nucleon electromagnetic form factors are used for the single-nucleon current and the model-independent two-body currents.

It is useful to define the quantities

$$F_M^{S,V}(Q) \equiv \frac{1}{2} [\mu(^3\text{He})F_M(Q; ^3\text{He}) \pm \mu(^3\text{H})F_M(Q; ^3\text{H})]. \quad (6.53)$$

If the ^3H and ^3He ground states were pure $T = \frac{1}{2}$ states, then the F_M^S and F_M^V linear combinations of the three-nucleon magnetic form factor would only be influenced by, respectively, the isoscalar (S) and isovector (V) parts of the current operator. However, small isospin admixtures with $T > \frac{1}{2}$, induced by the electromagnetic interaction as well as charge-symmetry-breaking and charge-independence-breaking terms present in the Argonne v_{18} interaction, are included in the present wave functions. As a consequence, isoscalar (isovector) current operators give small (otherwise vanishing) contributions to the F_M^V (F_M^S) magnetic form factor (Schiavilla and Viviani, 1996).

It is instructive to consider the contributions of individual components of the two-nucleon currents to the form factors. In the region of the diffraction minimum, the π -like current gives the dominant isovector contribution to $F_M^V(Q)$, while the ρ -like contributions are significantly smaller (by nearly an order of magnitude). The remaining terms are smaller still; the next most important isovector contributions are those associated with Δ and SO currents (the latter constructed from the spin-orbit components of the two-nucleon interaction). It is significant that calculations of perturbative and nonperturbative treatment of the Δ -isobar components in the wave function give significantly different results. In general, perturbation theory leads to a significant overprediction of the importance of Δ degrees of freedom in nuclei. This is particularly so in reactions as delicate as the radiative captures on ^2H and ^3He at very low energy (to be discussed below).

Among the two-body contributions to $F_M^S(Q)$, the most important is that due to the currents from the spin-

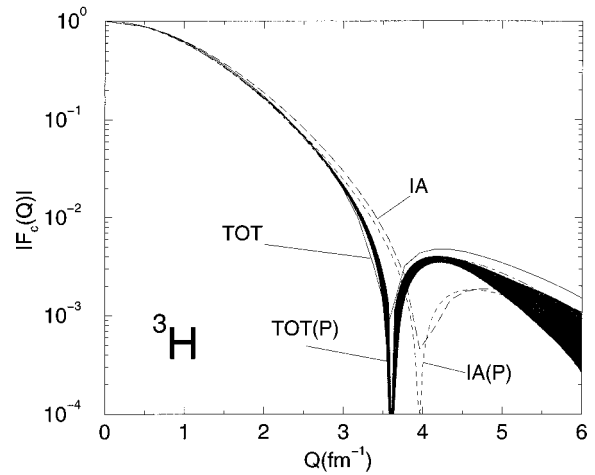


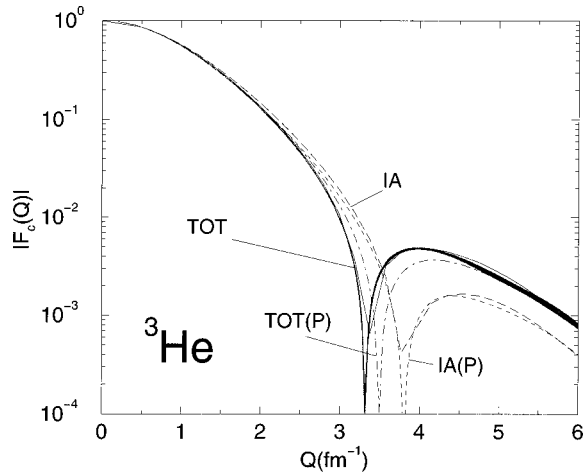
FIG. 27. The charge form factors of ^3H , obtained in the impulse approximation (IA) and with inclusion of two-body charge contributions and relativistic corrections (TOT), compared with data (shaded area) from Amroun *et al.* (1994). Theoretical results correspond to the Argonne v_{18} two-nucleon and Urbana IX three-nucleon (Schiavilla and Viviani, 1996) and Paris two-nucleon (P; Strueve *et al.*, 1987) interactions. They use, respectively, correlated hyperspherical harmonics and Faddeev wave functions and employ the dipole parameterization (including the Galster factor for $G_{E,n}$) for the nucleon electromagnetic form factors. Note that the Paris-based calculation also includes Δ -isobar admixtures in the ^3H wave function.

orbit interactions, and the next most important is that from the quadratic spin-orbit interactions. These two contributions have opposite sign, as has been found for the deuteron $B(Q)$ structure function (Wiringa, Stoks, and Schiavilla, 1995).

2. The charge form factors of ^3H , ^3He , and ^4He

In Figs. 27–29, the calculated ^3H , ^3He , ^4He charge form factors (Strueve *et al.*, 1987; Musolf, Schiavilla, and Donnelly, 1994; Schiavilla and Viviani, 1996) are compared with the experimental data (Collard *et al.*, 1965; Frosch *et al.*, 1968; McCarthy, Sick, and Whitney, 1977; Szalata *et al.*, 1977; Arnold *et al.*, 1978; Cavedon *et al.*, 1982; Dunn *et al.*, 1983; Juster *et al.*, 1985; Ottermann *et al.*, 1985; Beck *et al.*, 1987; Amroun *et al.*, 1994). The three-body wave functions used in the matrix elements of the charge operators are those discussed in the previous subsection. However, the four-nucleon wave function is that obtained in a variational Monte Carlo calculation corresponding to the older AV14/VIII model, which underestimates the ^4He binding energy by 3% (Wiringa, 1991).

The calculated charge form factors for the $A = 3$ and 4 nuclei are in excellent agreement with the experimental data. The important role of the two-body charge operator contributions above $\approx 3 \text{ fm}^{-1}$ is evident, consistent with what was found in earlier studies. The structure of these operators is the same in the AV18/IX and Paris-based calculations. However, in the former case their


 FIG. 28. Same as in Fig. 27, but for ${}^3\text{He}$.

short-range behavior is determined from the Argonne v_{18} according to the Riska prescription (Schiavilla, Pandharipande, and Riska, 1990; Schiavilla and Viviani, 1996), while in the latter case this behavior is taken into account by phenomenological form factors (Struete *et al.*, 1987).

The theoretical uncertainty caused by the lack of precise knowledge of the nucleon electromagnetic form factors is significant for ${}^3\text{H}$ only at the highest values of momentum transfer, as Fig. 30 makes clear. The effect of this uncertainty is even smaller in ${}^3\text{He}$.

Again, we can consider contributions of the different components of the nuclear charge operator to the combinations,

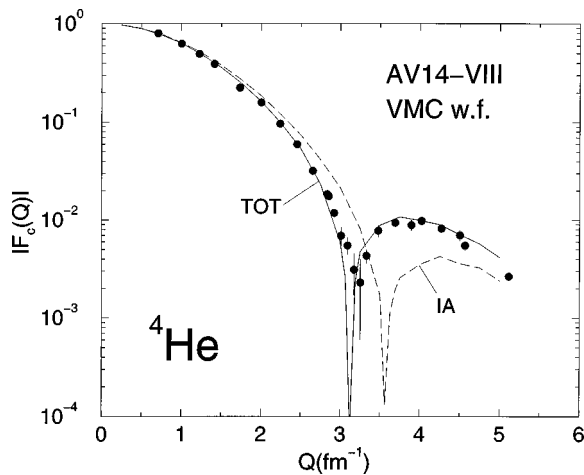


FIG. 29. The charge form factors of ${}^4\text{He}$, obtained in the impulse approximation (IA) and with inclusion of two-body charge contributions and relativistic corrections (TOT), compared with data from Frosch *et al.* (1968) and Arnold *et al.* (1978). Theoretical results correspond to the Argonne v_{14} two-nucleon and Urbana VIII three-nucleon interactions (AV14-VIII), using a variational Monte Carlo ${}^4\text{He}$ wave function (VMC w.f.) and employ the dipole parametrization (including the Galster factor for $G_{E,n}$) for the nucleon electromagnetic form factors. From Musolf, Schiavilla, and Donnelly (1994).

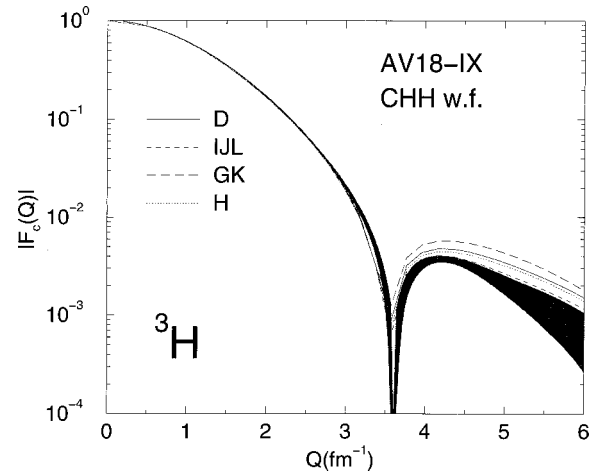


FIG. 30. The ${}^3\text{H}$ charge form factors, calculated with the IJL (Iachello, Jackson, and Lande, 1973), GK (Gari and Krümpelmann, 1986), H (Höhler *et al.*, 1976), and D (Galster *et al.*, 1971) parametrizations of the nucleon electromagnetic form factors, compared with data (shaded area) from Amroun *et al.* (1994). All theoretical results correspond to the Argonne v_{18} two-nucleon and Urbana IX three-nucleon interactions (AV18-IX), using a correlated hyperspherical harmonics ${}^3\text{H}$ wave function (CHH w.f.) and include two-body current contributions and relativistic corrections. From Schiavilla and Viviani (1996).

$$F_C^{S,V}(Q) \equiv \frac{1}{2} [2F_C(Q; {}^3\text{He}) \pm F_C(Q; {}^3\text{H})]. \quad (6.54)$$

As already mentioned in the previous subsection, the F_C^S (F_C^V) charge form factor will also include small contributions from isovector (isoscalar) operators, proportional to admixtures in the wave functions with $T > \frac{1}{2}$. The results reveal that, at low and moderate values of momentum transfer, the π -like charge operator is by far the most important two-body term. This term is more than a factor of 10 larger than the next largest contribution, the ρ -like term, in F_C^S , while it is roughly a factor of 5 larger in F_C^V .

Finally, the question of how the three-body interaction influences the charge form factor has been studied by Friar, Gibson, and Payne (1987) by calculating the trinucleon charge form factor from Faddeev wave functions obtained for several different combinations of two- and three-body interactions. These studies have conclusively shown that the effect of the three-nucleon interaction on the charge form factor is small.

D. The $A=6$ systems

In this section we discuss the ${}^6\text{Li}$ ground-state longitudinal and transverse form factors as well as transition form factors to the excited states with spin, parity and isospin assignments ($J^\pi; T$) given by $(3^+; 0)$ and $(0^+; 1)$. The calculations are based on variational Monte Carlo wave functions obtained from the AV18/IX Hamiltonian model (Pudliner *et al.*, 1995; Wiringa, Stoks, and Schiavilla, 1995). The calculated binding energies for the ground state and $(3^+; 0)$ and $(0^+; 1)$ low-lying excited

states are given in Table VII (Sec. IV.B). The ground state is underbound by nearly 4 MeV compared to experiment, and is only 0.4 MeV more bound than the corresponding ${}^4\text{He}$ calculation (27.8 MeV). This is above the threshold for breakup of ${}^6\text{Li}$ into an α and deuteron. In principle, it should be possible to lower the variational energy at least to that threshold, but the wave function would be too spread out. In the variational calculations reported by Wiringa and Schiavilla (1996), the parameter search was constrained to keep the rms radius close to the experimental value of 2.43 fm^{-1} . The (exact) Green's-function Monte Carlo results for this Hamiltonian, also listed in Tables VII and VIII, indicate that the ground-state binding energy and radius are in agreement with the experimental value, while the $(3^+;0)$ and $(0^+;1)$ experimental binding energies are underestimated by about 3%.

It should be emphasized that previous calculations of the elastic and inelastic six-body form factors have relied on relatively simple shell-model (Donnelly and Walecka, 1973; Vergados, 1974; Bergstrom, 1975) or α - d (Bergstrom, 1979) cluster wave functions. These calculations have typically failed to provide a satisfactory, quantitative description of all measured form factors. More phenomenologically successful models have been based on αNN (Kukulin *et al.*, 1990, 1995; Lehman and Parke 1983a, 1983b) clusterization, or on extensions of the basic α - d model with spherical clusters, in which the deuteron is allowed to deform, or stretch, along a line connecting the clusters' centers of mass (Bergstrom, Kowalski, and Neuhausen, 1982). However, while these models do provide useful insights into the structure of the $A=6$ nuclei, their connection with the underlying two- (and three-) nucleon dynamics is rather tenuous.

The calculated elastic form factors $F_L^2(Q)$ and $F_T^2(Q)$ (Wiringa and Schiavilla, 1996) are compared with the experimental values (Li *et al.*, 1971; Lapikas, 1978; Bergstrom, Kowalski, and Neuhausen, 1982) in Figs. 31 and 32. Since the ${}^6\text{Li}$ ground state is $(1^+;0)$, both $J=0$ and $J=2$ Coulomb multipoles contribute to F_L^2 , while only the $J=1$ magnetic multipole operator contributes to F_T^2 . In these figures, the results obtained in both the impulse approximation (empty squares) and with inclusion of two-body corrections in the charge and current operators (filled squares) are displayed, along with the statistical errors associated with the Monte Carlo integrations. The F_L^2 form factor is in excellent agreement with experiment. In particular, the two-body contributions (predominant due to the π -like charge operator) shift the minimum to lower values of momentum transfer Q , consistently with what has been found for the charge form factors of the hydrogen and helium isotopes. The T_2^{Coul} multipole contribution is much smaller than the T_0^{Coul} one, and at low Q it is proportional to the ground-state quadrupole moment. The theoretical prediction for the latter is significantly larger (though with a 50% statistical error) in absolute value than the measured value, but it does have the correct (negative) sign. It is interesting to point out that cluster models of the ${}^6\text{Li}$ ground

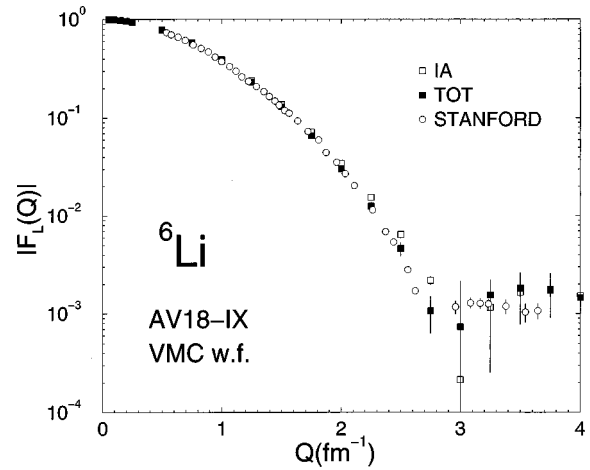


FIG. 31. The longitudinal form factors of ${}^6\text{Li}$, obtained in the impulse approximation (IA) and with inclusion of two-body charge operator contributions and relativistic corrections (TOT), compared with data from Li *et al.* (1971; Stanford). The theoretical results correspond to the Argonne v_{18} and Urbana IX three-nucleon interactions, use a variational Monte Carlo ${}^6\text{Li}$ wave function, and employ the dipole parameterization (including the Galster factor for $G_{E,n}$) of the nucleon electromagnetic form factors. From Wiringa and Schiavilla (1996).

state give large, positive values for the quadrupole moment, presumably due to the lack of D waves in the α particle and the consequent absence of destructive interference between these and the D wave in the α - d relative motion.

The experimental transverse form factor is not well reproduced by theory for Q values larger than 1 fm^{-1} .

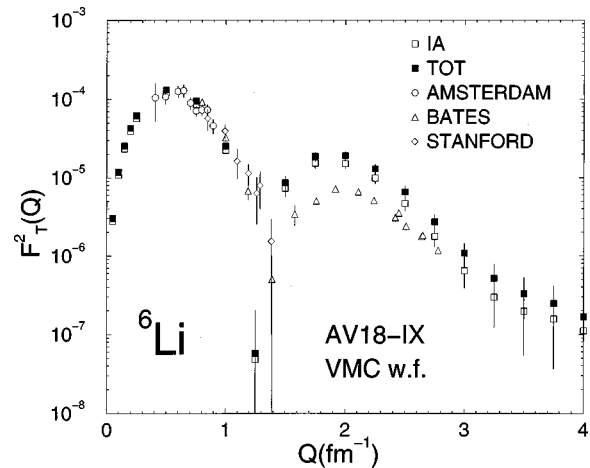


FIG. 32. The transverse form factors of ${}^6\text{Li}$, obtained in the impulse approximation (IA) and with inclusion of two-body current contributions (TOT), compared with data from Rand, Frosch, and Yearian (1966); Stanford Lapikas (1978; Amsterdam), and Bergstrom, Kowalski, and Neuhausen (1982; Bates). The theoretical results correspond to the Argonne v_{18} and Urbana IX three-nucleon interactions, use a variational Monte Carlo ${}^6\text{Li}$ wave function, and employ the dipole parameterization (including the Galster factor for $G_{E,n}$) of the nucleon electromagnetic form factors. From Wiringa and Schiavilla (1996).

TABLE XI. Magnetic moments in n.m., obtained with the Argonne v_{18} two-nucleon and Urbana IX three-nucleon interaction Hamiltonian model in the impulse approximation (IA) and with inclusion of two-body current contributions (TOT). For the trinucleons, Δ -isobar degrees of freedom are included nonperturbatively with the transition-correlation-operator method.

	${}^2\text{H}$	${}^3\text{H}$	${}^3\text{He}$	${}^6\text{Li}$
IA	0.847	2.571	-1.757	0.83
TOT	0.871	2.980	-2.094	0.86
Expt.	0.857	2.979	-2.127	0.822

Since the ${}^6\text{Li}$ ground state has $T=0$, only isoscalar two-body currents contribute to $F_T^2(Q)$. The associated contributions are small at low Q , but increase with Q , becoming significant for $Q > 3 \text{ fm}^{-1}$. However, the data cover the Q range 0 – 2.8 fm^{-1} . The observed discrepancy between theory and experiment might be due to deficiencies in the VMC wave function. Indeed, it will be interesting to see whether this discrepancy is resolved by using the more accurate GFMC wave functions. We also note that the calculated magnetic moment is about 4% larger than the experimental value, which is close to that of a free deuteron (see Table XI).

The measured longitudinal inelastic form factor to the $(3^+;0)$ state (Eigenbrod, 1969; Bergstrom and Tomusiak, 1976; Bergstrom, Deutschmann, and Neuhausen, 1979) is found to be in excellent agreement with the VMC predictions (Wiringa and Schiavilla, 1996), as can be seen in Fig. 33. We note that this transition is induced by $J=2$ and $J=4$ Coulomb multipole operators, and thus the associated form factor $F_L^2(Q)$ behaves as Q^4 at low Q . Good agreement between the experimental (Bergstrom, 1975; Bergstrom, Deutschmann, and Neuhausen, 1979) and VMC calculated values (Wiringa and Schiavilla, 1996) is also found for the transverse inelastic form factor to the state $(0^+;1)$ (see Fig. 34). The latter is an isovector magnetic dipole transition and, as expected, is significantly influenced, even at low values of Q , by two-body contributions, predominantly by those due to the π -like current operator. This is particularly evident when considering the radiative widths of the $(0^+;1)$ and $(3^+;0)$ states. This latter quantity is generally given by (Ring and Schuck, 1980)

$$\Gamma_{fi}(\lambda, J) = \frac{8\pi(J+1)}{J[(2J+1)!!]^2} E_\gamma^{2J+1} B(\lambda J, J_i \rightarrow J_f), \quad (6.55)$$

$$B(EJ, J_i \rightarrow J_f) = \frac{1}{4\pi} \frac{2J+1}{2J_i+1} |\langle J_f || Q_J || J_i \rangle|^2, \quad (6.56)$$

$$B(MJ, J_i \rightarrow J_f) = \frac{1}{4\pi} \frac{2J+1}{2J_i+1} |\langle J_f || \mu_J || J_i \rangle|^2, \quad (6.57)$$

where E_γ is the energy of the emitted photon, and Q_{JM} and μ_{JM} are the operators defined in Eqs. (6.18)–(6.20), respectively. Note that the $B(EJ)$ and $B(MJ)$ are, re-

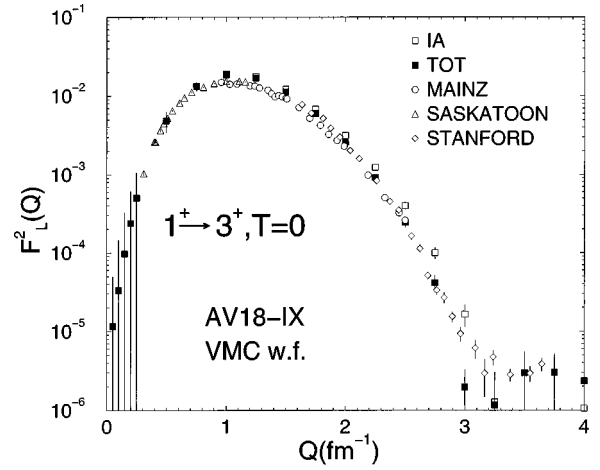


FIG. 33. The longitudinal form factors for the transition from the $1^+, T=0$ to the $3^+, T=0$ (2.18 MeV) levels of ${}^6\text{Li}$, obtained in the impulse approximation (IA) and with inclusion of two-body charge operator contributions and relativistic corrections (TOT), compared with data from Bergstrom (1979). The theoretical results correspond to the Argonne v_{18} and Urbana IX three-nucleon interactions, use variational Monte Carlo $1^+, T=0$ and $3^+, T=0$ ${}^6\text{Li}$ wave functions, and employ the dipole parametrization (including the Galster factor for $G_{E,n}$) of the nucleon electromagnetic form factors. From Wiringa and Schiavilla (1996).

spectively, in units of $e^2\text{-fm}^{2J}$ and $\mu_N^2\text{-fm}^{2J-2}$, and that, for electric multipole transitions, use of the identity in Eq. (6.21) (Siegert's theorem) has been made, which is valid only if the initial and final states are truly eigen-

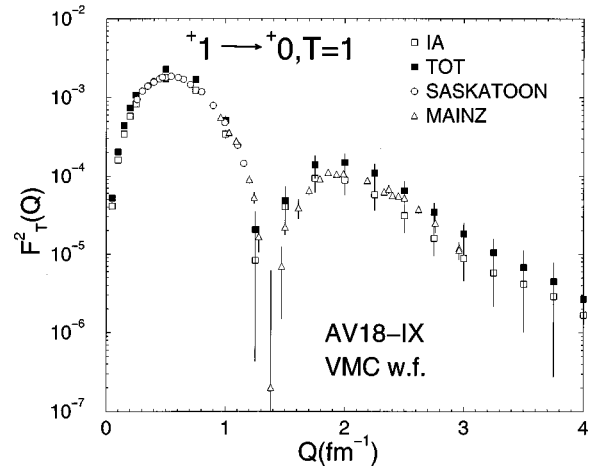


FIG. 34. The transverse form factors for the transition from the $1^+, T=0$ to the $0^+, T=1$ (3.56 MeV) levels of ${}^6\text{Li}$, obtained in impulse approximation (IA) and with inclusion of two-body current contributions (TOT), compared with data from Bergstrom, Deutschmann, and Neuhausen (1979; Saskatoon, Mainz). The theoretical results correspond to the Argonne v_{18} and Urbana IX three-nucleon interactions, use variational Monte Carlo $1^+, T=0$ and $0^+, T=1$ ${}^6\text{Li}$ wave functions, and employ the dipole parametrization (including the Galster factor for $G_{E,n}$) of the nucleon electromagnetic form factors. From Wiringa and Schiavilla (1996).

states of the Hamiltonian. Such is not the case for the VMC wave functions used here. The predicted radiative widths of the $(0^+;1)$ and $(3^+;0)$ states are, respectively, 7.5 eV and 3.4×10^{-4} eV in the impulse approximation, and 9.1 eV and 3.4×10^{-4} eV including two-body contributions (Wiringa and Schiavilla, 1996). These results should be compared with the corresponding experimental values (8.19 ± 0.17) eV and $(4.40 \pm 0.34) 10^{-4}$ eV. Thus the isovector two-body current contributions increase the γ width of the $(0^+;1)$ state by 20%, bringing it into reasonable agreement with experiment.

E. Some concluding remarks

In this section the electromagnetic structure of the $A=2-6$ nuclei has been discussed within a realistic approach to nuclear dynamics, based on nucleons interacting via two- and three-body potentials and consistent two-body currents. The only phenomenological input, beyond that provided by the underlying interactions, consists of the electromagnetic form factors of the nucleon, which are taken from experiment. Within this framework, a variety of electronuclear observables, including ground-state moments (listed in Table XI), as well as elastic and inelastic form factors, are reasonably well described by theory at a quantitative level. The only remaining discrepancies are those between the measured and calculated deuteron tensor polarizations at intermediate values of momentum transfers ($Q \approx 3.5-4.5$ fm $^{-1}$), and between the experimental and calculated positions of the first zero in the ^3He magnetic form factor. However, additional data are needed to confirm these discrepancies with theory. It should also be pointed out that simultaneously reproducing the observed deuteron $A(Q)$, $B(Q)$, and $T_{20}(Q)$ has proven, to date, difficult not only in the essentially nonrelativistic approach discussed above (Schiavilla and Riska, 1991; Plessas, Christian, and Wagenbrunn, 1995), but also in fully relativistic approaches based on quasipotential reductions of the Bethe-Salpeter equation (Hummel and Tjon, 1989; Van Orden, Devine, and Gross, 1995), and on light-front Hamiltonian dynamics (Chung *et al.*, 1988).

The special role played by the two-body charge and current operators associated with π exchange should be emphasized. Their contributions dominate both isoscalar and isovector charge form factors of the $A=2-4$ nuclei, as well as their isovector magnetic structure at intermediate values of momentum transfers $Q \approx 3.5-4.5$ fm $^{-1}$. In fact, a description in which the degrees of freedom associated with virtual-pion production were to be ignored would dramatically fail to reproduce the experimental data. That only the π -exchange currents required by gauge invariance (and chiral symmetry) should have (so far) clear experimental evidence is perhaps not surprising. This fact has been referred to in the past as the “chiral filter” paradigm (Rho and Brown, 1981).

Finally, the remarkable success of the present picture based on (essentially) nonrelativistic dynamics, even at large values of momentum transfer, should be stressed.

It suggests, in particular, that the present model for the two-body charge operators is better than one *a priori* should expect. These operators, such as the π -exchange charge operator, fall into the class of relativistic corrections. Thus evaluating their matrix elements with the usual nonrelativistic wave functions represents only the first approximation to a systematic reduction. A consistent treatment of these relativistic effects would require, for example, inclusion of the boost corrections on the nuclear wave functions (Friar, 1977). Yet, the excellent agreement between the calculated and measured charge form factors of the $A=3-6$ nuclei suggests that these corrections may be negligible in the Q range explored so far.

VII. CORRELATIONS IN NUCLEI

The two outstanding features of the nucleon-nucleon (NN) interaction v_{ij} are its short-range repulsion and long-range tensor character. These induce, among the nucleons in a nucleus, strong spatial spin-isospin correlations, which influence the structure of the ground- and excited-state wave functions. Several nuclear properties reflect these features of the underlying v_{ij} . For example, the two-nucleon density distributions in states with pair spin $S=1$ and isospin $T=0$ are very small at small inter-nucleon separations and exhibit strong anisotropies depending on the spin projection S_z (Forest *et al.*, 1996). Nucleon momentum distributions $N(\mathbf{p})$ (Zabolitzky and Ey, 1978; Ciofi degli Atti, Pace, and Salmè, 1984; Fantoni and Pandharipande, 1984; Schiavilla, Pandharipande, and Wiringa, 1986; Pieper, Wiringa, and Pandharipande, 1992) and, more generally, spectral functions $S(\mathbf{p}, E)$ (Meier-Hajduk *et al.*, 1983; Ramos, Polls, and Dickhoff, 1989; Benhar, Fabrocini, and Fantoni, 1989, 1991; Morita and Suzuki, 1991) have high-momentum components and, for $S(\mathbf{p}, E)$, energy components extending over a wide range of \mathbf{p} and E values, which are produced by short-range and tensor correlations. Finally, these correlations also affect the distribution of strength in response functions $R(\mathbf{q}, \omega)$, which characterize the response of the nucleus to a spin-isospin disturbance injecting momentum \mathbf{q} and energy ω into the system (Czyz and Gottfried, 1963; Fabrocini and Fantoni, 1989).

The present section is organized as follows: We first review, in Secs. VII.A and VII.B, how the short-range repulsive and tensor components of the NN interaction produce strong spatial anisotropies in the two-nucleon distribution functions, and their dependence on the pair spin-isospin states. The experimental evidence for these short-range structures is discussed for the deuteron in Sec. VII.C and for nuclei with $A > 2$ in Sec. VII.D. The longitudinal data from (e, e') inclusive scattering off nuclei have provided, at least in light nuclei, a rather clear indication for the presence of proton-proton correlations from Coulomb sum studies, as summarized in Sec. VII.E. Finally, the last two subsections, F and G, present the current status of momentum-distribution and spectral-function calculations in nuclei. These quantities,

by their very definition, are eminently sensitive to correlation effects and are in principle experimentally accessible via $(e, e'p)$ scattering from nuclei.

A. $T, S = 0, 1$ two-nucleon density distributions in nuclei

The two-nucleon density distributions in T, SM_S two-nucleon states are defined as (Forest *et al.*, 1996)

$$\rho_{T,S}^{M_S}(\mathbf{r}) = \frac{1}{2J+1} \sum_{M_J=-J}^J \langle JM_J | \sum_{i<j} P_{ij}(\mathbf{r}, T, S, M_S) | JM_J \rangle, \quad (7.1)$$

where $|JM_J\rangle$ denotes the ground state of the nucleus with total angular momentum J and projection M_J , and

$$P_{ij}(\mathbf{r}, T, S, M_S) = \delta(\mathbf{r} - \mathbf{r}_{ij}) P_{ij}^T |SM_S; ij\rangle \langle SM_S; ij|, \quad (7.2)$$

$$P_{ij}^{T=0} = (1 - \boldsymbol{\tau}_i \cdot \boldsymbol{\tau}_j) / 4, \quad (7.3)$$

$$P_{ij}^{T=1} = (3 + \boldsymbol{\tau}_i \cdot \boldsymbol{\tau}_j) / 4, \quad (7.4)$$

projects out the specific two-nucleon state, with $\mathbf{r}_{ij} \equiv \mathbf{r}_i - \mathbf{r}_j = \mathbf{r}$. The $\rho_{T,S}^{M_S}$ is normalized such that

$$\sum_{T,S,M_S} \int d\mathbf{r} \rho_{T,S}^{M_S}(\mathbf{r}) = \frac{1}{2} A(A-1), \quad (7.5)$$

i.e., the number of pairs in the nucleus. It is a function of r , θ , independent of the azimuthal angle ϕ . In fact, because of the average over the total angular momentum projections of the nucleus, these two-nucleon densities can simply be expanded as

$$\rho_{T,S}^{M_S}(\mathbf{r}) = \sum_{L=0,2} A_{T,S,L}^{M_S}(r) P_L(\cos\theta), \quad (7.6)$$

where the functions $A_{T,S,L}^{M_S}(r)$, which are explicitly given by

$$A_{T,S,L}^{M_S}(r) = \frac{1}{2J+1} \frac{2L+1}{4\pi} \sum_{M_J} \int d\mathbf{R} \Psi_{M_J}^\dagger(\mathbf{R}) \sum_{i<j} \frac{1}{r_{ij}^2} \times \delta(r - r_{ij}) P_L(\hat{\mathbf{r}}_{ij} \cdot \hat{\mathbf{z}}) P_{ij}(T, S, M_S) \Psi_{M_J}(\mathbf{R}), \quad (7.7)$$

vanish for $L > 2$, and

$$A_{T,S=1,L=0}^{M_S=0} = A_{T,S=1,L=0}^{M_S=\pm 1}, \quad (7.8)$$

$$A_{T,S=1,L=2}^{M_S=0} = -2A_{T,S=1,L=2}^{M_S=\pm 1}. \quad (7.9)$$

Note that in Eq. (7.7) \mathbf{R} represents the coordinates $\mathbf{r}_1, \dots, \mathbf{r}_A$, and $P_{ij}(T, S, M_S)$ is the spin-isospin part of the projection operator introduced in Eq. (7.2).

The two-nucleon densities defined above obviously will reflect features of the underlying NN interaction. Of particular relevance are those in the $T, S = 0, 1$ channel. The momentum-independent part of the NN interaction in this channel, which is dominated by pion exchange, is given by

$$v_{0,1}^{\text{stat}} = v_{0,1}^c(r) + v_{0,1}^t(r) S_{ij}. \quad (7.10)$$

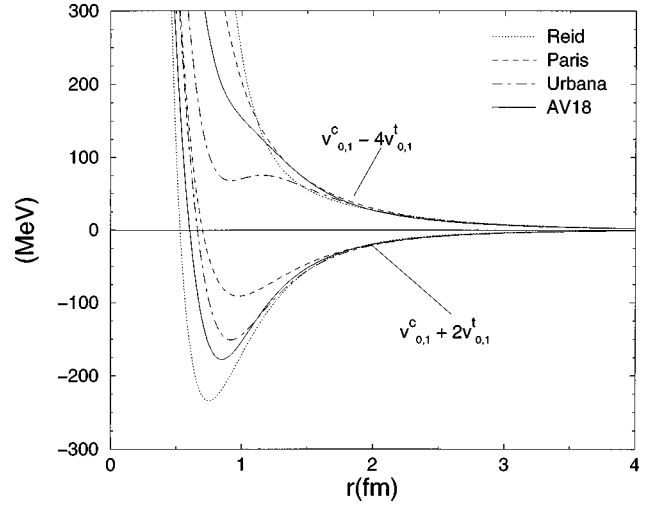


FIG. 35. The upper four lines show expectation values of $v_{0,1}^{\text{stat}}$ for $M_S=0$, $\theta=0$, and the lower four lines are for $M_S=0$, $\theta=\pi/2$ or equivalently $M_S=\pm 1$, $\theta=0$. The expectation values for $M_S=\pm 1$, $\theta=\pi/2$ (not shown) are half way in between. Reid model, Reid (1968); Paris model, Cottingham *et al.* (1973); Urbana model, Lagaris and Pandharipande (1981); AV18 model, Wiringa, Stoks, and Schiavilla (1995).

The tensor operator S_{ij} leads to a strong dependence of the $v_{0,1}^{\text{stat}}$ expectation values upon the relative spatial-spin configurations of the two nucleons:

$$\langle M_S=0 | v_{0,1}^{\text{stat}}(\mathbf{r}) | M_S=0 \rangle = v_{0,1}^c(r) - 4v_{0,1}^t(r) P_2(\cos\theta), \quad (7.11)$$

$$\langle M_S=\pm 1 | v_{0,1}^{\text{stat}}(\mathbf{r}) | M_S=\pm 1 \rangle = v_{0,1}^c(r) + 2v_{0,1}^t(r) P_2(\cos\theta), \quad (7.12)$$

where the angle θ is relative to the spin-quantization axis—i.e., the z axis. These expectation values are shown in Fig. 35 for the combinations $M_S=0$ and $\theta=0$ (particles along the z axis) or $\pi/2$ (particles in the xy plane), and $M_S=\pm 1$ and $\theta=\pi/2$ (Forest *et al.*, 1996). Note that by symmetry the expectation value in the state $M_S=\pm 1$ and $\theta=0$ is the same as that in the state $M_S=0$ and $\theta=\pi/2$. From Fig. 35 it can be seen that the interaction is very repulsive for $r < 0.5$ fm regardless of the M_S value. However, for distances ≈ 1 fm, it is very attractive when the two nucleons, in state $M_S=0$, are confined in the xy plane and very repulsive when they are along the z axis. In contrast, when the two nucleons are in state $M_S=1$, the interaction is repulsive (but not as repulsive as for $M_S=0$) when the two nucleons are in the xy plane and very attractive when they are located along the z axis. The energy difference between the two configurations $M_S=0$ and $\theta=0$ and $\pi/2$ is found to be very large—a few hundreds of MeV—in all realistic NN interactions. As a result, two-nucleon densities in nuclei are strongly anisotropic.

The deuteron is a particularly simple case, since for it the two-nucleon density $\rho_{0,1}^M(\mathbf{r}; d)$ is simply related to the one-nucleon density

$$\rho_{0,1}^M(\mathbf{r}; d) = \frac{1}{3} \times \frac{1}{16} \rho_d^M(\mathbf{r}' = \mathbf{r}/2), \quad (7.13)$$

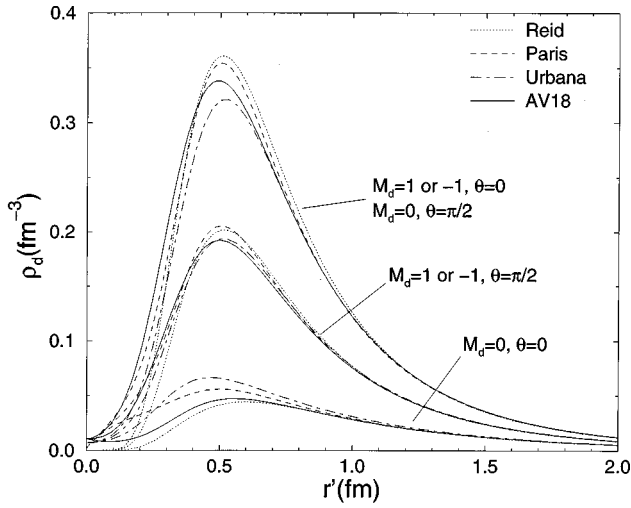


FIG. 36. Deuteron density $\rho_d^{M_d}$ for the indicated values of M_d and θ , obtained from various interaction models (Forest *et al.*, 1996). Note that in the deuteron the two-nucleon density $\rho_{T=0,S=1}^{M_S}(\mathbf{r}) = (1/48)\rho_d^{M_d=M_S}(\mathbf{r}' = \mathbf{r}/2)$. Reid model, Reid (1968); Paris model, Cottingham *et al.* (1973); Urbana model, Lagaris and Panharipande (1981); AV18 model, Wiringa, Stoks, and Schiavilla (1995).

with the normalization

$$\int d^3\mathbf{r}' \rho_d^{M_d}(\mathbf{r}') = 2. \quad (7.14)$$

This is because the relative distance between the two nucleons is twice the distance between each nucleon and the center of mass. Obviously, this property is only valid for a two-body system. Note that the spin-dependent two-body density on the left ($M_S = M$) is an average over projections M_d in the deuteron, while the polarized one-body density on the right ($M_d = M$) has been summed over spins.

The deuteron densities $\rho_d^{M_d}(\mathbf{r}')$ are displayed in Fig. 36 for a variety of NN interactions (and corresponding deuteron wave functions) and the spin-spatial configurations discussed above (Forest *et al.*, 1996). They are essentially model independent and show that the ratio $\rho_d^0(r', \theta=0)/\rho_d^0(r', \theta=\pi/2)$ is very small, indicating that the deuteron has near maximal tensor correlations for distances less than 2 fm.

The deuteron density distributions in $M_d=0$ and $M_d=1$ are plotted in Figs. 37 and 38, along with their contour projections on the xy plane (Forest *et al.*, 1996). The maximum value of ρ_d is large (0.35 fm^{-3}). The maxima of ρ_d^0 form a ring with a diameter of about 1 fm, denoted by d , in the xy plane, while the $\rho_d^{\pm 1}$ has two equal maxima on the z axis separated by a distance d . Equidensity surfaces $\rho_d^{M_d}(\mathbf{r}') = \rho_d$ are obtained by rotating the distributions shown in Figs. 37 and 38 about the z axis and are shown in Fig. 39 for $\rho_d = 0.24$ and 0.08 fm^{-3} (Forest *et al.*, 1996); all four sections are drawn to the same scale. The peculiar toroidal and dumbbell-like shapes result from the combined action of the repulsive core and tensor components of $v_{0,1}(\mathbf{r})$. In fact, the tor-

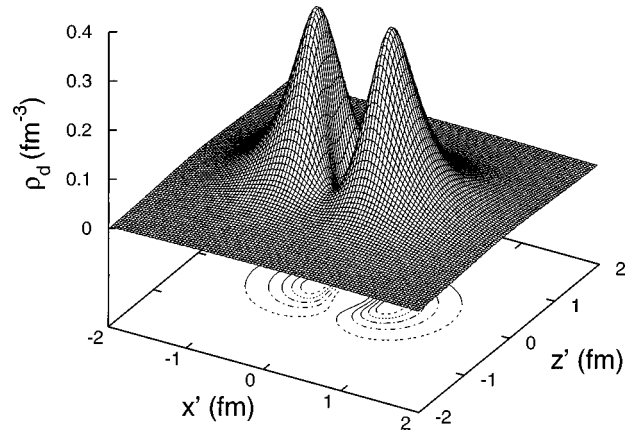


FIG. 37. Deuteron density $\rho_d^{M_d=\pm 1}(x', z')$ obtained from the Argonne v_{18} interaction. The peaks are located at $x'=0$ and $z' = \pm d/2$ (Forest *et al.*, 1996). Note that in the deuteron the two-nucleon density $\rho_{T=0,S=1}^{M_S=\pm 1}(\mathbf{r}) = (1/48)\rho_d^{M_d=\pm 1}(\mathbf{r}' = \mathbf{r}/2)$.

oidal shape is more compact, in the sense that it persists down to smaller values of ρ_d or, equivalently, to larger values of r . Note that, at very small densities (less than 0.05 fm^{-3}), the $\rho_d^0(\mathbf{r}')$ and $\rho_d^{\pm 1}(\mathbf{r}')$ surfaces collapse into disconnected inner and outer parts which, particularly for $M_d=0$, are not close to being spherical in shape. Of course, in the absence of the tensor interaction, the deuteron D state would vanish and the equidensity surfaces would consist of concentric spheres for any value of the density.

The $\rho_{0,1}^{M_S}$ in ${}^3,4\text{He}$, ${}^6,7\text{Li}$, and ${}^{16}\text{O}$ have been recently calculated (Forest *et al.*, 1996) using VMC wave functions, obtained from a realistic Hamiltonian with the Argonne v_{18} two-nucleon (Wiringa, Stoks, and Schiavilla, 1995) and Urbana IX three-nucleon (Pudliner *et al.*, 1995) interactions. The more accurate Faddeev and correlated hyperspherical harmonics wave functions for $A=3$ and GFMC wave functions for $A>3$ are not expected to produce $\rho_{0,1}^{M_S}$ significantly different from VMC.

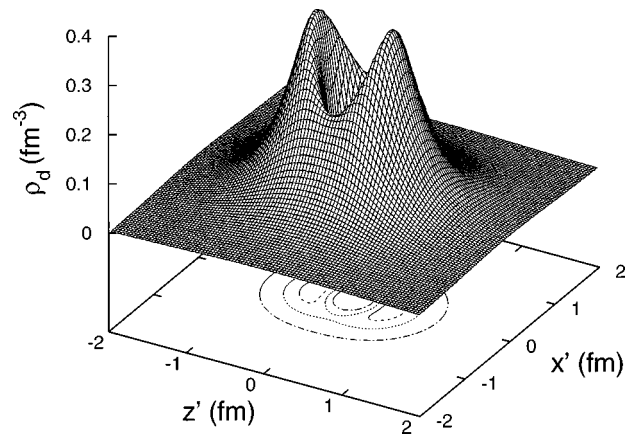


FIG. 38. Deuteron density $\rho_d^{M_d=0}(x', z')$ obtained from the Argonne v_{18} interaction. The peaks are located at $z'=0$ and $x' = \pm d/2$ (Forest *et al.*, 1996). Note that in the deuteron the two-nucleon density $\rho_{T=0,S=1}^{M_S=0}(\mathbf{r}) = (1/48)\rho_d^{M_d=0}(\mathbf{r}' = \mathbf{r}/2)$.

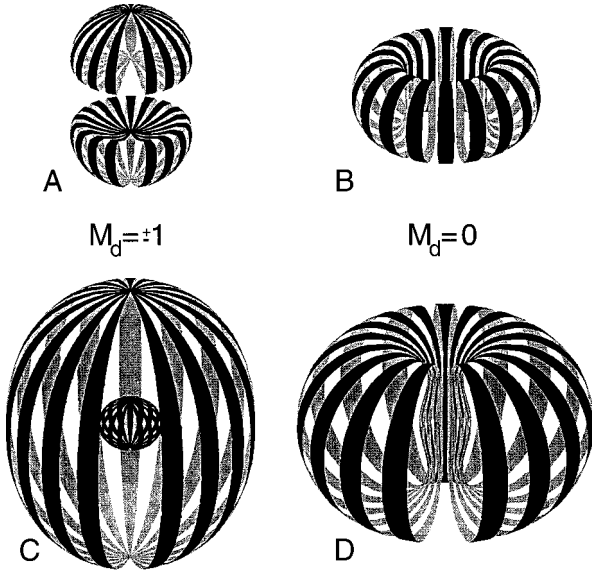


FIG. 39. The surfaces having $\rho_d^{M_d=\pm 1}(\mathbf{r}')=0.24 \text{ fm}^{-3}$ (A) and $\rho_d^{M_d=0}(\mathbf{r}')=0.24 \text{ fm}^{-3}$ (B). The surfaces are symmetric about the z' axis and have $r' \leq 0.74 \text{ fm}$; i.e., the length of the dumbbell along the z' axis as well as the diameter of the outer surface of the torus is 1.48 fm . Sections C and D are for $\rho_d^{M_d=\pm 1,0}(\mathbf{r}')=0.08 \text{ fm}^{-3}$; the maximum value of r' is 1.2 fm (Forest *et al.*, 1996). Note that in the deuteron the two-nucleon density $\rho_{T=0,S=1}^{M_S}(\mathbf{r})=(1/48)\rho_d^{M_d=M_S}(\mathbf{r}'=\mathbf{r}/2)$.

The calculated $\rho_{0,1}^{M_S}(A)$ have been found to have essentially the same shape as the $\rho_{0,1}^{M_S}(d)$ for internucleon separations less than 2 fm . This can be seen in Fig. 40, where the $\rho_{0,1}^{M_S}(\mathbf{r};A)$ densities, divided by the factor R_{Ad} ,

$$R_{Ad} = \frac{\max[\rho_{0,1}^{\pm 1}(\mathbf{r};A)]}{\max[\rho_{0,1}^{\pm 1}(\mathbf{r};d)]}, \quad (7.15)$$

are compared with the $\rho_{0,1}^{M_S}(\mathbf{r};d)$. Again, the smallness of the ratio $\rho_{0,1}^0(r, \theta=0)/\rho_{0,1}^0(r, \theta=\pi/2)$ indicates that ten-

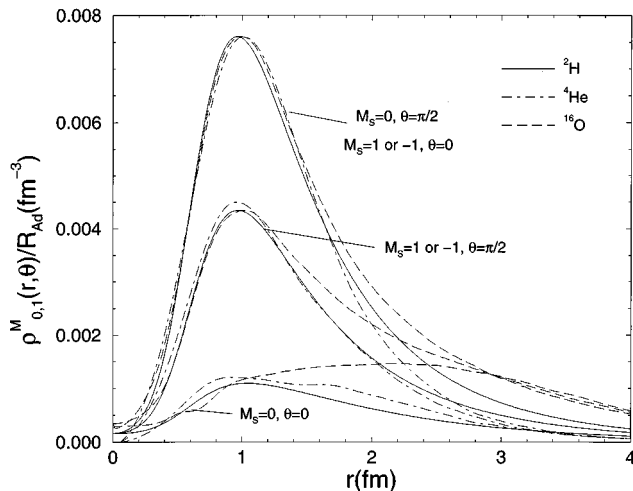


FIG. 40. $\rho_{T=0,S=1}^{M_S}(r, \theta)/R_{Ad}$ for various nuclei. From Forest *et al.* (1996).

TABLE XII. The calculated values of R_{Ad} and other ratios in various nuclei. IP=independent-particle model.

Nucleus	R_{Ad}	$\frac{\langle v_\pi \rangle_A}{\langle v_\pi \rangle_d}$	$\frac{\sigma_{ab,A}^\pi}{\sigma_{ab,d}^\pi}$	$\frac{\sigma_{ab,A}^\gamma}{\sigma_{ab,d}^\gamma}$	IP	$N_{0,1}^A$ Ψ_v
^3He	2.0	2.1	2.4(1) ^a	$\sim 2^d$	1.5	1.49
^4He	4.7	5.1	4.3(6) ^b	$\sim 4^c$	3	2.99
^6Li	6.3	6.3			5.5	5.46
^7Li	7.2	7.8		6.5(5) ^f	6.75	6.73
^{16}O	18.8	22	17(3) ^c	16(3) ^f	30	30.1

^aAltholz *et al.*, 1994.

^bMateos, 1995.

^cMack *et al.*, 1992.

^dFetisov, Gorbunov, and Varfolomeev, 1965; O'Fallon, Koester, and Smith, 1972.

^eArkato *et al.*, 1980.

^fAhrens 1985; Jenkins, Debevec, and Harty, 1994.

sor correlations have near maximal strength in all the nuclei considered. In ^{16}O , the $\rho_{0,1}^{M_S}$ become approximately independent of M_S only for $r \geq 3 \text{ fm}$.

That the neutron-proton relative wave function in a nucleus is similar, at small separations, to that in the deuteron had been conjectured by Levinger and Bethe (1950). Thus Fig. 40 provides a microscopic justification for that conjecture, which has become known since then as the quasideuteron model. As a consequence of this proportionality between the $\rho_{0,1}^{M_S}(\mathbf{r};A)$ and $\rho_{0,1}^{M_S}(\mathbf{r};d)$, the expectation value of any short-ranged $T, S=0,1$ operator is expected to scale, in an A -nucleon system, with R_{Ad} . This is illustrated in Table XII, where the values for R_{Ad} are listed along with the ratios of the calculated expectation values of the one-pion-exchange part of the Argonne v_{18} potential, the observed low-energy pion-absorption cross sections [118 MeV for ^3He (Altholz *et al.*, 1994) and ^4He (Mateos, 1995), and 115 MeV for ^{16}O (Mack *et al.*, 1992)], and the average value of the observed photon-absorption cross sections in the range $E_\gamma=80-120 \text{ MeV}$.⁹ All these processes are dominated by the $T, S=0,1$ pairs. However, while these ratios do suggest the validity of the quasideuteron approximation, their semiquantitative character should not be ignored. For example, the $\langle v_\pi \rangle$ in nuclei has a relatively small contribution from $T, S \neq 0,1$ states, absent in the deuteron, which makes $\langle v_\pi \rangle_A / \langle v_\pi \rangle_d$ slightly larger than R_{Ad} . The pion- and photon-absorption processes in a nucleus are significantly more complicated than the quasideuteron model would suggest, despite the overall agreement between the measured cross-section ratios and the predicted R_{Ad} . In particular, initial- and final-state interaction effects as well as three-body and, more

⁹Data for ^3He were from Fetisov, Gorbunov, and Varfolomeev (1965) and O'Fallon, Koester, and Smith (1972). Data for ^4He were from Arkato *et al.* (1980); for ^7Li and ^{16}O from Ahrens (1985) and Jenkins, Debevec, and Harty (1994).

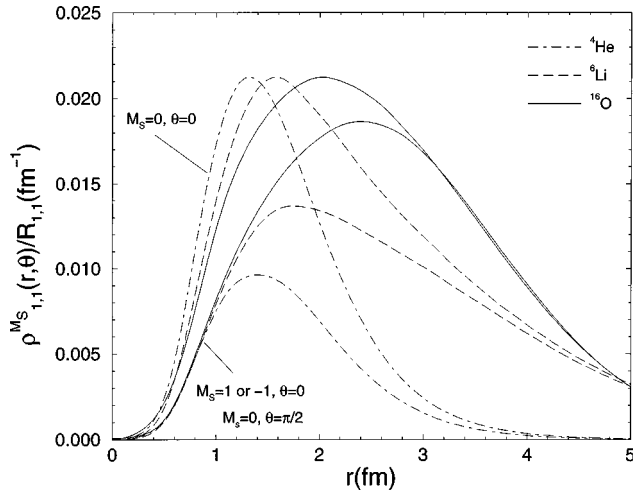


FIG. 41. $\rho_{1,1}^{M_S}(r, \theta)/R_{1,1}^A$ for various nuclei (Forest *et al.*, 1996). The upper three curves are for $M_S=0, \theta=0$ while the lower ones are for $M_S=0, \theta=\pi/2$ and equivalently $M_S=\pm 1, \theta=0$.

generally, many-body mechanisms—all of which are neglected in the quasideuteron approximation—are known to influence the measured absorption cross sections in an A -nucleon system at a quantitative level (Weyer, 1990).

B. $T, S \neq 0, 1$ two-nucleon density distributions in nuclei

It is interesting to study the two-nucleon density distributions in states with pair spin-isospin $TS=11, 00$, and 10 (Forest *et al.*, 1996). They are shown for ^4He , ^6Li , and ^{16}O in Figs. 41–43, where all curves have been normalized to have the same peak height as for ^{16}O .

The $T, S=1, 1$ interaction has a tensor component of opposite sign with respect to that of the $T, S=0, 1$ interaction. As a consequence, the $M_S=\pm 1$ ($=0$) density distributions are largest when the two nucleons are in the xy plane (along the z axis)—that is, the situation is the reverse of that illustrated in Fig. 40 for $T, S=0, 1$. However, Fig. 41 shows that the $T, S=1, 1$ densities are strongly A dependent; in particular, their anisotropy decreases as the number of nucleons increases.

This strong A dependence is also a feature of the $T, S=0, 0$ two-nucleon densities, as can be seen in Fig. 42. In contrast, the $T, S=1, 0$ density distributions, shown in Fig. 43, do display, for separation distances less than 2 fm, very similar shapes. This is not surprising, since the $T, S=1, 0$ interaction is attractive enough to produce a virtual bound state, which manifests itself as a pole on the second energy sheet of the 1S_0 -channel T -matrix.

It is also interesting to compare the total number of pairs in T, S states predicted by the present fully correlated wave functions with those obtained from simple independent-particle wave functions (Forest *et al.*, 1996). The total numbers of T, S pairs, defined as

$$N_{T,S}^A = \sum_{M_S} 2\pi \int \rho_{T,S}^{M_S}(r, \theta; A) r^2 dr d\cos\theta, \quad (7.16)$$

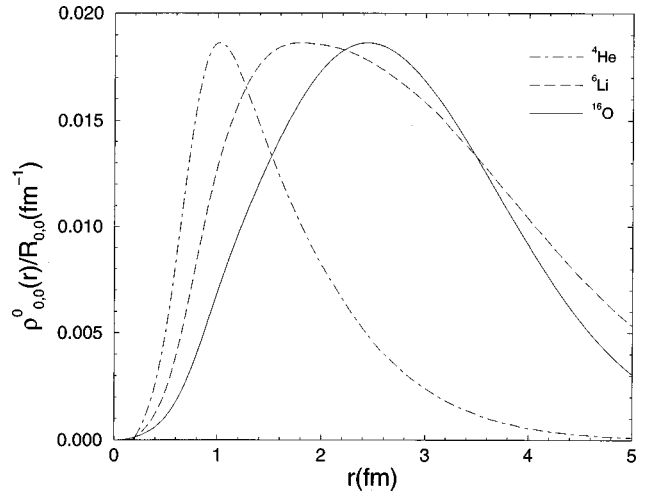


FIG. 42. $\rho_{0,0}^0(r)/R_{0,0}^A$ for various nuclei. From Forest *et al.* (1996).

are listed in Table XIII. Note that since both the correlated and independent-particle wave functions are eigenstates of total isospin T_A , the following relations have to be satisfied:

$$N_{0,0}^A + N_{0,1}^A = \frac{1}{8}[A^2 + 2A - 4T_A(T_A + 1)], \quad (7.17)$$

$$N_{1,0}^A + N_{1,1}^A = \frac{1}{8}[3A^2 - 6A + 4T_A(T_A + 1)]. \quad (7.18)$$

However, if the total spin

$$\mathbf{S}_A = \sum_i \frac{1}{2} \boldsymbol{\sigma}_i \quad (7.19)$$

were to commute with the Hamiltonian, there would be similar relations,

$$N_{0,0}^A + N_{1,0}^A = \frac{1}{8}[A^2 + 2A - 4S_A(S_A + 1)], \quad (7.20)$$

$$N_{0,1}^A + N_{1,1}^A = \frac{1}{8}[3A^2 - 6A + 4S_A(S_A + 1)], \quad (7.21)$$

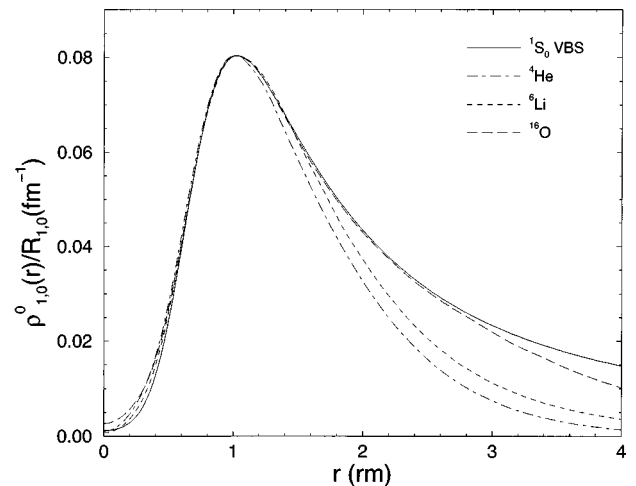


FIG. 43. $\rho_{1,0}^0(r)/R_{1,0}^A$ for various nuclei. From Forest *et al.* (1996).

TABLE XIII. The calculated values of $R_{T,S}^A$ and $N_{T,S}^A$ in various nuclei. IP=independent particle model.

Nucleus	$R_{1,0}^A$			$R_{0,0}^A$			$R_{1,1}^A$		
	IP	$N_{1,0}^A$	Ψ_v	IP	$N_{0,0}^A$	Ψ_v	IP	$N_{1,1}^A$	Ψ_v
^3He	0.087	1.5	1.35	0.0016	0	0.01	0.012	0	0.14
^4He	0.22	3	2.5	0.0085	0	0.01	0.060	0	0.47
^6Li	0.24	4.5	4.0	0.061	0.5	0.52	0.104	4.5	4.96
^7Li	0.37	6.75	6.1	0.118	0.75	0.77	0.18	6.75	7.41
^{16}O	1	30	28.5	1	6	6.05	1	54	55.5

for the total number of pairs with spin 0 and 1. This is the case for the independent-particle wave functions, which are indeed eigenstates of \mathbf{S}_A (the independent-particle ^2H , ^3He , ^4He , ^6Li , ^7Li , and ^{16}O wave functions have, respectively, $S_A=1, \frac{1}{2}, 0, 1, \frac{1}{2}$, and 0). However, tensor correlations in the realistic wave functions produce admixtures of states with larger S_A . These correlations reduce the $N_{1,0}^A$ and increase the $N_{1,1}^A$ by the same amount since their sum must be conserved. In fact, this conversion of $T=1$ pairs from spin 0 to spin 1 leads to a reduction in the binding energy of nuclei (Forest *et al.*, 1996), since the $T,S=1,0$ interaction is far more attractive than the $T,S=1,1$ interaction. As an example, in ^4He the $T,S=1,0$ interaction gives -14.2 MeV per pair, while the $T,S=1,1$ interaction gives only -0.8 MeV per pair. Thus the conversion of 0.47 $T=1$ pairs from the $S=0$ to the $S=1$ state raises the energy of ^4He by ~ 6.3 MeV. The mechanism discussed here—it is important to realize—is an intrinsically many-body effect. Indeed, a tensor correlation between nucleons i and j will not change the total spin S of this pair; however, by flipping the individual spins of i and j , it can convert pairs ik and/or jl from $S=0$ to $S=1$.

C. Experimental evidence for the short-range structure in the deuteron

The best experimental evidence, so far, for the presence of torus- and dumbbell-like short-range structures in the ground state of nuclei comes from deuteron elastic form-factor measurements.

The measured charge and quadrupole form factors of the deuteron (Arnold *et al.*, 1975; Simon, Schmitt, and Walther, 1981; Schulze *et al.*, 1984; Cramer *et al.*, 1985; Dmitriev *et al.*, 1985; Gilman *et al.*, 1990; Platchkov *et al.*, 1990; The *et al.*, 1991) are related, in the impulse approximation, to the Fourier transforms of the one-body densities (Forest *et al.*, 1996)

$$F_{C,M_d}(q) = \frac{1}{2} \int \rho_d^{M_d}(\mathbf{r}') e^{iqz'} d^3\mathbf{r}'. \quad (7.22)$$

In a naive model, in which the $M_d=1(-1)$ density is represented by the sum of two δ functions at $z' = \pm d/2$, the zeros of $F_{C,M_d=1}(q)$ would occur at $qd = \pi, 3\pi, \dots$. The cancellation between the contributions from the two peaks persists even when these have a finite width. Thus experimentally locating the position of the zeros provides an approximate determination of

the distance between the maxima of $\rho_d^{M_d=\pm 1}$. This distance coincides with the diameter of the ring of maximum density of $\rho_d^{M_d=0}$. Similarly, the zeros of $F_{C,M_d=0}(q)$ provide an estimate for the thickness t of the torus (at half maximum density, t is predicted to be about 0.9 fm by realistic NN interactions). This is most easily seen by considering the Fourier transform of a disk of thickness t located in a plane perpendicular to the momentum transfer \mathbf{q} .

If a small magnetic contribution to the deuteron tensor polarization is neglected, then this observable can be simply expressed as (Forest *et al.*, 1996)

$$T_{20}(q) \approx -\sqrt{2} \frac{F_{C,0}^2(q) - F_{C,1}^2(q)}{F_{C,0}^2(q) + 2F_{C,1}^2(q)}. \quad (7.23)$$

The minima of $T_{20}(q)$ occur when $F_{C,M_d=1}(q)$ vanishes, while the maxima occur when $F_{C,M_d=0}(q)$ vanishes. These minima and maxima correspond to those q values for which the recoiling deuteron is in state $M_d=0$ or $M_d=\pm 1$, respectively. The first minimum has been measured to be at $q \approx 3.5 \text{ fm}^{-1}$ (Dmitriev *et al.*, 1985; Gilman *et al.*, 1990; The *et al.*, 1991), in agreement with the value $d \approx 1$ fm predicted by realistic potentials. The first maximum of T_{20} is yet to be observed: it will provide a measure of the torus thickness. Of course, relativistic corrections and contributions from two-body charge operators will modify, at the 10% level for moderate q values (less than 5 fm^{-1}), the analysis outlined here. Nevertheless, the short-range structures present in the deuteron dominate the q behavior of T_{20} .

The analysis described above can be extended to the deuteron magnetic form factor. This observable is the Fourier transform of a transition density, since the photon changes the spin projection of the deuteron along \mathbf{q} by ± 1 . This transition density is in fact dominated by the toroidal structure. In particular, as shown in Forest *et al.* (1996), the zero of the B -structure function, which experimentally occurs at about $q=7 \text{ fm}^{-1}$, provides an estimate for the thickness of the torus: $t \approx 0.85$ fm.

Because of these short-range structures, the nucleon momentum distribution in the deuteron depends strongly on the M_d state. It may be experimentally accessible from cross-section asymmetry measurements in double-coincidence experiments of the type $\vec{d}(e,e'p)n$ (Forest *et al.*, 1996) and $d(e,e'\vec{p})\vec{n}$ (Schiavilla, 1997). However, experiments of this type have not yet been

TABLE XIV. The asymptotic D/S state ratios and D_2 coefficients in fm^2 for the dp , dd , and αd breakup channels of ${}^3\text{He}$, ${}^4\text{He}$, and ${}^6\text{Li}$, respectively. The ${}^3\text{He}$ - dp result for η is from a Faddeev calculation (Friar *et al.*, 1988), while all other results are from variational Monte Carlo calculations (Forest *et al.*, 1996).

	η		D_2 (fm^2)	
	Theory	Experiment	Theory	Experiment
${}^3\text{He}$ - dp	-0.043	-0.042 ± 0.007^a	-0.15	-0.20 ± 0.04^a
${}^4\text{He}$ - dd	-0.091		-0.12	-0.3 ± 0.1^b
${}^6\text{Li}$ - αd	-0.29		-0.07	

^aSen and Knutson, 1982; Eiró and Santos, 1990.

^bKarp *et al.*, 1984.

performed. It is important to stress the complementarity of these exclusive experiments to the elastic form-factor measurements. The former should allow us to ascertain to what extent these peculiar short-range structures are really due to nucleonic degrees of freedom, as has been implicitly assumed in the analysis presented here.

D. Short-range structure in $A > 2$ nuclei

In addition to two-nucleon densities, short-range and tensor correlations strongly influence two-cluster distribution functions, such as $\vec{d}\vec{p}$ in ${}^3\text{He}$, $\vec{d}\vec{d}$ in ${}^4\text{He}$, and $\alpha\vec{d}$ in ${}^6\text{Li}$. The two-cluster overlap functions are simply defined as (Forest *et al.*, 1996)

$$\begin{aligned}
 A_{ab}(M_a, M_b, M_J, \mathbf{r}_{ab}) &= \langle \mathcal{A} \Psi_{a, M_a} \Psi_{b, M_b} | \Psi_{M_J} \rangle \\
 &= \sum_{LM_L SM_S} \langle LM_L, SM_S | JM_J \rangle \\
 &\quad \times \langle J_a M_a, J_b M_b | SM_S \rangle R_L(r_{ab}) Y_{LM_L}(\hat{\mathbf{r}}_{ab}), \quad (7.24)
 \end{aligned}$$

where \mathbf{r}_{ab} is the relative coordinate between the centers of mass of the two clusters, and \mathcal{A} is an antisymmetrization operator for the two-cluster state. The $R_L(r_{ab})$ radial functions are obtained from

$$\begin{aligned}
 R_L(r_{ab}) &= \sum_{M_a M_b M_L M_S} \langle J_a M_a, J_b M_b | SM_S \rangle \\
 &\quad \times \langle LM_L, SM_S | JM_J \rangle \\
 &\quad \times \int d\mathbf{R} [\mathcal{A} \Psi_{a, M_a}(\mathbf{R}_a) \Psi_{b, M_b}(\mathbf{R}_b)]^\dagger Y_{LM_L}^*(\hat{\mathbf{r}}_{ab}) \\
 &\quad \times \frac{\delta(r - r_{ab})}{r_{ab}^2} \Psi_{M_J}(\mathbf{R}), \quad (7.25)
 \end{aligned}$$

where $\mathbf{R}_{a(b)}$ represents the coordinates of particles in cluster $a(b)$.

The $\vec{d}\vec{p}$, $\vec{d}\vec{d}$, and $\vec{d}\alpha$ overlap functions in, respectively, ${}^3\text{He}$, ${}^4\text{He}$, and ${}^6\text{Li}$ have recently been calculated with Monte Carlo methods using realistic wave functions (Schiavilla, Pandharipande, and Wiringa, 1986; Forest *et al.*, 1996). Angular momentum and parity selection rules restrict the sum over L in Eq. (7.24) to $L=0$ and 2.

Incidentally, the radial functions $R_L(r_{ab})$ provide information on the asymptotic properties of the overlap functions. These can be experimentally determined, although indirectly, from distorted-wave Born-approximation (DWBA) analyses of transfer reactions (Eiró and Santos, 1990). Two such properties are the D_2 parameter,

$$D_2^{ab} = \frac{\int R_2(r_{ab}) r_{ab}^4 dr_{ab}}{15 \int R_0(r_{ab}) r_{ab}^2 dr_{ab}}, \quad (7.26)$$

and the asymptotic D/S ratio $\eta_{ab} = C_2^{ab}/C_0^{ab}$, where C_0 and C_2 are the asymptotic normalization constants of $R_0(r)$ and $R_2(r)$, respectively:

$$R_L(r_{ab}) = \lim_{r_{ab} \rightarrow \infty} -i^L C_L^{ab} h_L(i\alpha_{ab} r_{ab}). \quad (7.27)$$

Here h_L is the spherical Hankel function of the first kind and α_{ab} is the wave number associated with the separation energy of the nucleus into clusters a and b . Theoretical estimates for D_2^{ab} and η_{ab} are compared with the values extracted from experiment (Sen and Knutson, 1982; Karp *et al.*, 1984) in Table XIV. It should be emphasized that the theoretical estimates obtained from variational wave functions may not be very accurate, as these wave functions minimize the energy, to which long-range configurations contribute very little.

Going back to the short-range structure, it is interesting to study the two-cluster densities defined as

$$\rho_{ab}^{M_a, M_b, M_J}(\mathbf{r}_{ab}) = |A_{ab}(M_a, M_b, M_J, \mathbf{r}_{ab})|^2. \quad (7.28)$$

They exhibit spin-dependent spatial anisotropies which are easily understood in terms of the toroidal or dumbbell structure of the polarized deuteron. To illustrate these features, the $\vec{d}\vec{d}$ densities in ${}^4\text{He}$ are shown in Fig. 44 for two different spatial configurations of the deuterons—along the spin-quantization axis (the “ z axis”) and in the plane perpendicular to it (the “ xy plane”); Forest *et al.*, 1996). The dd cluster density is largest when the two $M_d=0$ deuterons are positioned one on top of the other—that is, the two tori share a common axis—and the cluster density is smallest when the two $M_d=0$ deuterons lie one next to the other—that is, the two tori are both in the xy plane. A similar analy-

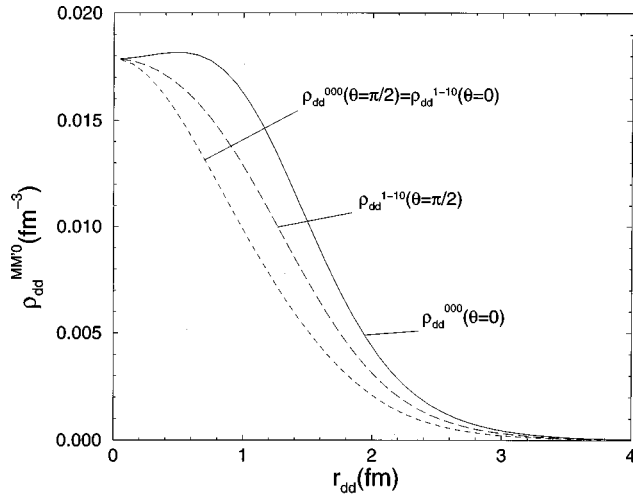


FIG. 44. Density distributions of $\vec{d}\vec{d}$ clusters in ${}^4\text{He}$ in parallel ($\theta=0$) and transverse ($\theta=\pi/2$) directions. From Forest *et al.* (1996).

sis can be made when the two deuterons are, respectively, in the states $M_d=1$ and $M_d=-1$, i.e., in the dumbbell-like shapes.

Similar features are shared by the $\vec{d}\vec{p}$ cluster densities in ${}^3\text{He}$ and the $\vec{d}\alpha$ cluster densities in ${}^6\text{Li}$: the density is enhanced in the direction corresponding to the most efficient or compact placement of the deuteron relative to the remaining cluster, and it is reduced in those directions that would lead to very extended structures (Forest *et al.*, 1996).

These structures are expected to produce cross-section asymmetries in experiments such as $(e, e' \vec{a}) \vec{b}$. In the plane-wave impulse approximation, the cross section for this latter process is in fact proportional to the momentum distribution $|\tilde{A}_{ab}(M_a, M_b, M_J, \mathbf{p})|^2$ obtained from the Fourier transform of the overlap function $A_{ab}(M_a, M_b, M_J, \mathbf{r}_{ab})$ (Jacob and Maris, 1966, 1973; Frullani and Mougey, 1984). These momentum distributions have been calculated by Forest *et al.* (1996) for the $\vec{d}\vec{p}$, $\vec{d}\vec{d}$, and $\alpha\vec{d}$ overlaps; they depend strongly on the relative orientation between the cluster-spin projections and the momentum \mathbf{p} (the missing momentum). Of course, final-state interaction effects and two-body corrections to the charge and current operators will complicate the analysis of these experiments (Schiavilla, 1990; Glöckle *et al.*, 1995), in particular the extraction, from the measured asymmetries, of the $|\tilde{A}_{ab}(M_a, M_b, M_J, \mathbf{p})|^2$ momentum distributions. However, the experimental confirmation, as of yet still lacking, of the short-range structures discussed above would be most interesting.

E. Evidence for short-range correlations from inclusive (e, e') longitudinal data

Perhaps the clearest experimental evidence for the presence of short-range correlations in the ground-state

wave function, at least in light nuclei, is from inclusive (e, e') longitudinal data. It has long been known that the total integrated strength of the longitudinal response function $R_L(q, \omega)$ measured in inclusive electron scattering [the so-called Coulomb sum rule $S_L(q)$],

$$S_L(q) = \frac{1}{Z} \int_{\omega_{el}^+}^{\infty} d\omega S_L(q, \omega),$$

$$S_L(q, \omega) \equiv R_L(q, \omega) / |G_{E,p}(q, \omega)|^2, \quad (7.29)$$

is related to the Fourier transform of the proton-proton distribution function (Drell and Schwartz, 1958; McVoy and Van Hove, 1962). In Eq. (7.29), $G_{E,p}$ is the proton electric form factor, and ω_{el} is the energy of the recoiling A -nucleon system with Z protons (the lower integration limit excludes the elastic electron-nucleus contribution). The $S_L(q)$ can be expressed as

$$\begin{aligned} S_L(q) &= \frac{1}{Z} \langle 0 | \rho_L^\dagger(\mathbf{q}) \rho_L(\mathbf{q}) | 0 \rangle - \frac{1}{Z} \langle 0 | \rho_L(\mathbf{q}) | 0 \rangle^2 \\ &\equiv 1 + \rho_{LL}(q) - Z |F_L(q)|^2, \end{aligned} \quad (7.30)$$

where $|0\rangle$ is the ground state of the nucleus, $\rho_L(\mathbf{q})$ is the nuclear charge operator, $F_L(q)$ is the longitudinal form factor [divided by $G_{E,p}(q, \omega_{el})$] normalized as $F_L(q=0)=1$, and a longitudinal-longitudinal distribution function has been defined as

$$\rho_{LL}(q) \equiv \frac{1}{Z} \int \frac{d\Omega_q}{4\pi} \langle 0 | \rho_L^\dagger(\mathbf{q}) \rho_L(\mathbf{q}) | 0 \rangle - 1. \quad (7.31)$$

If relativistic corrections and two-body contributions to the nuclear charge operator are neglected, then $\rho_L(\mathbf{q})$ (divided by the electric proton form factor) is simply given by

$$\rho_L(\mathbf{q}) \approx \sum_{i=1,A} e^{i\mathbf{q}\cdot\mathbf{r}_i} (1 + \tau_{z,i}) / 2, \quad (7.32)$$

and the resulting longitudinal-longitudinal distribution function can be written as

$$\rho_{LL}(q) = \int d\mathbf{r}_1 d\mathbf{r}_2 j_0(q|\mathbf{r}_1 - \mathbf{r}_2|) \rho_{LL}(\mathbf{r}_1, \mathbf{r}_2), \quad (7.33)$$

with

$$\begin{aligned} \rho_{LL}(\mathbf{r}_1, \mathbf{r}_2) &= \frac{1}{4Z} \sum_{i \neq j} \langle 0 | \delta(\mathbf{r}_1 - \mathbf{r}_i) \delta(\mathbf{r}_2 - \mathbf{r}_j) (1 + \tau_{z,i}) \\ &\quad \times (1 + \tau_{z,j}) | 0 \rangle, \end{aligned} \quad (7.34)$$

$$\int d\mathbf{r}_1 d\mathbf{r}_2 \rho_{LL}(\mathbf{r}_1, \mathbf{r}_2) = Z - 1. \quad (7.35)$$

Note that, within this approximation and in the limit $q \rightarrow \infty$, $S_L(q) \rightarrow 1$ (that is, in the large-momentum-transfer limit), the longitudinal cross section is due to the incoherent contributions from the Z protons. In this case, the longitudinal-longitudinal distribution function gives the probability of finding two protons at positions \mathbf{r}_1 and \mathbf{r}_2 , regardless of their spin-projection states. Such a quantity is, therefore, sensitive to the short-range correlations induced by the repulsive core of the NN interac-

tion (Schiavilla *et al.*, 1987). Naively, one would expect that for noninteracting nucleons

$$\rho_{LL,unc} \simeq (Z-1)\rho_L(\mathbf{r}_1)\rho_L(\mathbf{r}_2), \quad (7.36)$$

$$\rho_L(\mathbf{r}) = \frac{1}{2Z} \sum_{i=1,A} \langle 0 | \delta(\mathbf{r} - \mathbf{r}_i) (1 + \tau_{z,i}) | 0 \rangle. \quad (7.37)$$

However, the expression above ignores the statistical correlations due to the Pauli exclusion principle obeyed by the nucleons as well as the “minimal” correlations induced by the conservation of the center-of-mass position. In light nuclei, the first are negligible, while the second are important only at low momentum transfer (Schiavilla *et al.*, 1987). The corresponding “uncorrelated” Coulomb sum rule is given by

$$S_{L,unc}(q) = 1 - |F_L(q)|^2, \quad (7.38)$$

and therefore only the difference between $S_L(q)$ and $S_{L,unc}(q)$ [or between $\rho_{LL}(q)$ and $\rho_{LL,unc}(q)$] provides a measure of the strength of the correlations.

Direct comparison between the calculated Coulomb sum rule and the experimental data is not possible, since $S_L(q)$ includes contributions from both spacelike ($\omega < q$) and timelike ($\omega > q$) regions. In practice, $S_L(q)$ can be measured up to some $\omega_{max} < q$ by inclusive electron scattering. The residual integral from ω_{max} to ∞ is then obtained from estimates of $R_L(q, \omega > \omega_{max})$ that satisfy energy-weighted sum rules $W_L^{(n)}(q)$,

$$W_L^{(n)}(q) = \frac{1}{Z} \int_{\omega_{el}^+}^{\infty} d\omega \omega^n S_L(q, \omega), \quad (7.39)$$

calculated theoretically (Schiavilla, Fabrocini, and Pandharipande, 1987; Schiavilla, Pandharipande, and Fabrocini, 1989). These can simply be expressed as expectation values of commutators of the charge operator with the Hamiltonian. For example, the $n=1$ sum rule is given by

$$W_L^{(1)}(q) = \frac{1}{2Z} \langle 0 | [\rho_L^\dagger(\mathbf{q}), [H, \rho_L(\mathbf{q})]] | 0 \rangle - \frac{1}{Z} \omega_{el} |F_L(q)|^2 \quad (7.40)$$

$$= \frac{q^2}{2m} + \frac{1}{2Z} \langle 0 | [\rho_L^\dagger(\mathbf{q}), [v_2 + V_3, \rho_L(\mathbf{q})]] | 0 \rangle - \frac{1}{Z} \omega_{el} |F_L(q)|^2, \quad (7.41)$$

where v_2 and V_3 are the two- and three-body potentials. The charge-exchange part of the NN interaction, particularly the one-pion-exchange potential, leads to a strong enhancement of the energy-weighted sum rule over that obtained in the limit of noninteracting nucleons (the Fermi-gas limit)—that is, $q^2/2m$.

In light nuclei, reasonable agreement between theory and experiment is obtained for the Coulomb sum rule (Schiavilla, Pandharipande, and Fabrocini, 1989), as illustrated in Fig. 45 (${}^2\text{H}$ data from Dytman *et al.*, 1988; ${}^3\text{H}$ data from Dow *et al.*, 1988; ${}^3\text{He}$ data from Marchand *et al.*, 1985, and Dow *et al.*, 1988; ${}^4\text{He}$ data from von Reden *et al.*, 1990). The open dots labeled $S_{L,tr}$ in this

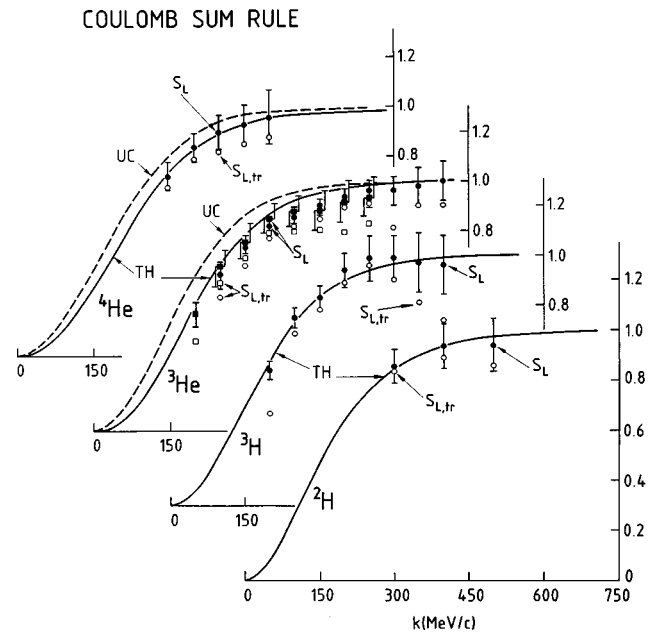


FIG. 45. The experimental $S_{L,tr}$ (open data points) and tail-corrected S_L (filled data points with error bars) compared with theory in ${}^2\text{H}$, ${}^3\text{H}$, ${}^3\text{He}$, and ${}^4\text{He}$. Solid lines, Schiavilla, Pandharipande, and Fabrocini, 1989; dashed curves, the $S_{L,unc}$ of ${}^3\text{He}$ and ${}^4\text{He}$. Data for ${}^3\text{He}$: O, Saclay (Marchand *et al.*, 1985); \square , Bates (Dow *et al.*, 1988). Data for ${}^2\text{H}$: Bates (Dytman *et al.*, 1988). Data for ${}^3\text{H}$, Dow *et al.*, 1988; for ${}^4\text{He}$ von Reden *et al.*, 1990.

figure show the integral of the experimental data up to ω_{max} ; the filled dots show the complete integral with the theoretically extrapolated $R_L(q, \omega > \omega_{max})$. The dashed lines show values for the $S_{L,unc}(q)$ in ${}^3\text{He}$ and ${}^4\text{He}$ obtained from Eq. (7.38), neglecting the correlations between the protons. Their effect is rather small. Note that in ${}^2\text{H}$ and ${}^3\text{H}$ the $S_L(q)$ is, in the approximation given by Eq. (7.32), exactly given by the $S_{L,unc}(q)$, since there is only a single proton.

Of course, the nuclear charge operator, in addition to the dominant proton contribution, also includes relativistic corrections and two-body components. Their effect on the $S_L(q)$ is very small in the q range covered by the present experiments, but it does reduce the small systematic discrepancies between the theoretical and measured Coulomb sum rules (Schiavilla, Wiringa, and Carlson, 1993). However, the importance of these contributions is enhanced when considering the longitudinal-longitudinal distribution function. This quantity is shown in Fig. 46 for ${}^4\text{He}$ (the Saclay data are from Zghiche *et al.*, 1993; the Bates data from von Reden *et al.*, 1990, give similar values for the longitudinal-longitudinal distribution function). The large error bars on the experimental $\rho_{LL}(q)$ reflect predominantly systematic uncertainties associated with the tail contribution (Beck, 1990; Schiavilla, Wiringa, and Carlson, 1993). The agreement between the experimental analysis and the results of calculations in which both one- and two-body terms are included in $\rho_L(\mathbf{q})$ is rather good. This situation is reminiscent of that encountered in the

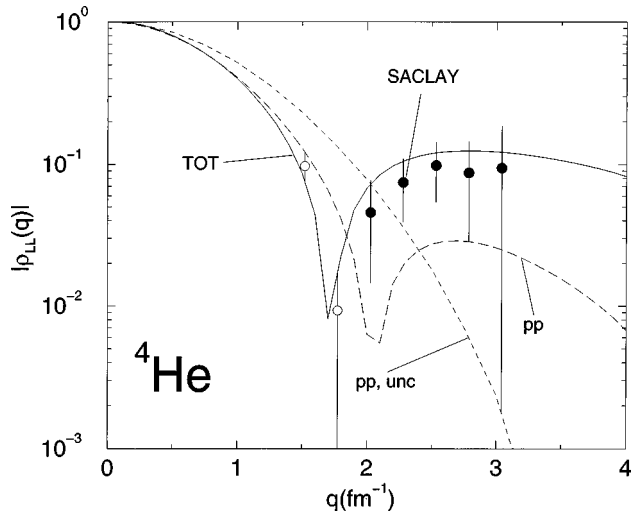


FIG. 46. The experimental longitudinal-longitudinal distribution function (LLDF) of ${}^4\text{He}$, obtained from the measured charge form factor and tail-corrected Coulomb sum-rule data (Saclay), compared with theory (Schiavilla, Wiringa, and Carlson, 1993). The curve labeled pp only takes into account the proton contributions to the nuclear charge operator, while that labeled TOT also includes contributions from two-body charge operators and relativistic corrections. Also shown is the LLDF for uncorrelated protons (curve labeled pp, unc). Note that the empty and filled circles denote positive and negative values for the experimental LLDF.

charge form factors of ${}^3\text{H}$, ${}^3\text{He}$, and ${}^4\text{He}$, in which the two-body charge operators play a crucial role in reproducing the data in the diffraction minimum. Figure 46 shows an interesting interplay between correlation effects in the ground-state wave function and relativistic and two-body corrections to the longitudinal transition operator. Note that the $\rho_{LL, \text{unc}}(q)$ is at variance with the data: the zero is shifted to much higher momentum transfer, and the strength of the secondary maximum is greatly underestimated.

As a final remark, we note that the present experimental situation with regard to the Coulomb sum rule in heavier nuclei is controversial. The original analysis of the Saclay data indicated substantial lack of strength, as much as 40%, in the longitudinal response of nuclei like ${}^{40}\text{Ca}$ and ${}^{56}\text{Fe}$ (Meziani *et al.*, 1984). More recently, however, an independent reanalysis of the ${}^{56}\text{Fe}$ world data shows that the resulting integrated longitudinal strength is not quenched with respect to the model-independent prediction $S_L(q) \approx 1$ at large q (Jourdan, 1995). This reanalysis combined Saclay, Bates, and SLAC data covering a wide range of values in the virtual-photon longitudinal polarization parameter ϵ [the longitudinal response is extracted from the slope of the (e, e') cross section as function of ϵ]. The analysis of inclusive electron scattering from heavy nuclei and, in particular, the separation of the cross section into its longitudinal and transverse contributions, is further complicated by distortion effects of the electron waves in the nuclear Coulomb field (Orlandini and Traini, 1991). The latter have been found to be negligible in light nuclei.

The current state of affairs with regard to Coulomb sum measurements in heavy nuclei is clearly unsatisfactory. The experimental controversy needs to be resolved.

F. Momentum distributions

The nucleon momentum distribution is given by

$$N_{\sigma\tau}(\mathbf{p}) = \langle 0 | a_{\sigma\tau}^\dagger(\mathbf{p}) a_{\sigma\tau}(\mathbf{p}) | 0 \rangle, \quad (7.42)$$

where $|0\rangle$ is the ground state of the nucleus, and $a_{\sigma\tau}(\mathbf{p})$ and $a_{\sigma\tau}^\dagger(\mathbf{p})$ are annihilation and creation operators for a nucleon in the spin-isospin state $\sigma\tau$ with momentum \mathbf{p} . In the coordinate representation, the $N_{\sigma\tau}(\mathbf{p})$ can be written as

$$N_{\sigma\tau}(\mathbf{p}) = \int d\mathbf{r}'_1 d\mathbf{r}_1 d\mathbf{r}_2 \cdots d\mathbf{r}_A \Psi_0^\dagger(\mathbf{r}'_1, \dots, \mathbf{r}_A) \times e^{i\mathbf{p} \cdot (\mathbf{r}'_1 - \mathbf{r}_1)} P_{\sigma\tau}(1) \Psi_0(\mathbf{r}_1, \dots, \mathbf{r}_A), \quad (7.43)$$

$$P_{\sigma\tau}(1) = \frac{1}{4} (1 + \sigma\sigma_{z,1})(1 + \tau\tau_{z,1}), \quad \sigma, \tau = \pm 1. \quad (7.44)$$

It has the normalization

$$\sum_{\sigma\tau=\pm 1} \int \frac{d\mathbf{p}}{(2\pi)^3} N_{\sigma\tau}(\mathbf{p}) = A. \quad (7.45)$$

Short-range and tensor correlations induce high-momentum components in the nuclear ground states. This is clearly seen in Fig. 47, where the momentum distributions of $\sigma = \pm 1$ neutrons in a ${}^3\text{He}$ nucleus with polarization $+\frac{1}{2}$ are shown (Carlson and Schiavilla, 1997). In the absence of tensor correlations (and, therefore, D-state admixtures in the ${}^3\text{He}$ ground state) the momentum distribution $N_{\sigma=-1, \tau=-1}$ would vanish. Indeed, these correlations are responsible for most of the high-momentum components in the nuclear ground states (Pieper, Wiringa, and Pandharipande, 1992).

It is interesting to compare the nucleon momentum distributions (normalized to one rather than to A) of ${}^2\text{H}$, ${}^3\text{H}$, ${}^4\text{He}$, ${}^{16}\text{O}$, and nuclear matter. The $A=3$ and 4 nuclei $N(\mathbf{p})$ (summed over σ and τ) have been calculated by several groups from a variety of interaction models (Zabolitzky and Ey, 1978; Akaishi, 1984; Ciofi degli Atti, Pace, and Salmè, 1984; Schiavilla, Pandharipande, and Wiringa, 1986; Ciofi degli Atti, Pace, and Salmè, 1991). Those shown in Fig. 48 are obtained from variational wave functions corresponding to a Hamiltonian that includes the Argonne v_{14} two-nucleon and Urbana model VIII three-nucleon interactions (Pieper, Wiringa, and Pandharipande, 1992). The nuclear matter $N(p)$, instead, has been calculated with chain-summation techniques from a correlated wave function, using the older Urbana v_{14} two-nucleon interaction, supplemented by density-dependent terms that simulate the effect of three-nucleon interactions (Fantoni and Pandharipande, 1984).

The momentum distributions of $A > 2$ nuclei are found to be approximately proportional, in the limit of

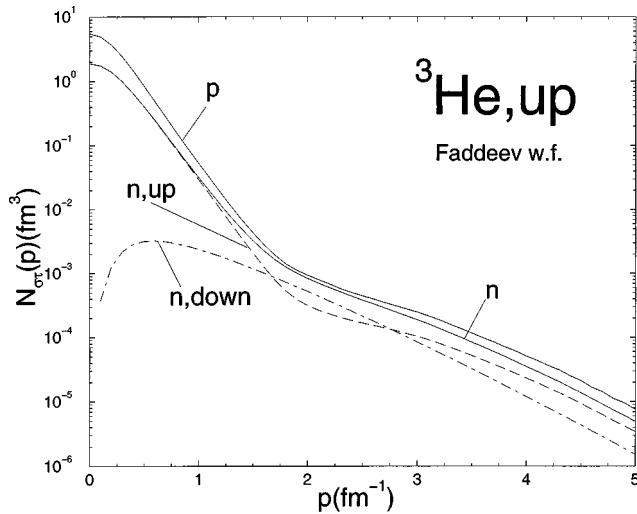


FIG. 47. Momentum distributions in a spin-up ${}^3\text{He}$ nucleus: p , proton; n neutron; (n,up) , neutron spin-up; (n,down) , neutron spin-down. From Carlson and Schiavilla (1997).

large momenta p , to that of the deuteron, as shown in Fig. 48. In particular, the high-momentum tails of the $A > 3$ nuclei $N(\mathbf{p})$ display a rather weak dependence on A .

G. Spectral functions

The probability for removing a nucleon of momentum \mathbf{p} in spin-isospin state $\sigma\tau$ from an A -nucleon system, and leaving the residual $A-1$ system with an internal excitation energy E , is given by the spectral function $S_{\sigma\tau}(\mathbf{p}, E)$,

$$S_{\sigma\tau}(\mathbf{p}, E) = \sum_f |\langle A-1; f | a_{\sigma\tau}(\mathbf{p}) | A; 0 \rangle|^2 \times \delta(E + E_0^A - E_f^{A-1}), \quad (7.46)$$

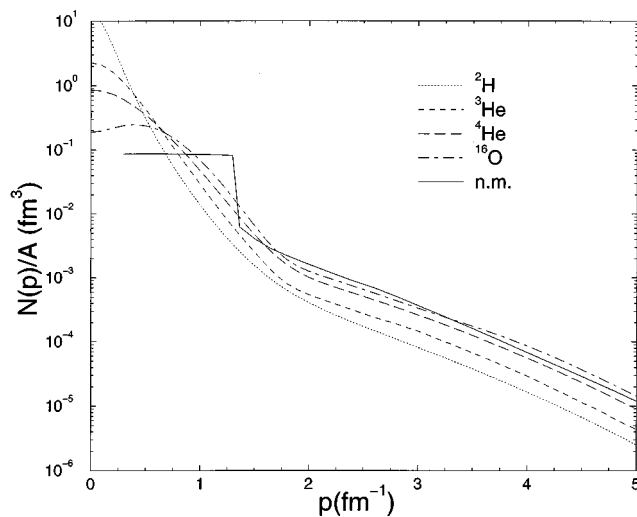


FIG. 48. The $N(\mathbf{p}) = \sum_{\sigma,\tau} N_{\sigma,\tau}(\mathbf{p})$ per nucleon in ${}^2\text{H}$, ${}^3\text{He}$, ${}^4\text{He}$, ${}^{16}\text{O}$, and nuclear matter (n.m.) From Pieper, Wiringa, and Pandharipande (1992).

where the sum is extended over all states of the $A-1$ system having energies E_f^{A-1} , and E_0^A is the energy of the A -nucleon ground state $|A; 0\rangle$. The spectral function obeys the sum rule

$$\int_{E_0^{A-1} - E_0^A}^{\infty} dE S_{\sigma\tau}(\mathbf{p}, E) = N_{\sigma\tau}(\mathbf{p}), \quad (7.47)$$

where E_0^{A-1} is the ground-state energy of the residual system. In fact, the contribution associated with the high-energy tail of the spectral function is crucial in saturating the sum rule at large p .

The spectral functions can in principle be measured in knockout reactions, such as $(e, e'p)$ reactions. In the plane-wave impulse approximation (PWIA), the cross section for these processes can be shown to be proportional to $S_p(\mathbf{p}_m, E_m)$ (summed over σ for unpolarized scattering), where $\mathbf{p}_m = \mathbf{p} - \mathbf{q}$ and $E_m = \omega - T_1 - T_{A-1}$ are, respectively, the so-called missing momentum and energy; T_1 and T_{A-1} are the kinetic energies of the knocked-out nucleon and recoiling $A-1$ system, and ω and \mathbf{q} are the energy and momentum transferred by the lepton probe. Of course, the PWIA ignores the final-state interactions between the outgoing and spectator nucleons. Furthermore, it requires for its validity that the probe-nucleus coupling be given by the sum of A one-body operators. Thus final-state interactions—as well as many-body components in the transition operators, such as meson-exchange currents in the case of $(e, e'p)$ reactions—complicate the interpretation of knockout processes and make the extraction of the spectral function from the data more difficult (Schiavilla, 1990; Glöckle *et al.*, 1995).

In the deuteron, the spectral function is simply given by $S_p(\mathbf{p}, E) = N_p(\mathbf{p}) \delta(E + E_0^d)$, where $E_0^d = -2.225$ MeV is the deuteron bound-state energy. The $S_p(\mathbf{p}, E)$ of ${}^3\text{He}$ (Meier-Hajduk *et al.*, 1983) and ${}^4\text{He}$ (Morita and Suzuki, 1991) have been calculated, respectively, with Faddeev and variational methods from realistic interactions [the ${}^3\text{He}$ $S(\mathbf{p}, E)$ is displayed in Fig. 49, after Meier-Hajduk *et al.*, (1983)]. Reliable approximations of these spectral functions (Ciofi degli Atti *et al.*, 1991; Benhar and Pandharipande, 1993) have also been obtained by using the momentum distributions of nucleons and nucleon clusters in the $A=3$ and $A=4$ ground states, such as, for example, dd and tp in ${}^4\text{He}$. The only other system for which realistic calculations of the spectral function have been carried out is nuclear matter. These latter calculations have used either correlated basis theory (Benhar, Fabrocini, and Fantoni, 1989, 1991) or the Green's-function method (Ramos, Polls, and Dickhoff, 1989), but both give quite similar predictions for the nuclear matter $S(\mathbf{p}, E)$.

The effect of correlations on the spectral function is easily understood by comparing realistic calculations of it with the Fermi gas model prediction. The latter is given by

$$S_{\text{FG}}(p, E) = \theta(p_F - p) \delta\left(E + \frac{p^2}{2m}\right), \quad (7.48)$$

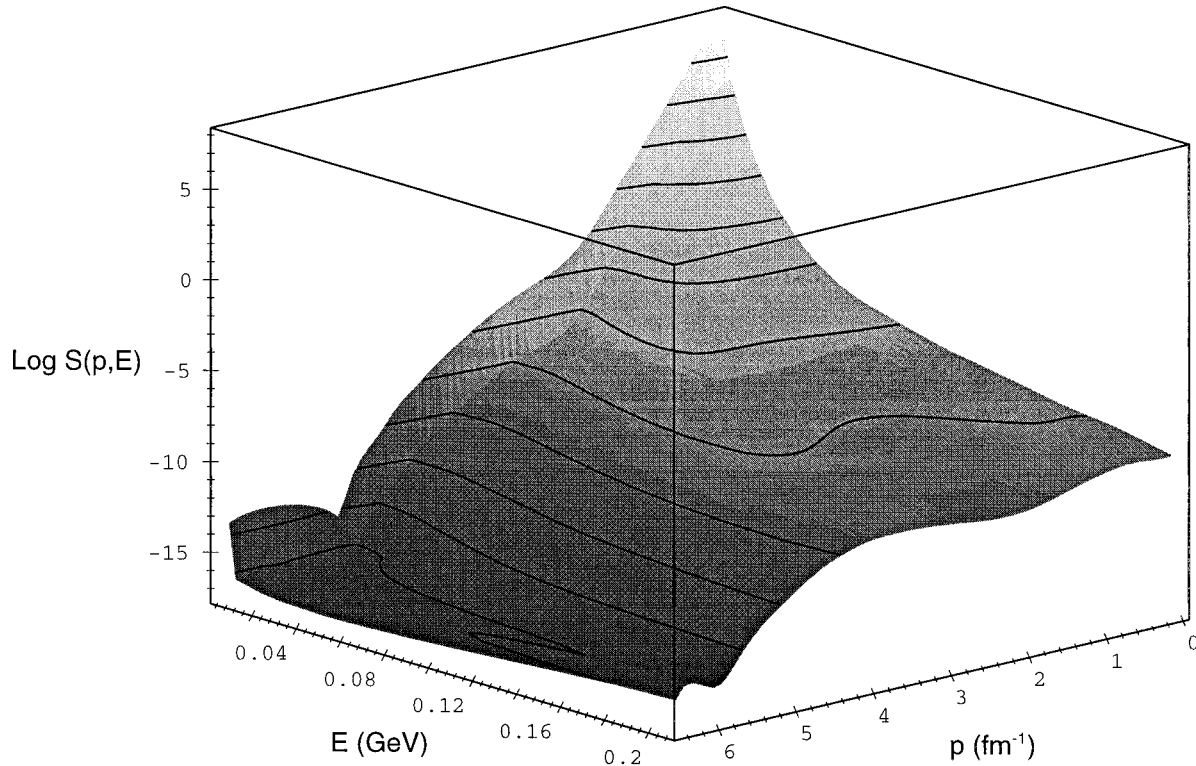


FIG. 49. The proton spectral function in ${}^3\text{He}$, as obtained by Meier-Hajduk *et al.* (1983).

where p_F is the Fermi momentum. As can be seen from Figs. 50 and 51 (Benhar, Fabrocini, and Fantoni, 1991), the nuclear matter $S(\mathbf{p}, E)$ (at equilibrium density, i.e., $p_F=1.33 \text{ fm}^{-1}$) is characterized by a large background extending over a wide energy range both above and below the Fermi level. This background is produced by dynamic (short-range and tensor) correlations. When $p < p_F$, the δ function of the Fermi gas model is replaced by a peak, the width of which gives the lifetime of the quasihole state. As p approaches p_F from below, this peak becomes sharper and sharper; its strength, which is denoted by $Z(p)$, has been shown by Migdal (1957) to be equal, in normal Fermi liquids and in the limit $p \rightarrow p_F$, to the magnitude of the discontinuity of the nuclear matter momentum distribution—that is, $Z(p \rightarrow p_F^-) = N(p_F^-) - N(p_F^+)$. Realistic calculations predict a value for $Z(p \approx p_F)$ of 0.71 in nuclear matter (Benhar, Fabrocini, and Fantoni, 1991). In the Fermi gas, $Z(p_F) = 1$, and so $1 - Z(p_F)$ is a measure of the strength of the correlations.

The notion of quasihole states is also useful in discussing the low-lying levels of finite systems (Pandharipande, 1990); for example, ${}^3\text{H}$ and ${}^{207}\text{Tl}$ can be viewed as $(1s1/2)^{-1}$ and $(3s1/2)^{-1}$ hole states in the doubly closed-shell nuclei ${}^4\text{He}$ and ${}^{208}\text{Pb}$, respectively. These states have zero width, since they cannot decay by strong interactions. In finite nuclei, quasihole wave functions are simply related to the $1 + (A-1)$ cluster amplitudes, defined above. In the shell model, in which nuclear wave functions are approximated by Slater determinants of single-nucleon wave functions ϕ_{nlj} , the quasihole orbital ψ_{nlj} coincides with ϕ_{nlj} . In particular,

the normalization of ψ_{nlj} , which is also known as the spectroscopic factor Z_{nlj} , would be one in this case. However, correlation effects reduce the spectroscopic factor and make the quasihole wave function more surface peaked than the mean-field one (Lewart, Pandharipande, and Pieper, 1988; Pandharipande, 1990). Of course, quasihole orbitals of nuclei with $A > 4$ have not yet been calculated from realistic interactions. In the α particle, the $Z_{1s1/2}$ is about 0.81. In heavy nuclei, the spectroscopic factors are expected to be even smaller

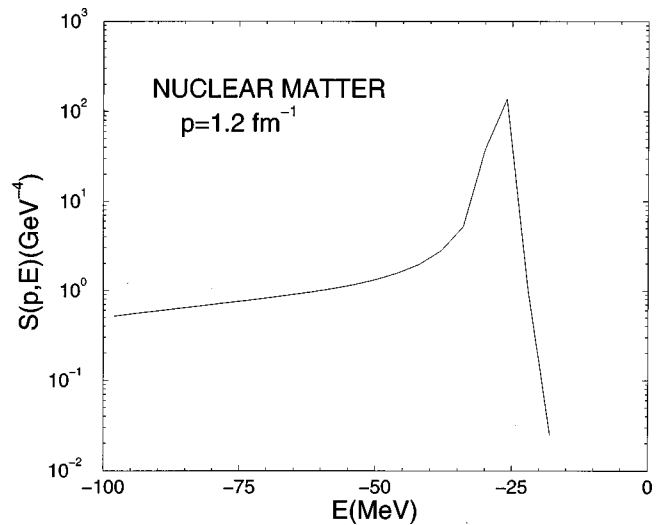


FIG. 50. The hole spectral function for $p=1.2 \text{ fm}^{-1}$ in nuclear matter at equilibrium $p_F=1.33 \text{ fm}^{-1}$, as obtained by Benhar, Fabrocini, and Fantoni (1989).

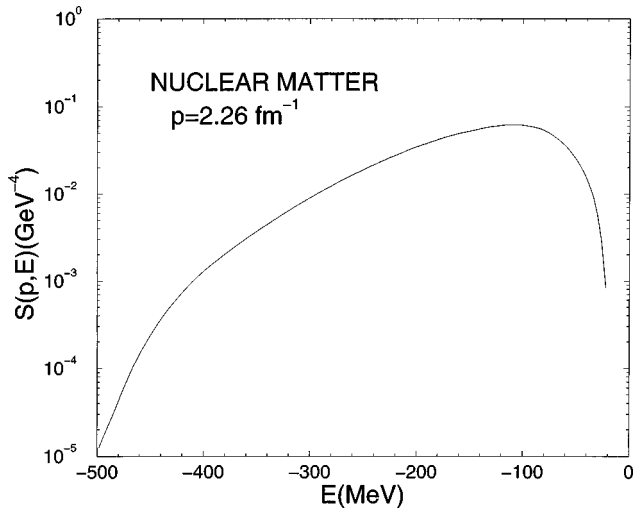


FIG. 51. The hole spectral function for $p = 2.26 \text{ fm}^{-1}$ in nuclear matter at equilibrium $p_F = 1.33 \text{ fm}^{-1}$, as obtained by Benhar, Fabrocini, and Fantoni (1989).

than the nuclear matter $Z(p_F) = 0.7$ because of surface effects (Pandharipande, Papanicolas, and Wambach, 1984). For example, the $^{208}\text{Pb } Z_{3s1/2}$ is estimated to be $\approx 0.6 \pm 0.1$.

VIII. SCATTERING METHODS

Two distinct energy regimes are of interest in few-nucleon scattering problems below the pion-production threshold. The first is low-energy scattering, where “low-energy” is defined to be the regime in which only breakup into two-body clusters is possible. In the nuclear three-body problem, this regime lies between zero and the deuteron binding energy $B_d = 2.225 \text{ MeV}$ in the center-of-mass (c.m.) frame, while for $A = 4$ it lies between zero and $B_t - B_d$, where $B_t = 8.48 \text{ MeV}$ is the triton binding energy. Many intriguing physical processes have been measured in this regime, including scattering lengths, total cross sections, polarization observables, and radiative-capture reactions. Of course, this is also the regime in which weak-capture reactions of astrophysical interest occur.

Scattering calculations naturally divide into low- and high-energy regimes because the dominant physical processes can be quite distinct. In low-energy reactions, the clustering properties of the nuclear wave function are extremely important, precisely because the relevant energies are near nuclear thresholds. For the same reason, a complete treatment of the long-ranged Coulomb interaction is crucial in many cases. In higher-energy (quasi-elastic) regimes, however, it is one- and two-body processes that typically dominate. Even so, it is often important and practical (at least for three-body problems) to treat multiple-scattering effects completely.

These distinctions also manifest themselves in the algorithms. In momentum-space calculations, the treatment of the poles of the Green’s functions is quite important. In configuration space, one must specify the

boundary conditions on the wave function for all possible breakup channels. Of course, the physical boundary conditions are the same in either the Faddeev or the correlated hyperspherical harmonics algorithms. Here we discuss them within the Faddeev description.

In both momentum and coordinate space, one must take care to obtain the solution corresponding to the physical process of interest—often incoming plane waves in one channel only. There are also important experiments in which different boundary conditions are appropriate, of course, including electromagnetic-scattering experiments. We shall postpone discussions of methods for inclusive response calculations to a later section.

A. Configuration-space Faddeev equations

One of the original motivations for using the Faddeev equations was to treat the scattering problem for three particles. Typically, a solution is to be constructed with an incoming plane wave in one channel only, and various possible final states. The Faddeev equations are well suited to studying this type of problem, because it is comparatively easy to obtain these physical scattering solutions. Furthermore, the partial-wave decomposition employed in Faddeev calculations is still quite valuable because the angular momentum barrier and the small size of nuclear ground states implies, at least at low energies, that one can still deal with a modest number of partial waves.

The boundary conditions for scattering, even below the three-nucleon breakup threshold, are somewhat more involved than for bound states. In general, more than one final state may be available. For three distinguishable particles, there are various possibilities, including elastic scattering, where asymptotically $1(23) \rightarrow 1(23)$ (the brackets indicating bound subclusters), as well as rearrangement scattering corresponding to $1(23) \rightarrow 2(13)$ or $1(23) \rightarrow 3(12)$. Of course, in the scattering regime the solution of the Schrödinger equation for a given energy E is in general not unique. It has been shown that simply converting the Schrödinger equation to a Lippman-Schwinger equation whose form guarantees outgoing waves in all channels does not provide a unique solution (Foldy and Tobocman, 1957). The difficulty is that the amount of incoming wave in each channel is not controlled. Various methods have been used to overcome this problem, including the triad (Glöckle, 1970) equations and the Faddeev equations (Faddeev, 1960). In this section we follow the discussion in Friar and Payne (1996). Interested readers should consult that article for a much more complete treatment.

In configuration space, the Faddeev equations [see Eq. (3.4)] are the most common technique for dealing with the rearrangement problem; since each equation deals with only one interacting pair, the boundary conditions are fairly straightforward. The first equation contains only v_{12} , so only particles 1 and 2 can be bound asymptotically in ψ_1 . The rearrangement channels are contained in ψ_2 and ψ_3 , which, for identical particles, are

the same function as ψ_1 but for different arguments. Hence this decomposition of the Schrödinger equation into three equations has solved the rearrangement problem.

For low-energy scattering, the Coulomb interaction is important, leading to dramatically different physics—hence the Faddeev equations need to be modified. A straightforward inclusion of the Coulomb interaction in the Faddeev equations via $v_{jk} \rightarrow v_{jk} + v_c(x_i)$ is far from optimum because there is no obvious Coulomb interaction in the \mathbf{y} coordinate that would describe the repulsion between an outgoing proton and a deuteron in pd scattering. Far better (Friar, Gibson, and Payne, 1983; Kuperin *et al.*, 1983) is to include the full Coulomb potential $\sum_i v_c(x_i)$ on the left-hand side of the equation for each Faddeev amplitude:

$$\left[E - H_0 - v_{23} - \sum_i v_c(x_i) \right] \psi_1(\mathbf{x}_1, \mathbf{y}_1) = v_{23} [\psi_2(\mathbf{x}_2, \mathbf{y}_2) + \psi_3(\mathbf{x}_3, \mathbf{y}_3)]. \quad (8.1)$$

Summing the three cyclic permutations again reproduces the Schrödinger equation, but now the amplitudes ψ obey physically meaningful boundary conditions. This form is called the Faddeev-Noble equation (Noble, 1967) and has been used by Merkuriev and collaborators (Merkuriev, 1976; Kuperin *et al.*, 1983).

Returning now to the boundary conditions, we require that the wave function be finite and consist of an initial plane wave plus outgoing scattered waves. The latter conditions are imposed for large \mathbf{x} and \mathbf{y} , or, equivalently, large $\rho \equiv (x^2 + y^2)^{1/2}$ as a function of θ , where $\cos\theta = \hat{\mathbf{x}} \cdot \hat{\mathbf{y}}$.

Below deuteron breakup, the boundary conditions are determined in a rather straightforward way as in standard two-body calculations. The amplitude at large values of y must be proportional to

$$\psi(\mathbf{x}, \mathbf{y}) \underset{y \rightarrow \infty}{\sim} \psi_d(\mathbf{x}) \phi_{Nd}(\mathbf{y}), \quad (8.2)$$

where ψ_d is the internal deuteron wave function and ϕ_{Nd} is the relative nucleon-deuteron wave function. In the absence of Coulomb forces, the asymptotic nd wave function ϕ_{nd} in each partial wave is proportional to

$$\phi_{nd}(\mathbf{y}) = e^{i\delta_L} [j_L(ky) \cos\delta_L - n_L(ky) \sin\delta_L] Y_{LM}(\hat{\mathbf{y}}), \quad (8.3)$$

where y is the distance between the n and d clusters, and the c.m. energy is given by $E = k^2/2\mu$. For cases of coupled channels or energies above breakup, the phase shift may be complex. For the Coulomb case, the asymptotic wave function is

$$\phi_{pd}(\mathbf{y}) = e^{i(\delta_L + \sigma_L)} [F_L(\eta, ky) \cos\delta_L + G_L(\eta, ky) \sin\delta_L] Y_{LM}(\hat{\mathbf{y}})/(ky), \quad (8.4)$$

where σ_L is the Coulomb phase shift, $\sigma_L = \arg[\Gamma(L + 1 + i\eta)]$, η is the Coulomb parameter related to the product of the two charges ($\eta = \mu Z_1 Z_2 \alpha/k$). F_L and G_L are the regular and irregular solutions of the Coulomb po-

tential, respectively, and δ_L is the additional phase shift produced by the nuclear interaction. Note that

$$\lim_{\eta \rightarrow 0} G_L(\eta, ky)/(ky) \rightarrow -n_L(ky). \quad (8.5)$$

This form is not directly suitable for zero-energy or very near zero-energy calculations. At very small energies, Coulomb calculations can be quite difficult due to suppression of the wave function near the origin, and hence one converts to asymptotic conditions normalized by an additional factor of $1/(ky C_L e^{i\sigma_L})$, where C_L is the Coulomb barrier penetration factor, which for $L=0$ is

$$C_0 = [2\pi\eta/(e^{2\pi\eta} - 1)]^{1/2}. \quad (8.6)$$

The regular part of the solution $F_L(\eta, ky)/(ky C_L e^{i\sigma_L}) \propto (\zeta y)^L/(2L+1)!$, where $\zeta = 2\eta k$. Dividing out the Coulomb penetration factors in this way yields well-behaved functions.

Above breakup, the amplitude $\psi(\mathbf{x}, \mathbf{y}) \equiv \psi(x, \rho, \theta)$ is nonzero everywhere for large ρ , not just in the regions corresponding to a bound deuteron subcluster. In the region of small x and large y , the amplitude corresponding to three-body breakup ψ_{br} decreases as $1/y^{5/2}$. This rapid decrease, when compared to the elastic ψ_{el} , enables one to separate the two contributions asymptotically:

$$\psi(\mathbf{x}, \mathbf{y}) = \psi_{br}(\mathbf{x}, \mathbf{y}) + \psi_{el}(\mathbf{x}, \mathbf{y}), \quad (8.7)$$

where ψ_{el} corresponds to elastic scattering.

In the asymptotic region, the interaction v_{23} can be dropped from the Faddeev equation to obtain an equation

$$\left[H_0 + \sum_i v_c(x_i) - E \right] \psi_{br} = 0. \quad (8.8)$$

Converting to hyperspherical coordinates, one can show that the solution of this equation has the asymptotic form

$$\psi_{br} \propto A \frac{\exp(ik\rho)}{\rho^{5/2}} \exp[i\bar{\eta} \ln(2k\rho)] [1 + \mathcal{O}(1/\rho)], \quad (8.9)$$

where A is a function of the angles in the c.m. frame and $\bar{\eta}$ is given by

$$\bar{\eta} = -\rho \left[\sum_i v_c(x_i) \right] \frac{m}{2k}, \quad (8.10)$$

which is the three-body equivalent of the two-body Coulomb parameter η . Taking the limit $\bar{\eta} \rightarrow 0$ gives the normal (non-Coulomb) solution.

To obtain the asymptotic solution for x within the range of the nuclear interaction, consider the Faddeev equation

$$\begin{aligned} & [E - T_x - T_y - v_{23}] \psi(\mathbf{x}_1, \mathbf{y}_1) \\ & = v_{23} [\psi(\mathbf{x}_2, \mathbf{y}_2) + \psi(\mathbf{x}_3, \mathbf{y}_3)]. \end{aligned} \quad (8.11)$$

For the non-Coulomb case, we can replace the right-hand side by $v_{23} \beta \exp(iky)/y^{5/2}$, where β is again a func-

tion depending upon angles that is determined by the breakup amplitude (to lowest order). The amplitude ψ in this regime is then

$$\psi(\mathbf{x}, \mathbf{y}) \propto \beta g(\mathbf{x}) \exp(iky)/y^{5/2} + \mathcal{O}(y^{-7/2}), \quad (8.12)$$

where $g(x)$ satisfies

$$[T_x + v]g(\mathbf{x}) = -v. \quad (8.13)$$

The homogeneous part of the solution for g is proportional to the zero-energy scattering solution $\psi^0(x)$, with a constant of proportionality denoted by γ . The inhomogeneous part is formally given by

$$g(\mathbf{x}) = \frac{-1}{T_x + v} v \equiv g_{\text{el}}(\mathbf{x}) + g_{\text{in}}(\mathbf{x}). \quad (8.14)$$

The inhomogeneous solution has been divided into the part proportional to the deuteron wave function (g_{el}) and the remainder (g_{in}). Thus we have for small x and large y

$$\begin{aligned} \psi(\mathbf{x}, \mathbf{y}) \propto & \psi_{\text{el}}(\mathbf{x}, \mathbf{y}) + [\beta[g_{\text{el}}(\mathbf{x}) + g_{\text{in}}(\mathbf{x})] + \gamma\psi_0(x)] \\ & \times \exp(iky)/y^{5/2}. \end{aligned} \quad (8.15)$$

The terms in this expression correspond to direct elastic scattering, elastic rearrangement, inelastic recombination, and direct inelastic scattering, respectively. This expression matches the previous expression for x larger than the range of the nuclear interaction and completes the asymptotic expressions for the Faddeev amplitudes. Of course, for a practical calculation one must determine where these asymptotic forms can be applied. Some results on this subject have been published by Glöckle and Payne (1992).

In addition to these leading terms at very small energies, one may wish to consider polarization effects, essentially evaluating the deuteron's dipole, quadrupole, etc., moments and adding these to the long-distance behavior of the wave function. A discussion of this specialized point can be found in Friar and Payne (1996).

Once the boundary conditions have been specified and a scattering solution obtained, it is extremely valuable to employ a variational principle both to check the calculations and to improve the estimate of the scattering matrix. For bound states, it is well known that an approximate wave function Ψ accurate to order $\delta\Psi$ in $\Psi - \Psi_0$ produces a variational estimate of the energy $\langle \Psi | H | \Psi \rangle$ accurate to order $(\delta\Psi)^2$. For scattering calculations, one can do something similar, although care must be taken with the boundary conditions.

Coordinate-space scattering calculations are necessarily performed within a finite volume and then matched at the boundary to the asymptotic wave functions. Within this boundary, one can construct a functional $I[\Psi]$,

$$I[\Psi] = \langle \Psi | \vec{H} - E | \Psi \rangle, \quad (8.16)$$

and vary the wave function $\Psi \rightarrow \Psi_0 + \delta\Psi$, yielding

$$\begin{aligned} \delta I &= \langle \Psi_0 + \delta\Psi | \vec{H} - E | \Psi_0 + \delta\Psi \rangle - \langle \Psi_0 | \vec{H} - E | \Psi_0 \rangle \\ &= \langle \delta\Psi | \vec{H} - E | \Psi_0 \rangle + \langle \Psi_0 | \vec{H} - E | \delta\Psi \rangle \end{aligned}$$

$$+ \langle \delta\Psi | \vec{H} - E | \delta\Psi \rangle, \quad (8.17)$$

where the arrow on the Hamiltonian is to remind one that H is not a Hermitian operator when acting within the finite volume. The first term on the right-hand side is zero since $(\vec{H} - E)|\Psi_0\rangle = 0$. The second term is given by a surface integral:

$$\begin{aligned} \delta S &= \langle \Psi_0 | \vec{H} - E | \delta\Psi \rangle \\ &= -(1/2\mu) \int dS \hat{\mathbf{n}} \cdot [(\nabla\Psi_0)^\dagger \delta\Psi - \Psi_0^\dagger \nabla \delta\Psi], \end{aligned} \quad (8.18)$$

which results from integrating by parts the kinetic energy operator and again using $(\vec{H} - E)|\Psi_0\rangle = 0$. Evidently, then, the variational principle for scattering states is given by

$$\delta I - \delta S = \langle \delta\Psi | H - E | \delta\Psi \rangle, \quad (8.19)$$

as originally formulated by Kohn (1948). Note that this is a stationary principle rather than an extremum, since $\delta I - \delta S$ is not necessarily positive. However, this variational principle is very important because, for any wave function accurate to order $\delta\Psi$, it can be used to obtain the elements of the scattering matrix accurate to order $(\delta\Psi)^2$.

A variety of coordinate-space scattering calculations have been carried out with Faddeev and CHH techniques. Below breakup, many interesting reactions have been studied, some of which will be presented in the next sections. Above breakup, comparisons between momentum- and coordinate-space representations indicate that both methods can be made to work reliably (Friar *et al.*, 1990a; Friar *et al.*, 1995). Many new results with full inclusion of the Coulomb interaction can be expected within the next several years.

B. Momentum-space Faddeev equations

In momentum space, additional issues are also present when addressing the scattering regime. Again, the problem has to be formulated in a way guaranteed to correspond to the physical process of interest. Numerically, the primary concern is the treatment of the singularities in the propagators. Let us first consider the case of distinguishable particles, in which an outgoing scattering state $\Psi^{(+)}$ obtained from an initial asymptotic arrangement of particles described by ϕ is given by

$$\Psi^{(+)} = \lim_{\epsilon \rightarrow 0} \frac{i\epsilon}{E + i\epsilon - H} \phi. \quad (8.20)$$

In the standard Faddeev decomposition, the following identity is useful:

$$\begin{aligned} \frac{1}{E + i\epsilon - H} &= \frac{1}{E + i\epsilon - H_0 - v_{jk}} + \frac{1}{E + i\epsilon - H_0 - v_{jk}} \\ &\quad \times (v_{ik} + v_{ij}) \frac{1}{E + i\epsilon - H}, \end{aligned} \quad (8.21)$$

where $H=H_0+v_{jk}+v_{ki}+v_{ij}$. A state ϕ_1 , which describes the initial scattering state and is an eigenstate of $H_1\equiv H_0+v_{23}$, will obey the Lippman identity (Lippman, 1956),

$$\lim_{\epsilon\rightarrow 0} \frac{i\epsilon}{E+i\epsilon-H_i} \phi_1 = \delta_{i,1} \phi_1, \quad (8.22)$$

and hence

$$\Psi_1^{(+)} = \delta_{i,1} \phi_1 + \lim_{\epsilon\rightarrow 0} \frac{1}{E+i\epsilon-H_i} \Psi_1^{(+)}. \quad (8.23)$$

This expression provides one inhomogeneous and two homogeneous equations which define $\Psi_1^{(+)}$ uniquely (Glöckle, 1970). Obviously this state is an eigenstate of the Schrödinger equation, and similar equations with inhomogeneous terms in $i=2,3$ define $\Psi_2^{(+)}$ and $\Psi_3^{(+)}$. Requiring the three equations to be fulfilled simultaneously rules out admixtures of Ψ_2 and Ψ_3 in Ψ_1 . Moreover, it is easy to see that this solution contains no admixtures of three free particles in the initial state.

From a solution of this triad of equations, the amplitude of the outgoing radial wave in the channel where particles j and k are bound together can be obtained from

$$A_{i,1} = \langle \phi_i | v_{ij} + v_{ik} | \Psi_1^{(+)} \rangle, \quad (8.24)$$

which can be used to define a transition operator from initial state 1 to final state i :

$$U_{i1} | \phi_1 \rangle \equiv (v_{ij} + v_{ik}) | \Psi_1^{(+)} \rangle. \quad (8.25)$$

The operators U_{i1} are the elastic (U_{11}) or rearrangement (U_{21} and U_{31}) operators, respectively. The breakup operator will be described below.

Writing out the equations for the U_{i1} and inserting the various expressions for $\Psi_1^{(+)}$, one obtains coupled equations for the U_{i1} acting on ϕ_1 in terms of the interactions v_{ij} and G_i , where $G_i \equiv \lim_{\epsilon\rightarrow 0} 1/(E+i\epsilon-H_i)$:

$$\begin{aligned} U_{11} \phi_1 &= v_{13} G_2 U_{21} \phi_1 + v_{12} G_3 U_{31} \phi_1, \\ U_{21} \phi_1 &= v_{23} \phi_1 + v_{23} G_1 U_{11} \phi_1 + v_{12} G_3 U_{31} \phi_1, \\ U_{31} \phi_1 &= v_{23} \phi_1 + v_{23} G_1 U_{11} \phi_1 + v_{13} G_2 U_{21} \phi_1. \end{aligned} \quad (8.26)$$

After some manipulations, one can use the identities $v_{23} \phi_1 = G_0^{-1} \phi_1$ and $v_{jk} G_i = T_j G_0$, in which the scattering operators T_i are again the three-particle propagators with only two particles interacting [see Eq. (3.10)], to derive a coupled set of equations for the U in terms of the T_i and G_0 :

$$U_{i1} \phi_1 = (1 - \delta_{i,1}) G_0^{-1} \phi_1 + \sum_{j \neq i} T_j G_0 U_{j1} \phi_1. \quad (8.27)$$

These equations are the Alt, Grassberger, and Sandhas (1967) or AGS equations for the transition operators U_{i1} .

For identical particles, one antisymmetrizes these equations, yielding an equation for the transition operator into final state i from an antisymmetrized initial

state. The outgoing wave function is $\Psi^{(+)} = \Psi_1^{(+)} + \Psi_2^{(+)} + \Psi_3^{(+)}$, and the transition operator is given by

$$U_i \phi_1 \equiv \sum_k U_{ik} \phi_k = \sum_{k \neq i} G_0^{-1} \phi_k + \sum_{j \neq i} T_j G_0 U_j \phi_1. \quad (8.28)$$

Of course, there is only one independent operator U for three identical particles, so the equation can be written

$$U \phi = G_0^{-1} E \phi + E T G_0 U \phi, \quad (8.29)$$

which generates the operator U appropriate for elastic scattering. The operator E is again the sum of the two cyclic permutations. For calculations with realistic forces, it is more convenient to define $\bar{T} \equiv T G_0 U$, which leads to an equation

$$\bar{T} \phi = T E \phi + T G_0 E \bar{T} \phi. \quad (8.30)$$

This is the central equation for scattering calculations. The elastic scattering transition is given by

$$U \phi = E G_0^{-1} \phi + E \bar{T} \phi. \quad (8.31)$$

The transition operator U_0 to states in the continuum is obtained from an amplitude

$$A_0 = \langle \phi_0 | (v_{ij} + v_{ik} + v_{jk}) | \Psi_1^{(+)} + \Psi_2^{(+)} + \Psi_3^{(+)} \rangle. \quad (8.32)$$

The transition operator U_0 to three-body continuum states is $U_0 \phi = (\sum_{ij} v_{ij}) (\Psi_1^{(+)} + \Psi_2^{(+)} + \Psi_3^{(+)})$, which yields

$$U_0 \phi \equiv (1 + E) T G_0 U \phi, \quad (8.33)$$

where U is the elastic-scattering operator. In terms of \bar{T} , this is

$$U_0 \phi = (1 + E) \bar{T} \phi. \quad (8.34)$$

Three-nucleon interactions can be treated in several ways. Complete treatments are presented in several articles (Kowalski, 1976; Glöckle, 1983; Glöckle and Brandenburg, 1983). One possibility is to add another equation to the triad, invoking a Green's function for the Hamiltonian consisting of three free particles plus the three-nucleon interaction (Glöckle *et al.*, 1996). It is also possible to incorporate the three-nucleon interaction directly into the standard Faddeev equations, as is done in configuration space. Recently, Hüber *et al.* (1997) developed a new partial-wave expansion scheme for three-nucleon interactions. This scheme is numerically more stable for high partial waves and hence will prove particularly useful for applications at higher energies.

Ignoring this complication, the basic equation to be solved is Eq. (8.30), which when decomposed into momentum magnitudes p, q and angular momentum, spin-isospin channels α is

$$\begin{aligned}
\langle pq\alpha|\bar{T}|\phi\rangle &= \langle pq\alpha|TE|\phi\rangle + \sum_{\alpha'} \int dq'q'^2 \int dp'p'^2 \\
&\times \sum_{\alpha''} \int dq''q''^2 \int dp''p''^2 \\
&\times \langle pq\alpha|T|p'q'\alpha'\rangle \langle p'q'\alpha'|E|p''q''\alpha''\rangle \\
&\times \langle p''q''\alpha''|G_0\bar{T}|\phi\rangle. \tag{8.35}
\end{aligned}$$

Again, the T matrix is diagonal in the spectator momenta and involves the standard two-body $t^{(2)}$ -matrix elements at an energy $E - 3q^2/4m$. The number of coupled equations is of the order of 60, as in coordinate-space calculations. If one chooses 30–40 grid points in p and q , the resulting matrix representation of the kernel is of dimension roughly 72 000 by 72 000. This is not inverted directly, but solved through an iterative procedure (Witala, Cornelius, and Glöckle, 1988a, 1988b; Cornelius, 1990; Hüber, 1993) that involves Padé approximants to the kernel of the scattering equation [Eq. (8.30)].

In order to solve these equations, one must confront the singularities in the propagators. The two-body $t^{(2)}$ matrix has a pole at the deuteron binding energy, of course, and hence in the three-body equation one hits this pole for a specific value of q for any energy E above deuteron threshold. The deuteron term in the $t^{(2)}$ matrix can be evaluated explicitly and the pole handled by a standard subtraction technique.

There are also free-propagator poles in this equation for suitable values of p and q . These are more difficult to treat, but can also be handled by subtraction techniques; a detailed discussion of their treatment is beyond the scope of this article. Detailed discussions can be found in Witala, Cornelius, and Glöckle (1988a, 1988b); Cornelius (1990); and Hüber (1993).

A large number of nd scattering reactions have been carried out with the momentum-space Faddeev scheme. Some of the impressive series of results are presented in Sec. X; a more complete treatment is found in the review article by Glöckle *et al.* (1996).

C. Monte Carlo methods

Due to the statistical error inherent in Monte Carlo methods, it has proven useful to approach the low-energy scattering problem in a slightly different manner from that used in Faddeev or CHH methods. The primary reason is that the Kohn variational principle as described above is a stationary principle, rather than an extremum. Although variational Monte Carlo methods could, in principle, be adopted, for the larger systems ($A \geq 4$), where the Monte Carlo methods have proven to be most valuable, such calculations could be quite difficult due to the statistical errors in the integration.

An alternative method has been formulated, however, which is quite useful in certain cases (Carlson, Pandharipande, and Wiringa, 1984). The essence of this method is to fix the boundary condition at the start of the calculation and again solve the eigenvalue problem. This is

not very different from the Kohn principle above, but instead of allowing arbitrary variations in Ψ as before, we allow only variations that do not change the boundary conditions on the wave function. With this restriction, the term δS in Eq. (8.18) is trivially zero, hence one is simply solving the eigenvalue equation.

Returning to the one-channel case, specifying the logarithmic derivative of the wave function and solving for the energy E is an approach that can be used to determine the phase shift at that energy. Assuming that the boundary condition on the logarithmic derivative D_L of the wave function is specified at a distance R , we have

$$\left. \frac{\nabla\Psi \cdot \hat{\mathbf{n}}}{\Psi} \right|_R = D_L = \frac{k[j'_L(kr)\cos\delta_L - n'_L(kr)\sin\delta_L]}{[j_L(kr)\cos\delta_L - n_L(kr)\sin\delta_L]}, \tag{8.36}$$

which provides a simple relation between the logarithmic derivative, k (determined by the energy), and the phase shift δ_L .

Since there is a variational upper bound, this method can easily be incorporated within standard VMC or GFMC algorithms. For a given boundary condition, the error is proportional to $(\delta\Psi)^2$. For zero-energy scattering, one simply takes the asymptotic form of the wave function ($\propto r - a$ for S waves) and adjusts the trial scattering length until a zero-energy eigenvalue is produced.

This procedure is more difficult for multichannel problems, however. In general, an arbitrary choice for the boundary conditions will not regulate the incoming flux in the various channels, and hence the solution will not correspond to a physical scattering process with an incoming plane wave in one channel only. One way to circumvent this difficulty would be to find different boundary conditions that reproduce the same energy, or, equivalently, to calculate the derivatives of energy with respect to changes in the boundary conditions. The latter may be feasible and could also prove useful in calculating widths of resonances, etc.

IX. THE $A=2-4$ RADIATIVE AND WEAK-CAPTURE REACTIONS AT LOW ENERGIES

Very low-energy radiative and weak-capture reactions involving few-nucleon systems have considerable astrophysical relevance for studies of stellar structure and evolution (Clayton, 1983) and big-bang nucleosynthesis (Kolb and Turner, 1990)—for example, in relation to the mechanism for energy and neutrino production in main-sequence stars, the process of protostellar evolution towards the main sequence, or the predictions for the primordial abundances of light elements.

These same reactions are also very interesting from the standpoint of the theory of strongly interacting systems, since their cross sections are very sensitive to the model used to describe both the ground-state and continuum wave functions, and the two-body electroweak current operators. Indeed, the ${}^1\text{H}(n, \gamma){}^2\text{H}$ radiative capture provided the first convincing case of a significant

(10%) and calculable two-body current effect in photo-nuclear reactions (Riska and Brown, 1972). Even more interesting are the ${}^2\text{H}(n, \gamma){}^3\text{H}$ and ${}^3\text{He}(n, \gamma){}^4\text{He}$ captures at thermal-neutron energies. Calculations of their cross sections based on realistic bound-state and continuum-state wave functions and one-body currents—in the impulse approximation (IA)—predict only about 50% and 10% of the corresponding experimental values (Friar, Gibson, and Payne, 1990; Schiavilla *et al.*, 1992). This is because the IA transition operator cannot connect the main S-state components of the deuteron and triton (or ${}^3\text{He}$ and ${}^4\text{He}$) wave functions. Hence the calculated cross section in the IA is small, since the reaction must proceed through the small components of the wave functions, in particular the mixed symmetry S'-state admixture (Schiff, 1937; Austern, 1951). Two-body currents, however, do connect the dominant S-state components, and the associated matrix elements are exceptionally large in comparison to those obtained in the IA (Friar, Gibson, and Payne, 1990; Schiavilla *et al.*, 1992).

The present section is organized into four subsections, A–D. Section IX.A summarizes the relevant formulas for the calculation of cross section and polarization observables. Formulas for the latter do not merely represent an academic exercise: in fact, vector and tensor analyzing powers have, in the last year, been measured in the energy range 0–150 keV at TUNL for the ${}^2\text{H}(\vec{p}, \gamma){}^3\text{He}$ and ${}^1\text{H}(\vec{d}, \gamma){}^3\text{He}$ reactions using beams of polarized protons and deuterons (Schmid *et al.*, 1995, 1996; Ma *et al.*, 1996). Sections IX.B–IX.D deal, in turn, with the $A=2$ ${}^1\text{H}(n, \gamma){}^2\text{H}$ and ${}^1\text{H}(p, e^+ \nu_e){}^2\text{H}$, $A=3$ ${}^2\text{H}(\vec{n}, \gamma){}^3\text{H}$, ${}^2\text{H}(\vec{p}, \gamma){}^3\text{He}$, ${}^1\text{H}(\vec{d}, \gamma){}^3\text{He}$, and $A=4$ ${}^3\text{He}(n, \gamma){}^4\text{He}$, ${}^2\text{H}(d, \gamma){}^4\text{He}$, ${}^3\text{He}(p, e^+ \nu_e){}^4\text{He}$ capture reactions at thermal-neutron and keV proton and deuteron incident energies.

A. Cross section and polarization observables

In the c.m. frame, the radiative transition amplitude between an initial two-cluster continuum state with clusters A_1 and A_2 having spins $J_1 M_1$ and $J_2 M_2$, respectively, and relative momentum \mathbf{p} , and a final A -nucleon bound state of spin $J_A M_A$ ($A_1 + A_2 = A$) is given by (Viviani, Schiavilla, and Kievsky, 1996)

$$j_{M_A M_2 M_1}^\lambda(\mathbf{p}, \mathbf{q}) = \langle \Psi_{A_1 A_2}^{J_A M_A} | \hat{\mathbf{e}}_\lambda^*(\mathbf{q}) \cdot \mathbf{j}^\dagger(\mathbf{q}) | \Psi_{\mathbf{p}, M_2 M_1}^{(+)} \rangle, \quad (9.1)$$

where \mathbf{q} and $\omega = q$ are the photon momentum and energy, and $\hat{\mathbf{e}}_\lambda(\mathbf{q})$, $\lambda = \pm 1$, are the spherical components of its polarization vector. The two-cluster wave function $\Psi^{(+)}$, satisfying outgoing wave boundary conditions, is normalized to unit flux and has the following partial-wave expansion:

$$\Psi_{\mathbf{p}, M_2 M_1}^{(+)} = 4\pi \sum_{SS_z} \langle J_1 M_1, J_2 M_2 | SS_z \rangle \sum_{LL_z JJ_z} \times i^L \langle SS_z, LL_z | JJ_z \rangle Y_{LL_z}^*(\hat{\mathbf{p}}) \bar{\Psi}_{A_1 + A_2}^{LSJJ_z}, \quad (9.2)$$

$$\bar{\Psi}_{A_1 + A_2}^{LSJJ_z} = e^{i\sigma_L} \sum_{L'S'} [1 - i^J R]_{LS, L'S'}^{-1} \Psi_{A_1 + A_2}^{L'S'JJ_z}, \quad (9.3)$$

where S is the channel spin, L is the relative orbital angular momentum between clusters A_1 and A_2 , ${}^J R$ is the R matrix in the subspace with total angular momentum J , and σ_L is the Coulomb phase shift, given by

$$\sigma_L = \arg[\Gamma(L + 1 + i\eta)], \quad (9.4)$$

$$\eta = \frac{Z_1 Z_2 \alpha}{v_{\text{rel}}}. \quad (9.5)$$

Here α is the fine-structure constant, and v_{rel} is the relative velocity between clusters A_1 and A_2 with charges Z_1 and Z_2 , respectively. If no Coulomb interaction is present between the clusters, then the factor $e^{i\sigma_L}$ in Eq. (9.3) should be omitted. The wave function $\Psi_{A_1 + A_2}^{LSJJ_z}$ in Eq. (9.3) describes the two interacting clusters and behaves asymptotically as

$$\Psi_{A_1 + A_2}^{LSJJ_z} \underset{r \rightarrow \infty}{\sim} \sqrt{(1 + \delta_{A_1, A_2})} \frac{A_1! A_2!}{A!} \sum_{\wp} (-1)^\wp \times \sum_{L'S'} [[\phi_{A_1; J_1} \otimes \phi_{A_2; J_2}]_{S'} \otimes Y_{L'}(\hat{\mathbf{r}})]_{JJ_z} \times \left[\delta_{LL'} \delta_{SS'} \frac{F_{L'}(\eta, pr)}{pr} + {}^J R_{LS}^{L'S'} \frac{G_{L'}(\eta, pr)}{pr} \right], \quad (9.6)$$

where $\phi_{A_1; J_1 M_1}$ and $\phi_{A_2; J_2 M_2}$ are the (antisymmetric and normalized) bound-state wave functions of clusters A_1 and A_2 , and F_L and G_L are the regular and irregular Coulomb functions, respectively. Again, in the absence of Coulomb interactions between the clusters, the $F_L(\eta, x)/x$ and $G_L(\eta, x)/x$ should be replaced by the regular and irregular spherical Bessel functions. The sum over $L'S'$ is over all values compatible with a given J and parity, while that over \wp is over all permutations [parity $(-1)^\wp$] of the nucleons between the two clusters, thus ensuring that the wave function $\Psi_{A_1 + A_2}^{LSJJ_z}$ is antisymmetric. The factor $1 + \delta_{A_1, A_2}$ is included to correct for the normalization of the wave function $\Psi_{A_1 + A_2}^{LSJJ_z}$ when the two clusters are identical (for example, two protons or two deuterons). To date, wave functions $\Psi_{A_1 + A_2}^{LSJJ_z}$ have been obtained from realistic two- and three-nucleon interactions for the trinucleons with Faddeev and CHH methods (Kievsky, Viviani, and Rosati, 1994), and for the $A=4$ nucleon systems with the VMC method (Carlson, Pandharipande, and Wiringa, 1984; Carlson *et al.*, 1990; Arriaga *et al.*, 1991; Carlson *et al.*, 1991).

Cross-section and polarization observables are easily obtained from the transition matrix elements $j_{M_A M_2 M_1}^\lambda(\mathbf{p}, \mathbf{q})$. The unpolarized differential cross section is written as (Viviani, Schiavilla, and Kievsky, 1996)

$$\sigma_u(\theta) = \frac{1}{(2J_1+1)(2J_2+1)} \sigma_0 \times \sum_{\lambda M_A M_2 M_1} |j_{M_A M_2 M_1}^{\lambda}(\mathbf{p}, \mathbf{q})|^2, \quad (9.7)$$

where the first factor comes from the average over the initial-state polarizations, θ is the angle between \mathbf{p} and \mathbf{q} (the vectors \mathbf{p} and \mathbf{q} define the xz plane), and

$$\sigma_0 = \frac{\alpha}{2\pi v_{\text{rel}}} \frac{q}{1+q/m_A}. \quad (9.8)$$

Here m_A is the rest mass of the final A -nucleon bound state. The c.m. energy of the emitted γ ray is given by

$$q = m_A \left[-1 + \sqrt{1 + \frac{2}{m_A} \left(\Delta m + \frac{p^2}{2\mu} \right)} \right], \quad (9.9)$$

where μ is $A_1 - A_2$ reduced mass, and $\Delta m \equiv m_1 + m_2 - m_A$, m_1 and m_2 are the rest masses of clusters A_1 and A_2 , respectively. The differential cross section $\sigma_{fi}(\theta)$ for a process in which an initial state with polarization defined by the density matrix ρ_i leads to a final polarization state with density matrix ρ_f can be expressed as

$$\begin{aligned} \sigma_{fi}(\theta) &= 2(2J_A+1) \sigma_0 \\ &\times \sum_{\lambda M_A M_2 M_1} \sum_{\lambda' M'_A M'_2 M'_1} [j_{M_A M_2 M_1}^{\lambda}(\mathbf{p}, \mathbf{q})] \\ &\times (\rho_i)_{M_2 M_1, M'_2 M'_1} [j_{M'_A M'_2 M'_1}^{\lambda'}(\mathbf{p}, \mathbf{q})]^* \\ &\times (\rho_f)_{\lambda' M'_A, \lambda M_A}. \end{aligned} \quad (9.10)$$

The initial density matrix is given by the product of the A_1 and A_2 density matrices, while the final density matrix is the product of the γ and A density matrices. The density matrices of clusters with spins $\frac{1}{2}$ and 1 (the only ones of interest here) are given by

$$\rho_{M, M'}^{[\mathbf{P}]} = \frac{1}{2} [1 + \boldsymbol{\sigma} \cdot \mathbf{P}]_{M, M'}, \quad (9.11)$$

$$\rho_{M, M'}^{[P^{\lambda\mu}]} = \frac{1}{3} \left[\sum_{\lambda\mu} P^{\lambda\mu} t^{\lambda\mu} \right]_{M, M'}, \quad (9.12)$$

with the matrices $t^{\lambda\mu}$ defined as

$$t_{MM'}^{\lambda\mu} = \sqrt{3} (-1)^{1-M} \langle 1M', 1-M | \lambda\mu \rangle. \quad (9.13)$$

Here \mathbf{P} and $P^{\lambda\mu}$ are the polarizations of the spin- $\frac{1}{2}$ and spin-1 clusters, respectively. For example, unpolarized proton and deuteron beams have $\mathbf{P}=0$ and $P^{\lambda\mu} = \delta_{\lambda 0} \delta_{\mu 0}$. Finally, the density matrix for the photon is written as

$$\rho_{\lambda, \lambda'}^{[P_{\ell}, P_c]} = \frac{1}{2} [\delta_{\lambda, \lambda'} + P_{\ell} \delta_{\lambda, -\lambda'} + \lambda P_c \delta_{\lambda, \lambda'}], \quad (9.14)$$

where P_{ℓ} is the linear and P_c the circular γ polarization. Note that $P_{\ell} = P_y - P_x$; that is, P_{ℓ} is defined as the difference between the γ polarizations out of and in the scattering plane (the xz plane).

The initial- and final-state polarizations are defined by assigning the quantities \mathbf{P} , $P^{\lambda\mu}$, P_{ℓ} and P_c . With the density matrices given in Eqs. (9.11), (9.12), and (9.14), polarization observables are then obtained from differences of cross sections:

$$\sigma_{fi}(\theta) \equiv \sigma(\theta; \mathbf{P}, P^{\lambda\mu}, P_{\ell}, P_c). \quad (9.15)$$

For example, the proton and deuteron vector and tensor analyzing powers $A_y(\theta)$ and $T_{20}(\theta)$ in the reactions ${}^2\text{H}(\vec{p}, \gamma){}^3\text{He}$ and ${}^1\text{H}(\vec{d}, \gamma){}^3\text{He}$ are given, respectively, by

$$\begin{aligned} \sigma_u(\theta) A_y(\theta) &= \frac{1}{2} [\sigma(\theta; \mathbf{P} = \hat{\mathbf{y}}, \delta_{\lambda 0} \delta_{\mu 0}, 0, 0) \\ &\quad - \sigma(\theta; \mathbf{P} = -\hat{\mathbf{y}}, \delta_{\lambda 0} \delta_{\mu 0}, 0, 0)], \end{aligned} \quad (9.16)$$

$$\begin{aligned} \sigma_u(\theta) T_{20}(\theta) &= \frac{1}{2} [\sigma(\theta; 0, +\delta_{\lambda 2} \delta_{\mu 0}, 0, 0) \\ &\quad - \sigma(\theta; 0, -\delta_{\lambda 2} \delta_{\mu 0}, 0, 0)]. \end{aligned} \quad (9.17)$$

Expressions for more complicated double-polarization observables are obtained in similar fashion. Another case of interest is the detection of the photon linear polarization coefficient $P_{\gamma}(\theta)$, defined as

$$\sigma_u(\theta) P_{\gamma}(\theta) = \frac{1}{2} [\sigma_{\parallel}(\theta) - \sigma_{\perp}(\theta)], \quad (9.18)$$

where

$$\sigma_{\parallel}(\theta) = \sigma(\theta; 0, \delta_{\lambda 0} \delta_{\mu 0}, P_{\ell} = -1, 0), \quad (9.19)$$

$$\sigma_{\perp}(\theta) = \sigma(\theta; 0, \delta_{\lambda 0} \delta_{\mu 0}, P_{\ell} = 1, 0). \quad (9.20)$$

Here $\sigma_{\parallel}(\theta)$ ($\sigma_{\perp}(\theta)$) corresponds to a capture cross section in which an unpolarized initial state leads to emission of a photon with linear polarization parallel (perpendicular) to the reaction plane. The observation of circular polarization $P_{\Gamma}(\theta)$,

$$\begin{aligned} \sigma_u(\theta) P_{\Gamma}(\theta) &= \frac{1}{2} [\sigma(\theta; \mathbf{P}, \delta_{\lambda 0} \delta_{\mu 0}, 0, P_c = 1) \\ &\quad - \sigma(\theta; \mathbf{P}, \delta_{\lambda 0} \delta_{\mu 0}, 0, P_c = -1)], \end{aligned} \quad (9.21)$$

requires the polarization of the initial proton (or neutron) beam. If the process is dominated by S-wave capture, as is the case for the ${}^2\text{H}(\vec{n}, \vec{\gamma}){}^3\text{H}$ reaction at thermal-neutron energies, then $P_{\Gamma}(\theta)$ is simply given by

$$P_{\Gamma}(\theta) = R_c \mathbf{P} \cdot \hat{\mathbf{q}} \quad (\text{S-wave capture only}), \quad (9.22)$$

where R_c is the so-called polarization parameter.

The expansion of the transition matrix element $j_{M_A M_2 M_1}^{\lambda}(\mathbf{p}, \mathbf{q})$ in terms of electric and magnetic multipoles is easily obtained from that given in Eq. (6.14):

$$\begin{aligned}
 & j_{M_A M_2 M_1}^\lambda(\mathbf{p}, \mathbf{q}) \\
 &= -\sqrt{\frac{8\pi^2}{(2J_A+1)}} \sum_{L S J_z \ell \ell_z} \sqrt{(2L+1)(2\ell+1)} i^L (-i)^{\ell} \\
 & \quad \times \langle J_1 M_1, J_2 M_2 | S J_z \rangle \langle S J_z, L 0 | J J_z \rangle \\
 & \quad \times \langle J J_z, \ell \ell_z | J_A M_A \rangle \mathcal{D}_{\ell_z, -\lambda}^{\ell} (0 \theta 0) [\lambda T_{\ell}^{\text{Mag}}(q; L S J) \\
 & \quad + T_{\ell}^{\text{El}}(q; L S J)], \tag{9.23}
 \end{aligned}$$

where $\mathcal{D}_{\ell_z, -\lambda}^{\ell}$ are standard rotation matrices (Messiah, 1961). The angle θ is defined as that between the \mathbf{p} direction (which is also taken as the quantization axis of the initial and final nuclear spins) and the \mathbf{q} direction.

By evaluating the sums in Eqs. (9.7) and (9.10) and using the product property of the \mathcal{D} matrices, one can make explicit the angular dependence of the unpolarized cross section as well as that of polarization observables. For example, the vector and tensor analyzing powers and photon linear coefficient can be expressed as (Seyler and Weller, 1979)

$$\sigma_u(\theta) = \sum_{m \geq 0} a_m P_m(\cos\theta), \tag{9.24}$$

$$\sigma_u(\theta) A_y(\theta) = \sum_{m \geq 1} b_m P_m^1(\cos\theta), \tag{9.25}$$

$$\sigma_u(\theta) T_{20}(\theta) = \sum_{m \geq 0} c_m P_m(\cos\theta), \tag{9.26}$$

$$\sigma_u(\theta) P_\gamma(\theta) = \sum_{m \geq 2} d_m P_m^2(\cos\theta), \tag{9.27}$$

where P_m (P_m^k) are Legendre polynomials (associated Legendre functions) and the coefficients a_m , b_m , c_m , and d_m denote appropriate combinations of electric and magnetic multipoles.

The weak-capture total cross section can simply be written, in the notation introduced above, as (Carlson, Pandharipande, and Schiavilla, 1991)

$$\begin{aligned}
 \sigma_T(E_{\text{c.m.}}) &= \frac{4}{(2\pi)^3} \frac{G_V^2 m_e^5}{v_{\text{rel}}} \frac{1}{(2J_1+1)(2J_2+1)} f(E_{\text{c.m.}}) \\
 & \quad \times \sum_{M_A M_2 M_1} |\langle \Psi_A^{J A M_A} | \mathbf{A}_a(\mathbf{q}=0) | \Psi_{\mathbf{p}, M_2 M_1}^{(+)} \rangle|^2, \tag{9.28}
 \end{aligned}$$

$$\begin{aligned}
 f(E_{\text{c.m.}}) &\equiv \frac{1}{m_e^5} \int \delta(E_{\text{c.m.}} + \Delta m - E_\nu - E_e) p_e E_e E_\nu^2 dE_e dE_\nu \\
 &= \int_1^{(E_{\text{c.m.}} + \Delta m)/m_e} dx x \sqrt{x^2 - 1} \left(\frac{E_{\text{c.m.}} + \Delta m}{m_e} - x \right)^2. \tag{9.29}
 \end{aligned}$$

Here G_V is the vector coupling constant ($G_V = 1.151 \times 10^{-5} \text{ GeV}^{-2}$), \mathbf{A}_a (a is an isospin index) is the nuclear axial current operator, and $E_{\text{c.m.}} = p^2/2\mu$ is the c.m. incident energy. The energy of the recoiling A -nucleon

bound state has been neglected, since incident energies are of the order of a few keV, that is, the energy range of relevance for the solar-burning reactions $^1\text{H}(p, e^+ \nu_e)^2\text{H}$ and $^3\text{He}(p, e^+ \nu_e)^4\text{He}$, which we shall discuss below. These processes are induced by the axial-vector (or Gamow-Teller) part of the weak-interaction Hamiltonian. Note that the dependence of \mathbf{A}_a upon the momentum transfer $\mathbf{q} = -\mathbf{p}_e - \mathbf{p}_\nu$, where \mathbf{p}_e and \mathbf{p}_ν are the outgoing lepton momenta, is ignored, again because of the very low energies involved. A more refined treatment of the phase-space factor $f(E_{\text{c.m.}})$ (the ‘‘Fermi function’’) includes the effect of the nuclear Coulomb potential due to the final A cluster, as well as its screening by atomic electrons, by multiplying the integrand in Eq. (9.29) by the ratio of the (relativistic) electron density at the nucleus to the density at infinity (Bahcall, 1966). These corrections are in fact very small for the reactions to be considered below.

Finally, for those reactions in which both clusters A_1 and A_2 carry charge, it is convenient to define the so-called astrophysical factor via

$$\sigma_T(E_{\text{c.m.}}) = \frac{S(E_{\text{c.m.}})}{E_{\text{c.m.}}} e^{-2\pi\eta}, \tag{9.30}$$

where $\sigma_T(E_{\text{c.m.}})$ is the total cross section for the process under consideration. The term $\exp(-2\pi\eta)$ is the Gamow penetration factor, proportional to the probability that two particles with charges Z_1 and Z_2 moving with relative velocity v_{rel} will penetrate their electrostatic repulsion. The factor $1/E_{\text{c.m.}}$ is essentially the geometrical factor λ^2 , λ being the de Broglie wavelength $\propto 1/p_{\text{rel}} \propto 1/\sqrt{E_{\text{c.m.}}}$. In this way, the strongly energy-dependent terms are explicitly factored out of $\sigma_T(E_{\text{c.m.}})$, and the residual function $S(E_{\text{c.m.}})$ is expected to be, at least for reactions that do not proceed through low-energy resonant states, weakly dependent on $E_{\text{c.m.}}$ (Clayton, 1983). In this situation, the measured astrophysical factor can be safely extrapolated to energies typical of the stellar interior, tens of keV or less, in which range direct measurements are often not possible.

In fact, it is interesting to investigate the energy dependence of the total cross section for radiative capture in a little more detail. In the naive direct-capture model (Christy and Duck, 1961; Bailey *et al.*, 1967; Rolfs, 1973; Lafferty and Cotanch, 1982), the total cross section for L -wave capture can be simply written as

$$\sigma_T^{(L)}(E_{\text{c.m.}}) = a^{(L)} \frac{1}{\sqrt{E_{\text{c.m.}}}} (\Delta m + E_{\text{c.m.}})^{2\ell+1} \left| \frac{F_L(\rho)}{\rho} \right|^2, \tag{9.31}$$

where $a^{(L)}$ is an energy-independent constant, the factors $1/\sqrt{E_{\text{c.m.}}}$ and $(\Delta m + E_{\text{c.m.}})^{2\ell+1}$ are, respectively, from $1/v_{\text{rel}}$ and from the energy and multipolarity ℓ of the emitted photon, and $|F_L(\rho)/\rho|^2$ is approximately the probability that clusters A_1 and A_2 approach to within some interaction radius R ($\rho \equiv p_{\text{rel}} R = \sqrt{2\mu E_{\text{c.m.}}} R$). At very low energies, $\eta \gg \rho$, and the Coulomb wave function F_L evaluated at ρ can be approximated as

$$\frac{F_L(\rho)}{\rho} \approx d_L \frac{C_L(\eta)}{\eta^L}, \quad (9.32)$$

$$C_L(\eta) = \frac{\sqrt{L^2 + \eta^2}}{L(2L+1)} C_{L-1}(\eta),$$

$$C_0(\eta) = \sqrt{\frac{2\pi\eta}{e^{2\pi\eta} - 1}}, \quad (9.33)$$

where d_L is a constant independent of energy. If no Coulomb repulsion is present in the initial channel, then the factor $|F_L(\rho)/\rho|^2$ should be replaced by $|j_L(\rho)|^2$, which shows that in this case the low-energy capture in L waves ≥ 1 is inhibited by the centrifugal barrier. However, such a suppression mechanism is not as effective when the Coulomb repulsion is present. In particular, since $\eta \propto 1/\sqrt{E_{\text{c.m.}}}$, the direct-capture model would predict, on the basis of Eqs. (9.31) and (9.32), a linear behavior for $S(E_{\text{c.m.}})$, when S- and P-wave capture are both important.

B. The $A=2$ capture reactions

1. The ${}^1\text{H}(n, \gamma){}^2\text{H}$ radiative capture

Historically, the radiative capture of thermal neutrons on protons has played a crucial role in establishing the quantitative importance of two-body current effects in photonuclear observables (Riska and Brown, 1972). Their inclusion resolves the long-standing 10% discrepancy between the calculated IA cross section and its measured value. We shall discuss it here for the sake of completeness.

At thermal energies, the ${}^1\text{H}(n, \gamma){}^2\text{H}$ capture proceeds entirely through the 1S_0 scattering state. Its cross section is related to that for threshold electrodisintegration of the deuteron, since the required matrix elements are connected to each other by time reversal. It has been most recently calculated with wave functions and currents corresponding to the Argonne v_{14} interaction (Schiavilla and Riska, 1991). The values for (successive) contributions to the cross section from the different components of the current operator are listed in Table XV. The calculated IA and total cross-section values are 304.1 mb and 331.4 mb, respectively. The latter is less than 1% below the empirical value (334.2 ± 0.5) mb (Cox, Wynchank, and Collie, 1965) and should thus be viewed as satisfactory. Note that the Argonne v_{14} model predicts singlet np scattering length and effective ranges of -23.67 fm and 2.77 fm, respectively, in good agreement with the corresponding experimental values (-23.749 ± 0.008) fm and (2.81 ± 0.05) fm (Koester and Nistler, 1975).

The two-body currents associated with Δ components are included perturbatively (see Sec. V). Their contribution is considerably smaller than that found in the original evaluation of them, which was also based on perturbation theory (Riska and Brown, 1972). This smaller contribution occurs for two reasons. First, the measured transition moment, in place of its static quark-model

TABLE XV. The ${}^1\text{H}(n, \gamma){}^2\text{H}$ cross section at thermal-neutron energies obtained with one-body currents in the impulse approximation (IA), and with inclusion of the two-body currents associated with, respectively, the leading model-independent terms due to π -like exchange (pseudoscalar PS), all model-independent terms from the Argonne v_{14} model (MI), $\omega\pi\gamma$ mechanism ($\omega\pi\gamma$), and perturbative Δ components (Δ_{PT}). The different contributions are added successively in the order stated above.

	σ_T (mb)
IA	304.1
IA+PS	322.7
IA+MI	326.9
IA+MI+ $\omega\pi\gamma$	328.2
IA+ \dots + Δ_{PT}	331.4
Expt.	334.2 ± 0.5^a

^aCox, Wynchank, and Collie, 1965.

prediction, is used here at the $\gamma N\Delta$ vertex (the former is about 30% smaller than the latter). Second, short-range cutoff parameters are included at the πNN and $\pi N\Delta$ vertices in the present treatment; these were neglected in the original work (Riska and Brown, 1972).

2. The ${}^1\text{H}(p, e^+ \nu_e){}^2\text{H}$ weak capture

The proton weak capture on protons is the most fundamental process in stellar nucleosynthesis: it is the first reaction in the p - p chain, which converts hydrogen into helium, and the principal source for the production of energy and neutrinos in stars like the sun (Clayton, 1983; Bahcall and Ulrich, 1988). The theoretical description of this hydrogen-burning reaction, whose cross section—it is important to realize—cannot be measured in the laboratory, was first given by Bethe and Critchfield (1938), who showed that the associated rate was large enough to account for the energy released by the sun. Since then, a series of calculations have refined their original estimate by using more precise values for the nucleon axial coupling and by computing the required nuclear matrix elements more accurately (Bahcall and May, 1968; Gari and Huffman, 1972; Dautry, Rho, and Riska, 1976; Gould and Guessoum, 1990; Carlson *et al.*, 1991).

Although the neutrinos from the p - p reaction are not energetic enough to have been detected in either the Davis (1994) or Kamiokande (Hirata *et al.*, 1989) experiments, the precise value for its cross section affects the flux due to higher-energy neutrinos, in particular those from the decay ${}^8\text{B}(e^+ \nu_e){}^8\text{Be}$, to which both the above experiments were sensitive. The reason for this lies in the following fact: Since the solar total luminosity and mass are known quantities, changing the pp cross section requires a modification in the solar-core density, radius, and temperature which, in turn, influences the computed rate for the production of ${}^8\text{B}$ in the p - p chain and associated neutrino flux. In particular, it has been shown by Bahcall, Bahcall, and Ulrich (1969) that the

TABLE XVI. The ${}^1\text{H}(p, e^+ \nu_e){}^2\text{H}$ cross sections at $E_{\text{c.m.}}=1, 2.5,$ and 5 keV obtained from the Argonne v_{14} model with one-body axial currents in the impulse approximation (IA) and with inclusion of the two-body axial currents associated with, respectively, π - and ρ -meson seagull terms, the $\rho\pi$ mechanism (mesonic), and perturbative Δ components (Δ_{PT}). The different contributions are added successively in the order stated above.

	$\sigma(E_{\text{c.m.}}=1 \text{ keV})$ 10^{-30} fm^2	$\sigma(E_{\text{c.m.}}=2.5 \text{ keV})$ 10^{-26} fm^2	$\sigma(E_{\text{c.m.}}=5 \text{ keV})$ 10^{-25} fm^2
IA	9.054	1.291	4.061
IA+mesonic	9.086	1.295	4.075
IA+...+ Δ_{PT}	9.188	1.310	4.121

neutrino counting rate in the Davis experiment was proportional to $(\sigma_T)^{-2.5}$, where σ_T is the p - p weak-capture cross section.

The total cross section for the proton weak capture on ${}^1\text{H}$ is easily obtained from Eq. (9.28) by considering the charge-lowering component of the axial current operator. The (dimensionless) Fermi function, including the correction for Coulomb focusing in the wave function of the emitted e^+ , is parametrized as $f(E_{\text{c.m.}})=0.142[1+9.04E_{\text{c.m.}}(\text{MeV})]$ (Bahcall and May, 1968).

Because of parity selection rules, only even L in the partial-wave expansion of the pp scattering state have a nonvanishing matrix element. Moreover, in the keV energy range, the contribution associated with $L \geq 2$ is found to be completely negligible. The expression for the transition matrix element is particularly simple in the IA; it is given by

$$\int_0^\infty dr u(r)u^{(+)}(r; E_{\text{c.m.}}, {}^1S_0), \quad (9.34)$$

where $u(r)$ and $u^{(+)}(r; E_{\text{c.m.}}, {}^1S_0)$ are, respectively, the S-wave component of the deuteron and 1S_0 scattering-state radial wave functions. The value of this expression is therefore sensitive to the pp scattering length.

The most recent and complete calculations have been based on the Argonne v_{14} interaction (Carlson *et al.*, 1991), in which, however, the central $T, S=1, 0$ component has been slightly modified so as to reproduce the experimental pp scattering length (-7.823 ± 0.01) fm (Bergervoet *et al.*, 1988) when the Coulomb repulsion is taken into account (the v_{14} interaction was originally fitted to np data only). The resulting value for the effective range parameter of 2.771 fm is also reasonably close to the experimental value (2.794 ± 0.015) fm (Bergervoet *et al.*, 1988).

As is evident from Table XVI, the two-body axial current operators lead to an increase of only 1.5% in the cross-section value predicted in the IA. The relative unimportance of these corrections has already been pointed out by Gari and Huffman (1972) and Dautry, Rho, and Riska (1976). The leading two-body contributions arising from Δ degrees of freedom are included perturbatively. The value used for the transition axial coupling $g_{\beta N \Delta}$ is taken from the naive quark model; however, the short-range cutoff in the transition $\pi N \Delta$ coupling is determined by fitting the Gamow-Teller matrix element of tritium β decay (Carlson *et al.*, 1991).

Finally, the values $S(E_{\text{c.m.}}=0)=4.00 \times 10^{-25}$ MeV-b and $dS(E_{\text{c.m.}})/dE_{\text{c.m.}}|_{E_{\text{c.m.}}=0}=4.67 \times 10^{-24}$ b are obtained from the results listed in Table XVI, which are close to the ‘‘standard’’ values $S(E_{\text{c.m.}}=0)=4.07 (1 \pm 0.051) \times 10^{-25}$ MeV-b and $dS(E_{\text{c.m.}})/dE_{\text{c.m.}}|_{E_{\text{c.m.}}=0}=4.52 \times 10^{-24}$ b quoted by Bahcall and Ulrich (1988).

C. The $A=3$ radiative-capture reactions

The low-energy three-body reactions we consider in this subsection are particularly important, since recent advances in numerical methods now make it possible to calculate bound and continuum (both dn and dp) wave functions very accurately. Thus the comparison with experimental data, which by now are quite extensive and include not only total cross sections but also spin observables, is not hindered by uncertainties in the many-body theory.

1. The ${}^2\text{H}(n, \gamma){}^3\text{H}$ radiative capture

The cross section for thermal-neutron radiative capture on deuterium was most recently measured to be $\sigma_T=0.508 \pm 0.015$ mb (Jurney, Bendt, and Browne, 1982), in agreement with the results of earlier experiments (Kaplan, Ringo, and Wilzbach, 1952; Merritt, Taylor, and Boyd, 1968). In the late eighties, measurements of both the photon polarization following polarized neutron capture (Konijnenberg *et al.*, 1988) and γ emission after polarized neutron capture from polarized deuterons (Konijnenberg, 1990) were also carried out.

The theory of the ${}^2\text{H}(n, \gamma){}^3\text{H}$ capture reaction has a long history. The ‘‘pseudo-orthogonality’’ between the ${}^3\text{H}$ ground state and nd doublet or quartet state inhibiting the T_1^{Mag} transition in IA for this process [and thus explaining the smallness of its cross section when compared to that for the ${}^1\text{H}(n, \gamma){}^2\text{H}$ reaction, $\sigma_T=334.5 \pm 0.5$ mb] was first pointed out by Schiff (1937). Later, Phillips (1972) emphasized the importance of initial-state interactions and two-body currents to the capture reaction in a three-body model calculation by considering a central, separable interaction. In more recent years, a series of calculations of increasing sophistication with respect to the description of both the initial- and final-state wave functions and two-body current model were carried out (Hadjimichael, 1973; Torre and Goulard, 1983). These efforts culminated in Friar

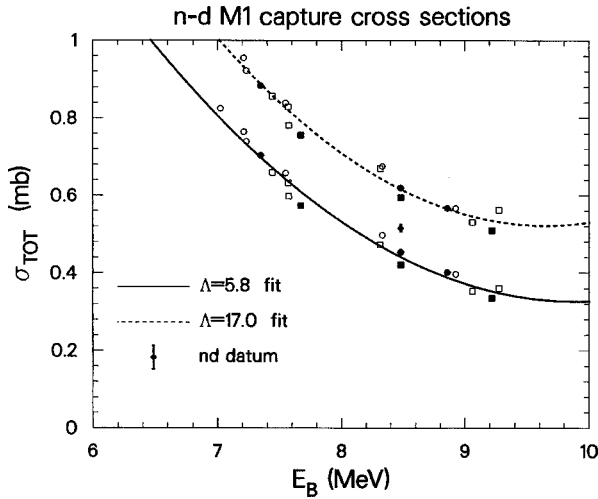


FIG. 52. The thermal nd radiative capture cross sections as a function of the triton binding energy: \circ , results obtained from a Hamiltonian based on the Reid soft-core two-nucleon interaction with and without the inclusion of the Tucson-Melbourne (Brasil) three-nucleon interaction; \square , results from a Hamiltonian based on the Argonne v_{14} two-nucleon interaction. Solid symbols denote 34-channel bound states. Results are also shown corresponding to 5, 9, and 18 channels. The pion-nucleon form-factor cutoff in the two-body currents is Λ (in units of m_π). The experimental value is from Jurney, Bendt, and Browne (1982).

et al.'s calculation (Friar, Gibson, and Payne, 1990) of the ${}^2\text{H}(n, \gamma){}^3\text{H}$ total cross section, quartet capture fraction, and photon polarization. The calculation was based on converged bound- and continuum-state Faddeev wave functions, which corresponded to a variety of realistic Hamiltonian models with two- and three-nucleon interactions, as well as a nuclear electromagnetic current operator, including the long-range two-body components associated with pion exchange and the virtual excitation of intermediate Δ resonances. Within this framework, Friar Gibson, and Payne clearly showed the importance of initial-state interactions and two-body current contributions. They also showed that both the calculated cross section and the photon polarization parameter could be in good quantitative agreement with the experimental values, if the cutoff Λ_π at the πNN vertices in the two-body currents was taken in the range $1050 \text{ MeV} \leq \Lambda_\pi \leq 1200 \text{ MeV}$, depending on the particular combination of two- and three-body interactions considered (see Figs. 52 and 53).

More recently, CHH wave functions obtained from either the Argonne v_{14} two-nucleon (Wiringa, Smith, and Ainsworth, 1984) and Urbana VIII three-nucleon (Wiringa, 1991) interactions (AV14/VIII), or the Argonne v_{18} two-nucleon (Wiringa, Stoks, and Schiavilla, 1995) and Urbana IX three-nucleon (Pudliner *et al.*, 1995) interactions (AV18/IX), and including Δ admixtures, were also used to study this reaction (Viviani, Schiavilla, and Kievsky, 1996). The nuclear electromagnetic current in these calculations consists of one- and two-body components, the latter constructed with the (current-conserving) Riska prescription. The low-energy

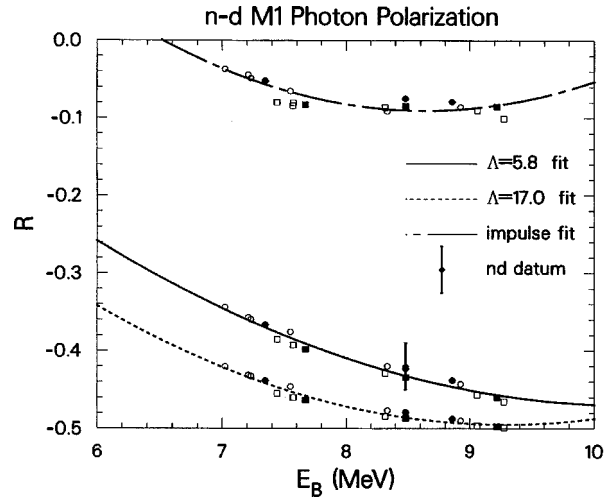


FIG. 53. The photon polarization parameter R_c in thermal $\vec{n}d$ radiative capture. Notation as in Fig. 52. The experimental value is from Konijnenberg *et al.* (1988).

scattering parameters obtained with the CHH $d+N$ wave functions corresponding to the AV14/VIII model are in excellent agreement with the Faddeev results (Hüber *et al.*, 1995).

At thermal energies, the reaction proceeds through S-wave capture predominantly via magnetic dipole transitions $T_1^{\text{Mag}}(0\frac{1}{2}\frac{1}{2})$ and $T_1^{\text{Mag}}(0\frac{3}{2}\frac{3}{2})$ from the initial doublet $J=\frac{1}{2}$ and quartet $J=\frac{3}{2}$ nd scattering states (the notation for the multipole operator reduced matrix elements is that introduced in Sec. IX.A). In addition, there is a small contribution due to an electric quadrupole transition $T_2^{\text{El}}(0\frac{3}{2}\frac{3}{2})$ from the initial quartet state.

The results for the cross section and photon polarization parameter, obtained with the AV14/VIII and AV18/IX Hamiltonian models, are listed in Table XVII, along with the experimental data (see table for notation). The cross section in the impulse approximation is calculated to be approximately a factor of 2 smaller than the measured value, while the $\text{IA} + \dots + \Delta$ calculations based on the AV14/VIII and AV18/IX Hamiltonians overestimate the experimental value by 18% and 14%, respectively. It should be noted, however, that the common perturbative treatment of Δ -isobar degrees of freedom (row labeled $\text{IA} + \dots + \Delta_{\text{PT}}$) leads to a significant increase in the discrepancy between theory and experiment (Viviani, Schiavilla, and Kievsky, 1996).

The photon polarization parameter is very sensitive to two-body currents, as can be seen from Table XVII and Fig. 53. More interesting is its sensitivity to the small E_2 reduced matrix element, particularly for the AV14/VIII Hamiltonian. In S-wave capture this matrix element is predominantly due to transitions $S({}^2\text{H}) \rightarrow D({}^3\text{H})$ and $D({}^2\text{H}) \rightarrow S({}^3\text{H})$, where S and D denote S- and D-wave components in the bound-state wave functions. In the case of the AV18/IX Hamiltonian, the contributions associated with these transitions interfere destructively, thus producing a small E_2 reduced matrix element; in contrast, for the AV14/VIII Hamiltonian, the interference between these contributions is constructive. Thus

TABLE XVII. Cumulative contributions to the cross section (in mb) and photon polarization parameter R_c of the reaction ${}^2\text{H}(n, \gamma){}^3\text{H}$ at thermal energies calculated with the Argonne v_{14} two-nucleon and Urbana VIII three-nucleon (AV14/VIII) and Argonne v_{18} two-nucleon and Urbana IX three-nucleon (AV18/IX) Hamiltonian models. Results obtained with one-body currents in the impulse approximation (IA), and with inclusion of the two-body currents associated with, respectively, the leading model-independent terms due to π -like exchange (pseudoscalar, PS), all model-independent terms from the interaction models Argonne v_{14} or Argonne v_{18} (MI), the $\rho\pi\gamma$ and $\omega\pi\gamma$ mechanisms (model-dependent, MD), and Δ components treated either perturbatively (Δ_{PT}) or nonperturbatively (Δ) with the transition-correlation-operator (TCO) method, are listed. $R_c(M_1)$ was calculated without inclusion of the electric quadrupole contribution, while $R_c(M_1 + E_2)$ was calculated with it.

	σ_T		$R_c(M_1)$		$R_c(M_1 + E_2)$	
	AV14/VIII	AV18/IX	AV14/VIII	AV18/IX	AV14/VIII	AV18/IX
IA	0.225	0.229	-0.089	-0.083	0.029	-0.068
IA+PS	0.409	0.383	-0.422	-0.397	-0.345	-0.385
IA+MI	0.502	0.481	-0.460	-0.446	-0.389	-0.437
IA+MI+MD	0.509	0.489	-0.464	-0.452	-0.394	-0.442
IA+...+ Δ_{PT}	0.658	0.631	-0.492	-0.487	-0.430	-0.478
IA+...+ Δ	0.600	0.578	-0.485	-0.477	-0.420	-0.469
Expt.	0.508 ± 0.015^a		-0.42 ± 0.03^b			

^aJurney, Bendt, and Browne, 1982.

^bKonijnenberg *et al.*, 1988.

the E_2 reduced matrix element appears to be very sensitive to the D-state content of the two- and three-nucleon bound-state wave functions and to the strength of the tensor force, as reflected in the large difference between the AV14/VIII and AV18/IX predictions. It is unfortunate that, due to the large two-body current contributions affecting the photon polarization parameter, the sensitivity displayed by this observable to the E_2 reduced matrix element cannot be exploited to gain information on the tensor interaction (Viviani, Schiavilla, and Kievsky, 1996).

Finally, we note that the AV14/VIII prediction for the cross section in the approximation $\text{IA} + \text{PS} + \Delta_{\text{PT}}$ is 0.545 mb. This result is about 15% smaller than that reported by Friar and collaborators (Friar, Gibson, and Payne, 1990) for the same Hamiltonian. The difference is mostly due to the different value used for the $N \rightarrow \Delta$ transition magnetic moment: Viviani, Schiavilla, and Kievsky (1996) take $\mu_{\gamma N\Delta} = 3\mu_N$, while Friar *et al.* used $\mu_{\gamma N\Delta} = 3\sqrt{2}/5\mu^V$ from the quark model, $\mu^V = 4.706\mu_N$ being the nucleon isovector magnetic moment. Indeed, if the latter value is used for $\mu_{\gamma N\Delta}$, the CHH result becomes 0.630 mb, in much better agreement with that reported by Friar *et al.* As a last remark, we note that the R_c parameter, obtained in the $\text{IA} + \text{PS} + \Delta_{\text{PT}}$ approximation by only including the M_1 reduced matrix element, is calculated to be -0.49 , again in excellent agreement with the value obtained by Friar *et al.*

2. The ${}^2\text{H}(p, \gamma){}^3\text{He}$ radiative capture

In an experiment performed in 1995 at TUNL (Schmid *et al.*, 1995, 1996), the total cross section and, for the first time, vector and tensor analyzing powers of the ${}^2\text{H}(\vec{p}, \gamma){}^3\text{He}$ and ${}^1\text{H}(\vec{d}, \gamma){}^3\text{He}$ reactions were measured at center-of-mass energies below 55 keV. The astrophysical S factor, extrapolated to zero energy from the cross-section data, was found to be $S(E_{\text{c.m.}} = 0)$

$= 0.165 \pm 0.014$ eV b, where the error includes both systematic and statistical uncertainties (Schmid *et al.*, 1996). This value for $S(0)$ is about 35% smaller than that obtained by Griffiths *et al.* (Griffiths, Lal, and Scarfe, 1963) more than thirty years ago, the only other experimental determination of $S(0)$. More recently, in another experiment performed at TUNL, a different group (Ma *et al.*, 1996) has extended the study of the ${}^2\text{H}(\vec{p}, \gamma){}^3\text{He}$ and ${}^1\text{H}(\vec{d}, \gamma){}^3\text{He}$ reactions to center-of-mass energies between 75 and 300 keV.

The radiative capture of protons on deuterons is the second reaction occurring in the pp chain, but its effect on the energy (and neutrino) production of stars is negligible, since its rate is controlled by the much slower pp weak-capture rate preceding it. However, the ${}^2\text{H}(p, \gamma){}^3\text{He}$ reaction plays a more prominent role in the evolution of protostars. As a cloud of interstellar gas collapses on itself, it begins to heat up, igniting, as its temperature reaches about 10^6 °K, the ${}^2\text{H}(p, \gamma){}^3\text{He}$ reaction. Deuterium burning via this reaction, which occurs first in the protostellar gas, plays the role of a thermostat in low-mass protostars, and maintains the temperature of the core at about 10^6 °K (Stahler, 1988). This puts tight constraints on the mass-radius relation of the protostar core and affects calculations of the “stellar birthline”—the sites on the H-R diagram where stars first become luminous. It also impacts the depletion of (primordial, in this case) deuterium. Of course, the precise value for the S factor of the ${}^2\text{H}(p, \gamma){}^3\text{He}$ reaction is essential to provide quantitative estimates for these phenomena.

The observed linear dependence upon the energy of the S -factor as well as the observed angular distributions of the cross section and polarization observables indicate that the ${}^2\text{H}(p, \gamma){}^3\text{He}$ reaction proceeds predominantly through S- and P-wave capture (Ma *et al.*, 1996; Schmid *et al.*, 1996). Such S- and P-wave capture pro-

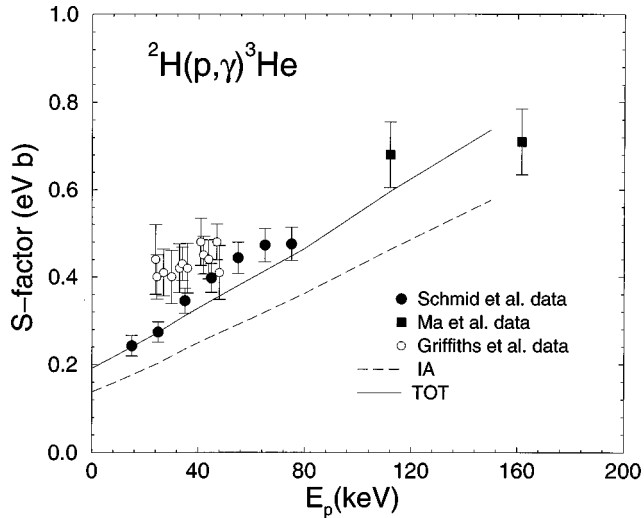


FIG. 54. The S factor of the ${}^2\text{H}(p, \gamma){}^3\text{He}$ reaction, obtained with the Argonne v_{18} two-nucleon and Urbana IX three-nucleon Hamiltonian model in the impulse approximation (IA) and with inclusion of two-body currents and Δ -isobar admixtures in the nuclear wave functions (TOT), compared with experimental results from Griffiths, Lal, and Scarfe (1963), Schmid *et al.* (1996), and Ma *et al.* (1996).

cesses have been theoretically studied, at very low energies, only in the past few years, with converged Faddeev and CHH wave functions obtained from realistic interactions that include Coulomb distortion effects in the initial channel (Friar *et al.*, 1991; Viviani, Schiavilla, and Kievsky, 1996).

The predicted S factor and angular distributions of the differential cross section $\sigma_u(\theta)$, and vector and tensor analyzing powers $A_y(\theta)$ and $T_{20}(\theta)$, are compared with the experimental data (Ma *et al.*, 1996; Schmid *et al.*, 1996) in Figs. 54–57. The results shown correspond to calculations based on the AV18/IX Hamiltonian and CHH wave functions (Viviani, Schiavilla, and Kievsky, 1996). Faddeev wave functions have only been used to calculate the zero-energy S -wave contribution to the S factor (Friar *et al.*, 1991).

The dominant contributions are those due to electric and magnetic dipole transitions between the initial dou-

plet or quartet scattering states and the final ${}^3\text{He}$ bound state. The transitions induced by electric and magnetic quadrupole operators have a much weaker strength. The calculated S - and P -wave capture contributions to the zero-energy S factor are compared with the most recent experimental determinations (Schmid *et al.*, 1996) in Table XVIII (see table for notation). The $S_S(E_{c.m.}=0)$ is found to be 0.105 eV b (Viviani, Schiavilla, and Kievsky, 1996), in good agreement with experiment, $S_S^{\text{exp}}(E_{c.m.}=0) = 0.109 \pm 0.01 \text{ eV b}$ (Schmid *et al.*, 1996) and with the value reported by Friar *et al.* (1991), 0.108 eV b . However, the experimental P -wave S factor, $S_P^{\text{exp}}(E_{c.m.}=0) = 0.073 \pm 0.007 \text{ eV b}$, is 15 (10)% smaller than calculated with the AV18/IX (AV14/VIII) Hamiltonian.

Results for the S factor in the energy range $E_p = 0\text{--}150 \text{ keV}$ ($E_{c.m.} = 0\text{--}100 \text{ keV}$) are shown in Fig. 54, where they are compared with the recent TUNL data (Ma *et al.*, 1996; Schmid *et al.*, 1996) and the much older data of Griffiths, Lal, and Scarfe (1963). Both the absolute values and the energy dependence of the TUNL data are well reproduced by the $\text{IA} + \dots + \Delta$ calculation. The enhancement due to two-body current and Δ -isobar contributions is substantial: the ratios $[S(\text{IA} + \dots + \Delta) - S(\text{IA})]/S(\text{IA})$ for the S - and P -wave S factors are found to be, respectively, 0.62 and 0.18 at 0 keV and increase to 0.75 and 0.22 at $E_p = 150 \text{ keV}$. The Griffiths *et al.* data have large errors and appear to be at variance with the TUNL data.

The measured angular distributions of the energy-integrated cross section, vector and tensor analyzing powers, and photon linear polarization (Schmid *et al.*, 1996) are compared with theory (Viviani, Schiavilla and Kievsky, 1996) in Figs. 55–57. Note that, since the energy binning of the data would substantially increase the statistical errors, the theoretical calculations, weighted by the energy dependence of the cross section and the target thickness, have been integrated for the purpose of comparing them with experiment (Rice, Schmid, and Weller, 1996). The energy dependence of these observables is, in any case, rather weak.

The overall agreement between theory and experiment is satisfactory for all observables with the exception of $A_y(\theta)$. The latter is particularly sensitive to two-

TABLE XVIII. Cumulative contributions in eV b to the S - and P -wave capture zero-energy S factor of the reaction ${}^2\text{H}(p, \gamma){}^3\text{He}$ calculated with the Argonne v_{14} two-nucleon and Urbana VIII three-nucleon (AV14/VIII) and Argonne v_{18} two-nucleon and Urbana IX three-nucleon (AV18/IX) Hamiltonian models. Notation is same as in Table XVII.

	S_S		S_P	
	AV14/VIII	AV18/IX	AV14/VIII	AV18/IX
IA	0.0605	0.0647	0.0650	0.0731
IA+PS	0.0880	0.0900	0.0794	0.0876
IA+MI	0.0939	0.0943	0.0822	0.0900
IA+MI+MD	0.0971	0.0972	0.0824	0.0901
IA + \dots + Δ_{PT}	0.117	0.117	0.0824	0.0901
IA + \dots + Δ	0.105	0.105	0.0800	0.0865
Expt.	$0.109 \pm 0.01^{\text{a}}$		$0.073 \pm 0.007^{\text{a}}$	

^aSchmidt *et al.*, 1996.

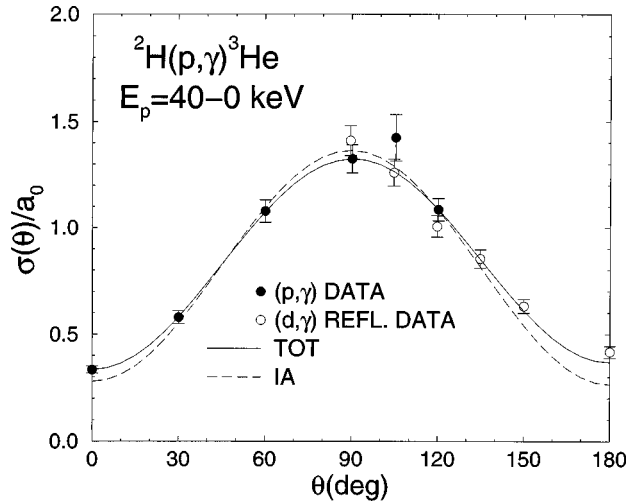


FIG. 55. The energy-integrated relative cross sections, $\sigma(\theta)/a_0$ where ($4\pi a_0$ is the total cross section), obtained with the Argonne v_{18} two-nucleon and Urbana IX three-nucleon Hamiltonian model in the impulse approximation (IA) and with inclusion of two-body currents and Δ -isobar admixtures in the nuclear wave functions (TOT), are compared with experimental results from Schmid *et al.* (1996). Note that this plot only shows data with $E_p=0-40$ keV ($E_{c.m.}=0-27$ keV). This is done to allow the (d,γ) data with $E_d=0-80$ keV ($E_{c.m.}=0-27$ keV) and the (p,γ) data to be shown in the same graph [with the (d,γ) data reflected].

body current contributions, whose effect is to reduce the results obtained in the IA by about a factor of 3, bringing them into better agreement with the data. However, an approximate 30% discrepancy between the predicted and measured A_y remains unresolved. It is important to recall here that these observables, unlike thermal cross

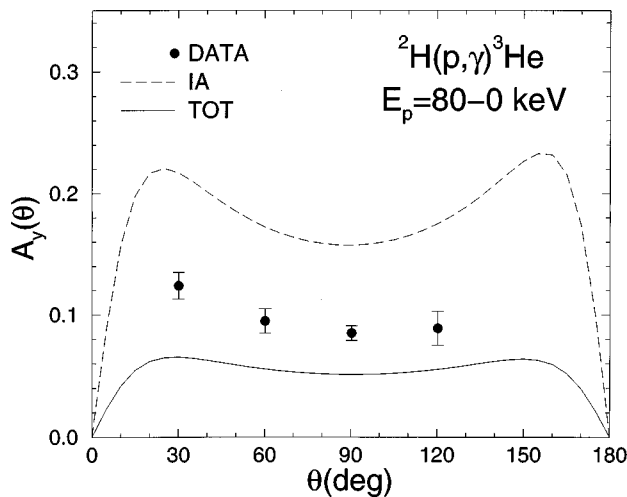


FIG. 56. The energy-integrated vector analyzing powers of the ${}^2\text{H}(\vec{p},\gamma){}^3\text{He}$ reaction, obtained with the Argonne v_{18} two-nucleon and Urbana IX three-nucleon Hamiltonian model in the impulse approximation (IA) and with inclusion of two-body currents and Δ -isobar admixtures in the nuclear wave functions (TOT), compared with experimental results from Schmid *et al.* (1996).

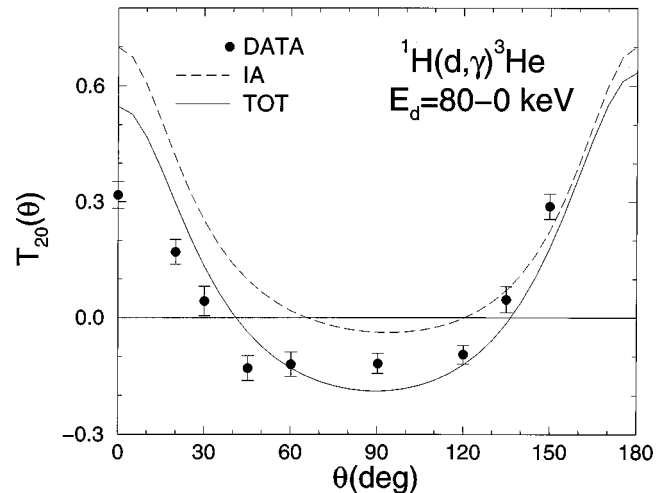


FIG. 57. The energy-integrated tensor analyzing powers of the ${}^1\text{H}(\vec{d},\gamma){}^3\text{He}$ reaction, obtained with the Argonne v_{18} two-nucleon and Urbana IX three-nucleon Hamiltonian model in the impulse approximation (IA) and with inclusion of two-body currents and Δ -isobar admixtures in the nuclear wave functions (TOT), compared with experimental results from Schmid *et al.* (1996).

sections, are independent of normalization issues in both theory and experiment. The origin of this discrepancy is, at present, unclear, but perhaps suggests an incomplete dynamic picture of the process.

D. The $A=4$ capture reactions

While the four-nucleon bound-state problem can nowadays be solved very accurately with a variety of different techniques and realistic interactions (see Secs. III and IV), solutions for the four-nucleon continuum problem, even at low excitation energies, have only been attempted with the variational Monte Carlo (VMC) method (Carlson, Pandharipande, and Wiringa, 1984; Carlson *et al.*, 1990; Arriaga *et al.*, 1991; Carlson *et al.*, 1991). It is expected that Faddeev-Yakubovsky, CHH, and GFMC $A=4$ scattering-state wave functions of quality comparable to those for the $A=3$ systems will become available in the next few years.

In this section, the focus is on the weak-capture ${}^3\text{He}(p,e^+\nu_e){}^4\text{He}$ and radiative captures ${}^3\text{He}(n,\gamma){}^4\text{He}$ and ${}^2\text{H}(d,\gamma){}^4\text{He}$. The thermal-neutron and keV proton captures on ${}^3\text{He}$ involve a transition from a 3S_1 scattering state to the $J^\pi=0^+$ ${}^4\text{He}$ ground state. As already pointed out, the matrix element of the one-body (electromagnetic or Gamow-Teller) operator between the dominant S-state components of the ${}^3\text{He}$ and ${}^4\text{He}$ bound states vanishes (Austern, 1951). Thus these reactions in the IA proceed through the small components of the wave functions—the S' mixed-symmetry states. For this reason, they are sensitive to models for the wave functions and two-body electroweak operators (for which the $S\rightarrow S$ transition is not inhibited).

Even more interesting is the dd fusion. Below 100 keV, the experimental data on the S factor suggest that the relevant orbital angular momentum between the dd clusters is $L=0$ (S wave) (Wilkinson and Cecil, 1985; Barnes *et al.*, 1987). As a consequence, because of the bosonic character of the two d clusters, only even channel-spin S values are allowed ($S=0$ or 2). Since $0^+ \rightarrow 0^+$ electromagnetic transitions with emission (or absorption) of a single photon are prohibited, it follows that the only allowed entrance channel is 5S_2 , and the transition to the ${}^4\text{He}$ ground state has T_2^{El} character. In the long-wavelength approximation, the T_2^{El} operator does not involve the nucleons' spin variables (it is proportional to the charge quadrupole operator), and therefore it can only connect the $S=2$ component of the ${}^4\text{He}$ ground state, namely its D-wave orbital part. Note that the dominant two-body currents have isovector character, and will not contribute to this $T=0 \rightarrow T=0$ transition. Furthermore, the less important isoscalar two-body currents associated, for example, with the momentum dependence of the two-nucleon interaction, are taken into account anyway in the long-wavelength approximation via Siegert's theorem. Thus the radiative fusion of two deuterons can, at low energies, provide information on the ${}^4\text{He}$ (and ${}^2\text{H}$) D-state components and, indirectly, on the tensor force which induces these components.

The above discussion should make clear that the $A=4$ reactions under consideration here put exceptional demands on the quality of models for the bound- and scattering-state wave functions and two-body electroweak operators.

1. The radiative ${}^3\text{He}(n, \gamma){}^4\text{He}$ and weak ${}^3\text{He}(p, e^+ \nu_e){}^4\text{He}$ captures

Most of the calculations of the ${}^3\text{He}(n, \gamma){}^4\text{He}$ and ${}^3\text{He}(p, e^+ \nu_e){}^4\text{He}$ cross sections have been based on shell-model descriptions of the initial- and final-state nuclear wave functions and simple meson-exchange models for the two-body components in the electroweak current operator [essentially the Chemtob and Rho (1971) prescription with some short-range modification]. These calculations have led to contradictory results. For example, in the radiative-capture reaction, Towner and Khanna (1981) have found that the cross section is dominated by exchange current contributions, whereas Tegnér and Bargholtz (1983) and, more recently, Wervelman *et al.* (1991) have found that these contributions provide only a small correction to the cross-section value obtained in the impulse approximation. Furthermore, large differences exist even between the IA values: Towner and Khanna quote results ranging from 2 to 14 μb , depending on whether harmonic-oscillator or exponential wave functions are used to describe the ${}^3\text{He}$ and ${}^4\text{He}$ ground states. However, Wervelman *et al.* quote an IA cross section of 50 μb . These discrepancies are presumably due to the schematic wave-function models used in these calculations and reiterate the need for a description of these reactions based on realistic wave functions.

More recently, VMC calculations based on the the AV14/VIII Hamiltonian model have been carried out (Carlson *et al.*, 1990; Schiavilla *et al.*, 1992). The Monte Carlo approach to the low-energy continuum was reviewed briefly in Sec. VIII.C. In essence, it converts the scattering problem, in which the asymptotic behavior of the wave function (phase shift) is to be determined for a given energy, into a bound-state problem within a finite volume, in which the energy corresponding to a prescribed boundary condition (and, therefore, phase shift) of the wave function on the surface of this volume is determined. The energy is determined variationally in VMC, but the method becomes exact if Faddeev or GFMC techniques are used to solve the bound-state problem in the finite volume. However, except for the GFMC studies of P-wave resonances in the $n+{}^4\text{He}$ system (Carlson and Schiavilla, 1994a), to date only VMC calculations have been attempted. These have been used to study the low-energy resonances in ${}^4\text{He}$ (Carlson, Pandharipande, and Wiringa, 1984), as well as the low-energy $N+{}^3\text{He}$ 3S_1 (Carlson *et al.*, 1990) and $d+d$ 5S_2 (Arriaga *et al.*, 1991; to be described below) scattering-state wave functions. The $p+{}^3\text{He}$ and $n+{}^3\text{He}$ scattering lengths are found to be (10.1 ± 0.5) fm (Carlson *et al.*, 1991) and (3.50 ± 0.25) fm (Carlson *et al.*, 1990), respectively. These are quite close to the values of (10.2 ± 1.4) fm (Tombrello, 1965; Berg *et al.*, 1980; Tegnér and Bargholtz, 1983) and (3.52 ± 0.25) fm (Kaiser *et al.*, 1977) obtained from effective range parametrizations of $p+{}^3\text{He}$ and $n+{}^3\text{He}$ scattering data at low energies. The uncertainties in the calculated values are due to statistical errors associated with the Monte Carlo integration technique.

In principle, the $n+{}^3\text{He}$ 3S_1 channel is coupled to the $p+{}^3\text{H}$ channel, as well as to the $n+{}^3\text{He}$ and $p+{}^3\text{H}$ 3D_1 channels. This coupling has been ignored in the calculations performed so far, although the method above can be generalized to treat multichannel problems. In the specific case of the $n+{}^3\text{He}$ state, it is not known how these couplings, which are found to be small in an R-matrix analysis of the $n+{}^3\text{He}$ reaction (Hale, 1990), would influence predictions for the ${}^3\text{He}(n, \gamma){}^4\text{He}$ cross section.

The cross sections for the $p+{}^3\text{He}$ and $n+{}^3\text{He}$ captures have also been shown to be quite sensitive to the treatment of Δ degrees of freedom (Schiavilla *et al.*, 1992). Indeed, perturbative estimates of the two-body current contributions associated with Δ excitation lead to a substantial overprediction of the measured $n+{}^3\text{He}$ cross section. To date, $N+\Delta$ coupled-channel calculations to describe the $A=4$ nuclei bound and continuum states have not been attempted. However, the correlation-operator method used in VMC has been generalized to include one- and two- Δ admixtures in the nuclear wave functions—the so-called transition-correlation-operator method, briefly discussed in Sec. V. The transition-correlation operator is constructed from interactions, such as the Argonne v_{28} (Wiringa, Smith, and Ainsworth, 1984), that include explicit Δ degrees of freedom.

TABLE XIX. Cumulative and normalized contributions to the total cross section of the radiative-capture ${}^3\text{He}(n, \gamma){}^4\text{He}$ at thermal-neutron energies. Notation is same as in Table XVII.

	$\sigma_T(\mu\text{b})$
IA	5.65
IA+MI	72.5
IA+MI+MD	83.7
IA+...+ Δ	85.9
Expt.	55 ± 3^a

^aWolfs *et al.*, 1989; Wervelman *et al.*, 1991.

The cross section for radiative capture of thermal neutrons on ${}^3\text{He}$ has most recently been measured by two groups (Wolfs *et al.*, 1989; Wervelman *et al.*, 1991); they quote values of (54 ± 6) and (55 ± 3) μb , respectively, in good agreement with each other and with two earlier measurements (Bollinger, Specht, and Thomas, 1973; Suffert and Berthollet, 1979), although not with the smaller value reported by Alfimenkov *et al.* (1990). The proton weak capture on ${}^3\text{He}$ cannot be measured in the energy range relevant for solar fusion, and earlier estimates for its cross section were based upon shell-model wave functions (Werntz and Brennan, 1967,1973). The neutrinos produced by this reaction possess the distinction, within the pp cycle, of having the larger energy. The associated small flux might be detectable in the next generation of solar neutrino experiments (Bahcall and Ulrich, 1988).

The VMC calculated values for the ${}^3\text{He}(n, \gamma){}^4\text{He}$ cross section at thermal-neutron energies and the ${}^3\text{He}(p, e^+ \nu_e){}^4\text{He}$ S factor at zero energy are listed in Tables XIX and XX, while those for the matrix elements of the one- and two-body current contributions—defined, respectively, as $\langle {}^4\text{He} | j_x | n {}^3\text{He}; J=1, J_z=1 \rangle$ and $\langle {}^4\text{He} | A_x | p {}^3\text{He}; J=1, J_z=1 \rangle / C_0$ [C_0 is defined in Eq. (9.33)]—are given in Tables XXI and XXII (from Schiavilla *et al.*, 1992).

Several comments are in order:

(1) The IA value for the radiative-capture cross section is one order of magnitude smaller than the experimental value.

(2) The matrix elements of the one- and (leading) two-body operators have opposite signs. Because of the

TABLE XX. Cumulative and normalized contributions to the S factor of the weak-capture ${}^3\text{He}(p, e^+ \nu_e){}^4\text{He}$ at zero energy, obtained with one-body currents in the impulse approximation (IA), with inclusion of the two-body axial currents associated with, respectively, the π - and ρ -meson seagull terms and $\rho\pi$ mechanism (IA+mesonic), and finally also including the two-body terms due to Δ -isobar degrees of freedom, generated with the transition-correlation-operator method.

	$10^{23}S$ (MeV b)
IA	6.88
IA+ mesonic	7.38
IA+...+ Δ	1.44

TABLE XXI. Contributions to the matrix element of the radiative capture ${}^3\text{He}(n, \gamma){}^4\text{He}$ at thermal-neutron energies. The rows labeled $[\Delta]_{d,r}$ correspond to contributions from, respectively, direct γ - Δ couplings and renormalization corrections. Notation is the same as in Table XVIII.

	10^2 M.E. ($\text{fm}^{3/2}$)
IA	-0.165
MI	0.756
MD	0.044
$[\Delta_\gamma]_d$	0.174
$[\Delta_\gamma]_r$	-0.125

resulting cancellation, the predicted value for the cross sections of the $n+{}^3\text{He}$ and, particularly, $p+{}^3\text{He}$ captures is exceptionally sensitive to the model for the two-body electroweak current operators.

(3) If the Δ contribution is estimated using perturbation theory, the radiative-capture cross section is calculated to be 112 μb , as compared to an experimental value of 55 μb . Explicit inclusion of Δ -isobar degrees of freedom in the nuclear wave functions, however, leads to a significant reduction of this discrepancy.

(4) In Tables XXI and XXII, the row labeled $[\Delta]_d$ denotes contributions due to the direct coupling of the photon or axial current to a Δ , while that labeled $[\Delta]_r$ denotes renormalization corrections, namely, the modification of the purely nucleonic matrix elements due to the presence of Δ -isobar components in the wave functions. These components, as expected, have the same sign as the IA matrix element. What may be surprising is the magnitude of the correction; the ratio $[\Delta]_r/\text{IA}$ is ≈ 0.75 (0.48) for radiative (weak) capture. However, this result is easily understood when one considers that the transition operators associated with this correction, in contrast to the one-body nucleon current, have a nonvanishing matrix element between the dominant S-wave components of the ${}^3\text{He}$ and ${}^4\text{He}$ ground states.

(5) The two-body model-dependent electromagnetic contributions due to the $\rho\pi\gamma$ and $\omega\pi\gamma$ mechanisms have been calculated using the rather “hard” cutoff values $\Lambda_\pi=1.2$ GeV and $\Lambda_\rho=\Lambda_\omega=2$ GeV at the meson- NN vertices. Use of “softer” values for them [as indicated for the $\rho\pi\gamma$ current by a study of the $B(Q)$ deuteron structure function] would significantly reduce their contribution.

TABLE XXII. Contributions to the matrix element of the weak-capture ${}^3\text{He}(p, e^+ \nu_e){}^4\text{He}$, multiplied by $[(\exp(2\pi\eta) - 1)/(2\pi\eta)]^{1/2}$, at zero energy. The rows labeled $[\Delta]_{d,r}$ correspond to contributions from, respectively, direct axial-vector- Δ couplings and renormalization corrections. Notation is the same as in Table XX.

	M.E. ($\text{fm}^{3/2}$)
IA	0.3849
mesonic	0.0137
$[\Delta_\beta]_d$	-0.3974
$[\Delta_\beta]_r$	0.1861

(6) The capture cross sections show a strong dependence on the scattering length. By varying the $n + {}^3\text{He}$ ($p + {}^3\text{He}$) scattering wave function so that the scattering length ranges from 3.25 fm (9.0 fm) to 3.75 fm (11.0 fm), which is the range given by the data analysis, the radiative-capture cross section varies from ≈ 1.3 to ≈ 0.7 times the present prediction, while the weak-capture cross section is ≈ 1.2 to ≈ 0.8 times the prediction listed in Table XX. Obviously, a more accurate experimental determination of the effective range parameters for low-energy $n + {}^3\text{He}$ and $p + {}^3\text{He}$ elastic scattering would be useful in ascertaining the quality of the interactions and/or the reliability of the variational description of the continuum states.

(7) Finally, the $N\Delta$ and $\Delta\Delta$ interactions and the axial $N \rightarrow \Delta$ coupling are not well known. Uncertainties on the precise value of the latter produce cross-section results which, in the case of the weak capture, may differ by as much as a factor of 2 (Schiavilla *et al.*, 1992). Clearly, the substantial overprediction of the $n + {}^3\text{He}$ cross section is unsatisfactory. At this point, it is unclear whether this discrepancy is due to deficiencies in the VMC wave functions, or two-body current operators, or more subtle dynamical effects (coupling to other channels or three-body currents, for example). Future calculations based on more accurate CHH, Faddeev-Yakuboisky, or GFMC wave functions should resolve some of these issues.

2. The ${}^2\text{H}(d, \gamma){}^4\text{He}$ radiative capture

${}^2\text{H}(d, \gamma){}^4\text{He}$ capture, at very low energies, occurs because of the presence of D-state components in the wave functions. Both states are generated by the tensor part of the two-nucleon interaction, and this reaction can therefore provide information, albeit indirect, on the tensor force in nuclei.

The radiative fusion of two deuterons also has important implications in nuclear astrophysics—it influences the predictions for the abundances of the primordial elements in the universe (Fowler, 1984)—and in fusion research (Cecil and Newman, 1984).

Experimental and theoretical studies of the ${}^2\text{H}(d, \gamma){}^4\text{He}$ reaction have been carried out since the early fifties (Flowers and Mandl, 1950; Meyerhof *et al.*, 1969; Skopik and Dodge, 1972; Poutissou and Del Bianco, 1973). In the eighties, advances in experimental techniques and, in particular, the availability of polarized ion beams made it possible to measure cross sections and polarization observables at energies ranging from 25 keV to about 50 MeV (Weller *et al.*, 1998, 1986; Mellema, Wang, and Heaberli, 1986; Barnes *et al.*, 1987; Langenbrunner *et al.*, 1988). It is fair to say, however, that progress in the theoretical description of this reaction has proceeded at a slower pace. Most of the calculations have been based on the resonating group method (Watcher, Mertelmeier, and Hofmann, 1988) or more phenomenological approaches (Weller *et al.*, 1984, 1986; Santos *et al.*, 1985; Arriaga, Eiró, and Santos, 1986; Mellema, Wang, and Heaberli, 1986; Tostevin, 1986; As-

senbaum and Langanke, 1987; Piekarewicz and Koonin, 1987; Arriaga *et al.*, 1988; Langenbrunner *et al.*, 1988), for which the connection with the underlying two- and three-nucleon interactions governing nuclear dynamics becomes rather tenuous.

In the early nineties, a VMC calculation of this reaction was performed (Arriaga *et al.*, 1991). The experimental data indicate that the S factor is constant below c.m. energies of 500 keV, suggesting that the reaction proceeds predominantly via S-wave capture. Thus the 5S_2 state should be the only important entrance channel at these energies. The corresponding VMC wave function ignores couplings to the 1D_2 and 5D_2 as well as to the $n + {}^3\text{He}$ and $p + {}^3\text{H}$ channels. However, D-wave contributions should be suppressed because of the centrifugal barrier. Contributions due to couplings to the 3+1 channels are also expected to be small, since angular momentum and parity selection rules require a relative orbital angular momentum of two units between these clusters, which should again be suppressed at low energies. These conclusions are corroborated by resonating-group-method calculations (Chwieroth, Tang, and Thompson, 1972; Hofmann, Zahn, and Stöwe, 1981; Kanada, Kaneko, and Tang, 1986).

The S factor obtained in the VMC calculation for energies below 500 keV was found to be about an order of magnitude smaller than measured. To shed some light on this disastrous result, Arriaga *et al.* (1991) wrote the T_2^{El} transition matrix element as (using a schematic notation)

$$\langle {}^4\text{He} | E_2 | dd \rangle \equiv \int_0^\infty dr \psi(r; {}^5S_2) Y(r; {}^5S_2), \quad (9.35)$$

where $\psi(r; {}^5S_2)$ is the relative wave function between the two deuteron clusters, and the function $Y(r; {}^5S_2)$ contains all information about the bound-state wave functions and transition operator. The Y function exhibits positive and negative regions, which nearly cancel out. Its positive portion is essentially due to $D \rightarrow S$ and its negative portion to $S \rightarrow D$ transitions. Thus the value of the E_2 matrix element becomes very sensitive to the relative wave function $\psi(r; {}^5S_2)$. Indeed, Arriaga *et al.* (1991) also showed that the S factor obtained with a wave function $\psi(r; {}^5S_2)$ slightly worse (variationally) than the optimal one was in reasonable agreement with data. This wave function had precisely the same asymptotic behavior (phase shift) as the optimal, but had a node in the interior region. The possible presence of inner oscillations in the relative wave function for clusters of nucleons is due to Pauli repulsion, as has been pointed out in the context of resonating-group-method calculations (Tamagaki and Tanaka, 1965; Okai and Park, 1966).

While the present VMC calculation is clearly unsatisfactory and needs to be improved, it is clear that this reaction shows an interesting interplay between the D states of the deuteron and α particle, both of which are determined by the tensor force, and the $d + d$ continuum wave function. It is expected that in the next few years advances in the description of the four-nucleon con-

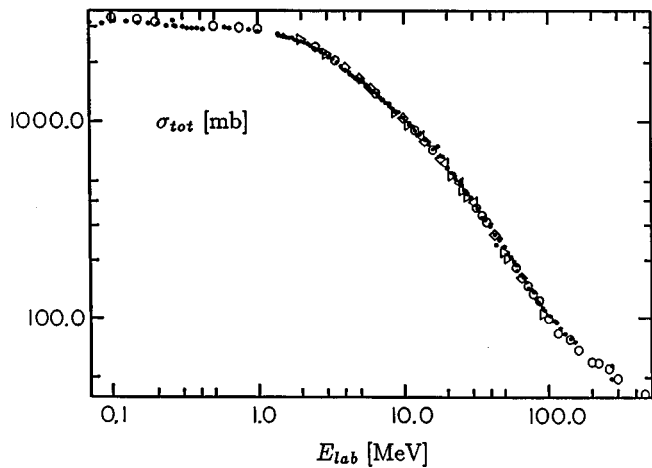


FIG. 58. Total cross section for nd scattering. Different NN interactions are shown: \circ , Bonn B (\diamond), Paris (\triangleright), Argonne v_{18} and (\triangleleft) Reid 93. Data are from Fox *et al.* (1950), deJuren (1950), deJuren and Knable (1950), Riddle *et al.* (1965), Measday and Palmieri (1966), Shirato and Koori (1968), Davis and Barschall (1971), Clement *et al.* (1972), Koori (1972), Phillips, Berman, and Seagrave (1980), and Schwarz *et al.* (1983).

tinuum will make it possible to study these subtle dynamic effects in a more precise way.

X. THREE-NUCLEON SCATTERING ABOVE BREAKUP

The pd and nd reactions provide a wealth of information about nuclear interactions. Many experiments have been carried out, including measurements of total and differential cross sections, polarization observables, and cross sections in specific kinematics. These experiments provide a host of stringent tests of the nuclear interaction models, in particular the three-nucleon interaction. An excellent review of this subject has recently been provided by Glöckle *et al.* (1996). In this section we present a few of the highlights.

To date, calculations above breakup with realistic interactions have been performed only with the momentum-space Faddeev method. However, comparisons of the breakup amplitude have been made using a simplified Malfliet-Tjon spin-dependent S-wave force (Friar *et al.*, 1990), and hence it is reasonable to believe that other methods will soon also be able to produce reliable results above breakup. Calculations that include the Coulomb interaction will be particularly valuable.

In general, theoretical predictions are in impressive agreement with experimental results. A first step in any comparison with data is to examine the total cross section, which is presented in Fig. 58. The total nd cross section is well reproduced by any of the modern realistic NN interaction models, many of which are shown in the figure. This cross section depends only upon the low partial waves of the NN interaction; the $J=4$ channels give only a modest two-percent contribution at 100 MeV. The experimental results are taken from many sources, including Juren and Knable (1950), Fox *et al.* (1950),

Riddle *et al.* (1965), Measday and Palmieri (1966), Shirato and Koori (1968), Davis and Barschall (1971), Clement *et al.* (1972), Koori (1972), Phillips, Berman, and Seagrave (1980), and Schwarz *et al.* (1983).

The total cross section is split into elastic and inelastic components, each of which has been measured. We turn first to elastic differential cross sections. As the momentum-space Faddeev calculations are performed without the Coulomb interaction, one would prefer to compare with nd data. The number of nd measurements is unfortunately rather small, although at a few energies both nd and pd data do exist. In Fig. 59 elastic pd and nd data are compared with nd Faddeev calculations. The calculations show little dependence on the NN interaction model and are dominated by quartet scattering (Aaron and Amado, 1966; Koike and Taniguchi, 1986). As is apparent in the figure, a substantial discrepancy exists between theory and experiment in the low-energy regime at forward and backward angles, as one would expect based upon the importance of the Coulomb interaction in these regions. The importance of these Coulomb effects has been confirmed in recent calculations of Kievsky, Viviani, and Rosati (1995).

The agreement is quite good at higher energies, from 8 to 35 MeV. At yet larger energies small discrepancies again appear, until at the largest energies (>140 MeV) these become quite significant. Clearly, at larger energies one should study results in a relativistic framework in order to develop a clearer understanding of the successes and failures of NN interaction models.

Spin observables in elastic scattering present a very significant challenge for nuclear interaction models. Consider an initial state with an incoming nucleon polarized along the direction \mathbf{P} and an unpolarized deuteron. The cross section can be defined as a sum of two terms, the unpolarized cross section plus a term proportional to the polarization:

$$I = I_0 \left(1 + \sum_k P_k A_k \right), \tag{10.1}$$

where the A_k are the nucleon analyzing powers. If $M_{m'_d, m'; m_d, m}$ represents the scattering amplitude for a transition $m_d, m \rightarrow m'_d, m'$, then the differential cross section is simply given by

$$\frac{d\sigma}{d\Omega} = |M_{m'_d, m'; m_d, m}(\mathbf{P}', \mathbf{P})|^2, \tag{10.2}$$

while the analyzing powers are obtained as a ratio,

$$A_k = \frac{\text{tr}(M \sigma_k M^\dagger)}{\text{tr}(M M^\dagger)}. \tag{10.3}$$

Note that, because of parity conservation, the analyzing-power components in the scattering plane (the xy plane) vanish—i.e., $A_x = A_z = 0$ —and only A_y is different from zero.

In contrast to the total cross-section measurements, in the nucleon analyzing power the $j=2$ NN forces can be significant even at energies as low as 10 MeV. At ener-

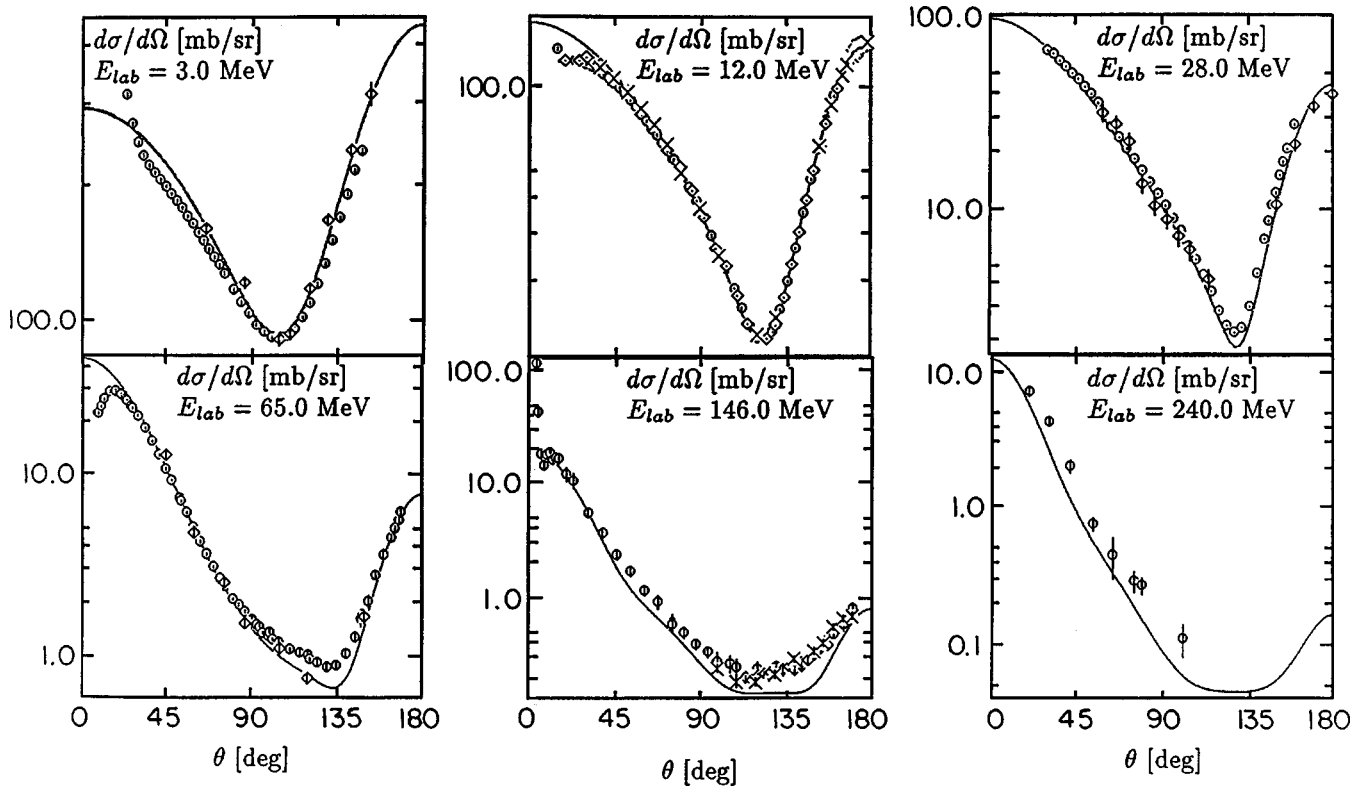


FIG. 59. Elastic pd and nd angular distributions, experiment and theory. Faddeev calculations are performed by the Bochum group (Glöckle, Witala, *et al.* (1996) for the indicated NN interaction models. The Coulomb interaction is not included (see discussion in text). 3 MeV: (\circ) pd data (Sagara *et al.*, 1994); (\diamond) nd data (Schwarz *et al.*, 1983); theory: solid line, Nijm I, long-dashed line, Nijm II, short-dashed line, Reid 93, dotted line, Argonne v_{18} . 12 MeV: (\circ) pd data (Sagara *et al.*, 1994), (\diamond) (Grüebler *et al.*, 1983), (\times) (Rauprich *et al.*, 1988); theory: dotted line Argonne v_{18} . 28 MeV: (\circ) pd data (Hatanaka *et al.*, 1984); (\diamond) nd data (Gouanere *et al.*, 1970); theory: solid line, Nijm I. 65 MeV: (\circ) pd data (Shimizu *et al.*, 1982); (\diamond) nd data (Rühl *et al.*, 1991); theory: dotted line, Argonne v_{18} . 146 MeV: (\circ) pd data (Postma and Wilson, 1961), (\diamond) (Igo *et al.*, 1972); nd data at 152 MeV (\times) (Palmieri, 1972); dotted line, Argonne v_{18} . 240 MeV: (\circ) pd data (Schamberger, 1952); theory: dotted line, Argonne v_{18} .

gies above 30 MeV (Fig. 60), very good agreement is found between theory and experiment, and little difference is found between nd and pd results (Glöckle and Witala, 1990; Tornow *et al.*, 1991; Witala and Glöckle, 1991).

A significant discrepancy exists between theory and experiment at lower energies, however. The calculations underestimate the data by approximately 30% at 10 MeV (Fig. 61). The 3P_J forces are dominant in determining the vector analyzing power A_y ; indeed, force models with different 3P_J phases can yield significantly different results. For example, the older Argonne v_{14} interaction model deviates most strongly from other results as its 3P_J phases are the most different. More recent NN interaction models all produce similar results, which are in sizable disagreement with the data.

Deuteron analyzing powers, describing experiments with an initial deuteron polarization, can be defined similarly. The deuteron, being a spin-1 system, can be vector or tensor polarized. The initial polarizations of the deuteron are described by a vector P_i and a tensor P_{jk} . For an unpolarized initial nucleon, the cross section is

$$I = I_0 \left(1 + \frac{3}{2} \sum_k P_k A_k + \frac{1}{3} \sum_{jk} P_{jk} A_{jk} \right). \quad (10.4)$$

The observables are often written in spherical tensor notation, in which, for example, $iT_{11} = (\sqrt{3}/2)A_y$. The experimental situation for the deuteron analyzing power is quite similar to that for the nucleon (Witala *et al.*, 1993; Sagara *et al.*, 1994)—agreement is quite good above 30–40 MeV, but serious disagreements exist at lower energies.

Current three-nucleon interaction models do not eliminate the A_y discrepancy. Indeed, Witala, Hüber, and Glöckle (1994) have performed calculations with the Bonn-B NN interaction and various components of the Tucson-Melbourne three-nucleon interaction model, including $\pi\pi$, $\pi\pi+\pi\rho$, and $\pi\pi+\pi\rho+\rho\rho$ exchanges. The corresponding results, shown in Fig. 62, do not improve agreement with the data. The present inability of theory to reproduce the A_y data constitutes one of the remaining open problems in the few-nucleon sector.

Other observables, including tensor analyzing powers and spin-transfer coefficients, have also been measured. The former are generally well described by the calcula-

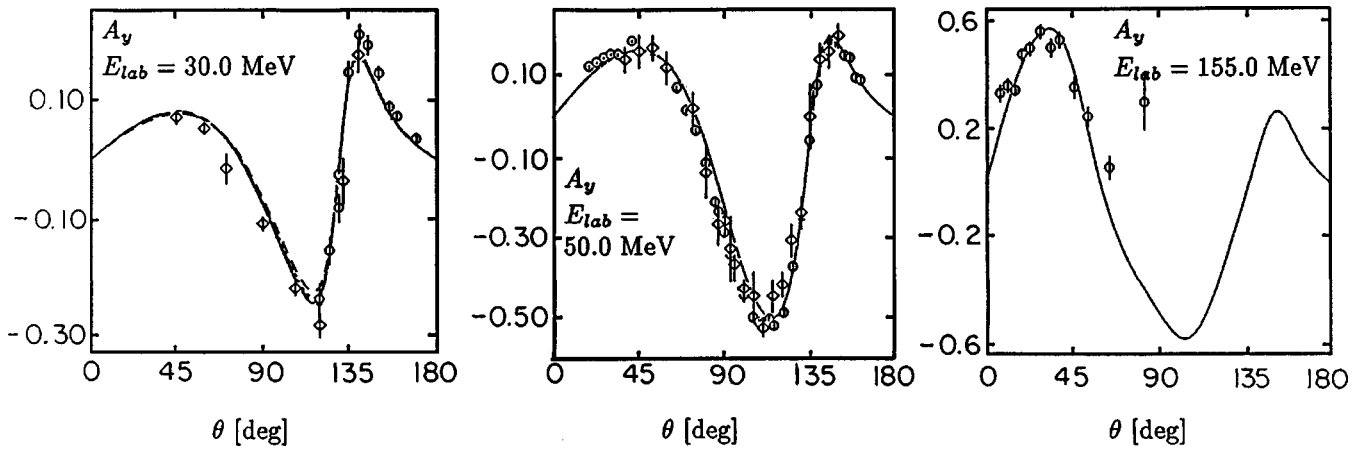


FIG. 60. The nucleon analyzing power A_y for elastic Nd scattering at 30 MeV and above. 30 MeV: (\circ) pd data (Johnston *et al.*, 1965); (\diamond) nd data (Dobiasch *et al.*, 1978); theory: solid line, Nijm I; long-dashed line, Nijm II; short-dashed, Reid 93, dotted line Argonne v_{18} . 50 MeV: (\circ) pd data (King *et al.*, 1977); (\diamond) nd data (Romero *et al.*, 1982; Watson *et al.*, 1982); theory: Argonne v_{18} . 155 MeV: (\circ) pd data (Kuroda, Michalowicz, and Poulet, 1966); theory: dotted line, Argonne v_{18} .

tions, except at low energies where one would expect Coulomb force corrections to be important (Witata *et al.*, 1993; Sagara *et al.*, 1994). The spin-transfer coefficients are obtained from experiments in which polarization of some of the spins in the final state are also measured; they indicate the transfer of polarization from an initially polarized nucleon to the final polarization of the outgoing nucleon. The spin-transfer coefficients show some limited dependence on the NN interaction model and can also be fairly well described in calculations using modern NN interaction models (Sydow *et al.*, 1994).

We now turn to the $3N$ breakup process. Here the available phase space is much larger (the number of in-

dependent momentum components is five after using energy and momentum conservation), so a much wider range of kinematics can in principle be measured. Two particular sets of kinematics have been particularly well studied. The first case occurs when in the final state, one nucleon is nearly at rest in the laboratory system—the so-called quasifree scattering process. The initial motivation for studying this case was the belief that the cross section would be dominated by the scattering of two nucleons, with the third near-zero-momentum nucleon acting essentially as a spectator.

In quasifree scattering kinematics, the dominant process should be single-nucleon scattering (Chew, 1950; Kottler, 1965), that is, $T \approx t^{(2)}E$, and thus

$$\langle \phi_0 | U_0 | \phi \rangle = \langle \phi_0 | (1 + E)t^{(2)}E | \phi \rangle. \quad (10.5)$$

This yields the product of an essentially on-shell NN $t^{(2)}$ matrix and the deuteron state at zero momentum. Such

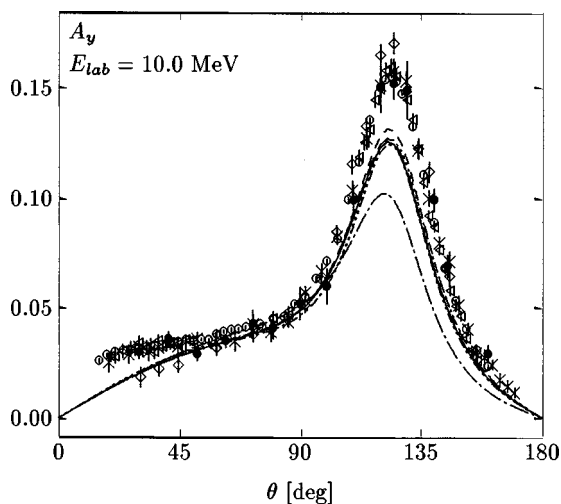


FIG. 61. The nucleon analyzing power A_y for elastic Nd scattering at 10 MeV. Comparison of experimental data and Faddeev calculations employing previous and current-generation NN interaction models. pd data: \circ , Sagara *et al.*, 1994); \times , Sperisen *et al.* (1984); \triangleleft , Rauprich *et al.* (1988); \bullet , Clegg and Haerberli (1967). nd data \diamond , Howell *et al.* (1987). Theory: solid curve, Nijm I; dashed curve, Nijm II; dotted curve, Reid 93; dotted curve, Argonne v_{18} , dot-dashed-curve, Argonne v_{14} , dash-dot-dot curve, Nijm 78.

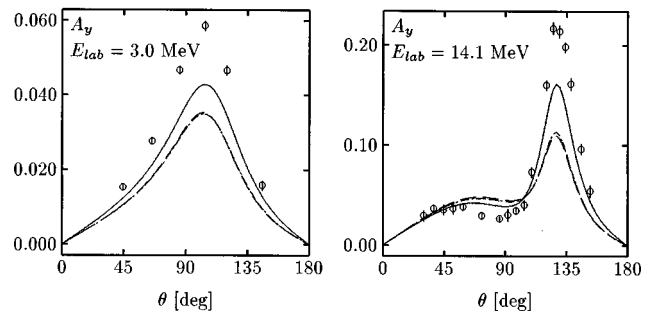


FIG. 62. Comparison of A_y data with calculations based upon an NN interaction alone, and with two- and three-nucleon interactions: Left, at 3 MeV; Right, at 14.1 MeV. Solid curves, calculations for the Bonn NN interaction alone; long-dashed curves, including the $\pi\pi$ interaction; short-dashed curves, $\pi\pi + \pi\rho$; dotted curves, $\pi\pi + \pi\rho + \rho\rho$ terms from the Tucson-Melbourne three-nucleon interaction. The nd data for 3 MeV are from McAninch *et al.* (1993) and McAninch, Lamm, and Haerberli (1994). The data for 14.1 MeV are from Howell *et al.* (1987).

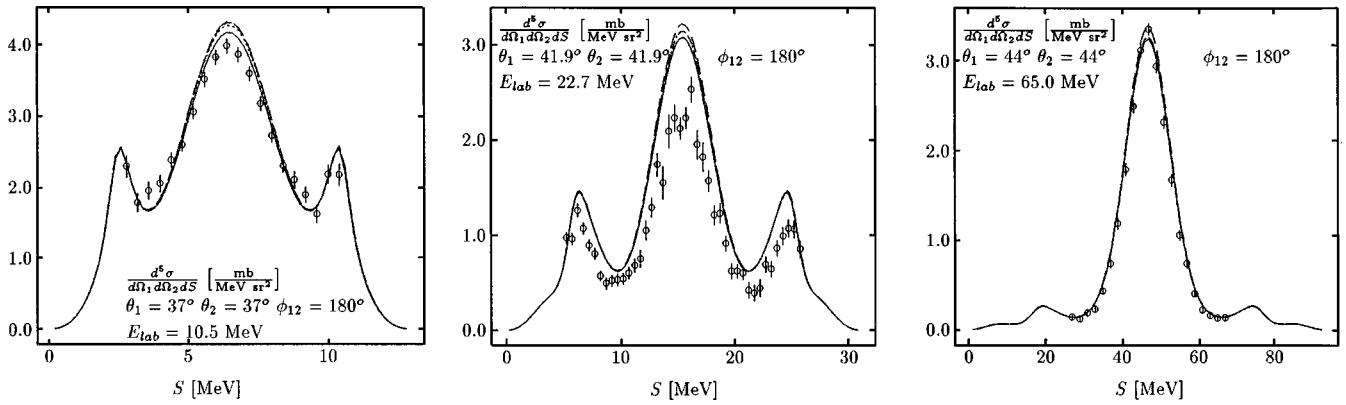


FIG. 63. Breakup cross sections in quasifree scattering kinematics. Comparison of pd data to calculations with different NN interaction models: Argonne v_{18} (—), Reid 93 (---), Nijm I (- - -), and Nijm II (· · ·).

calculations indeed see a peak near quasifree conditions, but higher order corrections can be important. The latter can in principle be calculated in a multiple-scattering series, but convergence in such a scheme can be problematic, particularly at energies significantly below 100 MeV (Glöckle *et al.*, 1996). Above 100 MeV, inclusion of the first-order term in the rescattering series leads to essentially converged results.

Complete calculations are also available and demonstrate that rescattering effects can be quite important at lower energies. Theoretical predictions for pd scattering at energies between 10 and 65 MeV are compared with experimental data in Fig. 63. Again different NN interaction models produce similar results. Except at the highest energy, theory always overestimates data in the region of the quasielastic peak. Discrepancies at lower energies could be due to Coulomb effects—it will be quite valuable to have full calculations including the Coulomb interaction.

The second set of kinematics often considered is when two nucleons leave the interaction region with nearly equal momenta. In such a case the final-state interactions between these two outgoing nucleons are necessarily strong. Indeed, this configuration has been seen as providing information on the nn scattering length. In the past, the Watson-Migdal approximation (Watson, 1952; Golberger and Watson, 1964) has often been used to extract the nn scattering length from final-state interaction peaks in the nd breakup process. In that approximation, the absolute square of the breakup amplitude is factored into an energy-independent constant C and an enhancement factor:

$$\frac{d^5\sigma}{d\Omega_1 d\Omega_2 dS} = k_s C (r_0/2)^2 \times \frac{p^2 + [1/r_0 + \sqrt{1/r_0^2 - 2/(r_0 a)}]^2}{p^2 + (-1/a + r_0 p^2/2)^2}, \quad (10.6)$$

where r_0 and a are the effective range and scattering length for the nn system and p is the relative momentum of the two neutrons. Complete calculations indicate that such an analysis should be adequate to determine the scattering length to approximately 0.5 fm. Investiga-

tion of charge-symmetry-breaking effects will require smaller uncertainties, however.

A first test of the possibility of extracting the nn scattering length is to try to reproduce the experimentally well-known np scattering lengths from np final-state interaction peaks measured in pd scattering. Comparisons of theory to experimental pd and nd results in the region of the np final-state interaction peak are presented in Fig. 64; the agreement between theory and experiment is quite good. The experimental np scattering length is -23.74 fm, and one comes closest to reproducing this value at $E=13$ MeV, where an extraction from pd scattering yields approximately (-23.3 ± 0.2) fm for the CD Bonn and Nijmegen interactions and (-23.5 ± 0.2) fm for the Reid 93. Extractions at other energies range from (-23.0 ± 0.3) fm at 10.5 MeV to (-24.2 ± 0.3) fm at 19 MeV. Obviously, the three-nucleon and Coulomb interactions can affect the extracted scattering lengths. Comparisons between experiment and theory also require a precise simulation of the experimental acceptance in the detectors.

Though quite a few nn final-state interaction peak measurements were published quite some time ago, the details are not specific enough to reproduce in numerical simulations. A fairly recent nn final-state interaction peak has been measured at 13 MeV (Gebhardt *et al.*, 1993). The results of this experiment have been analyzed by Witala *et al.* (1995) and again, with more modern NN interaction models, by Glöckle *et al.* (1996). The extracted value of a_{nn} is -14.40 fm and is nearly independent of which of the modern NN interactions is chosen. However, the shape of the data is not well reproduced by theory. This extracted value is far from the result of $-18.6(3)$ fm obtained from analyses of π absorption on the deuteron (Gabioud *et al.*, 1979; Schori *et al.*, 1987). Other measurements in this kinematic regime are underway (Tornow, Witala, and Brown, 1995).

Two other “special” final-state configurations have drawn some interest: the collinear and star configurations. In the former, one nucleon is at rest in the center-of-mass system. In the star configuration, the nucleons emerge each with the same energy and their momentum directions are separated by 120 degrees. If the plane of

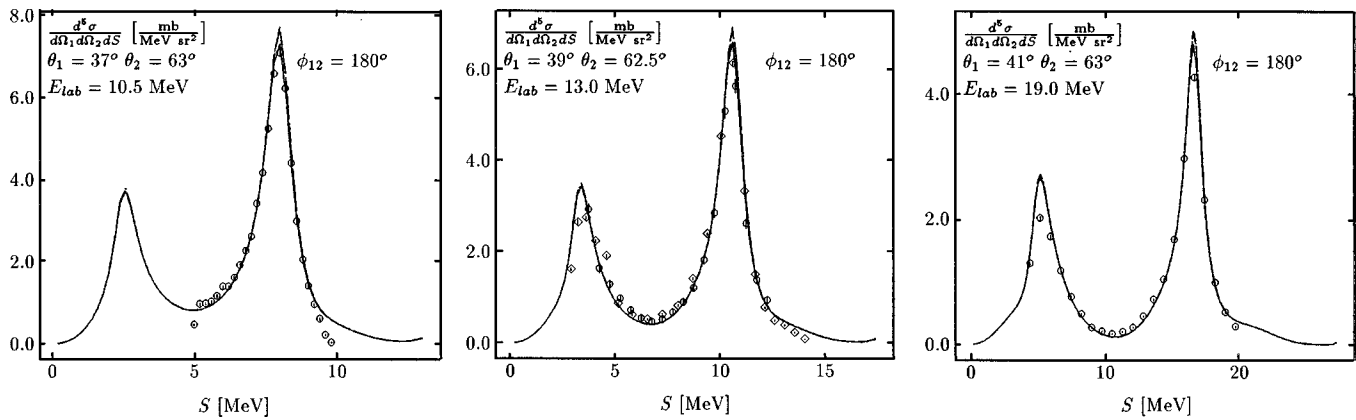


FIG. 64. Breakup cross sections near np final-state interaction peak kinematics. Data at 10 MeV: (\circ) pd data (Grossman, 1993); 13 MeV: (\circ) nd data (Strate *et al.*, 1988; Strate 1989), (\diamond) pd data (Rauprich *et al.*, 1991); 19 MeV: (\circ) pd data (Patberg, 1995). Calculations are for Argonne v_{18} , Reid 93, Nijm I, and Nijm II NN interaction models.

the momenta lies perpendicular to the beam axis, this configuration is often called the space-star configuration. The earliest motivation for studying these two configurations is that the spin-averaged two-pion-exchange three-nucleon interaction is repulsive in a collinear geometry and attractive in an equilateral triangle configuration.

The results obtained in the collinear configuration are generally in good agreement with experiment (Witala, Cornelius, and Glöckle, 1988a, 1988b; Rauprich *et al.*, 1991; Witala, Glöckle, and Kamada, 1991; Allet *et al.*, 1994). Experiments are sometimes contradictory, however. In one case a hump is seen in the nd data near the point of collinearity, although no such hump is apparent in the pd data. Therefore more accurate data are needed before definite conclusions can be drawn.

Experimental results in the star configuration are at variance with theory, at least at low energies, where the partial waves with $j \leq 2$ are important. The results are fairly insensitive to the choice of NN interaction, however. Studies of this configuration were originally motivated by the fact that three-nucleon interaction effects could be particularly important. Again, though, the Coulomb distortion of the initial and final wave functions must be included before rigorous conclusions can be drawn. At 10 MeV, theory agrees with one set of nd data (Stephan *et al.*, 1989) but is in disagreement with another (Finckh, 1990). At 13 MeV, the nd and pd data differ strongly and theory lies in between. A recent re-measurement by Tornow *et al.* (1995) supports the earlier nd data, and hence the discrepancies do seem significant.

Many other experiments and calculations have been performed, including breakup results in different kinematics and measurement of spin-transfer observables. In general, the calculations now seem to be able to describe the scattering data quite well. In the few exceptions that exist, notably the low-energy A_y observables, current three-nucleon interaction models do not seem to improve the situation. Significant advances in theory can be expected as it becomes possible to perform scattering calculations above breakup with the Coulomb interac-

tion. The combination of a huge amount of experimental data and an accurate calculational ability will provide an important regime for testing and improving three-nucleon interaction models.

XI. NUCLEAR RESPONSE

The response to electromagnetic and hadronic probes provides direct information on dynamics in the nucleus. The rich structure of nuclear interactions and currents, combined with the availability of different probes, offers the opportunity to study many intriguing aspects of nuclear dynamics. A comprehensive study of nuclear response requires an understanding of the nuclear ground-state wave function, couplings of the various probes to the nucleus, and final-state interactions. In this section we first describe the theoretical framework for studying nuclear response and then discuss electromagnetic and hadronic response.

A. Theory and calculations

Response functions are obtained from inclusive experiments, in which we essentially assume that the cross section is dominated by the exchange of a single (virtual) boson. In the electromagnetic case, a virtual photon is coupled to the nucleus through the nuclear charge or current operators, Eqs. (5.1) and (5.2). For unpolarized electrons and nuclei, the inclusive cross section in the one-photon-exchange approximation is given by

$$\frac{d^2\sigma}{d\omega d\Omega} = \sigma_M [v_L R_L(\mathbf{q}, \omega) + v_T R_T(\mathbf{q}, \omega)], \quad (11.1)$$

where σ_M , v_L , and v_T have been defined in Eqs. (6.2)–(6.4). Thus the longitudinal [$R_L(\mathbf{q}, \omega)$] and transverse [$R_T(\mathbf{q}, \omega)$] response functions can be extracted from measurements at different angles and fixed \mathbf{q} and ω . For hadrons, a high-energy nucleon passes near the nucleus and interacts once by exchanging a virtual meson. In the approximation where there is only time for a single scattering to take place, a nuclear response function can be extracted.

Here we consider response functions in a nonrelativistic framework. Extensions of the definitions of the response to the relativistic case are straightforward. However, relativistic schemes that include final-state interaction and two-nucleon processes while respecting Poincaré and gauge invariance are less well developed. Generically, a response function is given by

$$R(\mathbf{q}, \omega) = \sum_f \langle 0 | \rho^\dagger(\mathbf{q}) | f \rangle \langle f | \rho(\mathbf{q}) | 0 \rangle \delta[\omega - (E_f - E_0)], \quad (11.2)$$

where the sum runs over all final states of the system $|f\rangle$. The coupling ρ is determined by the probe. Initially we discuss a generic coupling. This coupling can depend on one- and two-nucleon operators (and possibly more), including dependence upon the orientation of the nucleon's spin and isospin.

In the simplest models of nuclear response, the plane-wave impulse approximation (PWIA), the response functions are obtained solely from the nuclear ground-state momentum distributions and the nucleon form factors. The response is assumed to be given by an incoherent sum of scattering off single nucleons that propagate freely in the final state. This simple model provides a baseline with which to gauge more realistic calculations.

In the PWIA, the sum over final states is carried out by assuming that the struck nucleon is transferred from an initial momentum \mathbf{p} to a free-particle state of final momentum $\mathbf{q} + \mathbf{p}$, and that the residual $A-1$ system is unaffected. The PWIA is expected to be accurate at high-momentum transfers, where coherent scattering effects and final-state interactions are small. For a momentum-independent coupling, the PWIA response is obtained from a convolution of the nucleon's initial momentum distribution with the energy-conserving δ function. For example, for the dominant proton coupling in the longitudinal response, it is given by (after dividing out the square of the proton charge form factor)

$$R_{L, \text{PWIA}}(\mathbf{q}, \omega) = \int d\mathbf{p} N_p(\mathbf{p}) \delta \left[\omega - E_s - \frac{(\mathbf{p} + \mathbf{q})^2}{2m} - \frac{\mathbf{p}^2}{2(A-1)m} \right], \quad (11.3)$$

where $N_p(\mathbf{p})$ is the proton momentum distribution in the ground state. The PWIA ignores the effects of nuclear binding in the initial state, replacing it with an average binding energy E_s . The remaining terms in the brackets are the final energies of the struck nucleon and the recoiling $A-1$ particle system, respectively.

To go beyond the PWIA, it is useful to write the response in terms of the real-time propagation of the final state:

$$R(\mathbf{q}, \omega) = \frac{1}{\pi} \text{Re} \int_0^\infty dt e^{i(\omega + E_0)t} \langle 0 | \rho^\dagger(\mathbf{q}) e^{-iHt} \rho(\mathbf{q}) | 0 \rangle, \quad (11.4)$$

$$\equiv \frac{1}{\pi} \text{Re} \int_0^\infty dt e^{i(\omega + E_0)t} A(\mathbf{q}, t). \quad (11.5)$$

By introducing the spectral function, we can also include the effects of binding in the initial ground-state wave function and the residual interactions of the ‘‘spectator’’ nucleons. The spectral function $S(\mathbf{p}, E)$ is defined as the probability of removing a nucleon of momentum \mathbf{p} in the nuclear ground state and leaving the residual $A-1$ system with an excitation energy $E = E_{\text{res}}^{A-1} - E_0^A$ [see Eq. (7.46)]. Ignoring coherent scattering processes and the interaction of the struck nucleon with the remaining nucleons, we obtain

$$A(\mathbf{q}, t) = \int d\mathbf{p} dE S(\mathbf{p}, E) e^{-i[E + E_0 + (\mathbf{p} + \mathbf{q})^2/2m]t}, \quad (11.6)$$

where $S(\mathbf{p}, E)$ is the spectral function defined in Eq. (7.46). The integral over time in Eq. (11.5) then yields a simple energy-conserving delta function. For example, the longitudinal response is given by

$$R_{L, \text{SF}}(\mathbf{q}, \omega) = \int d\mathbf{p} dE S_p(\mathbf{p}, E) \delta \left[\omega - E - \frac{(\mathbf{p} + \mathbf{q})^2}{2m} \right], \quad (11.7)$$

where $S_p(\mathbf{p}, E)$ is the proton spectral function.

Ignoring the energy dependence in the spectral function reproduces the PWIA approximation, as integrating $S(\mathbf{p}, E)$ over the energy loss recovers the momentum distribution. At large values of the momentum transfer, the spectral-function approximation is accurate because the cross section is dominated by striking a single nucleon, and that nucleon is ejected faster than the typical time scale of a nuclear interaction. Indeed, this approximation has been used extensively to study y scaling (Ciofi degli Atti, 1992), at least in part to obtain information about the nuclear momentum distributions.

Often, though, we are interested in experiments at more modest values of momentum transfer, where final-state interactions and two-nucleon couplings are important. In light nuclei, it is feasible to go beyond the simple approximations discussed above. Indeed, much of the interesting physics is obtained only when ground-state correlations, two-body currents, and final-state interactions are included. We first address the methods used to address these physics issues.

In the deuteron, it is relatively straightforward to calculate explicitly the final scattering states and sum over them to obtain the response. Experimentally, the deuteron can be used to study a variety of interesting physics, including, for example, relativistic effects in electron scattering and reaction mechanisms in hadronic experiments. Since the deuteron is so weakly bound, the interesting interaction effects are comparatively small.

In three-nucleon systems, it is still possible to calculate the final states explicitly, and hence compute the response by summing over final states. To date, calculations have been performed for longitudinal and transverse electron scattering in $A=3$ (Golak *et al.*, 1995). However, present calculations include only single-nucleon couplings. Inclusion of the two-body currents is necessary for a realistic comparison with data in the transverse channel. Proceeding much along the lines of

the $3N$ scattering equations described previously, we wish to calculate the nuclear matrix element

$$N = \langle \Psi_f^{(-)} | \rho(\mathbf{q}) | \Psi_0 \rangle. \quad (11.8)$$

The final state $\Psi_f^{(-)}$ is decomposed in terms of Faddeev amplitudes as

$$| \Psi_f^{(-)} \rangle = (1 + E) \psi, \quad (11.9)$$

where E is the permutation operator $E = E_{12}E_{23} + E_{13}E_{23}$. The Faddeev amplitude ψ obeys the equation

$$\psi^{(-)} = \psi_0 + G_0^{(-)} T \psi^{(-)}, \quad (11.10)$$

where the driving term ψ_0 is different for two- and three-body fragmentation. For nd breakup, ψ_0 is just the product of a deuteron state and a plane wave in the relative motion of the neutron and deuteron. Inserting Eq. (11.10) into Eq. (11.8) yields

$$N = \langle \psi_0 | (1 + E) \rho(\mathbf{q}) | \Psi_0 \rangle + \langle \psi_0 | E T G_0 (1 + E) \rho(\mathbf{q}) | \Psi_0 \rangle. \quad (11.11)$$

The first term is the PWIA and the second recovers the final-state interaction. This rescattering term can be written (Glöckle *et al.*, 1996)

$$N^{\text{rescat}} = \langle \psi_0 | (1 + E) | U \rangle, \quad (11.12)$$

where U is obtained as a solution of a Faddeev-type integral equation:

$$U = T G_0 (1 + E) \rho(\mathbf{q}) | \Psi_0 \rangle + T G_0 E | U \rangle. \quad (11.13)$$

The kernel in this equation is the same as for $3N$ scattering in Eq. (8.30), but the driving term is different, as it contains the current operator acting upon the ground state.

Beyond $A=3$, calculations have so far been performed by considering transforms of the nuclear response functions. This subject has quite a long history, both within nuclear physics and elsewhere (Baym and Mermin, 1961; Thirumalai and Berne, 1983; Silver, Sivia, and Gubernatis, 1990; Gubernatis *et al.*, 1991; Boninsegni and Ceperley, 1996). The basic idea is to sum over a set of final states in order to make as “complete” a calculation as possible. Complete here means full inclusion of final-state interactions and realistic couplings. Summing over final states allows one to avoid having to implement specific boundary conditions, one of the most difficult parts of dealing with quantum few- and many-body problems in the scattering regime.

We first consider the Lorenz-kernel transform. To date, this method has been applied with realistic interactions to the longitudinal scattering of electrons in $A=3$ (Martinelli *et al.*, 1995) and with approximate treatment of tensor interactions in $A=4$ (Efros, Leidemann, and Orlandini, 1997). The Lorenz-kernel transformed response is given by

$$L(\mathbf{q}, \sigma_R, \sigma_I) = \int d\omega \frac{S(\mathbf{q}, \omega)}{\sigma_I^2 + (\omega - \sigma_R)^2}. \quad (11.14)$$

This transformation allows one to emphasize the response for the energies near $\omega = \sigma_R$, with a width of σ_I . The response L can be calculated directly from an amplitude Φ :

$$| \Phi \rangle = \frac{1}{H - E_0 - \sigma_R + i\sigma_I} \rho(\mathbf{q}) | 0 \rangle, \quad (11.15)$$

where the transformed response is given by the norm of $| \Phi \rangle$; that is, $L(\mathbf{q}, \sigma_R, \sigma_I) = \langle \Phi | \Phi \rangle$. The advantage in this formulation is that, for nonzero σ_I , the boundary conditions are simple because the state $| \Phi \rangle$ is exponentially damped at large distances.

The state $| \Phi \rangle$ can be written in terms of Faddeev components $| \Phi \rangle = \sum_i \phi_i$. Using standard manipulations, one obtains

$$| \Phi \rangle = \frac{1}{E_0 + \sigma_R - i\sigma_I - H_0} (H - H_0) | \Phi \rangle - \frac{1}{E_0 + \sigma_R - i\sigma_I - H_0} \rho(\mathbf{q}) | 0 \rangle, \quad (11.16)$$

where H is the full Hamiltonian and H_0 is the kinetic-energy operator. This can again be recast into an inhomogeneous Faddeev equation, here evaluated at complex energy $E_0 + \sigma_R - i\sigma_I$.

It is easier to compute L for larger σ_I , because one is averaging over more final states. Consequently, larger σ_I implies fewer oscillations in the function $[1/(H - E_0 - \sigma_R - i\sigma_I)] \rho(\mathbf{q}) | 0 \rangle$, the norm of which yields $L(\mathbf{q}, \sigma_R, \sigma_I)$. For the same reason, though, it is more difficult to obtain the desired response function $S(\mathbf{q}, \omega)$ from the transformed response with larger values of σ_I . In the quasielastic regime, a value of σ_I around 10 MeV is deemed sufficient. Near threshold, it may prove advantageous to subtract the response of isolated states when calculating $L(\mathbf{q}, \sigma_R, \sigma_I)$, as the response to these states can be calculated explicitly.

Exact calculations beyond $A=3$ have so far relied upon another integral transform of the response: the Euclidean response, or Laplace transform of $S(\mathbf{q}, \omega)$. The Euclidean response is defined as

$$E(\mathbf{q}, \tau) = \int d\omega \exp[-(H - E_0)\tau] S(\mathbf{q}, \omega). \quad (11.17)$$

Its name derives from the fact that it can be obtained by the replacement of the real time t in the nuclear propagator [Eq. (11.5)], by an imaginary time τ . The Euclidean response integrates over even more final states than the Lorenz kernel, and hence it is more difficult to go back directly to $S(\mathbf{q}, \omega)$. However, it is easier to calculate than L , particularly for systems with many degrees of freedom.

This is principally because $E(\mathbf{q}, \tau)$ can be cast in a path-integral form which can be naturally evaluated with Monte Carlo techniques:

$$E(\mathbf{q}, \tau) = \langle 0 | \rho^\dagger(\mathbf{q}) \exp[-(H - E_0)\tau] \rho(\mathbf{q}) | 0 \rangle. \quad (11.18)$$

Indeed, for condensed-matter systems with spin-independent interactions, systems with hundreds of interacting particles can be treated (Boninsegni and Ceperley, 1996). The path-integral representation of $E(\mathbf{q}, \tau)$ is useful both from a computational point of view as a way of understanding some of the important experimental features of nuclear response in the quasielastic regime.

At $\tau=0$, the Euclidean response is equivalent to the associated sum rule [for example, Eq. (7.29)], while the derivatives with respect to τ are just the energy-weighted sum rules [Eq. (7.39)]. For larger τ , increasingly lower-energy contributions to the response are weighted more strongly, until, in the large- τ limit, the elastic form factors are recovered. The fact that the calculation is placed in a path-integral framework means that there are strong correlations in the calculation between closely spaced values of τ in the response. This fact has been exploited in the attempt to recover information on $S(\mathbf{q}, \omega)$ from path-integral calculations using Bayesian probability theory (Gubernatis *et al.*, 1991; Boninsegni and Ceperley, 1996). This attempt has proven successful in the quasielastic regime in the condensed-matter problem of the response of helium, but less so at lower energies where strong resonances occur (Boninsegni and Ceperley, 1966).

To illustrate the basic concept of the path-integral calculation, consider the response of a probe that is coupled to nucleons only [$\rho(\mathbf{q}) = \sum_i \exp(i\mathbf{q} \cdot \mathbf{r}_i)$]. This would be given by the sum over paths:

$$E(q, \tau) = \sum_{\text{paths}, i < j} j_0(q|r_i - r'_j|), \quad (11.19)$$

where the paths run from initial points $\mathbf{R} = \{\mathbf{r}_1, \dots, \mathbf{r}_i, \dots\}$ to $\mathbf{R}' = \{\mathbf{r}'_1, \dots, \mathbf{r}'_i, \dots\}$ and are weighted with a probability proportional to $\langle \Psi_0 | \mathbf{R}' \rangle \langle \mathbf{R}' | \exp[-(H - E_0)\tau] | \mathbf{R} \rangle \langle \mathbf{R} | \Psi_0 \rangle$. In the simplest model of longitudinal electron scattering, where the coupling ρ is only to individual protons, the Euclidean response would also be given by the sum over paths:

$$E(q, \tau) = \sum_{\text{paths}, i < j} j_0(q|r_i - r'_j|), \quad (11.20)$$

but the sum now extends only over the initial and final positions of the protons. Thus the charge dependence of the nuclear interaction means that the charge propagates much faster than the nucleons. This distinction is an important point in understanding the various nuclear response functions, which we discuss below.

B. Comparison with experiment

By now a rich set of experimental data is available on the nuclear response. In light nuclei, the electromagnetic longitudinal and transverse responses have been measured in the deuteron, the trineutrons, and the alpha particle. In addition, hadronic experiments have been used to extract the spin-isospin responses in both the deuteron and heavier systems.

When compared with simple PWIA results, these experiments show several intriguing features, features that may enhance our understanding of the nuclear response. Particularly striking is the suppression in the ratio of longitudinal to transverse electromagnetic response near the quasielastic peak. This suppression occurs in all nuclei with $A \geq 4$, but is absent for $A = 2$ and 3. In addition, the longitudinal response shows significantly greater

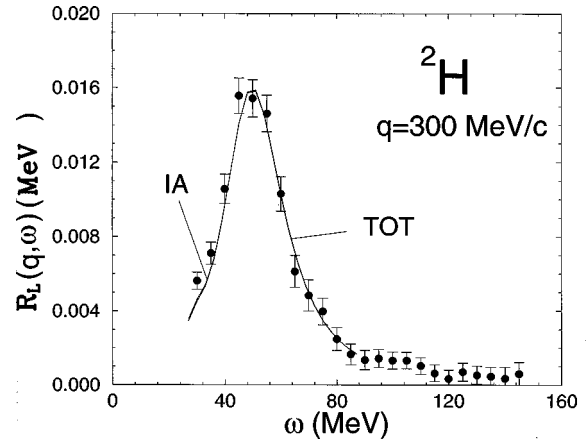


FIG. 65. Deuteron longitudinal response at 300 MeV/c; theory from Carlson and Schiavilla (1992) and experiment from Dytman *et al.* (1988). Calculations include final-state interactions and show results with one- and two-body charge operators.

strength at energies away from the quasielastic peak than occurs in PWIA estimates of the response.

Hadronic probes have provided additional important information. In particular, the peak of the (p, n) response is shifted toward significantly higher energies than the standard peak $\omega = q^2/2m$ observed in (p, p) measurements (Chrien *et al.*, 1980; Taddeucci, 1991; Carlson and Schiavilla, 1994b). Finally, there has been much discussion of recent measurements of the spin-longitudinal and spin-transverse response (Taddeucci *et al.*, 1994). Comparisons of all these results with “complete” calculations are extremely valuable in understanding nuclear dynamics in the quasielastic regime.

We first discuss the results obtained in electron scattering. For unpolarized electrons and targets, the inclusive cross section is obtained as a sum of longitudinal and transverse response functions multiplied by the associated couplings of the virtual photon. The longitudinal and transverse responses have been obtained at the Bates (Dow *et al.*, 1988; Dytman *et al.*, 1988; von Reden *et al.*, 1990) and Saclay (Marchand *et al.*, 1985; Zghiche *et al.*, 1993) accelerator facilities for different nuclei and a sizable range of kinematics.

In any experiment, the cross section is a sum of longitudinal and transverse terms, and hence one must extrapolate the results at different kinematics to obtain the longitudinal and transverse response. In light nuclei, this appears to be well under control, as the experimental results from different laboratories are in agreement. In heavier systems, considerable discrepancies persist even at the same kinematics, and an unambiguous separation into longitudinal and transverse response is problematic (Jourdan, 1995, 1996).

The longitudinal response is given by

$$R_L(\mathbf{q}, \omega) = \sum_f \langle 0 | \rho^\dagger(\mathbf{q}) | f \rangle \langle f | \rho(\mathbf{q}) | 0 \rangle \delta(\omega + E_0 - E_f), \quad (11.21)$$

where $\rho(\mathbf{q})$ is the nuclear charge operator in Eq. (5.1). In the nonrelativistic limit, recall

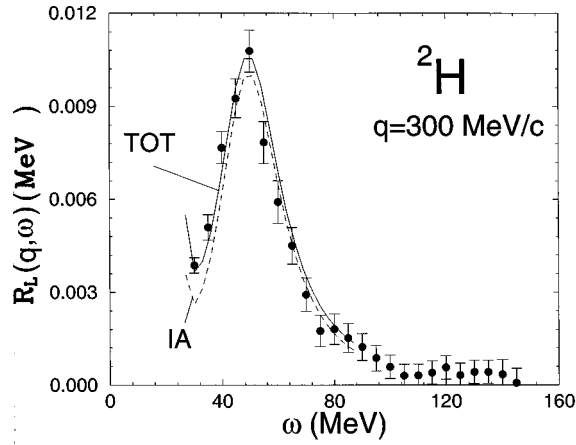


FIG. 66. Deuteron transverse response at 300 MeV/c, as in Fig. 65.

$$\rho(\mathbf{q}) = \sum_i e^{i\mathbf{q}\cdot\mathbf{r}_i} \frac{1 + \tau_{z,i}}{2}. \quad (11.22)$$

Relativistic corrections and two-body contributions to the charge operator have also been considered, but numerically they have been found to be quite small.

The transverse response is given by

$$R_T(\mathbf{q}, \omega) = \sum_f \langle 0 | \mathbf{j}^\dagger(\mathbf{q}) | f \rangle \langle f | \mathbf{j}(\mathbf{q}) | 0 \rangle \delta(\omega + E_0 - E_f). \quad (11.23)$$

Here the current operator $\mathbf{j}(\mathbf{q})$ contains both one- and two-body terms, the latter being required for current conservation.

Experimentally, after scaling by the appropriate single-nucleon couplings, the ratio of the transverse to longitudinal response is significantly enhanced in the regime of the quasielastic peak ($\omega \approx \omega_{qe} \equiv q^2/2m$) for ${}^4\text{He}$ and larger nuclei, but for $A=2$ and 3 it is very near one. Plane-wave impulse-approximation calculations yield too much strength in the longitudinal response near the peak, and too little at energies well below or above the

peak. Various exotic mechanisms, including a static nucleon “swelling,” have been introduced to explain one or more of these effects. However, as we shall see, this occurs quite naturally in complete calculations of the nuclear response.

We first consider the longitudinal and transverse responses of the deuteron, which are presented in Figs. 65 and 66. The figures present the calculation in the impulse approximation (with one-body charge and current operators) and the full response. Note that for the special case of the deuteron, the full calculation is quite close to the impulse approximation. The primary reason is that the struck nucleon can interact with only one other nucleon, and the average separation between the two nucleons is twice the deuteron’s rms radius, or about 4 fm. Consequently, the effects of two-body currents in the deuteron are quite small. In addition, the effects of final-state interactions are also quite small, except in the very low-energy part of the response. As is apparent in the figures, the calculations agree quite well with experimental results in the case of the deuteron. In the longitudinal case, the impulse and full charge operators produce nearly identical results. In the transverse channel, the two-body currents do have some effect.

We next present results for the trinucleons: the longitudinal responses at 250 and 300 MeV/c are given in Figs. 67 and 68. The momentum-space Faddeev calculations are reproduced from Golak *et al.* (1995). In general the responses are quite well reproduced, except for a slight overprediction of the ${}^3\text{He}$ response at 300 MeV/c. Calculations of the transverse response have also been presented. These significantly underpredict the available data at both momentum transfers. However, only single-nucleon current operators have been included in these calculations.

Complete Faddeev calculations that include two-nucleon currents are not yet available. Consequently, we also show the Euclidean longitudinal and transverse responses for ${}^3\text{He}$ at 400 MeV/c in Figs. 69 and 70. In the figures, a scaled response $\bar{E}(\mathbf{q}, \tau) = \exp[q^2\tau/(2m)]E(\mathbf{q}, \tau)$ has been plotted. This scaling removes trivial kinematic

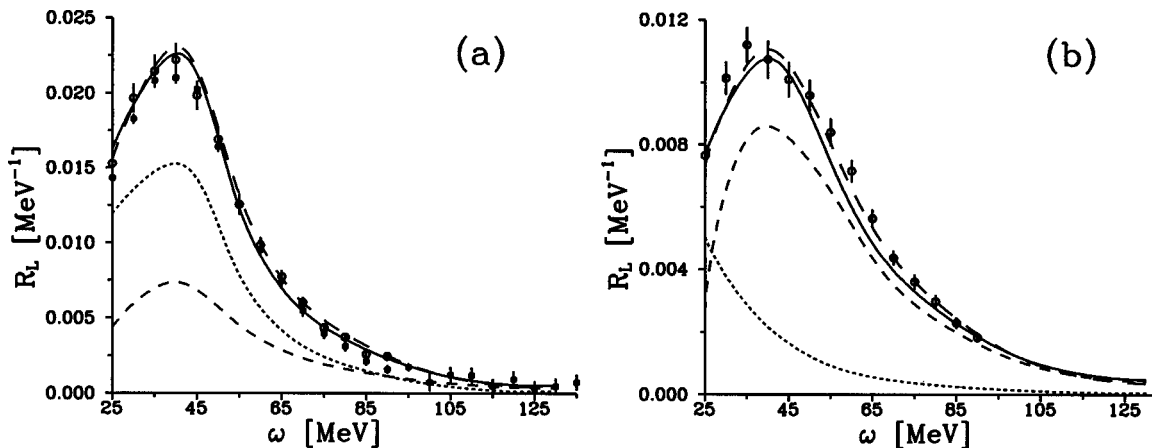


FIG. 67. ${}^3\text{He}$ (a) and ${}^3\text{H}$ (b) longitudinal response at 250 MeV/c. Calculations are from Golak *et al.* (1995): solid line, Bonn B NN interaction; I-III long-dashed line, Malfliet-Tjon, NN interactions; dotted line, Bonn B contributions from the Nd channel; short-dashed line, contribution from the Npn channel. Experimental data: \square , Marchand *et al.* (1985); \circ , Dow *et al.* (1988).

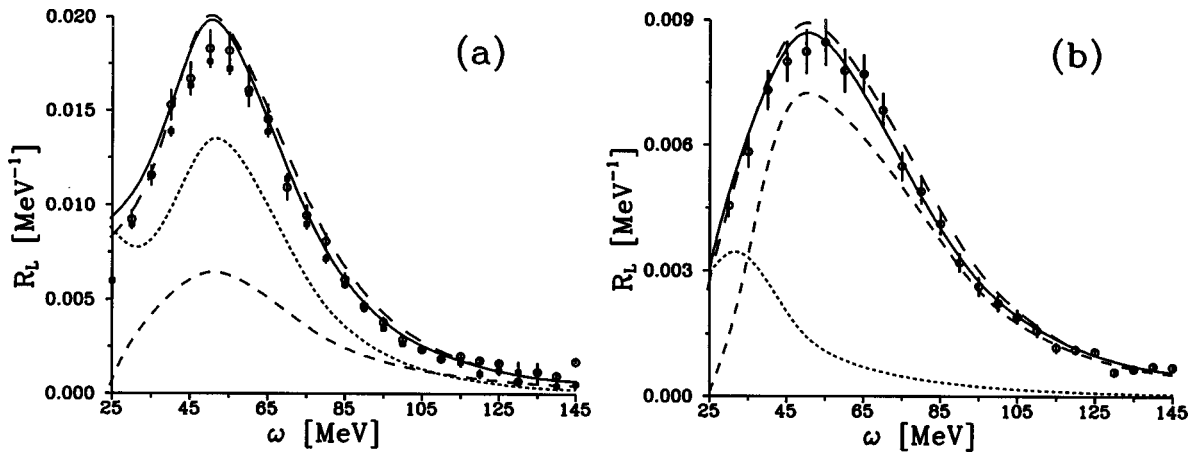


FIG. 68. ^3He (a) and ^3H (b) longitudinal response at 300 MeV/c, as in Fig. 67.

effects and emphasizes the more interesting interaction effects. The scaled response of an isolated proton would simply be given by $\bar{E}(\mathbf{q}, \tau) = 1$.

For the longitudinal response, we show only the “full” response—that obtained with one- and two-body charge operators. In the transverse case, several curves are presented: the measured response as well as responses for the impulse (one-body) and full (one- and two-body) current operators. In the longitudinal channel, the contributions due to the neutron charge operator, relativistic corrections, and two-nucleon couplings are found to be quite small; the response from the single-proton coupling is nearly identical to the full result.

The imaginary-time response $E_p(q, \tau)$ measures the propagation of charge with imaginary time in a nucleus. In the limit $\tau \rightarrow 0$, the propagator $\langle \mathbf{R} | \exp[-(H - E_0)\tau] | \mathbf{R}' \rangle \rightarrow \delta(\mathbf{R} - \mathbf{R}')$. As τ increases, the nucleons move, and the imaginary-time propagator is proportional to $\exp[-m/(2\tau)(\mathbf{R} - \mathbf{R}')^2]$. This is the part of the response that comes from the PWIA. In the limit that we consider a struck nucleon only (imagining that the propagator acting on the spectator nucleons can be ap-

proximated as one), we obtain the response due to the nucleon’s momentum distribution in the ground state. Including the interactions of the spectator nucleons with each other recovers the spectral-function approximation to the response.

However, another effect is also important. As the system evolves with imaginary time, the charge can propagate by charge-exchange interactions, the most important being one-pion exchange. The charge exchange implies a hardening of the response, a shift to higher energy, as the portion of the response due to single-nucleon processes is reduced. In a static picture of the longitudinal response, the part of the response due to the isovector part of the charge operator is shifted to higher energy, as it costs energy to change the isospin of the nucleus. In the path-integral picture, the hardening appears as an increased propagation distance (or equivalently, a reduced effective mass) associated with nuclear charge exchange. In effect, the virtual photon sees an “enlarged” nucleon for processes in which the momen-

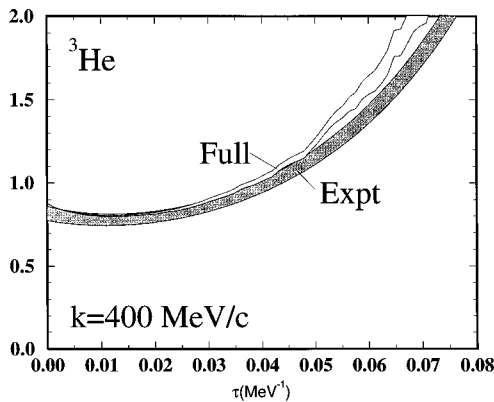


FIG. 69. Scaled Euclidean longitudinal response of ^3He at 400 MeV/c compared to the Laplace transform of experimental data from Marchand *et al.* (1985). The shaded bands represent the approximate experimental uncertainty and statistical errors in the Monte Carlo calculation.

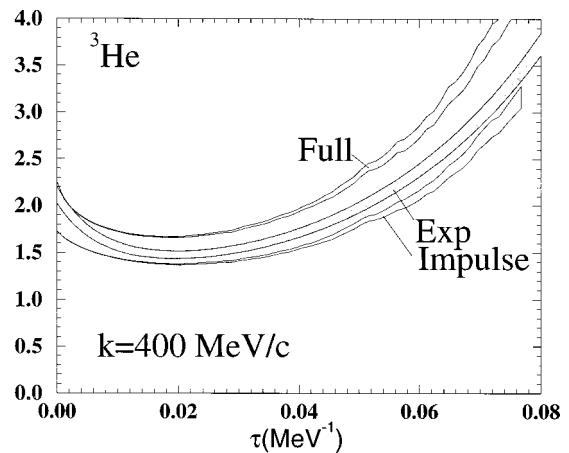


FIG. 70. Scaled Euclidean transverse response of ^3He at 400 MeV/c compared to the Laplace transform of experimental data from Marchand *et al.* (1985). The curves marked “impulse” and “full” represent results with single-nucleon and the complete current operators, respectively. In each case the calculations includes a full treatment of final-state interactions.

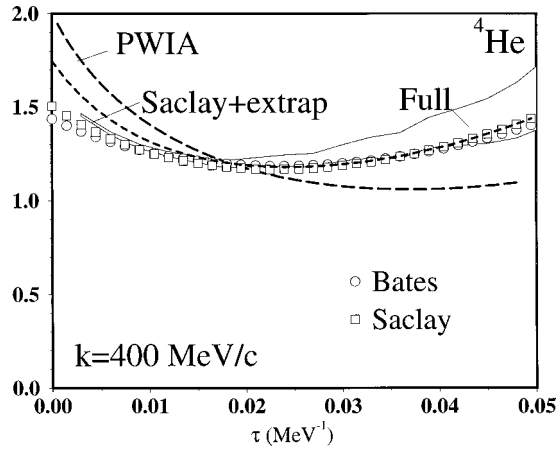


FIG. 71. Scaled Euclidean longitudinal response as in Fig. 69, but for ${}^4\text{He}$. Experimental data are from Bates (Dytman, 1988; von Reden, 1990) and Saclay (Zghiche *et al.*, 1993 and erratum 1995). The long-dashed line includes an estimate of the response beyond the high-energy limit of the experiment. Plane-wave impulse approximation and full calculations are from Carlson and Schiavilla, 1994b.

tum of the photon is comparable to that of typical pions in the nucleus. At even larger τ (lower energies), this effect saturates because only a finite number of nucleons are exchanging charge and the total charge must be conserved. In this regime, the attractive nature of the average nuclear interaction increases the response.

Of course, this charge-exchange mechanism should also exist in the single-nucleon transverse coupling, since it is largely isovector. The scaled transverse data for $A=3$ are plotted in Fig. 70. In fact, this does occur, as the response that would be obtained from single-nucleon couplings alone is substantially quenched due to charge exchange. However, when the full current is included, the exchange currents add to the final response and yield a result rather different from that obtained for single-nucleon (impulse) currents. As is apparent in the figures, the agreement with experiment is fairly satisfactory. The energy dependence is reproduced quite well, and the normalization is within 10%.

The situation is even more dramatic in the α particle, as the difference between PWIA and “complete” calculations is much larger. This is not entirely surprising, since the α particle has twice as many pairs as the trinucleons, and the density is somewhat larger. Hence the effect of charge exchange in the longitudinal response is even larger. The scaled Euclidean response \bar{E} is presented in Fig. 71. The figure shows both the truncated response, which assumes that there is *no* response above the experimental ω_{max} , and the extrapolated response obtained from sum-rule considerations.

The experimental values of the response are available only up to a finite energy ω_{max} . It is possible to estimate the response at higher energies through sum-rule techniques (Carlson and Schiavilla, 1994b). This extrapolation introduces an uncertainty in the measured response at small τ , which is indicated by the difference between the dashed line and the points labeled “Saclay” in the

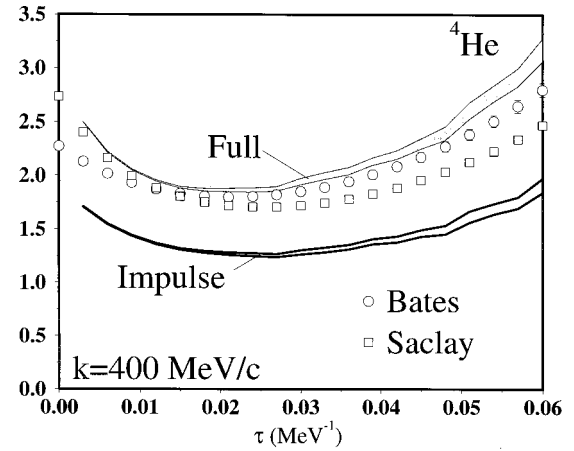


FIG. 72. Transverse Euclidean responses as in Fig. 71, but for ${}^4\text{He}$. Experimental data are from Bates (Dytman, 1988) and Saclay (Zghiche *et al.* 1993 and erratum 1995). Impulse (one-body current) and full calculations are taken from Carlson and Schiavilla, 1994b.

figure. The response above ω_{max} is exponentially suppressed at larger τ , and by $\tau \approx 0.015$ MeV this difference is negligible.

Again, the charge-exchange mechanism produces a quenching of the response in the longitudinal channel. At large τ (low ω), though, the overall attractive nature of the nuclear interaction increases the response. The PWIA or spectral-function approximations do not really contain information on the low-lying states of the A -body system, so such calculations cannot be expected to work well in this regime. As is apparent in the figure, both the normalization and the energy dependence of the PWIA calculation are quite poor.

In the transverse channel, two-body currents provide a very important enhancement to the response. Again, the calculated responses are in good agreement with experimental results (see Fig. 72). We should stress that this agreement is not obtained if realistic ground-state correlations, final-state interactions, and two-body currents are not all considered.

To further the understanding of the dynamic mechanisms in the nuclear quasielastic response, one can also consider the response of the nucleus to idealized single-nucleon couplings. The nucleon, proton, isovector, spin-longitudinal, and spin-transverse couplings are defined, respectively, as

$$\rho_N(\mathbf{q}) = \sum_i e^{i\mathbf{q}\cdot\mathbf{r}_i}, \quad (11.24)$$

$$\rho_p(\mathbf{q}) = \sum_i e^{i\mathbf{q}\cdot\mathbf{r}_i} \frac{1 + \tau_{z,i}}{2}, \quad (11.25)$$

$$\rho_\tau(\mathbf{q}) = \sum_i e^{i\mathbf{q}\cdot\mathbf{r}_i} \tau_{+,i}, \quad (11.26)$$

$$\rho_{\sigma\tau L}(\mathbf{q}) = \sum_i e^{i\mathbf{q}\cdot\mathbf{r}_i} (\boldsymbol{\sigma}_i \cdot \hat{\mathbf{q}}) \tau_{+,i}, \quad (11.27)$$

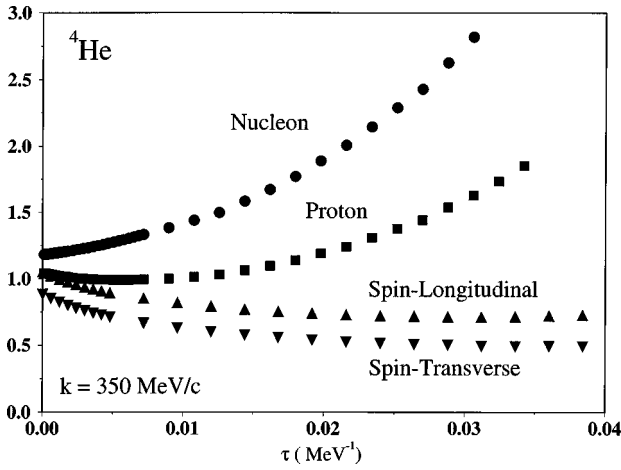


FIG. 73. Scaled Euclidean response for a variety of idealized single-nucleon couplings in the α -particle.

$$\rho_{\sigma\tau T}(\mathbf{q}) = \sum_i e^{i\mathbf{q}\cdot\mathbf{r}_i} (\boldsymbol{\sigma}_i \times \hat{\mathbf{q}}) \tau_{+,i}. \quad (11.28)$$

For each coupling ρ_α one obtains an associated response, which we normalize such that $\bar{E}_\alpha(q \rightarrow \infty, \tau = 0) = 1$. These responses are shown in the α particle in Fig. 73, except for \bar{E}_τ , which is a simple weighted average of the spin-longitudinal and spin-transverse isovector responses. In the large- τ limit, the only contribution to $\bar{E}_{N,p}$ is from elastic-scattering, and hence here $\bar{E}_N = \bar{E}_p/2$, given the normalization above. There is no elastic-scattering contribution to the isovector responses in the α particle, and hence they are much smaller at large τ . The rapid increase of $\bar{E}_{N,p}$ at large τ and decrease of $(\bar{E}_{\sigma\tau L}, \bar{E}_{\sigma\tau T})$ at small τ indicate that there is substantial response at $\omega < \omega_{qe}$ and $\omega > \omega_{qe}$, respectively.

The charge-exchange effect described above occurs in all isovector responses. Indeed, this effect has been observed in comparisons of quasielastic spectra obtained in (p, p') and (p, n) reactions (Fig. 74; Chrien *et al.* 1980; Taddeucci, 1991; Carlson and Schiavilla, 1994b). More recent experiments have measured the spin-longitudinal and spin-transverse responses in heavier nuclei (Taddeucci *et al.*, 1994). These experiments find a transverse response much larger than that obtained in traditional RPA calculations.

In contrast to a simple interpretation of the experimental results, microscopic calculations find an excess strength in the spin-longitudinal response, both in sum-rule calculations in ^{16}O and in the Euclidean response in the alpha particle (Pandharipande *et al.*, 1994). However, this enhancement is significantly smaller than those obtained in RPA calculations. A variety of physics issues, including couplings to more than single nucleons and multiple-scattering effects, need to be better understood before this situation is satisfactorily resolved. Experiments on several light nuclei could prove extremely valuable in this regard, as they have in electron scattering.

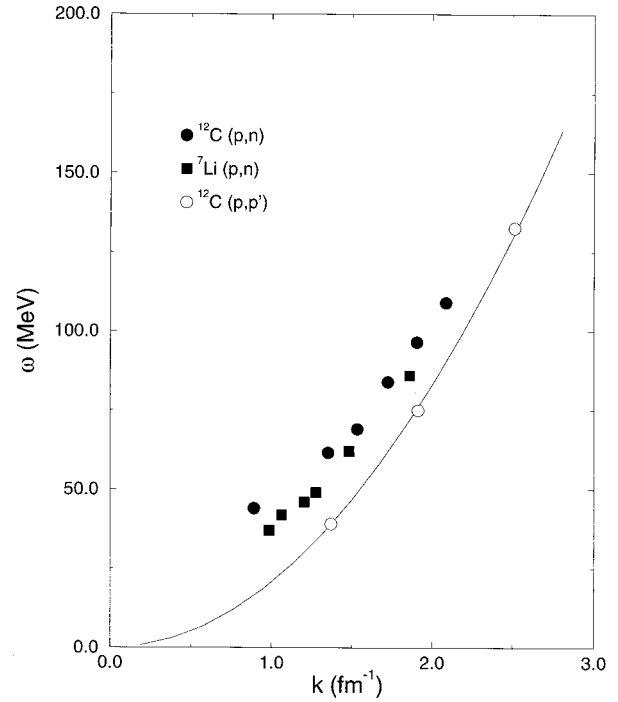


FIG. 74. Peak position measured for quasielastic scattering with different experiments. The solid line is the free-particle peak position.

Before leaving the subject of nuclear response, we should also consider recent measurements of inclusive scattering of polarized electrons from polarized ^3He (Woodward *et al.*, 1990; Thompson *et al.*, 1992; Gao *et al.*, 1994; Hansen *et al.*, 1995; Milner *et al.*, 1996). By polarizing the electrons and the target nucleus, one can obtain additional response functions (Donnelly and Raskin, 1986). For a spin- $\frac{1}{2}$ nucleus, the additional response functions are R'_{LT} and R'_T , and the related spin-dependent asymmetry is

$$A = - \frac{\cos\theta^* v'_T R'_T + 2\sin\theta^* \cos\phi^* v_{TL} R'_{TL}}{v_L R_L + v_T R_T}, \quad (11.29)$$

where the v_K are again kinematic factors and ϕ^* and θ^* are the polar and azimuthal angles of the target spin with respect to the three-momentum transfer \mathbf{q} .

The initial motivation for these experiments was to try to extract the neutron electric and magnetic form factors by exploiting the fact that in ^3He the neutron is largely polarized parallel to the spin of the nucleus (the two protons coupling to spin-0). This idea was first investigated by Blankleider and Woloshyn (1984) in a closure approximation, and then by Friar *et al.* (1990b). Later, impulse-approximation calculations were performed by Ciofi degli Atti, Pace, and Salmè (1992) and Schulze and Sauer (1993). These calculations use realistic spin-dependent spectral functions to calculate the asymmetry, but do not include the effects of final-state interactions or two-body currents. Gao *et al.* (1994) extracted a value of the neutron magnetic form factor at $Q^2 = 0.19 \text{ GeV}/c^2$ that is consistent with the dipole parametrization. Given the substantial effects of exchange currents

and final-state interactions, however, significant uncertainty remains in the extraction. More complete calculations, as well as a wider range of measurements, are likely to provide as much information about nuclear dynamics as about the nucleon form factors.

A variety of important physics issues remain in inclusive electron-scattering experiments. They include microscopic calculations of the response in heavier nuclei, more accurate descriptions of the pion and delta electroproduction region, effects of final-state interactions and two-body currents on polarization observables, and responses to other probes, including the weak-interaction couplings probed in parity-violating electron scattering. Inclusive scattering remains an important tool for studying nuclear dynamics and a rich field for both theory and experiment.

XII. OUTLOOK

The last few years have seen the maturing of our techniques for predicting and calculating the properties of light nuclei using nonrelativistic quantum mechanics and have witnessed extensive development of relativistic methods for the treatment of few-body systems.

Nuclear many-body theory based on nonrelativistic Hamiltonians with two- and three-nucleon interactions and one- and two-body electroweak current operators constructed consistently with these interactions, has been shown, so far, to provide a satisfactory, quantitative description of many of the nuclear properties that can be reliably calculated. The success achieved within this framework suggests that: (i) nucleons are the dominant degrees of freedom in nuclei; (ii) meson and (particularly) pion degrees of freedom can be eliminated in favor of effective two- and many-body operators involving only nucleonic coordinates; (iii) so far, no experimental evidence exists for in-medium modifications of the nucleon's structure, such as its electromagnetic form factors. Clearly, the validity of these conclusions is based on the ability, developed in the past few years, to solve nuclear bound- and scattering-state problems very accurately. In this respect, it is worth emphasizing that this progress could not have been realized without the parallel and tremendous progress in computational resources.

Is there any clear breakdown of the above outlined view of nuclear dynamics? Its present failure to reproduce correctly (Schiavilla and Riska, 1991; Plessas, Christian, and Wagenbrunn, 1995; Van Orden, Devine, and Gross, 1995) the observed deuteron structure functions and tensor polarization at relatively low-momentum-transfer values suggests that this may be the case, although more accurate data, particularly on T_{20} , are needed in order to resolve the issue firmly. These data will be forthcoming in the next few years from experiments currently underway at NIKHEF and TJNAF. A second failure consists in the inability of present two- and three-nucleon interaction models to predict accurately the nucleon and deuteron vector analyzing powers, measured in elastic $\vec{N}d$ and $\vec{d}N$ scattering at ener-

gies below the three-body breakup threshold (Kievsky *et al.*, 1996). The A_y and iT_{11} observables appear to be very sensitive, at the few percent level, to the values of the ${}^4P_{1/2}$ phase shift and $\epsilon_{3/2-}$ mixing angle, which in turn are influenced by the 3P_J phase shifts in the NN interaction. Three-nucleon interaction terms only marginally modify present theoretical predictions. It is indeed an open question whether present NN interaction models, including only mild nonlocalities via momentum-dependent components, can provide a simultaneous, satisfactory description of the polarization observables mentioned above. Finally, another relevant discrepancy is that between the spin-longitudinal and spin-transverse response functions measured in quasi-elastic (\vec{p}, \vec{n}) reactions and existing theoretical predictions, particularly the substantial underestimate of strength by the latter in the transverse channel (Taddeucci *et al.*, 1994). Again, forthcoming data on few-body nuclei from IUCF will be very helpful in clarifying the situation. In this respect, Faddeev and, possibly, hyperspherical-harmonics-based calculations of the cross section and polarization-transfer coefficients measured in the $d(\vec{p}, \vec{n})pp$ reaction should allow us to assess the validity of the factorized impulse-approximation assumption made in the analysis of the data and the impact on the latter of effects presently ignored—specifically, multistep contributions to the inclusive spectrum, spin-dependent distortions, and medium modification of the NN amplitudes.

With regard to future prospects, it now appears possible to carry out exact GFMC calculations of the low-lying spectra of H, He, Li, Be, and B isotopes with mass numbers ≤ 10 (Pieper and Wiringa, 1996) and of the associated elastic and inelastic electroweak transitions. These studies should allow us to test and refine the present models of three-nucleon interactions and electroweak current operators. To date, results on the $A=6$ spectra indicate that the binding energies of low-lying states of p-shell nuclei are underestimated by theory (Pieper *et al.*, 1996). Although three-nucleon interactions are much weaker than two-nucleon ones, they nevertheless contribute $\approx 15\%$ of nuclear binding, due to the large cancellation between kinetic and two-body potential energies. Current models for them include a long-range part arising from two-pion exchange via excitation of intermediate Δ resonances; however, the spin-isospin structure of their short-range components is not known. It is an open question whether, in a nonrelativistic framework, it is possible to reproduce correctly the spectra of nuclei via a two-nucleon interaction, fitted to NN data, and a three-nucleon interaction, constrained by fitting the bound-state energies of the few nucleons.

The GFMC method will also allow the study of neutron drops with ≈ 10 neutrons (Pudliner *et al.*, 1996). These studies will put useful constraints on the spin-orbit and pairing interactions in nuclei, as well as on the energy-density functionals commonly employed to model neutron star crusts and nuclei far from stability.

Of course, continuing progress in the hyperspherical harmonics (Kievsky *et al.*, 1996) and Faddeev-Yakubovsky (Glöckle, 1996) approaches will lead to very precise determinations of the binding energy of the α particle (at the fraction-of-keV level) and low-energy scattering parameters in the 3+1 and 2+2 elastic channels. These calculations will be useful, for example, in setting bounds on the contribution of four-nucleon interactions to nuclear binding.

Nuclear astrophysics is another area in which substantial progress can be expected in the next few years. Low-energy electroweak capture reactions involving light nuclei have great astrophysical importance in relation to the mechanism for energy and neutrino production in main-sequence stars—in particular, the determination of the solar neutrino flux—and in relation to the abundances of primordial elements in the universe. Examples of these are ${}^2\text{H}(d, \gamma){}^4\text{He}$, ${}^3\text{He}(p, e^+ \nu_e){}^4\text{He}$, ${}^4\text{He}({}^3\text{He}, \gamma){}^7\text{Be}$, and ${}^7\text{Be}(p, \gamma){}^8\text{B}$. The rates for some of these reactions cannot be measured in terrestrial laboratories in the energy range typical of the stellar interior, and it is therefore crucial to have accurate theoretical predictions for them, given their relevance for studies of stellar structure and evolution. The hyperspherical harmonics and Faddeev-Yakubovsky methods for $A=4$, and quantum Monte Carlo techniques, in the VMC and possibly GFMC versions, appear suitable for attacking these problems. The calculations of experimentally accessible reactions should provide stringent tests for models of two- and many-body electroweak current operators. In particular, they will allow the study of a variety of related issues: the role of Δ degrees of freedom in nuclei; the contribution of three-body currents associated with the three-nucleon interaction; the effect of nonlocalities in the two-body currents due to relativistic corrections; the influence of charge-independence-breaking terms in the NN interaction; and, in a more speculative vein, the problem of electron screening in very-low-energy nuclear reactions, and its impact on the extrapolation of the astrophysical factor from the corresponding low-energy data.

The prospects for an *ab initio* microscopic description of lepton and hadron scattering from light nuclei in the quasielastic regime are also quite promising. The full response of the trinucleons to polarized and unpolarized probes will be mapped out in Faddeev (Glöckle, 1996) and hyperspherical harmonics (Kievsky *et al.*, 1996) calculations. These techniques may not be easily extended to heavier systems, however, because of the large number of channels that need to be included for converged solutions of the scattering state at the relatively high energies of interest in quasielastic processes.

On the other hand, the integral transform method, both in its Laplace and its Lorenz kernel versions (Carlson and Schiavilla, 1994b; Martinelli *et al.*, 1995), should be very useful, at least in dealing with inclusive scattering from $A \geq 4$. These techniques are in principle also applicable to exclusive channels (Efros, 1993), but whether they will provide accurate predictions for the cross section of reactions like $A(e, e'p)$ or $A(e, e'd)$ is

unclear at this point, simply because practical calculations have not yet been attempted.

This aspect of few-nucleon physics is of great importance, particularly in view of the experimental effort currently underway or already in progress at facilities such as TJNAF, Mainz, and Bates. For example, a substantial part of the experimental program is directed toward parity-violating scattering of spin-polarized electrons. The goal is to study the distribution and polarization of virtual strange quarks in nuclei. The proper interpretation of these experiments requires a detailed understanding of many-body effects (Musolf, Donnelly, *et al.*, 1994; Musolf, Schiavilla, and Donnelly, 1994), including those, for example, due to pair currents, strange-hadron admixtures in the nuclear wave function, or dispersive effects associated with $Z_0-\gamma$ exchanges.

Finally, the next few years should also see substantial advances in the relativistic treatment of few-nucleon dynamics—a topic we have not discussed in the present review. Broadly speaking, it is possible to identify three lines of attack: (1) quasipotential reductions of the Bethe-Salpeter equation, such as the Blankenbecler-Sugar (Blankenbecler and Sugar, 1966) or Gross (1969, 1974, 1982) equations; (2) the light-front Hamiltonian dynamics (Keister and Polyzou, 1991); and (3) the Bakamjian-Thomas-Foldy (Bakamjian and Thomas, 1953; Foldy, 1961; Krajcik and Foldy, 1974; Friar, 1975) approach to the many-body theory of particles interacting via potentials.

Covariant two-body quasipotential equations have been solved with realistic one-boson-exchange interactions and have been found to give a reasonable overall description of low-energy NN data (Gross, Van Orden, and Holinde, 1992) and deuteron elastic (Hummel and Tjon, 1989; Van Orden, Devine, and Gross, 1995) and inelastic (Hummel and Tjon, 1990) electromagnetic observables. Initial calculations of the ${}^3\text{H}$ binding energy have also been carried out with the Gross equation and a realistic two-nucleon interaction, including some off-shell couplings for the exchanged (scalar and pseudoscalar) bosons (Stadler and Gross, 1997). Within this context, Stadler and Gross have shown that these off-shell couplings play an important role in improving the description of the two-body data and in predicting the ${}^3\text{H}$ binding energy. They have also argued that these couplings, in a nonrelativistic theory, lead to strong energy dependence of the two-body interaction as well as to many-body effective interactions. However, a more thorough examination of these issues is necessary to assess their full impact. These studies will, no doubt, be forthcoming in the next few years.

The other approach to the relativistic dynamics of few-nucleon systems is that pioneered by Bakamjian and Thomas (1953) and further developed by Foldy and others (Foldy, 1961; Krajcik and Foldy, 1974; Friar, 1975). This approach, discussed in Sec. II, appears to be particularly convenient from the computational standpoint (Carlson, Pandharipande, and Schiavilla, 1993). Variational Monte Carlo methods have been developed to treat the nonlocalities in the kinetic energy and v_{ij} (For-

est, Pandharipande, and Arriaga, 1997), and calculations have been carried out for the $A=3$ and 4 nuclei. When compared to results obtained with a nonrelativistic Hamiltonian containing a phase-equivalent two-body interaction, the total relativistic effects produce a repulsive contribution of a few hundred keV in ^3H and about 2 MeV in ^4He , most of which is due to boost corrections (Forest, Pandharipande, and Arriaga, 1997).

In Bethe-Salpeter-equation-based approaches, the nucleons are described by Dirac spinors, interacting via the exchange of observed or “effective” mesons. The lower components of the spinors, associated with antinucleon degrees of freedom, play an important role in these theories. On the other hand, in the Bakamijan-Thomas-Foldy method antinucleon degrees of freedom, and indeed the composite nature of the nucleons, are subsumed into effective phenomenological interactions v_{ij} (and V_{ijk}), constrained by data. Thus the latter approach should be useful if the compositeness of the nucleon is crucial in suppressing antinucleon degrees of freedom.

Quantum Monte Carlo methods (both VMC and GFMC) are currently being extended to calculate accurately, using the relativistic Hamiltonian, properties that depend upon the ground and scattering states of systems with $A \leq 6$. Electromagnetic properties are of particular interest, since future experiments at TJNAF and other facilities will involve large momentum transfers, in which relativistic effects may be important. Clearly, this will require the consistent treatment of the electromagnetic current operator and the “boost” effects (such as the Lorentz contraction and Wigner spin rotation) on the wave function. The next few years should see substantial progress made along these lines.

Although quark models of mesons and baryons (not discussed here) have been developed which give an excellent account of the observed spectrum, their implications have not been fully incorporated in current models of the nuclear force. In this respect, the ability to calculate six-fermion ground states with relativistic Hamiltonians may allow us to calculate the properties of the deuteron and the NN scattering states directly from the interactions of six constituent quarks. However, any progress in this direction will depend on our ability to define a realistic six-quark Hamiltonian.

In summary, substantial progress has been made in our understanding of few-nucleon physics, progress which is due to rapid development in both experimental and theoretical techniques. The developments that we have highlighted cover a broad range, from nuclear structure studies, to low-energy reactions, to hadronic and electroweak reaction studies at intermediate energies. We look forward to continued development and growth in the field of few-nucleon physics.

ACKNOWLEDGMENTS

We wish to thank our close collaborators, J. L. Friar, V. R. Pandharipande, S. C. Pieper, D. O. Riska, M. Viviani, and R. B. Wiringa for their input and many contri-

butions to the subject matter. We also thank H. Arenhövel, A. Arriaga, O. Benhar, A. Fabrocini, J. L. Forest, F. Gross, A. Kievsky, W. Plessas, B. S. Pudliner, S. Rosati, P. U. Sauer, I. Sick, and J. W. Van Orden for providing us with many of their results, and W. Glöckle for a critical reading of the manuscript. The support of the U.S. Department of Energy is gratefully acknowledged. Many of the calculations reported in the present article were made possible by grants of computer time from the National Energy Research Supercomputer Center, Cornell Theory Center, and Mathematics and Computer Science Division of Argonne National Laboratory.

REFERENCES

- Aaron, R., and R. D. Amado, 1996, *Phys. Rev.* **150**, 857.
 Ahrens, J., 1985, *Nucl. Phys. A* **446**, 229c.
 Akaishi, Y., 1984, *Nucl. Phys. A* **416**, 409c.
 Albrecht, W., *et al.*, 1968, *Phys. Lett.* **26B**, 642.
 Alfimenzov, V. P., S. B. Borzakov, G. G. Bunatyon, Ya. Vezhbitski, L. B. Pikelner, and E. I. Sharapov, 1980, *Sov. J. Nucl. Phys.* **31**, 21.
 Allet, M., *et al.*, 1994, *Phys. Rev. C* **50**, 602.
 Alt, E. O., P. Grassberger, and W. Sandhas, 1967, *Nucl. Phys. B* **2**, 167.
 Alteholz, T., *et al.*, 1994, *Phys. Rev. Lett.* **73**, 1336.
 Amaldi, E., S. Fubini, and G. Furlan, 1979, *Electroproduction at Low Energy and Hadron Form Factors*, Springer Tracts in Modern Physics No. 83, 1.
 Amroun, A., *et al.*, 1994, *Nucl. Phys. A* **579**, 596.
 Anderson, J. B., 1975, *J. Chem. Phys.* **63**, 1499.
 Arkatov, Y. M., P. I. Vatsset, V. I. Voloshchuck, V. A. Zoltenko, and I. M. Prokhorets, 1980, *Sov. J. Nucl. Phys.* **31**, 726.
 Arnold, R. G., *et al.*, 1975, *Phys. Rev. Lett.* **35**, 776.
 Arnold, R. G., *et al.*, 1978, *Phys. Rev. Lett.* **40**, 1429.
 Arnold, R. G., *et al.*, 1987, *Phys. Rev. Lett.* **58**, 1723.
 Arnold, R. G., *et al.*, 1990, *Phys. Rev. C* **42**, 1.
 Arndt, R. A., L. D. Roper, R. L. Workman, and M. W. McNaughton, 1992, *Phys. Rev. D* **45**, 3995.
 Arndt, R. A., I. I. Strakovsky, and R. L. Workman, 1995, *Phys. Rev. C* **52**, 2246.
 Arndt, R. A., R. L. Workman, and M. M. Pavan, 1994, *Phys. Rev. C* **49**, 2729.
 Arriaga, A., A. M. Eiró, and F. D. Santos, 1986, in *Weak and Electromagnetic Interactions in Nuclei*, edited by H. V. Klapdor (Springer, Heidelberg), p. 61.
 Arriaga, A., A. M. Eiró, F. D. Santos, and J. E. Ribeiro, 1988, *Phys. Rev. C* **37**, 2312.
 Arriaga, A., V. R. Pandharipande, and R. Schiavilla, 1991, *Phys. Rev. C* **43**, 983.
 Arriaga, A., V. R. Pandharipande, and R. B. Wiringa, 1995, *Phys. Rev. C* **52**, 2362.
 Assenbaum, H. J., and K. Langanke, 1987, *Phys. Rev. C* **36**, 17.
 Auffret, S., *et al.*, 1985a, *Phys. Rev. Lett.* **54**, 649.
 Auffret, S., *et al.*, 1985b, *Phys. Rev. Lett.* **55**, 1362.
 Austern, N., 1951, *Phys. Rev.* **83**, 672.
 Bahcall, J. N., 1966, *Nucl. Phys.* **75**, 10.
 Bahcall, J. N., N. A. Bahcall, and R. K. Ulrich, 1969, *Astrophys. J.* **156**, 559.
 Bahcall, J. N., and R. M. May, 1968, *Astrophys. J. Lett.* **152**, L17.
 Bahcall, J. N., and R. K. Ulrich, 1988, *Rev. Mod. Phys.* **60**, 297.

- Bailey, G. M., G. M. Griffiths, M. Lal, and T. W. Donnelly, 1967, *Nucl. Phys. A* **94**, 502.
- Bakamjian, B., and L. H. Thomas, 1953, *Phys. Rev.* **92**, 1300.
- Barnes, C. A., K. H. Chang, T. R. Donoghue, C. Rolfs, and J. Kammeraad, 1987, *Phys. Lett. B* **197**, 315.
- Barroso, A., and E. Hadjimichael, 1975, *Nucl. Phys. A* **238**, 422.
- Baym, G., and N. D. Mermin, 1961, *J. Math. Phys.* **2**, 232.
- Beck, D. H., 1990, *Phys. Rev. Lett.* **64**, 268.
- Beck, D. H., *et al.*, 1987, *Phys. Rev. Lett.* **59**, 1537.
- Benayoun, J. J., and C. Gignoux, 1972a, *Nucl. Phys. A* **190**, 419.
- Benayoun, J. J., and C. Gignoux, 1972b, *Lett. Nuovo Cimento* **5**, 313.
- Benhar, O., A. Fabrocini, and S. Fantoni, 1989, *Nucl. Phys. A* **505**, 267.
- Benhar, O., A. Fabrocini, and S. Fantoni, 1991, in *Modern Topics in Electron Scattering*, edited by B. Frois and I. Sick (World Scientific, Singapore), p. 460.
- Benhar, O., and V. R. Pandharipande, 1993, *Phys. Rev. C* **47**, 2218.
- Berg, D., *et al.*, 1980, *Phys. Rev. Lett.* **44**, 706.
- Berg, H., W. Arnold, E. Huttel, H. H. Krause, W. Ulbricht, and G. Clausnitzer, 1980, *Nucl. Phys. A* **334**, 21.
- Bergervoet, J. R., P. C. van Campen, W. A. van der Sanden, and J. J. de Swart, 1988, *Phys. Rev. C* **38**, 15.
- Bergstrom, J. C., *Phys. Rev. C* **11**, 1514.
- Bergstrom, J. C., 1979, *Nucl. Phys. A* **327**, 458.
- Bergstrom, J. C., I. P. Auer, and R. S. Hicks, 1975, *Nucl. Phys. A* **251**, 401.
- Bergstrom, J. C., U. Deutschmann, and R. Neuhausen, 1979, *Nucl. Phys. A* **327**, 439.
- Bergstrom, J. C., S. B. Kowalski, and R. Neuhausen, 1982, *Phys. Rev. C* **25**, 1156.
- Bergstrom, J. C., and E. L. Tomusiak, 1976, *Nucl. Phys. A* **262**, 196.
- Bernabéu, J., 1982, *Nucl. Phys. A* **374**, 593c.
- Bernheim, M., *et al.*, 1981, *Phys. Rev. Lett.* **46**, 402.
- Bethe, H. A., and C. L. Critchfield, 1938, *Phys. Rev.* **54**, 248.
- Bishop, D. M., and L. M. Cheung, 1979, *Phys. Rev. A* **20**, 381.
- Bjorken, J. D., and S. D. Drell, 1964, *Relativistic Quantum Mechanics* (McGraw-Hill, New York).
- Blankenbecler, R., and R. Sugar, 1966, *Phys. Rev.* **142**, 1051.
- Blankleider, B., and R. M. Woloshyn, 1984, *Phys. Rev. C* **29**, 538.
- Blomqvist, J., 1970, *Phys. Lett.* **32B**, 1.
- Blunden, P. G., and D. O. Riska, 1992, *Nucl. Phys. A* **536**, 697.
- Bollinger, L. M., J. R. Specht, and G. E. Thomas, 1973, *Bull. Am. Phys. Soc.* **18**, 591.
- Bond, J. E., and F. W. K. Firk, 1977, *Nucl. Phys. A* **287**, 317.
- Boninsegni, M., and D. M. Ceperley, 1996, *J. Low Temp. Phys.* **104**, 339.
- Bopp, P., *et al.*, 1986, *Phys. Rev. Lett.* **56**, 919.
- Borkowski, F., G. G. Simon, V. H. Welther, and R. D. Wending, 1975a, *Z. Phys. A* **275**, 29.
- Borkowski, F., G. G. Simon, V. H. Walther, and R. D. Wending, 1975b, *Nucl. Phys. B* **93**, 461.
- Brandenburg, R. A., Y. E. Kim, and A. Tubis, 1974a, *Phys. Rev. Lett.* **28**, 1533.
- Brandenburg, R. A., Y. E. Kim, and A. Tubis, 1974b, *Phys. Rev. Lett.* **32**, 1325.
- Brandenburg, R. A., Y. E. Kim, and A. Tubis, 1975, *Phys. Rev. C* **12**, 1368.
- Brown, G. E., and W. Weise, 1975, *Phys. Rep.* **22**, 279.
- Bryan, R., and B. L. Scott, 1969, *Phys. Rev.* **177**, 1435.
- Buchmann, A., W. Leidemann, and H. Arenhövel, 1985, *Nucl. Phys. A* **443**, 726.
- Bugg, D. V., and R. A. Bryan, 1992, *Nucl. Phys. A* **540**, 449.
- Bugg, D. V., and R. Machleidt, 1995, *Phys. Rev. C* **52**, 1203.
- Carlson, C. E., 1986, *Phys. Rev. D* **34**, 2704.
- Carlson, J., 1987, *Phys. Rev. C* **36**, 2026.
- Carlson, J., 1988, *Phys. Rev. C* **38**, 1879.
- Carlson, J., 1990, *Nucl. Phys. A* **508**, 141c.
- Carlson, J., 1991, *Nucl. Phys. A* **522**, 185c.
- Carlson, J., 1995, unpublished.
- Carlson, J., V. R. Pandharipande, and R. Schiavilla, 1991, in *Modern Topics in Electron Scattering*, edited by B. Frois and I. Sick (World Scientific, Singapore), p. 177.
- Carlson, J., V. R. Pandharipande, and R. Schiavilla, 1993, *Phys. Rev. C* **47**, 484.
- Carlson, J., V. R. Pandharipande, and R. B. Wiringa, 1983, *Nucl. Phys. A* **401**, 59.
- Carlson, J., V. R. Pandharipande, and R. B. Wiringa, 1984, *Nucl. Phys. A* **424**, 47.
- Carlson, J., D. O. Riska, R. Schiavilla, and R. B. Wiringa, 1990, *Phys. Rev. C* **42**, 830.
- Carlson, J., D. O. Riska, R. Schiavilla, and R. B. Wiringa, 1991, *Phys. Rev. C* **44**, 619.
- Carlson, J., and R. Schiavilla, 1992, *Phys. Rev. Lett.* **68**, 3682.
- Carlson, J., and R. Schiavilla, 1994a, *Few-Body Syst., Suppl.* **7**, 349.
- Carlson, J., and R. Schiavilla, 1994b, *Phys. Rev. C* **49**, R2880.
- Carlson, J., and R. Schiavilla, 1997, unpublished.
- Cavedon, J. M., *et al.*, 1982, *Phys. Rev. Lett.* **49**, 978.
- Cecil, F. E., and D. E. Newman, 1984, *Nucl. Instrum. Methods Phys. Res. A* **221**, 449.
- Ceperley, D. M., and B. J. Alder, 1980, *Phys. Rev. Lett.* **45**, 566.
- Chemtob, M., E. J. Moniz, and M. Rho, 1974, *Phys. Rev. C* **10**, 334.
- Chemtob, M., and M. Rho, 1971, *Nucl. Phys. A* **163**, 1; **212**, 628(E).
- Chen, C. R., G. L. Payne, J. L. Friar, and B. F. Gibson, 1985, *Phys. Rev. C* **31**, 2266.
- Chew, G. F., 1950, *Phys. Rev.* **80**, 196.
- Chrien, R. E., *et al.*, 1980, *Phys. Rev. C* **21**, 1014.
- Christy, R. F., and I. Duck, 1961, *Nucl. Phys.* **24**, 89.
- Chung, P. L., *et al.*, 1988, *Phys. Rev. C* **37**, 2000.
- Chwieroth, F. S., Y. C. Tang, and D. R. Thompson, 1972, *Nucl. Phys. A* **189**, 1.
- Ciechanowicz, S., and E. Truhlik, 1984, *Nucl. Phys. A* **414**, 508.
- Ciofi degli Atti, C., 1992, *Nucl. Phys. A* **543**, 183c.
- Ciofi degli Atti, C., E. Pace, and G. Salmè, 1984, *Phys. Lett.* **141B**, 14.
- Ciofi degli Atti, C., E. Pace, and G. Salmè, 1991, *Phys. Rev. C* **43**, 1155.
- Ciofi degli Atti, C., E. Pace, and G. Salmè, 1992, *Phys. Rev. C* **46**, R1591.
- Ciofi degli Atti, C., S. Simula, L. L. Frankfurt, and M. I. Strikman, 1991, *Phys. Rev. C* **44**, 7.
- Clayton, D. D., 1983, *Principles of Stellar Evolution and Nucleosynthesis* (University of Chicago, Chicago, IL).
- Clegg, T. B., and W. Haeblerli, 1967, *Nucl. Phys. A* **95**, 608.
- Clement, J. M., P. Stoler, C. A. Goulding, and R. W. Fairchild, 1972, *Nucl. Phys. A* **183**, 51.
- Coester, F., 1965, *Helv. Phys. Acta* **38**, 7.

- Coester, F., and D. O. Riska, 1994, *Ann. Phys. (N.Y.)* **234**, 141.
- Collard, H., *et al.*, 1965, *Phys. Rev.* **138**, 357.
- Coon, S. A., and J. L. Friar, 1986, *Phys. Rev. C* **34**, 1060.
- Coon, S. A., and M. T. Peña, 1993, *Phys. Rev. C* **48**, 2559.
- Coon, S. A., M. D. Scadron, P. C. McNamee, B. R. Barrett, D. W. E. Blatt, and B. H. J. McKellar, 1979, *Nucl. Phys. A* **317**, 242.
- Cornelius, Th., 1990, Ph. D. thesis (University of Bochum).
- Cottingham, W. N., *et al.*, 1973, *Phys. Rev. D* **8**, 800.
- Cox, A. E., S. A. R. Wynchank, and C. H. Collie, 1965, *Nucl. Phys.* **74**, 497.
- Cramer, R., *et al.*, 1985, *Z. Phys. C* **29**, 513.
- Czyz, W., and K. Gottfried, 1963, *Ann. Phys. (N.Y.)* **21**, 47.
- Dautry, F., M. Rho, and D. O. Riska, 1976, *Nucl. Phys. A* **264**, 507.
- Davis, J. C., and H. H. Barschall, 1971, *Phys. Rev. C* **3**, 1798.
- Davis, R., Jr., 1994, *Prog. Part. Nucl. Phys.* **32**, 13.
- deForest, T., and J. D. Walecka, 1966, *Adv. Phys.* **15**, 1.
- deJuren, J., 1950, *Phys. Rev.* **80**, 27.
- deJuren, J., and N. Knable, *Phys. Rev.* **77**, 606.
- Dmitriev, V. F., *et al.*, 1985, *Phys. Lett.* **157B**, 143.
- Dobiasch, H., *et al.*, 1978, *Phys. Lett.* **76B**, 195.
- Donnelly, T. W., and A. S. Raskin, 1986, *Ann. Phys. (N.Y.)* **169**, 247.
- Donnelly, T. W., and I. Sick, 1984, *Rev. Mod. Phys.* **56**, 461.
- Donnelly, T. W., and J. D. Walecka, 1973, *Phys. Lett.* **44B**, 330.
- Dow, K., *et al.*, 1988, *Phys. Rev. Lett.* **61**, 1706.
- Drell, S. D., and C. L. Schwartz, 1958, *Phys. Rev.* **122**, 568.
- Dubach, J., 1980, *Nucl. Phys. A* **340**, 271.
- Dubach, J., J. H. Koch, and T. W. Donnelly, 1976, *Nucl. Phys. A* **271**, 279.
- Dunn, P. C., *et al.*, 1983, *Phys. Rev. C* **27**, 71.
- Dymarz, R., and F. C. Khanna, 1990a, *Nucl. Phys. A* **507**, 560.
- Dymarz, R., and F. C. Khanna, 1990b, *Phys. Rev. C* **41**, 828.
- Dymarz, R., C. J. Morningstar, R. Gourishankar, and F. C. Khanna, 1990, *Nucl. Phys. A* **507**, 531.
- Dytman, S., *et al.*, 1988, *Phys. Rev. C* **38**, 800.
- Efros, V. D., 1993, *Yad. Fiz.* **56**, 22.
- Efros, V. D., W. Leideman, and G. Orlandini, 1997, *Phys. Rev. Lett.* **78**, 4015.
- Eigenbrod, F., 1969, *Z. Phys.* **228**, 337.
- Eiró, A. M., and F. D. Santos, 1990, *J. Phys. G* **16**, 1139.
- Ericson, T. E. O., and M. Rosa-Clot, 1983, *Nucl. Phys. A* **405**, 497.
- Ericson, T. E. O., and W. Weise, 1988, *Pions and Nuclei* (Clarendon, Oxford).
- Ericson, T. E. O., *et al.*, 1995, *Phys. Rev. Lett.* **75**, 1046.
- Fabian, W., and H. Arenhövel, 1976, *Nucl. Phys. A* **258**, 461.
- Fabian, W., and H. Arenhövel, 1978, *Nucl. Phys. A* **314**, 253.
- Fabian, W., and H. Arenhövel, 1979, *Nucl. Phys. A* **314**, 253.
- Fabrocini, A., and S. Fantoni, 1989, *Nucl. Phys. A* **503**, 375.
- Faddeev, L. D., 1960, *Zh. Éksp. Teor. Fiz.* **39**, 1459 [*Sov. Phys. JETP* **12**, 1041 (1961)].
- Fantoni, S., and V. R. Pandharipande, 1984, *Nucl. Phys. A* **427**, 473.
- Fetisov, V. N., A. N. Gorbunov, and A. T. Varfolomeev, 1965, *Nucl. Phys.* **71**, 305.
- Finckh, E., 1990, unpublished.
- Flowers, B. H., and F. Mandl, 1950, *Proc. R. Soc. London, Ser. A* **206**, 131.
- Foldy, L. L., 1961, *Phys. Rev.* **122**, 275.
- Foldy, L. L., and W. Tobocman, 1957, *Phys. Rev.* **105**, 1099.
- Forest, J. L., V. R. Pandharipande, and A. Arriaga, 1997, private communication.
- Forest, J. L., V. R. Pandharipande, and J. Carlson, and R. Schiavilla, 1995, *Phys. Rev. C* **52**, 576.
- Forest, J. L., V. R. Pandharipande, and J. L. Friar, 1995, *Phys. Rev. C* **52**, 568.
- Forest, J. L., *et al.*, 1996, *Phys. Rev. C* **54**, 646.
- Fowler, W. A., 1984, *Rev. Mod. Phys.* **56**, 169.
- Fox, R., C. Leith, L. Wouters, K. R. MacKenzie, 1950, *Phys. Rev.* **50**, 23.
- Friar, J. L., 1973, *Ann. Phys. (N.Y.)* **81**, 332.
- Friar, J. L., 1975, *Phys. Rev. C* **12**, 695.
- Friar, J. L., 1977, *Ann. Phys. (N.Y.)* **104**, 380.
- Friar, J. L., and S. A. Coon, 1994, *Phys. Rev. C* **49**, 1272.
- Friar, J. L., B. F. Gibson, H. C. Jean, and G. L. Payne, 1991, *Phys. Rev. Lett.* **66**, 1827.
- Friar, J. L., B. F. Gibson, D. R. Lehman, and G. L. Payne, 1988, *Phys. Rev. C* **37**, 2859.
- Friar, J. L., B. F. Gibson, and G. L. Payne, 1983, *Phys. Rev. C* **28**, 983.
- Friar, J. L., B. F. Gibson, and G. L. Payne, 1987, *Phys. Rev. C* **35**, 1502.
- Friar, J. L., B. F. Gibson, and G. L. Payne, 1990, *Phys. Lett. B* **251**, 11.
- Friar, J. L., and G. L. Payne, 1996, in *Coulomb Interactions in Nuclear and Atomic Few-Body Collisions*, edited by F. S. Levin and D. A. Micha (Plenum, New York), p. 97.
- Friar, J. L., G. L. Payne, V. G. J. Stoks, and J. J. de Swart, 1993, *Phys. Lett. B* **311**, 4.
- Friar, J. L., *et al.*, 1990a, *Phys. Rev. C* **42**, 1838.
- Friar, J. L., *et al.*, 1990b, *Phys. Rev. C* **42**, 2310.
- Friar, J. L., *et al.*, 1995, *Phys. Rev. C* **51**, 2356.
- Frosch, R. F., *et al.*, 1968, *Phys. Rev.* **160**, 874.
- Frullani, S., and J. Mougey, 1984, *Adv. Nucl. Phys.* **14**, 1.
- Fujita, J., and H. Miyazawa, 1957, *Prog. Theor. Phys.* **17**, 360.
- Gabioud, *et al.*, 1979, *Phys. Rev. Lett.* **42**, 1508.
- Galster, S., H. Klein, J. Moritz, K. H. Schmidt, and D. Wegener, 1971, *Nucl. Phys. B* **32**, 221.
- Gao, H., *et al.*, 1994, *Phys. Rev. C* **50**, R546.
- Gari, M., and A. H. Huffman, 1972, *Astrophys. J.* **178**, 543.
- Gari, M., and H. Hyuga, 1976, *Nucl. Phys. A* **264**, 409.
- Gari, M., and W. Krümpelmann, 1986, *Phys. Lett. B* **173**, 10.
- Gari, M., and W. Krümpelmann, 1992, *Phys. Lett. B* **274**, 159.
- Gebhardt, K., W. Jäger, C. Jeitner, M. Vitz, E. Finckh, T. N. Frank, T. Januschke, W. Sandhas, and H. Habermann, 1993, *Nucl. Phys. A* **561**, 232.
- Gilman, R., *et al.*, 1990, *Phys. Rev. Lett.* **65**, 1733.
- Glöckle, W., 1970, *Nucl. Phys. A* **141**, 620.
- Glöckle, W., 1982, *Nucl. Phys. A* **381**, 343.
- Glöckle, W., 1983, *The Quantum-Mechanical Few-Body Problem* (Springer, Berlin-Heidelberg).
- Glöckle, W., 1996, private communication.
- Glöckle, W., and R. Brandenburg, 1983, *Phys. Rev. C* **27**, 83.
- Glöckle, W., and H. Kamada, 1993a, *Phys. Rev. Lett.* **71**, 1971.
- Glöckle, W., and H. Kamada, 1993b, *Nucl. Phys. A* **560**, 541.
- Glöckle, W., H. Kamada, H. Witala, D. Huber, J. Golak, K. Miyagawa, and S. Ishikawa, 1995, *Few-Body Syst., Suppl.* **8**, 9.
- Glöckle, W., T.-S. H. Lee, and F. Coester, 1986, *Phys. Rev. C* **33**, 709.
- Glöckle, W., and G. L. Payne, 1992, *Phys. Rev. C* **45**, 974.
- Glöckle, W., and H. Witala, 1990, *Nucl. Phys. A* **508**, 115c.
- Glöckle, W., H. Witala, D. Hüber, H. Kamada, and J. Golak, 1996, *Phys. Rep.* **274**, 107.

- Glöckle, W., H. Witala, H. Kamada, D. Huber, and J. Golak, 1995, in *Few Body Problems in Physics*, AIP Conf. Proc. No. **334**, edited by F. Gross (AIP, New York), p. 45.
- Golak, J., *et al.*, 1995, *Phys. Rev. C* **52**, 1216.
- Golberger, M. L., and K. M. Watson, 1964, in *Collision Theory*, edited by M. L. Goldberger (Wiley, New York), p. 270.
- Gouanere, M., M. Chemarin, G. Nicolai, and J.-P. Burq, 1970, *Nucl. Phys. A* **144**, 607.
- Gould, R. J., and N. Guessoum, 1990, *Astrophys. J. Lett.* **359**, L67.
- Green, A. M., 1976, *Rep. Prog. Phys.* **39**, 1109.
- Griffiths, G. M., M. Lal, and C. D. Scarfe, 1963, *Can. J. Phys.* **41**, 724.
- Gross, F., 1969, *Phys. Rev.* **186**, 1448.
- Gross, F., 1974, *Phys. Rev. D* **10**, 223.
- Gross, F., 1982, *Phys. Rev. C* **26**, 2203.
- Gross, F., and H. Henning, 1992, *Nucl. Phys. A* **537**, 344.
- Gross, F., J. W. Van Orden, and K. Holinde, 1992, *Phys. Rev. C* **45**, 2094.
- Grossman, R., 1993, Diplom thesis (University of Köln).
- Grüebler, W., V. König, P. A. Schmelzbach, F. Sperisen, B. Jenny, R. E. White, F. Seiler, and H. W. Roser, 1983, *Nucl. Phys. A* **398**, 445.
- Gubernatis, J. E., M. Jarrel, R. N. Silver, and D. S. Sivia, 1991, *Phys. Rev. B* **44**, 6011.
- Guichon, P. A. M., M. Giffon, and C. Samour, 1978, *Phys. Lett.* **74B**, 15.
- Hadjimichael, E., 1973, *Phys. Rev. Lett.* **31**, 183.
- Hadjimichael, E., B. Goulard, and R. Bornais, 1983, *Phys. Rev. C* **27**, 831.
- Hajduk, Ch., and P. U. Sauer, 1979, *Nucl. Phys. A* **322**, 329.
- Hajduk, Ch., P. U. Sauer, and W. Strueve, 1983, *Nucl. Phys. A* **405**, 581.
- Hale, G., 1990, private communication.
- Hamada, T., and I. D. Johnston, 1962, *Nucl. Phys.* **34**, 382.
- Hansen, *et al.*, 1995, *Phys. Rev. Lett.* **74**, 654.
- Harper, E. P., Y. E. Kim, and A. Tubis, 1972, *Phys. Rev. Lett.* **28**, 1533.
- Hatanaka, K., *et al.*, 1984, *Nucl. Phys. A* **426**, 77.
- Henneck, R., 1993, *Phys. Rev. C* **47**, 1859.
- Hirata, K. S., *et al.*, 1989, *Phys. Rev. Lett.* **63**, 16.
- Hockert, J., D. O. Riska, M. Gari, and A. Huffman, 1973, *Nucl. Phys. A* **217**, 14.
- Hofmann, H. M., W. Zahn, and H. Stöwe, 1981, *Nucl. Phys. A* **357**, 139.
- Höhler, G., E. Pietarinen, I. Sabba-Stafanesco, F. Borowkowski, G. G. Simon, V. H. Walther, and R. D. Wendling, 1976, *Nucl. Phys. B* **114**, 505.
- Howell, C. R., *et al.*, 1987, *Few-Body Syst.* **2**, 19.
- Hüber, D., 1993, Ph. D. thesis (University of Bochum).
- Hüber, D., H. Witala, A. Nogga, W. Glöckle, and H. Kamada, 1997, *Acta Phys. Pol. B* **28**, 1677.
- Hüber, D., *et al.*, 1995, *Phys. Rev. C* **51**, 1100.
- Hummel, E., and J. A. Tjon, 1989, *Phys. Rev. Lett.* **63**, 1788.
- Hummel, E., and J. A. Tjon, 1990, *Phys. Rev. C* **42**, 423.
- Iachello, F., A. D. Jackson, and A. Lande, 1973, *Phys. Lett.* **43B**, 191.
- Igo, G., *et al.*, 1972, *Nucl. Phys. A* **195**, 33.
- Jacob, G., and Th. A. J. Maris, 1966, *Rev. Mod. Phys.* **38**, 121.
- Jacob, G., and Th. A. J. Maris, 1973, *Rev. Mod. Phys.* **45**, 6.
- Jäger, H.-U., M. Kirchbach, and E. Truhlik, 1984, *Sov. J. Nucl. Phys.* **39**, 243.
- Jenkins, D. A., P. T. Debevec, and P. D. Harty, 1994, *Phys. Rev. C* **50**, 74.
- Johnston, A. R., *et al.*, 1965, *Phys. Lett.* **19**, 289.
- Jourdan, J., 1995, *Phys. Lett. B* **353**, 189.
- Jourdan, J., 1996, *Nucl. Phys. A* **603**, 117.
- Jurney, E. T., P. J. Bendt, and J. C. Browne, 1982, *Phys. Rev. C* **25**, 2810.
- Juster, F. P., *et al.*, 1985, *Phys. Rev. Lett.* **55**, 2261.
- Kaiser, H., H. Rauch, W. Bauspiess, and U. Bonse, 1977, *Phys. Lett.* **71B**, 321.
- Kallio, A. J., P. Toropainen, A. M. Green, and T. Kouki, 1974, *Nucl. Phys. A* **231**, 77.
- Kalos, M. H., 1962, *Phys. Rev.* **128**, 1791.
- Kanada, H., T. Kaneko, and Y. C. Tang, 1986, *Phys. Rev. C* **34**, 22.
- Kaplan, L., G. R. Ringo, and K. E. Wilzbach, 1952, *Phys. Rev.* **87**, 785.
- Karp, B. C., E. J. Ludwig, W. J. Thompson, and F. D. Santos, 1984, *Phys. Rev. Lett.* **53**, 1619.
- Keister, B. D., and W. N. Polyzou, 1991, *Ann. Phys. (Leipzig)* **20**, 225.
- Kievsky, A., S. Rosati, and M. Viviani, 1993, *Nucl. Phys. A* **551**, 241.
- Kievsky, A., S. Rosati, W. Tornow, and M. Viviani, 1996, *Nucl. Phys. A* **607**, 402.
- Kievsky, A., S. Rosati, and M. Viviani, 1996, private communication.
- Kievsky, A., M. Viviani, and S. Rosati, 1994, *Nucl. Phys. A* **577**, 511.
- Kievsky, A., M. Viviani, and S. Rosati, 1995, *Phys. Rev. C* **52**, R15.
- King, N. S. P., *et al.*, 1977, *Phys. Lett.* **69B**, 151.
- Kirchbach, M., 1986, *Czech. J. Phys.* **36**, 372.
- Kirchbach, M., H.-U. Jäger, and M. Gmitro, 1984, *Z. Phys. A* **320**, 689.
- Kirchbach, M., S. Kamalov, and H.-U. Jäger, 1984, *Phys. Lett.* **144B**, 319.
- Kirk, P. N., *et al.*, 1973, *Phys. Rev. D* **8**, 63.
- Kitagaki, T., *et al.*, 1983, *Phys. Rev. D* **28**, 436.
- Kloet, W. M., and J. A. Tjon, 1974, *Phys. Lett.* **49B**, 419.
- Koester, L., and W. Nistler, 1975, *Z. Phys. A* **272**, 189.
- Kohn, W., 1948, *Phys. Rev.* **74**, 1763.
- Koike, Y., and Y. Taniguchi, 1986, *Few-Body Syst.* **1**, 13.
- Kolb, E. W., and M. S. Turner, 1990, *The Early Universe* (Addison-Wesley, Redwood City, CA).
- Konijnenberg, M. W., 1990, Ph.D. thesis (Netherlands Energy Research Foundation).
- Konijnenberg, M. W., K. Abrahams, J. Kopecky, F. Stecher-Rasmussen, R. Wervelman, and J. H. Koch, 1988, *Phys. Lett. B* **205**, 215.
- Koori, N., 1972, *J. Phys. Soc. Jpn.* **32**, 306.
- Kottler, H., and K. L. Kowalski, 1965, *Phys. Rev. B* **138**, 619.
- Kowalski, K. L., 1976, *Nucl. Phys. A* **264**, 173.
- Krajcik, R. A., and L. L. Foldy, 1974, *Phys. Rev. D* **10**, 1777.
- Kukulin, V. I., V. N. Pomerantsev, Kh. D. Razikov, V. T. Voronchev, and G. G. Ryzhikh, 1995, *Nucl. Phys. A* **586**, 151.
- Kukulin, V. I., V. T. Voronchev, T. D. Kaipov, and R. A. Eramzhyan, 1990, *Nucl. Phys. A* **517**, 221.
- Kuperin, Yu., A. Kuperin, S. P. Merkuriev, and A. A. Kvitsinsky, 1983, *Yad. Fiz.* **37**, 1440 [*Sov. J. Nucl. Phys.* **37**, 857 (1983)].
- Kuroda, K., A. Michalowicz, and M. Poulet, 1966, *Nucl. Phys.* **88**, 33.

- Lafferty, J. M., and S. R. Cotanch, 1982, Nucl. Phys. A **373**, 363.
- Lagaris, I. E., and V. R. Pandharipande, 1981, Nucl. Phys. A **359**, 331.
- Langenbrunner, J. L., *et al.*, 1988, Phys. Rev. C **38**, 565.
- Lapikás, L., 1978, in *Proceedings of the Conference on Modern Trends in Elastic Electron Scattering*, edited by C. De Vries (NIKHEF-K, Amsterdam), p. 49.
- Lavern, A., and C. Gignoux, 1973, Nucl. Phys. A **203**, 597.
- Lehman, D. R., and W. C. Parke, 1983a, Phys. Rev. Lett. **50**, 98.
- Lehman, D. R., and W. C. Parke, 1983b, Phys. Rev. C **28**, 364.
- Leidemann, W., and H. Arenhövel, 1983, Nucl. Phys. A **393**, 385.
- Leidemann, W., and H. Arenhövel, 1987, Nucl. Phys. A **465**, 573.
- Leidemann, W., K.-M. Schmitt, and H. Arenhövel, 1990, Phys. Rev. C **42**, 826.
- Levinger, J. S., and H. A. Bethe, 1950, Phys. Rev. **78**, 115.
- Lewart, D. S., V. R. Pandharipande, and S. C. Pieper, 1988, Phys. Rev. B **37**, 4950.
- Li, G. C., I. Sick, R. R. Whitney, and M. R. Yearian, 1971, Nucl. Phys. A **162**, 583.
- Lin, D., and M. K. Liou, 1991, Phys. Rev. C **43**, R930.
- Lindgren, I., 1965, in *Alpha-, Beta-, and Gamma-Ray Spectroscopy*, Vol. 2, edited by K. Siegbahn (North Holland, Amsterdam), p. 1620.
- Lippman, B. A., 1956, Phys. Rev. **102**, 264.
- Lock, J. A., and L. L. Foldy, 1975, Ann. Phys. (N.Y.) **93**, 276.
- Ma, L., H. J. Karwowski, C. R. Brune, Z. Ayer, T. C. Black, J. C. Blackman, E. J. Ludwig, M. Viviani, A. Kievsky, and R. Schiavilla, 1996, Phys. Rev. C **55**, 588.
- Machleidt, R., 1989, Adv. Nucl. Phys. **19**, 189.
- Machleidt, R., K. Holinde, and Ch. Elster, 1987, Phys. Rep. **149**, 1.
- Machleidt, R., F. Sammarruca, and Y. Song, 1996, Phys. Rev. C **53**, R1483.
- Mack, D. J., *et al.*, 1992, Phys. Rev. C **45**, 1767.
- Maize, M. A., and Y. E. Kim, 1984, Nucl. Phys. A **420**, 365.
- Malfliet, R. A., and J. A. Tjon, 1969a, Nucl. Phys. A **127**, 161.
- Malfliet, R. A., and J. A. Tjon, 1969b, Phys. Lett. **29B**, 391.
- Marchand, C., *et al.*, 1985, Phys. Lett. **153B**, 29.
- Martinelli, S., H. Kamada, G. Orlandini, and W. Glöckle, 1995, Phys. Rev. C **52**, 1778.
- Martorell, J., D. W. L. Sprung, and D. C. Zheng, 1995, Phys. Rev. C **51**, 1127.
- Mateos, A. O., 1995 Ph. D. thesis (Massachusetts Institute of Technology).
- Mathiot, J. F., and B. Desplanques, 1981, Phys. Lett. **101B**, 141.
- Mathiot, J. F., 1984, Nucl. Phys. A **412**, 201.
- McAninch, J. E., W. Haeberli, H. Witala, W. Glöckle, and J. Golak, 1993, Phys. Lett. B **307**, 13.
- McAninch, J. E., L. O. Lamm, and W. Haeberli, 1994, Phys. Rev. C **50**, 589.
- McCarthy, J. S., I. Sick, and R. R. Whitney, 1977, Phys. Rev. C **15**, 1396.
- McVoy, K. W., and L. Van Hove, 1962, Phys. Rev. **125**, 1034.
- Measday, J. F., and J. N. Palmieri, 1966, Nucl. Phys. **85**, 142.
- Meier-Hajduk, H., Ch. Hajduk, P. U. Sauer, and W. Theis, 1983, Nucl. Phys. A **395**, 332.
- Mellema, S., T. R. Wang, and W. Haeberli, 1985, Phys. Lett. **166B**, 282.
- Merkuriev, S. P., 1976, Yad. Fiz. **24**, 289 [Sov. J. Nucl. Phys. **24**, 150 (1976)].
- Merritt, J. S., J. G. V. Taylor, and A. W. Boyd, 1968, Nucl. Sci. Eng. **34**, 195.
- Messiah, A., 1961, *Quantum Mechanics* (North-Holland, Amsterdam).
- Metropolis, N., A. W. Rosenbluth, M. N. Rosenbluth, A. H. Teller, and E. Teller, 1953, J. Chem. Phys. **21**, 1087.
- Meyerhof, W. E., W. Feldman, S. Gilbert, and W. O'Connell, 1969, Nucl. Phys. A **131**, 489.
- Meziani, Z. E., *et al.* 1984, Phys. Rev. Lett. **52**, 2130.
- Migdal, A. B., 1957, Sov. Phys. JETP **5**, 333.
- Milner, R. G., *et al.*, 1996, Phys. Lett. B **379**, 67.
- Miyazawa, H., 1951, Prog. Theor. Phys. **6**, 801.
- Morita, H., and T. Suzuki, 1991, Prog. Theor. Phys. **86**, 671.
- Musolf, M. J., T. W. Donnelly, J. Dubach, S. J. Pollock, S. Kowalski, and E. J. Beise, 1994, Phys. Rep. **239**, 1.
- Musolf, M. J., R. Schiavilla, and T. W. Donnelly, 1994, Phys. Rev. C **50**, 2173.
- Nagels, M. M., T. A. Rijken, and J. J. de Swart, 1978, Phys. Rev. D **17**, 768.
- Noble, J. V., 1967, Phys. Rev. **161**, 945.
- Nogga, A., D. Hüber, H. Kamada, and W. Glöckle, 1997, preprint nucl-th/9704001.
- Nozawa, S., Y. Kohyama, and K. Kubodera, 1982, Prog. Theor. Phys. **67**, 1240.
- Nozawa, S., Y. Kohyama, and K. Kubodera, 1984, Phys. Lett. **140B**, 11.
- Nyman, E. M., 1967, Nucl. Phys. B **1**, 535.
- Nyman, E. M., and D. O. Riska, 1986, Phys. Rev. Lett. **57**, 3007.
- Nyman, E. M., and D. O. Riska, 1987, Nucl. Phys. A **468**, 473.
- O'Fallon, N. M., L. J. Koester, Jr., and J. H. Smith, 1972, Phys. Rev. C **5**, 1926.
- Ohta, K., 1989a, Nucl. Phys. A **495**, 564.
- Ohta, K., 1989b, Phys. Rev. C **39**, 2302.
- Okai, S., and S. C. Park, 1966, Phys. Rev. **145**, 787.
- Ordóñez, C., L. Ray, and U. van Kolck, 1994, Phys. Rev. Lett. **72**, 1982.
- Orlandini, G., and M. Traini, 1991, Rep. Prog. Phys. **54**, 257.
- Ottermann, C. R., G. Kobschall, K. Maurer, K. Rohrich, Ch. Schmitt, and V. N. Walther, 1985, Nucl. Phys. A **435**, 688.
- Palmieri, J., 1972, Nucl. Phys. A **188**, 72.
- Pandharipande, V. R., 1990, in *Structure of Hadrons and Hadronic Matter*, edited by O. Scholten and J. Koch (World Scientific, Singapore), p. 1.
- Pandharipande, V. R., C. N. Papanicolas, and J. Wambach, 1984, Phys. Rev. Lett. **53**, 1133.
- Pandharipande, V. R., and S. C. Pieper, 1992, Phys. Rev. C **45**, 791.
- Pandharipande, V. R., *et al.*, 1994, Phys. Rev. C **49**, 789.
- Patberg, H., 1995, Ph. D. thesis (University of Köln).
- Payne, G. L., 1987, in *Models and Methods in Few-Body Physics*, Lecture Notes in Physics No. 273 (Springer, New York), p. 64.
- Peña, M. T., P. U. Sauer, A. Stadler, and G. Kortemeyer, 1993, Phys. Rev. C **48**, 2208.
- Phillips, A. C., 1972, Nucl. Phys. A **184**, 337.
- Phillips, D. R., and T. D. Cohen, 1997, Phys. Lett. B **390**, 7.
- Phillips, T. W., B. L. Berman, and J. D. Seagrave, 1980, Phys. Rev. C **22**, 384.
- Picklesimer, A., R. A. Rice, and R. Brandenburg, 1991, Phys. Rev. C **44**, 1359.

- Picklesimer, A., R. A. Rice, and R. Brandenburg, 1992a, *Phys. Rev. Lett.* **68**, 1484.
- Picklesimer, A., R. A. Rice, and R. Brandenburg, 1992b, *Phys. Rev. C* **45**, 547.
- Picklesimer, A., R. A. Rice, and R. Brandenburg, 1992c, *Phys. Rev. C* **45**, 2045.
- Picklesimer, A., R. A. Rice, and R. Brandenburg, 1992d, *Phys. Rev. C* **45**, 2624.
- Picklesimer, A., R. A. Rice, and R. Brandenburg, 1995, *Few-Body Syst.* **19**, 47.
- Piekarewicz, J., and S. E. Koonin, 1987, *Phys. Rev. C* **36**, 875.
- Pieper, S. C., and V. R. Pandharipande, 1993, *Phys. Rev. Lett.* **70**, 2541.
- Pieper, S. C., and R. B. Wiringa, 1996, private communication.
- Pieper, S. C., R. B. Wiringa, and V. R. Pandharipande, 1990, *Phys. Rev. Lett.* **64**, 364.
- Pieper, S. C., R. B. Wiringa, and V. R. Pandharipande, 1992, *Phys. Rev. C* **46**, 1741.
- Pieper, S. C., *et al.*, 1996 private communication.
- Platchkov, S., *et al.*, 1990, *Nucl. Phys. A* **510**, 740.
- Plessas, W., V. Christian, and R. F. Wagenbrunn, 1995, *Few-Body Syst., Suppl.* **9**, 429.
- Polyzou, W. N., and W. Glöckle, 1990, *Few-Body Syst.* **9**, 97.
- Postma, H., and R. Wilson, 1961, *Phys. Rev.* **121**, 1229.
- Poutissou, J. M., and W. R. Del Bianco, 1973, *Nucl. Phys. A* **199**, 517.
- Pudliner, B. S., V. R. Pandharipande, J. Carlson, and R. B. Wiringa, 1995, *Phys. Rev. Lett.* **74**, 4396.
- Pudliner, B. S., *et al.*, 1996, *Phys. Rev. Lett.* **76**, 2416.
- Pudliner, B. S., V. R. Pandharipande, J. Carlson, S. C. Pieper, and R. B. Wiringa, 1997, *Phys. Rev. C* **56**, 1720.
- Ramos, A., A. Polls, and W. H. Dickhoff, 1989, *Nucl. Phys. A* **503**, 1.
- Rand, R. E., R. F. Frosch, and M. R. Yearian, 1966, *Phys. Rev.* **144**, 859.
- Rauprich, G., H. J. Hahn, M. Karus, P. Niessen, K. R. Nyga, H. Oswald, L. Sydow, H. Paetz-gen-Schieck, and Y. Koike, 1988, *Few-Body Syst.* **5**, 67.
- Rauprich, G., S. Lemaitre, P. Niessen, K. R. Nyga, R. Reckenfelderbaumer, L. Sydow, H. Paetz-gen-Schieck, H. Witala, and W. Glöckle, 1991, *Nucl. Phys. A* **535**, 313.
- Reid, R. V., 1968, *Ann. Phys. (N.Y.)* **50**, 411.
- Renard, R. M., J. Tran Thanh Van, and M. Le Bellac, 1965, *Nuovo Cimento* **38**, 565.
- Rho, M., and G. E. Brown, 1981, *Comments Nucl. Part. Phys.* **10**, 201.
- Rice, B. J., G. J. Schmid, and H. R. Weller, 1996, private communication.
- Riddle, R. A. J., A. Langsford, P. H. Bown, and G. C. Cox, 1965, *Nucl. Phys.* **61**, 467.
- Ring, P., and P. Schuck, 1980, *The Nuclear Many-Body Problem* (Springer, Heidelberg).
- Riska, D. O., 1980, *Nucl. Phys. A* **350**, 227.
- Riska, D. O., 1984, *Prog. Part. Nucl. Phys.* **11**, 199.
- Riska, D. O., 1985a, *Phys. Scr.* **31**, 107.
- Riska, D. O., 1985b, *Phys. Scr.* **31**, 471.
- Riska, D. O., 1989, *Phys. Rep.* **181**, 207.
- Riska, D. O., and G. E. Brown, 1970, *Phys. Lett.* **32B**, 662.
- Riska, D. O., and G. E. Brown, 1972, *Phys. Lett.* **38B**, 193.
- Riska, D. O., and M. Poppius, 1985, *Phys. Scr.* **32**, 581.
- Riska, D. O., and M. Radomski, 1977, *Phys. Rev. C* **16**, 2105.
- Robilotta, M. R., 1987, *Few-Body Syst., Suppl.* **2**, 35.
- Robilotta, M. R., and M. P. Isidro Filho, 1984, *Nucl. Phys. A* **414**, 394.
- Robilotta, M. R., and M. P. Isidro Filho, 1986, *Nucl. Phys. A* **451**, 581.
- Robilotta, M. R., M. P. Isidro Filho, H. T. Coelho, and T. K. Das, 1985, *Phys. Rev. C* **31**, 646.
- Rock, S., *et al.*, 1982, *Phys. Rev. Lett.* **49**, 1139.
- Rodning, N. L., and L. D. Knutson, 1990, *Phys. Rev. C* **41**, 898.
- Rolfs, C., 1973, *Nucl. Phys. A* **217**, 29.
- Romero, J. L., *et al.*, 1982, *Phys. Rev. C* **25**, 2214.
- Rühl, H., *et al.*, 1991, *Nucl. Phys. A* **524**, 377.
- Rupp, G., and J. A. Tjon, 1992, *Phys. Rev. C* **45**, 2133.
- Sachs, R. G., 1948, *Phys. Rev.* **74**, 433; **75**, 1605(E).
- Sachs, R. G., 1962, *Phys. Rev.* **126**, 2256.
- Sagara, K., *et al.*, 1994, *Phys. Rev. C* **50**, 576.
- Saito, T.-Y., Y. Wu, S. Ishikawa, and T. Sasakawa, 1990, *Phys. Lett. B* **242**, 12.
- Santos, F. D., A. Arriaga, A. M. Eiró, and J. A. Tostevin, 1985, *Phys. Rev. C* **31**, 707.
- Sauer, P. U., 1986, *Prog. Part. Nucl. Phys.* **16**, 35.
- Sauer, P. U., 1992, *Nucl. Phys. A* **543**, 291c.
- Schamberger, R. D., 1952, *Phys. Rev.* **85**, 424.
- Schiavilla, R., 1990, *Phys. Rev. Lett.* **65**, 835.
- Schiavilla, R., 1996a, in *Perspectives in Nuclear Physics at Intermediate Energies*, edited by S. Boffi, C. Ciofi degli Atti, and M. M. Giannini (World Scientific, Singapore), p. 490.
- Schiavilla, R., 1996b, unpublished.
- Schiavilla, R., 1997, unpublished.
- Schiavilla, R., A. Fabrocini, and V. R. Pandharipande, 1987, *Nucl. Phys. A* **473**, 290.
- Schiavilla, R., D. S. Lewart, V. R. Pandharipande, S. C. Pieper, R. B. Wiringa, and S. Fantoni, 1987, *Nucl. Phys. A* **473**, 267.
- Schiavilla, R., V. R. Pandharipande, and A. Fabrocini, 1989, *Phys. Rev. C* **40**, 1484.
- Schiavilla, R., V. R. Pandharipande, and D. O. Riska, 1989, *Phys. Rev. C* **40**, 2294.
- Schiavilla, R., V. R. Pandharipande, and D. O. Riska, 1990, *Phys. Rev. C* **41**, 309.
- Schiavilla, R., V. R. Pandharipande, and R. B. Wiringa, 1986, *Nucl. Phys. A* **449**, 219.
- Schiavilla, R., and D. O. Riska, 1991, *Phys. Rev. C* **43**, 437.
- Schiavilla, R., and M. Viviani, 1996, unpublished.
- Schiavilla, R., R. B. Wiringa, and J. Carlson, 1993, *Phys. Rev. Lett.* **70**, 3856.
- Schiavilla, R., R. B. Wiringa, V. R. Pandharipande, and J. Carlson, 1992, *Phys. Rev. C* **45**, 2628.
- Schiff, L. I., 1937, *Phys. Rev.* **52**, 242.
- Schmid, G. J., *et al.*, 1995, *Phys. Rev. C* **52**, 1732.
- Schmid, G. J., *et al.*, 1996, *Phys. Rev. Lett.* **76**, 3088.
- Schmidt, K. E., and M. H. Kalos, 1984, in *Applications of the Monte Carlo Method in Statistical Physics*, edited by K. Binder (Springer, Heidelberg), p. 125.
- Schori, O., *et al.*, 1987, *Phys. Rev. C* **35**, 2252.
- Schulze, M. E., *et al.*, 1984, *Phys. Rev. Lett.* **52**, 597.
- Schulze, R.-W., and P. U. Sauer, 1993, *Phys. Rev. C* **48**, 38.
- Schwarz, P., H. O. Klages, P. Doll, B. Haesner, W. Wilczynski, B. Zietnitz, and J. Kecskemeti, 1983, *Nucl. Phys. A* **398**, 1.
- Sen, S., and L. D. Knutson, 1982, *Phys. Rev. C* **26**, 257.
- Seyler, R. G., and H. R. Weller, 1979, *Phys. Rev. C* **20**, 453.
- Shimizu, H., K. Imai, N. Tamura, K. Nisimura, K. Hatanaka, T. Saito, Y. Koike, and Y. Taniguchi, 1982, *Nucl. Phys. A* **382**, 242.
- Shirato, S., and N. Koori, 1968, *Nucl. Phys. A* **120**, 387.

- Silver, R. N., D. S. Sivia, and J. E. Gubernatis, 1990, *Phys. Rev. B* **41**, 2380.
- Simon, G., F. Borkowski, Ch. Schmitt, and V. N. Walther, 1980, *Z. Naturforsch. A* **35**, 1.
- Simon, G., Ch. Schmitt, and V. H. Walther, 1981, *Nucl. Phys. A* **364**, 285.
- Skopik, D. M., and W. R. Dodge, 1972, *Phys. Rev. C* **6**, 43.
- Sperisen, F., W. Gruebler, V. Konig, P. A. Schmelzbach, K. Elsener, B. Jenny, C. Schweizer, J. Ulbricht, and P. Dole-schall, 1984, *Nucl. Phys. A* **422**, 81.
- Stadler, A., J. Adam, H. Henning, and P. U. Sauer, 1995, *Phys. Rev. C* **51**, 2896.
- Stadler, A., W. Glöckle, and P. U. Sauer, 1991, *Phys. Rev. C* **44**, 2319.
- Stadler, A., and F. Gross, 1994, in *Few-Body Problems in Physics*, AIP Conf. Proc. No. **334**, edited by F. Gross (AIP, New York), p. 867.
- Stadler, A., and F. Gross, 1997, *Phys. Rev. Lett.* **78**, 26.
- Stahler, S. W., 1988, *Astrophys. J.* **322**, 804.
- Stephan, M., *et al.*, 1989, *Phys. Rev. C* **39**, 2133.
- Stoks, V. G. J., and J. J. de Swart, 1990, *Phys. Rev. C* **42**, 1235.
- Stoks, V. G. J., R. A. M. Klomp, M. C. M. Rentmeester, and J. J. de Swart, 1993, *Phys. Rev. C* **48**, 792.
- Stoks, V. G. J., R. A. M. Klomp, C. P. F. Terheggen, and J. J. de Swart, 1994, *Phys. Rev. C* **49**, 2950.
- Stoks, V. G. J., R. Timmermans, and J. J. de Swart, 1993, *Phys. Rev. C* **47**, 512.
- Strate, J., *et al.*, 1988, *J. Phys. G* **14**, L229.
- Strate, J., *et al.*, 1989, *Nucl. Phys. A* **501**, 51.
- Strueve, W., Ch. Hajduk, P. U. Sauer, and W. Theis, 1987, *Nucl. Phys. A* **465**, 651.
- Suffert, M., and R. Berthollet, 1979, *Nucl. Phys. A* **318**, 54.
- Sugawara, H., and F. von Hippel, 1968, *Phys. Rev.* **172**, 1764.
- Suzuki, T., H. Hyuga, A. Arima, and K. Yazaki, 1981a, *Nucl. Phys. A* **358**, 421.
- Szuki, T., H. Hyuga, A. Arima, and K. Yazaki, 1981b, *Phys. Lett.* **106B**, 19.
- Sydow, L., *et al.*, 1994, *Nucl. Phys. A* **567**, 55.
- Szalata, Z. M., *et al.*, 1977, *Phys. Rev. C* **15**, 1200.
- Taddeucci, T. N., 1991, in *Spin and Isospin in Nuclear Interactions*, edited by S. W. Wissink, C. D. Goodman, and G. E. Walker (Plenum, New York), p. 393.
- Taddeucci, T. N., *et al.*, 1994, *Phys. Rev. Lett.* **73**, 3516.
- Tamagaki, R., and H. Tanaka, 1965, *Prog. Theor. Phys.* **34**, 191.
- Tégner, P. E., and C. Bargholtz, 1983, *Astrophys. J.* **272**, 311.
- The, I., *et al.*, 1991, *Phys. Rev. Lett.* **67**, 173.
- Thirumalai, D., and B. Berne, 1983, *J. Chem. Phys.* **79**, 5029.
- Thompson, A. K., *et al.*, 1992, *Phys. Rev. Lett.* **68**, 2901.
- Tjon, J. A., 1975, *Phys. Lett.* **56B**, 217.
- Tombrello, T. A., 1965, *Phys. Rev.* **138**, 40B.
- Tornow, W., R. T. Braun, and H. Witala, 1996, *Phys. Rev. C* **54**, 42.
- Tornow, W., *et al.*, 1991, *Phys. Lett. B* **257**, 273.
- Tornow, W., *et al.*, 1995, *Few-Body Syst. Suppl.* **8**, 161.
- Torre, J., and B. Goulard, 1983, *Phys. Rev. C* **28**, 529.
- Tostevin, J. A., 1986, *Phys. Rev. C* **34**, 1497.
- Towner, I. S., 1984, *Prog. Part. Nucl. Phys.* **11**, 9.
- Towner, I. S., 1987, *Phys. Rep.* **155**, 263.
- Towner, I. S., and F. C. Khanna, 1981, *Nucl. Phys. A* **356**, 445.
- Tsushima, K., D. O. Riska, and P. G. Blunden, 1993, *Nucl. Phys. A* **559**, 543.
- van der Leun, C., and C. Alderliesten, 1982, *Nucl. Phys. A* **380**, 261.
- van Faassen, E. E., and J. A. Tjon, 1984, *Phys. Rev. C* **30**, 285.
- Van Orden, J. W., N. Devine, and F. Gross, 1995, *Phys. Rev. Lett.* **75**, 4369.
- Vergados, J. D., 1974, *Nucl. Phys. A* **220**, 259.
- Villars, F., 1947, *Helv. Phys. Acta* **20**, 476.
- Viviani, M., 1997, private communication.
- Viviani, M., A. Kievsky, and S. Rosati, 1995, *Few-Body Syst.* **18**, 25.
- Viviani, M., R. Schiavilla, and A. Kievsky, 1996, *Phys. Rev. C* **54**, 534.
- von Reden, K. F., *et al.*, 1990, *Phys. Rev. C* **41**, 1084.
- Wakamatsu, M., and W. Weise, 1988, *Nucl. Phys. A* **477**, 559.
- Walker, R. C., *et al.*, 1989, *Phys. Lett. B* **224**, 353.
- Watcher, B., T. Mertelmeiser, and H. M. Hofmann, 1988, *Phys. Lett. B* **200**, 246.
- Watson, J. W., *et al.*, 1982, *Phys. Rev. C* **25**, 2219.
- Watson, K. M., 1952, *Phys. Rev.* **88**, 1163.
- Weinberg, S., 1990, *Phys. Lett. B* **251**, 288.
- Weinberg, S., 1991, *Nucl. Phys. B* **363**, 3.
- Weller, H. R., P. Colby, N. R. Roberson, and D. R. Tilley, 1984, *Phys. Rev. Lett.* **53**, 1325.
- Weller, H. R., *et al.*, 1986, *Phys. Rev. C* **34**, 32.
- Werntz, C., and J. G. Brennan, 1967, *Phys. Rev.* **157**, 759.
- Werntz, C., and J. G. Brennan, 1973, *Phys. Rev. C* **8**, 1545.
- Wervelman, R., *et al.*, 1991, *Nucl. Phys. A* **526**, 265.
- Weyer, H. J., 1990, *Phys. Rep.* **195**, 295.
- Wilkinson, F. J., III, and F. E. Cecil, 1985, *Phys. Rev. C* **31**, 2036.
- Wiringa, R. B., 1991, *Phys. Rev. C* **43**, 1585.
- Wiringa, R. B., V. Fiks, and A. Fabrocini, 1988, *Phys. Rev. C* **38**, 1010.
- Wiringa, R. B., and R. Schiavilla, 1996, unpublished.
- Wiringa, R. B., R. A. Smith, and T. L. Ainsworth, 1984, *Phys. Rev. C* **29**, 1207.
- Wiringa, R. B., V. G. J. Stoks, and R. Schiavilla, 1995, *Phys. Rev. C* **51**, 38.
- Witala, H., Th. Cornelius, and W. Glöckle, 1988a, *Few-Body Syst.* **3**, 123.
- Witala, H., Th. Cornelius, and W. Glöckle, 1988b, *Few-Body Syst.* **5**, 89.
- Witala, H., and W. Glöckle, 1991, *Nucl. Phys. A* **528**, 48.
- Witala, H., W. Glöckle, and H. Kamada, 1991, *Phys. Rev. C* **43**, 1619.
- Witala, H., D. Hüber, and W. Glöckle, 1994, *Phys. Rev. C* **49**, R14.
- Witala, H., D. Huber, W. Glöckle, J. Golak, A. Stadler, and J. Adam, Jr., 1995, *Phys. Rev. C* **52**, 1254.
- Witala, H., D. Hüber, W. Tornow, and D. E. Gonzales Trotter, 1998, *Few-Body Syst.* (in press.)
- Witala, H., 1993, *Few-Body Systm.* **15**, 67.
- Wolfs, F. L. H., *et al.*, 1989, *Phys. Rev. Lett.* **63**, 2721.
- Woodward, C. E., *et al.*, 1990, *Phys. Rev. Lett.* **65**, 698.
- Yakubovsky, O. A., 1967, *Sov. J. Nucl. Phys.* **5**, 937.
- Yukawa, H., 1935, *Proc. Phys. Math. Soc. Jpn.* **17**, 48.
- Zabolitzky, J. G., and W. Ey, 1978, *Phys. Lett.* **76B**, 527.
- Zghiche, A., *et al.*, 1993, *Nucl. Phys. A* **572**, 513; **584**, 757(E).
- Zhang, S., J. Carlson, and J. E. Gubernatis, 1995, *Phys. Rev. Lett.* **74**, 3652.
- Zheng, D. C., *et al.*, 1995, *Phys. Rev. C* **52**, 2488.